Solubilization of lipids and membrane proteins into nanodiscs

Mode of action and applications of SMA copolymers

Stefan Scheidelaar

S. Scheidelaar

Solubilization of lipids and membrane proteins into nanodiscs
Mode of action and applications of SMA copolymers

PhD Thesis, Utrecht University, 2016
In English, with a summary in Dutch

ISBN: 978-90-393-6635-6

Cover Design: Stefanie van den Herik, Proefschriftmaken.nl || Uitgeverij BOXpress
Printed by: Proefschriftmaken.nl || Uitgeverij BOXpress
Published by: Uitgeverij BOXPress, Vianen

The research presented in this thesis was performed in the Membrane Biochemistry & Biophysics group, Bijvoet Center for Biomolecular Research, Faculty of Science, Utrecht University, The Netherlands. The Printing of this thesis was financially supported by Stichting FOM, and Polyscope Polymers B.V., Geleen, The Netherlands.

Solubilization of lipids and membrane proteins into nanodiscs
Mode of action and applications of SMA copolymers

Solubilizatie van lipiden en membraaneiwitten in nanodiscs
Werkingsmechanisme en toepassingen van SMA copolymeren
(met een samenvatting in het Nederlands)

Proefschrift

ter verkrijging van de graad van doctor aan de Universiteit Utrecht op gezag van de rector magnificus, prof. dr. G.J. van der Zwaan, ingevolge het besluit van het college voor promoties in het openbaar te verdedigen op woensdag 26 oktober 2016 des middags te 2.30 uur

door

Stefan Scheidelaar

geboren op 12 juli 1988
te Nieuw-Lekkerland

Promotor:
Prof. dr. J.A. Killian

The research described in this thesis is part of the research programme of the Foundation for Fundamental Research on Matter (FOM), which is part of the Netherlands Organisation for Scientific Research (NWO).

Table of contents

CHAPTER 1

INTRODUCTION

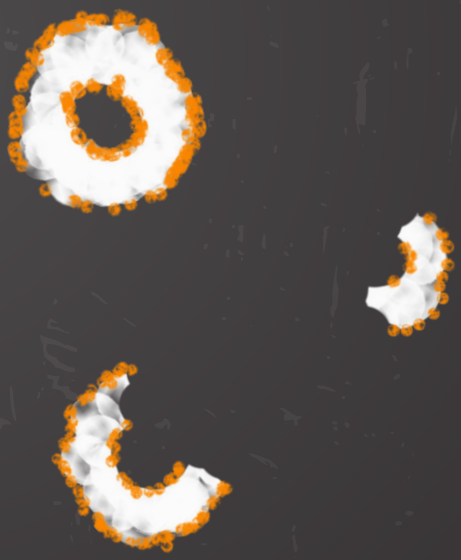

THIS CHAPTER IS PARTLY BASED ON THE PUBLICATION:

J.M. DÖRR, **S. SCHEIDELAAR**, M.C. KOORENGEVEL, J.J. DOMINGUEZ, M. SCHÄFER, C.A. VAN WALREE AND J.A. KILLIAN, (2016), THE STYRENE-MALEIC ACID COPOLYMER: A VERSATILE TOOL IN MEMBRANE RESEARCH. *EUR. BIOPHYS. J.* 45, 3-21.

1.1 Cell membranes

A cell is considered to be the smallest unit of life capable to function independently. There are many different type of cells and well-known examples include skin cells, lung cells, and red blood cells. Cells are part of a tissue in which many cells work together to make that specific tissue function. Although the cells that build up the different tissues have different functions, they all have at least one thing in common: a lipid membrane that surrounds the cell contents and is called the cell membrane.

The cell membrane acts as a barrier separating the inside of the cell from the outside world. But the cell membrane is much more than that. It is an active part of cellular processes inside the cell that are crucial for survival: it regulates the transport of solutes over the membrane both inwards and outwards, and is involved in the communication between cells, which is important for proper function of the tissue. The cell membrane has a sheet-like structure and consists mainly lipids and membrane proteins (figure 1), which will be briefly introduced below. Not only the cell itself, but also the organelles inside the cell, such as mitochondria and the endoplasmic reticulum (ER) have a lipid membrane that act as a barrier and a place for many cellular processes. Those membranes also consist of lipids and membrane proteins but their compositions are very different. It is the unique composition of membranes, and their interactions with their direct environment that gives them their specific function in life.

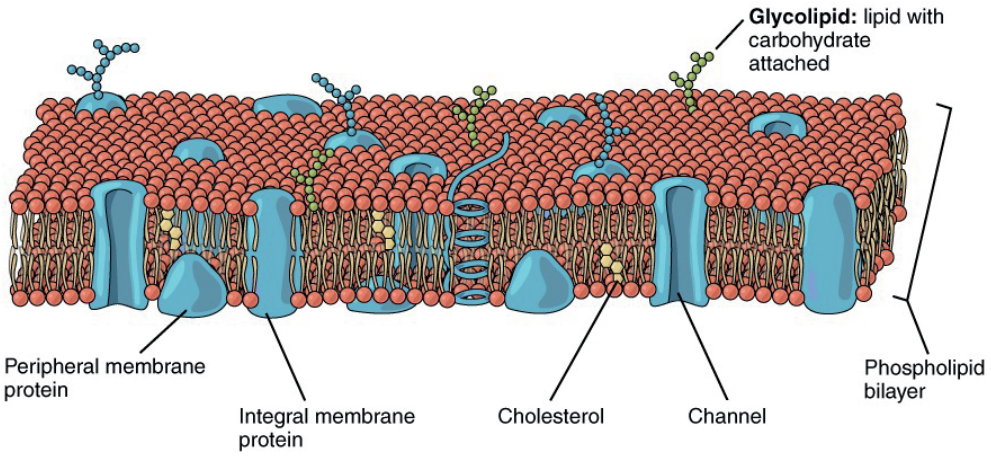

Figure 1

Cartoon of a biological membrane with its lipid and membrane protein components. Adapted from ref [1].

Lipids. The properties of a cell membrane are for a large part determined by lipids. Lipids are amphipathic molecules that have a hydrophilic headgroup that is connected to two hydrophobic tails. In mammalian cells, the most abundant types of lipids are phospholipids, glycolipids, and sterols (like cholesterol). In this thesis, phospholipids

and in particular glycerophospholipids is the main class of lipids that will be discussed. Glycerophospholipids consist of a glycerol backbone to which a phosphate group is esterified which make up the hydrophilic headgroup, and two fatty acids which make up the hydrophobic tails. Figure 2 shows some examples of this type of phospholipid. The diversity in glycerophospholipids originates from the different groups that are attached to the phosphate group, but also from the different length, branching and degree of unsaturation of the fatty acids. For instance, lipids can be charged: while phosphatidylcholine (PC) and PE are zwitterionic lipids, phosphatidic acid (PA), phosphatidylserine (PS), phosphatidylglycerol (PG), and cardiolipin (CL) are negatively charged. The charge state of lipids is important for the interactions they have with each other and proteins.

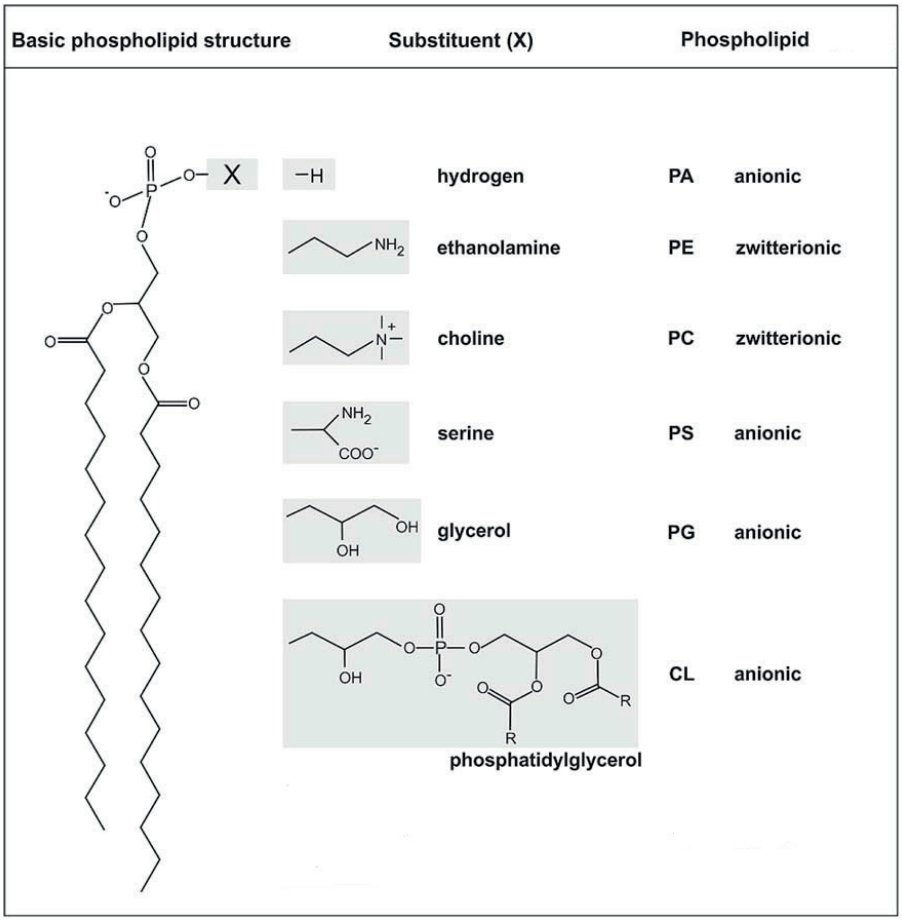

Figure 2
Structural overview of common glycerophospholipids and their ionic state. Adapted from ref [8].

Due to their amphipathic structure lipids generally organize themselves in a bilayer in which two monomolecular layers of lipids build a hydrophobic core made by the acyl chains and a hydrophilic surface that faces the aqueous solution made by the headgroups.

Lipids are also part of many cellular processes and pathways. For example, in signal transduction where lipids acts as messenger molecules that convey signals from the cell membrane to various targets within the cell [2,3]. But they also play roles in cellular process such as energy transduction, cellular trafficking, endocytosis/exocytosis, and programmed cell-death or apoptosis [4—7].

The lipid bilayer architecture of membranes, and specifically the hydrophobic core, forms an excellent barrier for most solutes and ions. However, the transport of molecules across the membrane, for instance the uptake of drug molecules, is vital for the survival of cells. It is the other main component of cell membranes, membrane proteins, that is responsible for molecular transport over the membrane, as well as for processes such as initializing signaling pathways in the cell, and performing enzymatic activities.

Membrane proteins. About 20-30% of all genes identified to date encode for membrane proteins [9,10], which illustrates their importance in the cell proteome. There are mainly two classes of membrane proteins: those that are embedded in the lipid bilayer (integral membrane proteins) and those that are associated to the surface of the membrane (peripheral membrane proteins) (figure 3). Most of the proteins are integral and span the bilayer once or more with their transmembrane segments that are interconnected by loops. Some proteins also have a water soluble domain that is attached to the membrane spanning part. The transmembrane segments are mostly α-helical in structure and appear in various configurations. They can span the membrane straight along the membrane normal, but they can also, for example, be tilted or have a kink in the helix. Multiple α-helices can associate together in the membrane to form a channel or pump to facilitate transport of solutes or ions over the membrane. The number of α-helices that associate together and the amino acid sequence in general determine the function of a membrane protein.

Peripheral membrane proteins are not embedded in the membrane but rather interact with the lipid headgroups by hydrogen bonds and electrostatic interactions and/or with the more hydrophobic core of the membrane by an amphipathic domain that shallowly penetrates into the membrane with hydrophobic side chains. For both classes of membrane proteins it not only the protein itself, but also the interactions that these proteins have with the direct lipid environment that determine their precise structure and function in the cell membrane.

Lipid-protein interactions. The lipid membrane does not just serve as a matrix for membrane proteins, it is also actively involved in the processes that membrane proteins carry out, for example by specific protein-lipid interactions

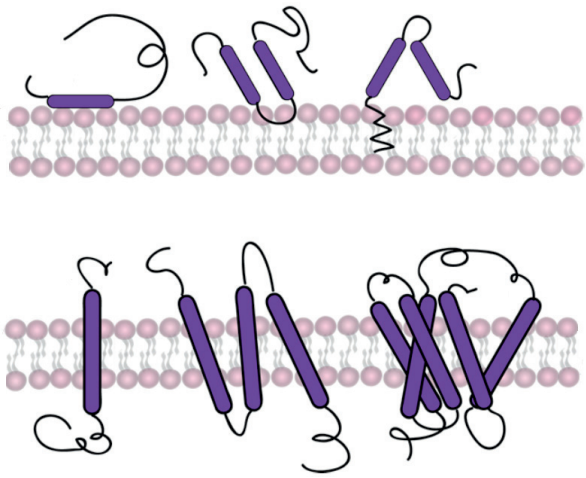

Figure 3
Schematic representation of various types of peripheral membrane proteins (above) and integral membrane proteins (below). Adapted from ref [11].

between a protein and an individual lipid molecule in the membrane [12].

Membrane lipids can be sorted in three classes based on their position in the membrane [13]. Lipids that are positioned inside integral proteins, and are not part of the lipid bilayer, are called integral lipids. Such lipids usually are tightly bound to the proteins and they are often found in large protein complexes that exist of multiple domains where lipids may be found for example at the interface where the domains connect to each other to assist correct protein structure. A lipid in the first shell around a membrane protein is called an annular lipid. Although they are part of the lipid bilayer they are often restricted in their motional freedom due to interactions with the protein surface by for instance hydrogen bonding or electrostatic interactions. Classic examples of annular lipids that interact with proteins come from mechanosensitive proteins such as MscL [14] and potassium channels such as KcsA [15—20], in which negatively charged bind to positively charged residues of the protein. The third and last class of lipids in the membrane is the bulk lipid. These lipids are at least one shell away from the protein and are considered to be structural lipids. However, bulk lipids can affect protein structure and function by macroscopic properties of the membrane. These properties include membrane fluidity and lateral pressure, which will be introduced later.

Outline of the introduction. A short and general introduction into lipid membranes and its components was given above. In the rest of the introduction, a more detailed overview is given about the topics that play a key role in the studies described in this thesis.

First we describe the photosynthetic membranes of plants and bacteria. In particular the photosynthetic membrane of *Rhodobacter sphaeroides*, a purple bacterium, is the

object of study in this thesis. Second, the concept of model membranes along with some of its properties is discussed. Third, several approaches that aim to solubilize membrane proteins from membranes and to stabilize them in aqueous solution for the purpose of research is discussed. Finally, the styrene-maleic acid (SMA) copolymer is introduced and discussed, an amphipathic macromolecule that was recently found to solubilize and stabilize membrane proteins. The SMA copolymer is the central topic of study in this thesis as will be outlined at the end of the introduction.

1.2 Photosynthetic membranes

Photosynthesis is the process by which plants, algae, and some types of bacteria convert the energy of sunlight into biochemical energy. Most of the processes in photosynthesis are carried out in a lipid membrane in which all the involved pigment-protein complexes reside. Photosynthesis is initiated by the absorption of a photon with certain energy by pigments that are located in pigment-protein complexes. The absorption of a photon creates excited state energy which is most of the time funneled in a down-hill direction over multiple pigments toward a reaction center (RC) where charge separation takes place. In general, an electron is transported from the luminal side of the membrane to the opposite stromal side, while a proton is transferred in the opposite direction. This results in a transmembrane pH gradient that drives a protein complex called ATP-synthase to generate ATP which is used in downstream reactions for the production of carbohydrates. In plants, water is often used as an electron donor in photosynthesis and oxidized into oxygen. This allows the production of carbohydrates to be summarized in the well-known chemical equation: $6\ CO_2 + 6\ H_2O \rightarrow C_6H_{12}O_6 + 6\ O_2$, where glucose and oxygen are produced from carbon dioxide and water. All oxygen and carbon consuming organisms are reliant on this reaction, and as such, photosynthesis is essential for sustaining all life on earth.

Membrane architecture in plants. In plants, the photosynthetic apparatus is found in thylakoid membranes. The thylakoid membrane consists of membrane stacks called grana and flat lipid bilayers called stromal lamellae which are connected by margins (figure 4). Each part of the thylakoid membrane has its own specific composition of lipids and pigment-protein complexes including photosystems and light harvesting complexes [23].

Photosystem I is mostly located in the stromal lamellae, whereas photosystem II is mostly located in the stacked grana. Both photosystems are RCs that are attached to different type of light harvesting complexes (LHCs) termed LHCI and LHCII. The function of the LHCs is to increase the absorption cross-section of sunlight, analogously to a satellite dish for antennas. The LHCs then transport the light energy as excitation energy to the RC where the excitation energy is stabilized and used to drive processes like proton pumping.

The lipid composition of thylakoid membranes is highly conserved among

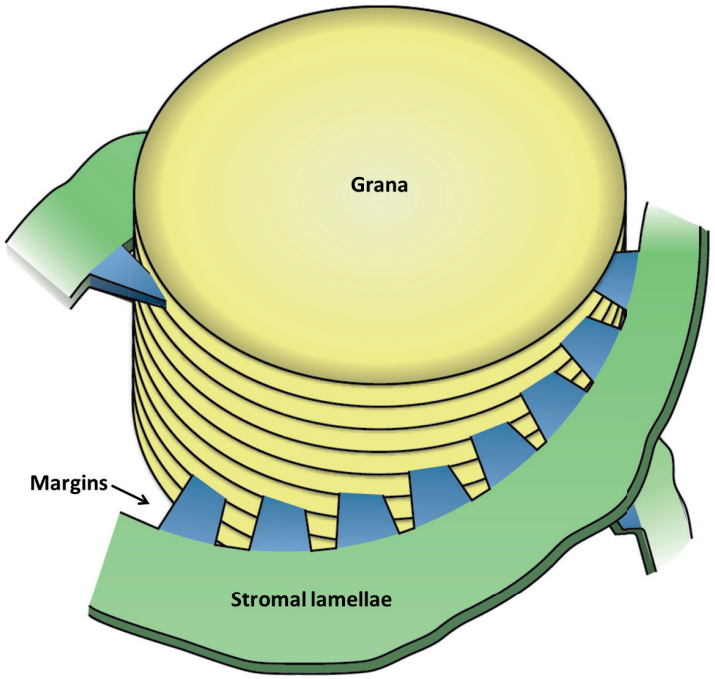

Figure 4
Model of the thylakoid membrane organization in plants based on cryo-EM data in ref [21] and ref [22]. Adapted from ref [23].

different photosynthetic organisms and is largely made up of the neutral glycolipids monogalactosyldiacylglycerol (MGDG), and digalactosyldiacylglycerol (DGDG), and the anionic sulfoquinovosyldiacylglycerol (SQDG) and glycerophospholipid phosphoglycerol (PG) (figure 5). While most biological membranes found in nature have phospholipids as their major building block, thylakoids have around 90% of glycolipids and only 5-10% of the phospholipid PG. The function of the different lipids is still the subject of many studies, but MGDG and DGDG are generally considered as bulk lipids, of which the conical shaped non-bilayer lipid MGDG is thought to be important for the highly curved parts of the thylakoid membrane, whereas the anionic PG and SQDG are thought to have specific interactions with various pigment-protein complexes [20].

For more details on the molecular structure of thylakoids, LHCs, RCs, lipids and the different steps of photosynthesis in plants, the reader is directed to different reviews and books on this topic [23-29].

Membrane architecture in bacteria. There are many classes of photosynthetic bacteria including purple bacteria, green sulfur bacteria, and heliobacteria. In this thesis, the purple bacterium *Rhodobacter (Rba.) sphaeroides* is the subject of study and in particular the RC and the LHC attached to it. In contrast to plants, the photosynthetic apparatus

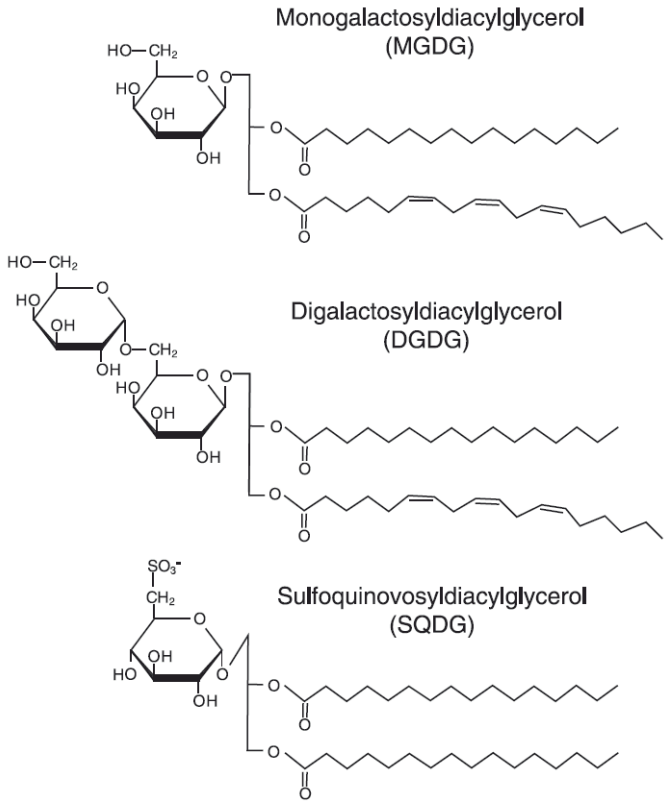

Figure 5
Structure of lipids that are largely found in thylakoid and other photosynthetic membranes, i.e., MGDG, DGDG, and SQDG. This figure shows the typical fatty acids bound to each class of lipid found in a variety of photosynthetic organisms. Adapted from ref [24].

of *Rba. sphaeroides* is not housed in thylakoid membranes but in intracytoplasmic vesicles named chromatophores as illustrated in figure 6. Three pigment-protein complexes therein are responsible for the capture and stabilization of light energy. The light harvesting complex 2 (LH2), which is typically arranged with others in a ring-like structure, absorbs light by its pigments and transfers the excitation energy from one to another until it reaches a LH1 protein complex. The LH1 surrounds the RC and brings the excitation energy into the RC for charge separation. Together the LH1 and RC form a so-called core complex as which it does exist in the native membrane.

Photosynthetic proteins. The LH2 protein complex is a circular nonamer (sometimes it is an octamer) consisting of nine pairs of so-called αβ-apoproteins of which each apoprotein has a single transmembrane α-helix [32]. The inner-ring is made up of nine α-apoproteins, while the outer-ring is made up of nine β-apoproteins. These proteins act mainly as a scaffold

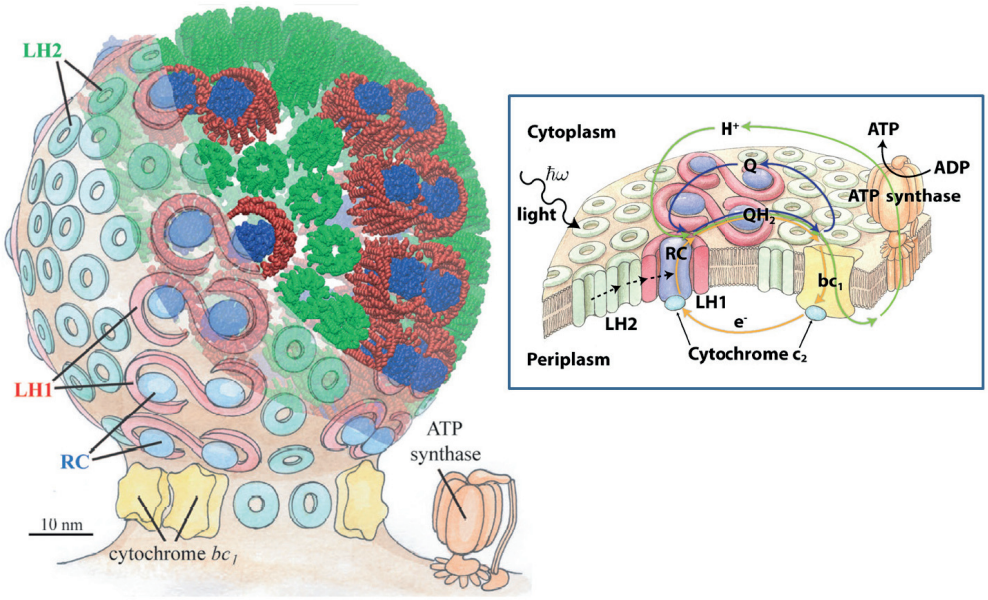

Figure 6
Architecture and constituents of a spherical chromatophore vesicle from *Rba. sphaeroides.* LH2 is shown in green and LH1 red, while the RC is shown in blue, the cytochrome bc_1 in yellow and ATP-synthase in orange. The inset shows the process of ATP generation which is driven by sunlight energy that is captured and converted by various protein complexes in and at the membrane. Details of this process are given in the text. Adapted from ref [30] and ref [31].

for the correct positioning of various pigments like bacteriochlorophylls (BChl) that capture light energy and transfer the excitation energy towards the RC-LH1 (core) complex.

The core complex consists of a RC that is surrounded by the LH1 protein complex. The LH1 receives excitation energy from the LH2s and funnels it into the RC where charge separation takes place. The LH1 is structurally similar to LH2 and is also composed of αβ-apoproteins that are organized in a ring-like structure that hold various pigments. However, the exact number of αβ-apoprotein pairs may differ between bacteria species with reported numbers of 15 and 16 [32]. The reason for this is that another protein called PufX can be a component of the LH1 ring which seems to be responsible for the dimerization of the core complex. In *Rba. sphaeroides*, when PufX is present the cores form dimers, but when deleted the cores exist as monomers [32, 33].

The RC consists of three polypeptides termed L-, M-, and H-polypetide which together hold ten cofactors (figure 7). While the L- and M-polypetides are integral membrane protein subunits, the H-polypetide has only a single transmembrane segment and a water soluble domain that caps the cytoplasmic face of the entire RC. The cofactors in the RC comprise four bacteriochlorophylls (BChl), two bacteriopheophytin (BPhe), one carotenoid, two ubiquinones, and an iron atom. Two

of the BChls form a dimer called the 'special pair' (P) which is positioned near the periplasmic side of the membrane. Charge separation is initiated in the special pair where excitation energy arrives from the pigments in the LHs and creates an excited state in the special pair (P*). This transforms the special pair into a strong reductant which is now able to donate an electron to a nearby BChl named B_a forming a $P^+B_a^-$ radical pair. The electron is passed to a BPhe pigment named H_a forming a $P^+H_a^-$ state. Then the electron is passed to a ubiquinone (Q_a) forming a $P^+Q_a^-$ radical pair, after which charge separation ends at ubiquinone Q_b where the $P^+Q_b^-$ radical pair is formed.

Whereas Q_a is fixed in the RC, Q_b is able to move freely and becomes reduced to QH_2 with the help of a second electron that is transferred from Q_a^- to Q_b^-. The QH_2 is a substrate for the integral membrane protein cytochrome bc_1 that facilitates the transfer of protons over the membrane by oxidizing QH_2 again, the protons being consumed by the ATP-synthase for the production of ATP. The special pair is reduced by gaining an electron from the water soluble cytochrome c_2 protein complex which completes the electron cycle in the RC. Interestingly, this process of excitation energy absorption and electron transfer happens only via the A-branch (inset in figure 7). Excellent reviews on the precise structure and function of the RC from *Rba. sphaeroides* can be found in refs [31, 32, 34, 35].

The BChl and BPhe pigments have distinct absorption spectra and thereby provide a sensitive probe for the functional integrity of the RC and provide a way to monitor the route and rate of electron transfer through the protein complex [35]. In addition, the protein concentration is conveniently followed in experiments by evaluating the absorption spectrum, something that is not possible for non-photosynthetic proteins.

Lipids. In contrast to the thylakoid membrane of plants, the photosynthetic membrane of *Rba. sphaeroides* contains mostly glycerophospholipids. The major lipid components are PE, PG, PC, CL, and SQDG. Three of them (PG, CL, SQDG) are negatively charged of which mainly CL has been identified to interact with the RC [36—38], but also with cytochrome bc_1 [39] and thus seems to be important for proper structure/function of the protein. In addition, seven PE lipids have been identified in the cytochrome bc_1 protein as well [40,41]. The exact role of the diverse lipids remains elusive but the increasing toolkit of lipid biosynthesic mutants and the high-throughput of membrane protein production ability of *Rba. sphaeroides* give scientists the opportunity to study the specific role of lipids in more detail and to reveal novel lipid-protein interactions [42].

1.3 Model membrane systems

Although a lipid membrane consists primarily of lipids and membrane proteins, the diversity of these components can lead to a very complex biological system. The investigation of a particular process in such a complex environment is at least challenging and perhaps even impossible. Many events are happening at the same time,

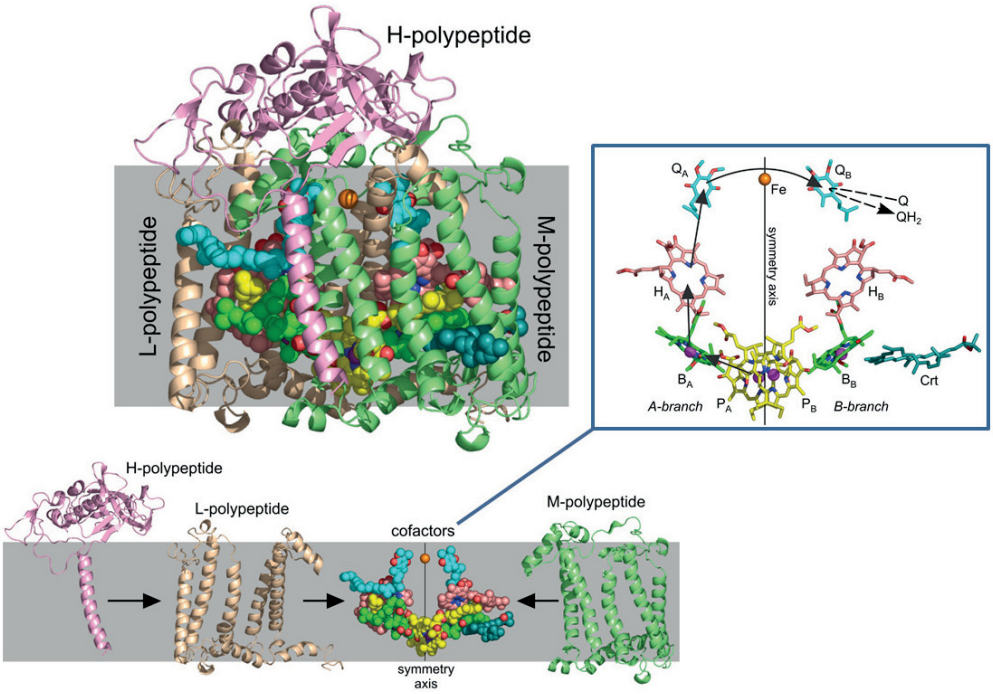

Figure 7
Overall structure of the RC from *Rba. sphaeroides* with the separate components shown below. The grey box represents the lipid membrane. The inset displays details on the cofactors and shows the direction of electron transfer trough the RC which happens only via the A-branch. Adapted from ref [35] with kind permission of the author.

which might influence each other. In order to study a particular process it is necessary to reduce the complexity of biological membranes by deleting some components, while retaining vital properties such as the bilayer architecture and lipid composition. By using model membranes, reduction of the complexity of the membrane can be achieved. The concept of model membranes can be considered as a trade-off: the more the complexity of a biological membrane is reduced, the less it represents a native biological membrane, but the more experimental accessible it becomes.

Many types of model membranes exist of which examples are vesicles, lipid monolayers, supported lipid bilayers, and in silico membranes (computational modeling). Below, the model membranes that have been used in this thesis along with some of their properties are briefly described.

Vesicles. Lipid membrane vesicles or liposomes (lipo= fat and soma = body in Greek) are spherical particles composed of curved lipid bilayers and have been very important for the understanding of biological membranes since their discovery by A.L. Bangham in the early sixties of the last century [43-45]. Vesicles can have different morphologies, lipid

compositions, sizes and they have the ability to enclose water soluble solutes and hold hydrophobic molecules. This makes them also interesting particles in the fields of drug delivery [46-48], food technology [49,50] and even in the field of cosmetics [51,52].

Different type of vesicles can be prepared by the spontaneous self-assembly of synthetic lipids (or lipid extracts from biological membranes) upon the addition of an aqueous solution to a lipid film. A vesicle is largely characterized by its diameter and number of lipid bilayers. The different type of vesicles are schematically shown in figure 8. After hydration of a lipid film, multi-lamellar vesicles (MLVs) and multi-vesicular vesicles (MVVs) are formed with sizes in the range of several micrometers. Extrusion of such vesicles through a polycarbonate filter with holes of a certain size yields large unilamellar vesicles (LUVs). These vesicles have a single lipid bilayer and a well-defined size in the range of 0.1-1 μm. Upon sonication of MLVs and MVVs small unilamellar vesicles (SUVs) can be prepared. The size of these vesicles can be as small as 25 nm. SUVs are used less frequently, because the small diameter results in packing difficulties of the lipids. The surface area of lipids in the outer layer is about twice that of the inner lipids, and about 70% of the lipids are in the outer layer. Under special conditions giant unilamellar vesicles (GUVs) can be made which can have a diameter up to 50 μm [53]. This type of vesicle is particularly useful in for instance light microscopy studies where the diffraction limit of light determines the resolution of the experiment.

In this thesis the large unilamellar vesicle (LUV) is the most used type of vesicle. The lipid composition was varied in order to vary its physical properties, in particular membrane fluidity, membrane surface charge, and the lateral pressure profile. Short descriptions of these physical properties are given below.

1.4 Physical properties of lipids and membranes

Lipid polymorphism. In aqueous solution, lipids self-assemble into a specific organization. The exact organization depends on the individual physical properties of lipids such as headgroup size, headgroup charge, acyl chain length and the acyl chain degree of unsaturation.

A molecular packing parameter P has been introduced to link the individual properties of a lipid to the type of aggregate it forms in solution (figure 9) [55]. This P value is defined as $P = v / l^{*}a$, in which v is the effective volume of the hydrophobic tail, l is the length of the hydrophobic tail, and a is the effective surface area of the polar headgroup. When $P < 1/3$, the lipids have an inverted cone-like shape and pack preferably in micellar structures. If P has a value between 1/3 and 1/2, the lipid forms a hexagonal phase which consists of tubes that have a hydrophilic surface and a hydrophobic interior. Between 1/2 and 1, the lipid is shaped is like a truncated-cone becoming more cylindrical approaching a P value of 1. Around a value of P=1, the cross-sectional area of the headgroup is similar to that of the tail and the lipid is cylindrically

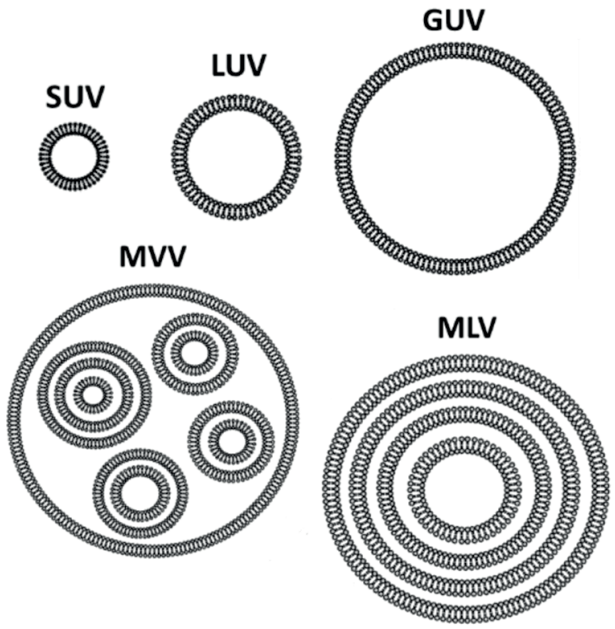

Figure 8
Overview of the different classes of vesicles which are characterized by their diameter and number of lipid bilayers. Adapted from ref [54].

shaped, which leads to the formation of lamellar bilayers. Finally, when $P>1$ the lipid is shaped like a cone and inverted micelles can be formed, but also lipid phases such as the cubic and inverted hexagonal phase can be formed.

The effective shape of the lipid is also determined by environmental factors such as pH, salt concentration, temperature, and hydration of the headgroups. Hence, these environmental factors also affect the type of aggregate formed by lipid molecules in solution [56].

As mentioned before, cell membrane are organized in lamellar bilayers. However, they sometimes contain a large fraction of lipids that have a P value larger than 1. These lipids are also called non-bilayer lipids and have an effect on the physical properties of membranes as discussed below. Phosphatidylethanolamine (PE) is a well-known non-bilayer lipid with $P>1$ and is abundant in biological membranes such as the inner membrane of *E. coli* bacteria [58].

Lateral pressure profile. Lipid membranes have an internal lateral pressure that results from the interfacial tension between the hydrophobic core and the polar membrane-water region of the membrane. The interfacial tension is minimized by squeezing the headgroups together creating a negative pressure at the interface. This is opposed by the repulsive ionic and entropic interactions between the headgroups, and the repulsive

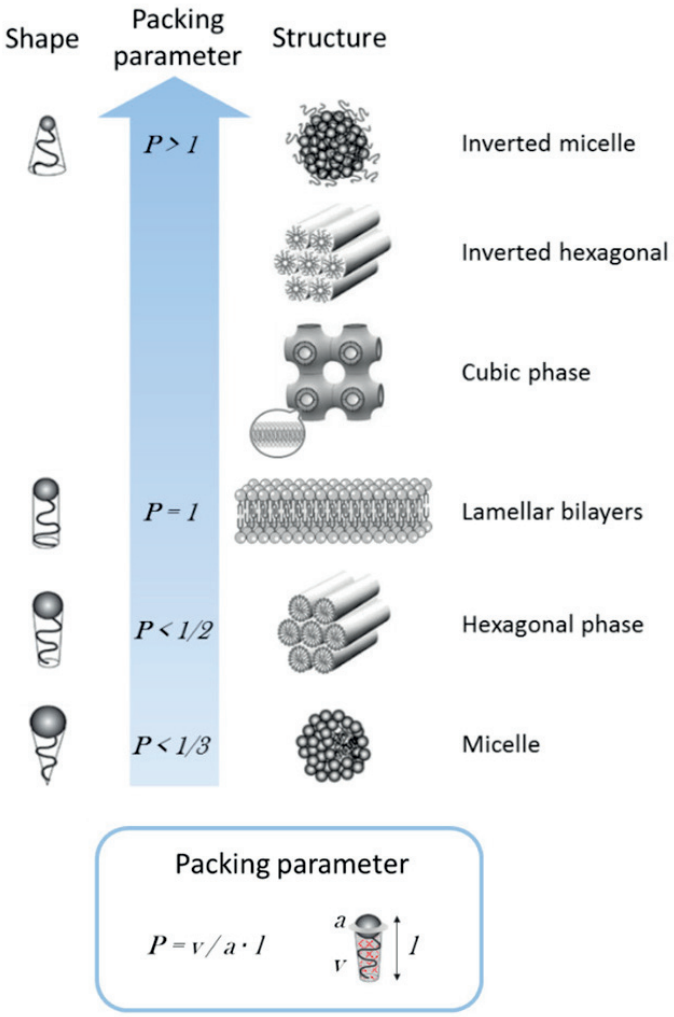

Figure 9
Overview of the different shapes that lipids can have, the associated packing parameter P, and type of aggregate/phase they form in aqueous solution. Biological membranes have a lamellar bilayer structure. Adapted from ref [57].

entropic interactions between the fatty acids in the hydrophobic core of the membrane. The inhomogeneous pressure distribution across the membrane is named the lateral pressure profile which is illustrated in figure 10. At equilibrium, the total lateral pressure across the membrane is zero (also called zero tension), but the total magnitude of the positive pressure in the core of the membrane (internal pressure) is estimated to be around 30 mN/m [59,60]. The lateral pressure profile is affected by the lipid composition and plays an important role in the adsorption of molecules and the structure and function of membrane protein [61,62]. The non-bilayer lipid PE, for instance, occupies a larger effective volume in the hydrophobic core increasing the acyl chain pressure, while the

small effective volume of the headgroups decreases the pressure at the interface. A protein in a membrane with considerable amount of PE lipids has to perform work against the internal pressure if it wants to change its conformation in the core of the membrane, but has more freedom of motion at the interfacial part of the membrane [62].

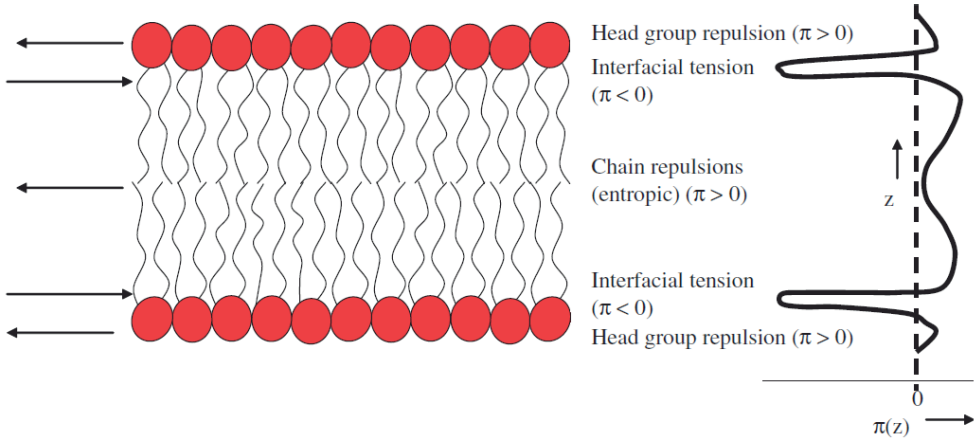

Figure 10
Schematic illustration and description of the lateral pressure profile across a lipid bilayer membrane. Adapted from ref [57].

Membrane surface charge. Most biological membranes possess as much as 10-20% of lipids that are negatively charged. Examples of abundant negatively charged glycerophospholipids lipids are PA, PS, PG and CL (figure 2). The anionic groups are localized at the membrane surface and they are neutralized by counterions. These counterions are mobile which results in the appearance of a diffuse double layer that generates a surface potential at the membrane that falls off with the distance from the membrane. The magnitude of the potential depends on the concentration of anionic lipids, ionic strength of the solution, and valence of the counterions, and is well described by the Gouy-Chapman-Stern theory [63—65]. The presence of a surface potential will modulate the binding of anionic hydrophobic molecules to a membrane and is therefore an important concept in, for example, drug delivery studies.

Membrane fluidity. The lipid membrane may be considered as a two-dimensional fluid in which lipids and proteins can diffuse freely in the lateral direction. The fluidity or viscosity of the membrane is an important property of the membrane which affects the rate of diffusion of its components. Membrane fluidity is largely determined by the packing of the lipid acyl chains and gives rise to the existence of different phases and phase transitions (figure 11). In the gel phase the acyl chains are highly ordered and the lipids are arranged in a regular structure, which leads to a low water permeability of

the membrane and low hydration level of the lipid headgroups. When the temperature increases, the thermal motion of the acyl chains increases leading to a disorder in lipid packing. At the melting temperature of the membrane (Tm) a cooperative transition from the gel phase to the liquid-crystalline phase occurs. In this lipid-phase, the acyl chains are much more disordered, the water permeability is higher and the lipids show a high degree of lateral motion. At the Tm, the gel phase and the liquid-crystalline phase co-exist which induces large surface defects in the membrane allowing solutes and ions to pass the membrane easily. The Tm of a lipid membrane is determined by van der Waals interactions between the fatty acids and depends mainly on the length and degree and positon of unsaturation. The introduction of an unsaturation gives a kink in the fatty acid decreasing the number of van der Waals contacts and thereby decreasing the Tm. When the fatty acids become longer the number of van der Waals contacts will increase and the Tm will increase as well.

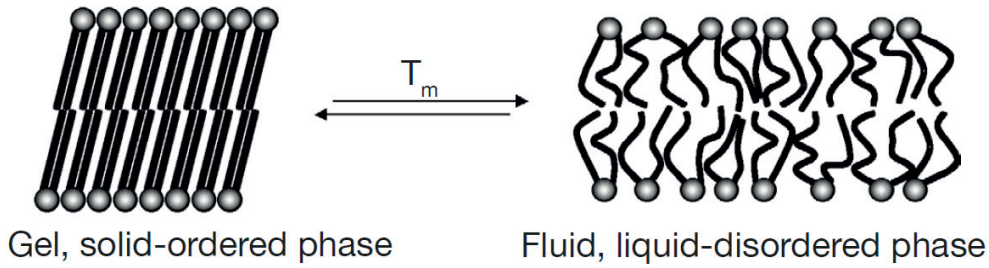

Figure 11
Schematic representation of the lipids in a bilayer membrane that is either in the gelphase or liquid-crystalline phase. The transition from one to another is characterized by the melting temperature Tm. Adapted from ref [66].

Lipid monolayers. A completely different kind of model membrane system is the lipid monolayer at an air-water interface. Lipids form a monomolecular oriented layer with the polar headgroups in contact with the aqueous solution and the hydrophobic chains extended in the air and can be thought of as a half of a lipid bilayer (figure 12). This water-insoluble layer is also called a Langmuir-Blodgett film and has the major advantage as model system that one can vary the lipid surface density and surface pressure allowing accurate control over the lipid surface area (A) and lateral pressure of the monolayer (π). This technique is often used to study lipid-lipid interactions and the insertion of membrane active molecules such as peptides and drugs [67,68]. This can be either done by compressing the lipid monolayer by a movable barrier to record pressure-area curves, or by monitoring the change in surface pressure at constant area upon the addition of surface active molecules to record pressure-time curves. In this thesis, the latter approach has been used.

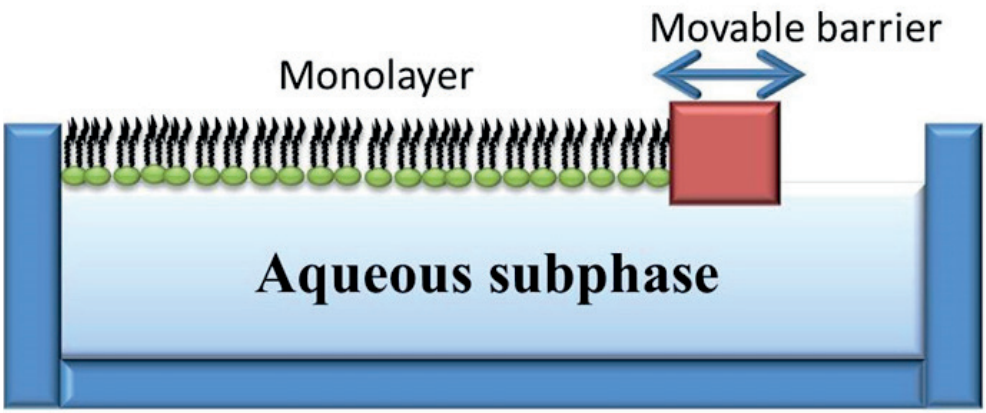

Figure 12
Schematic drawing of lipid monolayer at the air-water interface compressed at a certain surface pressure. Adapted from ref [69].

The surface pressure π is actually defined as the difference in surface tension between the pure air-water interface (y_0) and the surface with the lipid monolayer (y): $\pi = y_0 - y$. The magnitude of the surface pressure n of a lipid monolayer when the lipid area is similar to those of lipids in a bilayer membrane (A_0), is often estimated to be equal to the magnitude of the internal pressure in bilayer membranes [60,67]. In addition, electrostatic phenomena at the surface of a lipid monolayer are similarly described as those at a membrane surface and thus lipid monolayer experiments may be compared and related to experiments performed on lipid membrane vesicles [60,67].

1.5 Solubilization and purification of membrane proteins

For detailed structural and functional studies of membrane proteins, they need to be isolated from there complex membrane environment and purified while maintaining both their stability and activity. This has proven to be a far more demanding task than the isolation and purification of soluble proteins. Structures of membrane proteins are largely underrepresented in the protein database: to date only 556 unique structures of membrane proteins have been deposited [70], accounting for less than 2% of all structures. The difficulty for membrane proteins lies in the fact that this class of proteins is very hydrophobic and need to be stabilized in aqueous solution after removal from the lipid membrane. Ideally, the environment after isolation should stabilize the protein, allow for its purification, and enable the study of its structural and functional properties while the protein displays native behavior. Below, three approaches for the solubilization and stabilization of membrane proteins are briefly discussed. There are more options available and a comprehensive overview is given in ref [71].

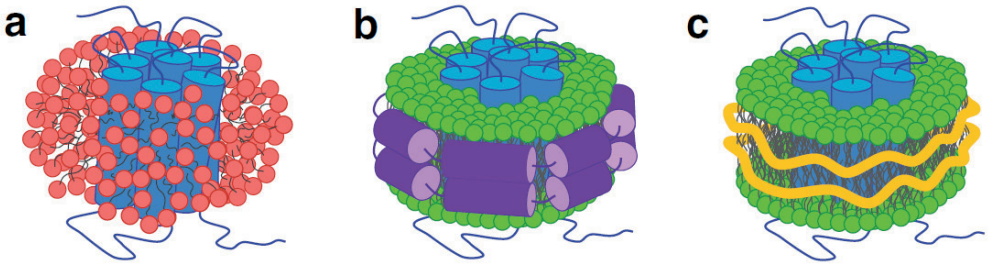

Figure 13
Membrane-mimetic systems for membrane protein stabilization after solubilization. The protein is indicated in blue and lipids in bilayers are indicated in green. (a) Protein in detergent (red) micelle. (b) Protein in nanodisc stabilized by MSP (purple). (c) Protein in nanodisc stabilized by SMA (yellow). Adapted from ref [71].

Detergents. The most used strategy for membrane protein isolation is the solubilization of the lipid bilayer matrix with detergents, which generally leads to the formation of spherical micelles, comprising membrane proteins, detergent molecules, and possibly some remaining lipids [72,73] (figure 13a). Although this approach without any doubt has contributed much to our understanding of membrane proteins, detergent solubilization has some inherent disadvantages. First, working with a membrane protein with unknown properties requires an extensive, mainly empirical screening to find a suitable detergent (mix) for each specific case [74,75]. Second, detergent addition strips the protein of its native lipid environment and thus generally leads to a loss of native interactions with both lipids and other proteins. Third, and probably most importantly, detergent micelles are a rather poor mimic of a lipid bilayer since they exhibit very different physicochemical properties [76,77]. Micelles have a single hydrophilic surface that is highly curved and their hydrophobic parts show a low degree of order. As a result, membrane proteins generally show a lower stability in micelles and transient solvent exposure of the hydrophobic membrane proteins surface can lead to inactivation or aggregation of the protein. Furthermore, the use of detergents may interfere with membrane protein function [78] or cause the protein to adopt a non-physiological conformation [79,80]. Because of these problems, much effort is being directed towards the development of new detergents with improved properties. In particular, fluorinated compounds [81] and maltose neopentyl glycol detergents [82] have proven to be powerful with respect to their ability to stabilize membrane proteins and hence may develop into more general tools in membrane research.

Nanodiscs bounded by membrane scaffold proteins. A relatively new approach to incorporate membrane proteins in a lipid bilayer environment was developed by Sligar and coworkers. They designed a method to transfer membrane proteins from detergent micelles into lipid nanodiscs, which are small patches of a lipid bilayer, bounded by

membrane scaffold proteins (MSPs) [83] (figure 13b). To achieve this, they engineered amphipathic helical proteins derived from human apolipoprotein A-1 that serve to shield the hydrophobic core of the lipids from the aqueous phase. Reconstitution of membrane proteins into these soluble particles seems to be generically applicable irrespective of the type of protein and they convey a relatively high protein stability (for reviews see [84,85]). The diameter of nanodiscs is typically in the order of ~10 nm, but generation of specific MSP variants allows the formation of smaller (~6–7 nm) [86,87] and larger (16–17 nm) [88] nanodiscs. Furthermore, the use of different apolipoproteins or derived peptides and the variation of the peptide/protein–lipid ratio enable the preparation of larger particles [89,90]. This control over size renders them excellent tools in many biophysical methods for structural and functional characterization of membrane proteins. The lipid composition in nanodiscs can be controlled by mixing in certain lipids along the formation of nanodiscs, enabling systematic studies [91]. Membrane proteins can even be incorporated into nanodiscs with exclusively native lipid material from detergent-solubilized membranes [92]. An additional advantage of nanodiscs is that, in contrast to other bilayer systems, membrane proteins can be trapped in a defined oligomeric state, allowing studies on how oligomerization influences protein function [93,94]. MSP nanodiscs thus are a particularly promising system for MP research and they are being used in a growing number of studies.

Nanodiscs bounded by styrene–maleic acid (SMA) copolymers. Much progress has been made with the introduction of MSP nanodiscs to stabilize membrane proteins. However, this system has still one disadvantage: it requires detergents to extract native membrane proteins from cellular membranes. Therefore, the problem of transient protein destabilization by detergent still persists. In order to attenuate this problem, alternative approaches are being developed, such as cell-free protein production [95,96], membrane protein-enriched cell-derived extracellular vesicles [97], genetic engineering of the membrane protein by fusion [98] or minimization of the exposure time with detergent [99]. However, arguably the most promising new method as an alternative to detergent extraction has become available by the recent discovery of the membrane-solubilizing effect of amphipathic styrene-maleic acid (SMA) copolymers [100-102]. SMA molecules exhibit a distinctly different mode of action than detergents: addition of the polymer to synthetic or biological lipid membranes leads to the spontaneous formation of discoidal particles with diameters of ~10 nm (figure 13c and figure 14). In this new type of polymer-bounded nanodiscs, the bilayer organization of the incorporated lipid molecules is conserved [103,104]. In different studies, these particles have been referred to as SMA–lipid particles (SMALPs) [100], Lipodisq particles [104], or native nanodiscs [105]. Depending on the origin of the lipid material, we here use the terms *SMALPs* for particles derived from synthetic liposomes and *native nanodiscs* for isolations from

biological membranes. The most striking feature of this novel system is the possibility to directly extract membrane proteins from cells without an intermediate step of conventional detergent solubilization [106]. Thus, the native nanodisc system combines a solubilizing power similar to detergents with the small particle size of nanodiscs, while conserving a minimally perturbed native lipid environment that stabilizes the protein.

The SMA approach is the central topic in this thesis. Therefore, the chemico-physical properties of the SMA copolymer will be discussed in the next section.

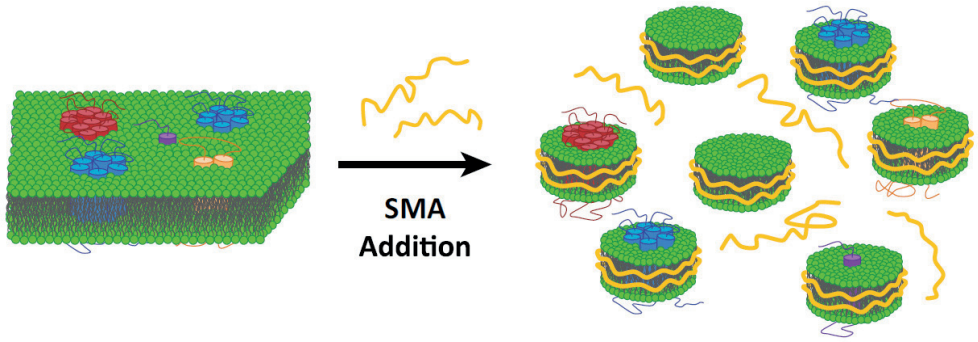

Figure 14
Extraction of membrane proteins from a lipid membrane with SMA. SMA addition leads to the formation of native nanodiscs containing different membrane proteins or only lipid material with the possible existence of a pool of free SMA copolymers in solution. Adapted from ref [71].

1.6 The styrene–maleic acid copolymer

Styrene–maleic acid (SMA) is the hydrolyzed form of the styrene–maleic anhydride (SMAnh) copolymer, which is synthesized by the copolymerization of styrene and maleic anhydride monomers (figure 15, Reaction 1). Both forms of the polymer are widely used in industry and they have many different applications. For instance, SMAnh is commonly used as thermal stabilizer in plastic blends, while SMA can be used as a dispersing agent for ink formulations and coatings. The SMA/SMAnh copolymers are produced by several suppliers worldwide. The major ones are TOTAL Cray Valley (Beaufort, TX, USA) and Polyscope (Geleen, NL), the latter using the brand name "Xiran" for their SMA/SMAnh copolymers. The products are typically sold in large quantities to companies that process the polymers for downstream products. SMA copolymers also have a long-standing history in life sciences, originally being described as conjugates for drugs in cancer therapy [107,108]. Later, it was found that SMA can interact with phospholipids to form discoidal structures that can incorporate hydrophobic molecules and therefore would be useful as a drug delivery system [101,109]. Based on this observation, new applications using SMA for the solubilization of lipid bilayers were developed and commercialized, as described in a patent by Malvern Cosmeceutics

(Worcester, UK) [102]. In particular, the application of SMA to solubilize membrane proteins, as first reported by the groups of Dafforn and Overduin [100], has led to a rapidly increasing interest in SMA as a novel tool in membrane research. Following these developments, SMA/SMAnh copolymers are now also commercially available in small quantities from Sigma Aldrich (St. Louis, MO, USA). Both SMA and SMAnh copolymers can be obtained in different commercial grades that vary in styrene–maleic anhydride/acid ratio and in average molecular weight. However, even within a single preparation of SMA/SMAnh copolymers there are large variations in molecular weight and in composition. The reason for this lies in the synthesis of SMAnh, as will be discussed next.

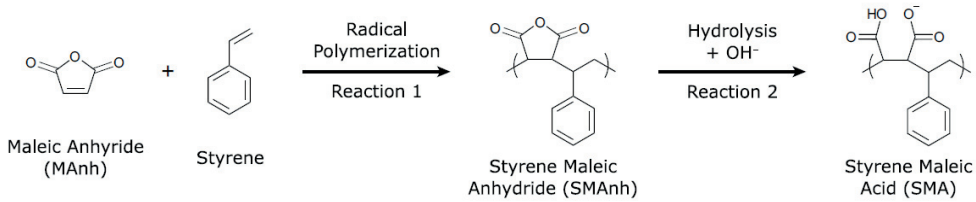

Figure 15
Schematic representation of the synthesis of styrene–maleic anhydride copolymers (Reaction 1) and the preparation of styrene–maleic acid copolymers (Reaction 2) as illustrated here for a 1:1 styrene-to-maleic anhydride/ acid molar ratio. When styrene is present in excess, the monomer sequence distribution in the polymer becomes more complex (see text for details). Adapted from ref [71].

Synthesis and composition of styrene–maleic anhydride copolymers. The polymerization of styrene and maleic anhydride (MAnh) monomers is a radical chain reaction that leads to the formation of SMAnh copolymers with a wide distribution in molecular weights. This distribution is characterized by the so-called polydispersity index (PDI), which for SMA is typically in the range of 2.0–2.5. The PDI is defined as the ratio of the weight-average molecular weight (M_w) and the number-average molecular weight (M_n) as:

$$\mathrm{PDI} \equiv \frac{M_w}{M_n}; \qquad M_w \equiv \frac{\sum M_i^2 n_i}{\sum M_i n_i}; \qquad M_n \equiv \frac{\sum M_i n_i}{\sum n_i}$$

where n_i is the number of polymer molecules of a molecular weight M_i. The concept of PDI can be illustrated by a simple calculation. Let us consider a distribution of three polymer molecules with molecular weights of 500, 1000, and 10,000 Da which are present in a molar mass ratio of (1:1:1). In this example, M_w is ~8800 Da, and M_n is ~3900 Da, resulting in a PDI of ~2.25. For a typical SMAnh polymer with a PDI of ~2.5 this means that the polymer chains have a broad size distribution with the smallest and largest chains differing by more than at least one order of magnitude in molecular

weight and thus chain length. The styrene–maleic anhydride/acid monomer ratio in the polymer can simply be varied by changing the feed monomer ratio used in the polymerization process. However, the resulting polymer generally does not consist of regular repeating building blocks of styrene and MAnh units with this feed ratio, nor does it exhibit a completely random distribution of the monomers along the chain. This is because of the differences in reactivity between chains with end radicals of styrene and MAnh. MAnh-terminated growing chains do not react with MAnh monomers, but they almost exclusively react with styrene monomers [110,111]. Therefore, the maximum content of MAnh units that can potentially be reached in SMAnh copolymers is 50 mol%. Only in this particular case a polymer with almost perfectly alternating building blocks can be obtained, by mixing styrene and MAnh monomers in a 1:1 molar ratio. This is not possible when styrene is present in excess, because styrene-terminated chains are capable of reacting with both styrene and MAnh monomers, the reaction with MAnh monomers being strongly favored [110,112]. If synthesis is performed in a batch-wise manner, this would result in polymers in which the overall ratio of styrene-to-maleic anhydride will be the same as the starting ratio, but in which the sequence distribution among the individual polymer chains may vary significantly: some chains will almost completely consist of alternating styrene and MAnh units, and others will have a high styrene content [113,114]. In order to minimize this heterogeneity, the polymerization of SMAnh is typically performed in a continuous manner in which the monomer ratio is controlled by the continuous feed of monomers and the simultaneous collection of polymer product to create a steady-state condition during polymerization [115]. In this way, the composition of the collected is proportional to the comonomer ratio in the reactor and SMAnh polymerizes in a statistical manner, yielding a much more homogenous distribution of monomer units among the individual polymer chains [115,116]. However, even under such steady-state conditions the synthesis of SMAnh leads to a rather inhomogeneous distribution of polymer chains differing in length and composition instead of well-defined molecules with a unique architecture and molecular weight. It is not clear yet whether or how this heterogeneity affects the membrane-solubilizing properties of SMA.

Hydrolysis of styrene–maleic anhydride to form styrene–maleic acid. The use of SMA in the solubilization of lipid membranes and formation of nanodiscs is not based on the anhydride form SMAnh, but on the hydrolyzed acid form SMA (figure 15, Reaction 2). When SMAnh is mixed with water or alkaline solution, its anhydride units will be converted to the acid form with two carboxyl groups that become partly deprotonated, yielding water-soluble SMA. Hydrolysis of SMAnh is relatively slow due to the hydrophobic character of the polymer, but it may be accelerated by (1) using the anhydride as powder instead of granulate, (2) elevating the temperature, and (3) adding

base (KOH or NaOH) during the reaction. After hydrolysis, the SMA solution can be processed or purified in different ways. If a minimal amount of base has been used, the required pH can usually be obtained just by addition of extra base or acid. When an excess of base has been used, one can bring the SMA solution into a desired buffering environment either by using dialysis [100] or by making use of their insolubility at low pH [117]. In the latter case, SMA can be precipitated by addition of excess hydrochloric acid (HCl). After several washing steps with diluted HCl, the polymer can then be dried by lyophilization causing the residual HCl to evaporate, yielding fully protonated SMA. This can be dissolved in water and the pH can be readily adjusted by the addition of KOH or NaOH.

pH–dependent properties of the styrene–maleic acid copolymer. SMA has amphipathic properties due to the hydrophobic styrene units and the hydrophilic carboxyl/carboxylate ([COOH]/[COO–]) groups. The degree of hydrophobicity depends not only on the ratio of styrene and maleic acid units in the polymer itself, but also strongly on pH. The two carboxyl groups in a maleic acid unit have different p*K*a values: the first p*K*a is close to 6, whereas the second one is close to 10 [118]. This implies that at low pH, SMA essentially is non-charged, at neutral pH most of the maleic acid units will carry a single negative charge, and at high pH the maleic acid units will be charged at both carboxyl groups. This pH dependence has major consequences for the conformation and solubility of SMA, as has been described for several other amphipathic polymers [109,119]. In the case of SMA, at neutral and high pH, electrostatic repulsions between the carboxylate groups dominate the hydrophobic effect and the polymer adopts a random coil conformation that dissolves relatively easily in aqueous solution. A decrease of the pH well below the lower p*K*a of the maleic acid unit will lead to complete protonation of SMA. Charge repulsion is then lost and the hydrophobic effect causes SMA to adopt a globular conformation and eventually to precipitate as aggregates [109,120,121]. The exact pH range that mediates this structural transition will depend on the composition of the polymer and also on the ionic strength in the solution.

SMA variants in membrane research. In all available studies on SMA and lipid membranes, the copolymers used had a ratio of styrene-to-maleic acid of 2:1 or 3:1, with an *M*w in the range of 7.5–10 kDa. For membrane solubilization, the polymers are commonly used at a pH between 7.0 and 8.0, at which values the balance between the hydrophobic effect and electrostatic interactions will be optimal for interactions with lipid membranes. For particular applications, SMAnh copolymers can also be covalently modified at the highly reactive anhydride moiety. In addition to hydrolysis to form SMA, this enables the introduction of different functional groups, via covalent binding

in the form of esters, amides, or imides (see e.g., [119]). In this way, a large variety of SMAnh based copolymers can be realized, each with its own properties and potential applications in membrane research.

1.7 Scope and outline of this thesis

The introduction provided a description of the most important topics that are required to understand this thesis. More detailed information on the theoretical background and used experimental techniques is described in the different chapters and can be found in references within.

This thesis can predominantly be divided in two parts. The first part (Chapter 2 & 3) describes the study on the mode of action of SMA copolymers as solubilizing agent on model membrane systems, while the second part (Chapter 4 & 5) mainly describes the study of the application of SMA: the solubilization, purification and photophysical characterization of membrane proteins involved in bacterial photosynthesis, with a leading role for the reaction center (RC) from the purple bacterium *Rhodobacter (Rba.) sphaeroides*.

The outline of this thesis is as follows:

Chapter 2 discusses the mode of action of the SMA copolymer and its efficiency of membrane solubilization on model membranes of various lipid compositions. The efficiency of solubilization of SMA is compared to that of the widely used membrane scaffold protein MSP1D1. Furthermore, the solubilization of membranes by SMA is investigated by different biophysical techniques including electron microscopy (EM), dynamic light scattering (DLS), and size exclusion chromatography (SEC). From the results, a three-stage model is proposed that summarizes the main steps in the solubilization of lipid membranes by the SMA copolymer.

In ***Chapter 3*** the influence of SMA composition, i.e. different styrene-to-maleic acid ratios in the polymer, and effect of pH on membrane solubilization is investigated and an optimal polymer composition and pH range are discussed. In addition, the molecular conformation in solution and the monomer sequence are studied by fluorescence and theoretical approaches, respectively, which turn out to be two key properties for efficient membrane solubilization.

In ***Chapter 4*** the SMA copolymer is used for the solubilization and purification of the RC from *Rba. sphaeroides*. This well-studied protein is used as a model to investigate the stability and photophysical properties of the protein in nanodiscs stabilized by SMA. A comparison with RCs in the native membrane and purified in detergent is made to see whether RCs in SMA nanodiscs are stable and show native-like behavior.

In ***Chapter 5*** oligomers of the RC are used to investigate the effect of protein size on solubilization by SMA. In addition, solubilization of the core complex (RC surrounded by the light harvesting complex I) from *Rba. sphaeroides* is described. This protein complex is tightly packed in the membrane, which might inhibit efficient membrane solubilization by SMA.

Finally, in ***Chapter 6*** a summarizing discussion is given on the main results of this thesis and possible applications of the SMA technique are discussed.

References

[1] Anatomy & Physiology, OpenStax, Download for free at http://cnx.org/content/col11496/latest/.

[2] van Meer, G., D.R. Voelker, and G.W. Feigenson. Membrane lipids: where they are and how they behave. Nat Rev Mol Cell Biol (2008), 9(2): p.112-24.

[3] Knaevelsrud, H. and A. Simonse., Lipids in autophagy: constituents, signaling molecules and cargo with relevance to disease. Biochim Biophys Acta (2012), 1821(8): p. 1133-45.

[4] Santos, A.X. and H. Riezman, Yeast as a model system for studying lipid homeostasis and function. FEBS Lett (2012), 586(18): p. 2858-67.

[5] Pohnert, G. Phospholipase A2 activity triggers the wound-activated chemical defense in the diatom Thalassiosira rotula. Plant Physiol (2002), 129(1): p. 103-11.

[6] Williamson, S.I., et al. LPS regulation of the immune response: separate mechanisms for murine B cell activation by lipid A (direct) and polysaccharide (macrophage-dependent) derived from Bacteroides LPS. J Immunol (1984), 133(5): p. 2294-300.

[7] Massimo, C., and Degli Esposti, M. Apoptosis-induced changes in mitocondrial lipids. BBA Mol. Cell Res (2011), 1813 (4): 551-557

[8] Aktas M, Danne L, Möller P, Narberhaus F. Membrane lipids in *Agrobacterium tumefaciens*: biosynthetic pathways and importance for pathogenesis.*Frontiers in Plant Science*. (2014), 5:109. doi:10.3389/fpls.2014.00109.

[9] Wallin E, von Heijne G Genome-wide analysis of integral membrane proteins from eubacterial, archaean, and eukaryotic organisms. *Protein Sci.* (1998) 7:1029–103

[10] Von Heijne, G., The membrane protein universe: what's out there and why bother? J Int Medi, 2007. 261: p. 543-57.

[11] Arioz, C. Exploring the interplay of lipids and membrane proteins, Doctoral Thesis, Stockholmi University, 2014.

[12] Dowhan, W., and Bogdanov, M. Chapter 1, Functional roles of lipids in membranes. Biochemistry of lipids, lipoproteins, and membrane (4th ed.), Vance, E.E>, and Vance, J.E. (Eds.) (2002), Elsevier Science B.V.

[13] Specificity of Intramembrane Protein–Lipid Interactions Francesc-Xabier Contreras, Andreas Max Ernst, Felix Wieland and Britta Brügger, *Cold Spring Harbor Perspectives in Biology* (2011), DOI:10.1101/cshperspect.a004705

[14] Powl, A.M., J.M. East, and A.G. Lee, Different effects of lipid chain length on the two sides of a membrane and the lipid annulus of MscL. Biophys J, (2007). 93(1): p. 113-22.

[15] Valiyaveetil FI, Zhou Y, MacKinnon R, Lipids in the structure, folding, and function of the KcsA K+ channel. Biochemistry (2002) , 41(35):10771–10777.

[16] Van Dalen A, Hegger S, Killian JA, de Kruijff B, Influence of lipids on membrane assembly and stability of the potassium channel KcsA. FEBS Lett (2002) , 525(1-3):33–38

[17] Marius, P., et al., The interfacial lipid binding site on the potassium channel KcsA is specific for anionic phospholipids. Biophys J, (2005), 89(6): p. 4081-9.

[18] Raja M, Spelbrink REJ, de Kruijff B, Killian JA, Phosphatidic acid plays a special role in stabilizing and folding of the tetrameric potassium channel KcsA. FEBS Lett (2007), 581(29):5715–5722.

[19] Triano I, et al. Occupancy of nonannular lipid binding sites on KcsA greatly increases the stability of the

tetrameric protein. Biochemistry (2010) , 49(25):5397–5404.

[20] Dörr JM et al Detergent-free isolation, characterization, and functional reconstitution of a tetrameric K+ channel: the power of native nanodiscs. Proc Natl Acad Sci USA (2014), 111:18607–18612

[21] Daum, B., Nicastro, D., Austin, J., McIntosh, J. R. & Kühlbrandt, W. Arrangement of photosystem II and ATP synthase in chloroplast membranes of spinach and pea. Plant Cell 22 (2010), 1299–1312.

[22] Austin, J. R. II & Staehelin, L. A. Three-dimensional architecture of grana and stroma thylakoids of higher plants as determined by electron tomography. Plant Physiol. (2011), 155, 1601–1611.

[23] Ruban, A.V. & Johnson, M.P., Visualizing the dynamic structure of the plant photosynthetic membrane, *Nature Plants* (2015), doi:10.1038/nplants.2015.161

[24] Mizusawa, N. & Wada, H., The role of lipids in photosystem II, Biochimica et Biophysica Acta (BBA) - Bioenergetics (2012), 1817, 1 , Pages 194–208

[25] J. Kern, A. Zouni, A. Guskov, N. Krauβ, Lipid in the structure of photosystem I, photosystem II and the cytochrome b6f complex, in: H. Wada, N. Murata (Eds.), Lipids in Photosynthesis: Essential nd Regulatory Functions, Springer, Dordrecht, 2009, pp. 203–242.

[26] Nakamura, Y. & Li-Beisson, Y. (Eds.), Lipids in Plant and Algae Development, Subcellular Biochemistry (2016), 86, Springer International Publishing

[27] Blankenship, R.E., Molecular mechanisms of Photosynthesis, 2nd Edition, John Wiley and Sons, 2014.

[28] Dekker J.P. & Boekema E.J., Supramolecular organization of thylakoid membrane proteins in green plants, Biochimica et Biophysica Acta (2005), 1706, 12-39.

[29] Mathias, P., Mathias, L., and Leister, D., Structure and dynamics of thylakoids in land plants, Journal of Experimental Botany (2014), Vol. 65, No. 8, pp. 1955–1972, 2014 doi:10.1093/jxb/eru090

[30] Sener, M.K., Olsen, J.D., Hunter, C.N., and Schulten, K., Atomic-level structural and functional model of a bacterial photosynthetic membrane vesicle, PNAS (2007) , vol. 104, no. 40: 15723–15728

[31] Strümpfer, J., Hsin, J., Şener, M., Chandler, D., and Schulten, K. , The Light-Harvesting Apparatus in Purple Photosynthetic Bacteria. Introduction to a Quantum Biological Device, Chapter 2, Molecular Machines, Edited by: Benoît Roux ,World Scientific.

[32] Cogdell, R.J., Gall, A., and Köhler, J., The architecture and function of the light-harvesting apparatus of purple bacteria :from single molecules to *in vivo* membranes, Quarterly Reviews of Biophysics 39, 3 (2006), pp. 227–324.

[33] Olsen JD, Adams PG, Jackson PJ, Dickman MJ, Qian P, Hunter CN. Aberrant Assembly Complexes of the Reaction Center Light-harvesting 1 PufX (RC-LH1-PufX) Core Complex of *Rhodobacter sphaeroides* Imaged by Atomic Force Microscopy. *The Journal of Biological Chemistry*. 2014;289(43):29927-29936. doi:10.1074/jbc.M114.596585.

[34] Law, C.J., Roszak, A.W., Southall, J., Gardiner, A.T., Isaacs, N.W., Cogdell, R.J., The structure and function of bacterial light-harvesting complexes (Review), Molecular Membrane Biology (2004), Vol. 21, Iss. 3.

[35] Jones, M.R., The petite purple photosynthetic powerpack, Biochemical Society Transactions (2009), 37 (2), 400-407, DOI: 10.1042/BST0370400.

[36]. McAuley, K. E., Fyfe, P. K., Ridge, J. P., Isaacs, N. W., Cogdell, R. J., and Jones M. R., Structural details of an interaction between cardiolipin and an integral membrane protein , *Proc. Natl. Acad. Sci. U.S.A.* (1999) , *96*, 14706-14711.

[37] Camara-Artigas, A., Brune, D., and Allen J. P.,Interactions between lipids and bacterial reaction centers determined by protein crystallography, *Proc. Natl. Acad. Sci. U.S.A.* (2002) , *99*, 11055-11060.

[38] Fyfe, P. K., Isaacs, N. W., Codgell, R. J., and Jones, M. R., Disruption of a specific molecular interaction with a bound lipid affects the thermal stability of the purple bacterial reaction centre, *Biochim. Biophys. Acta* (2004) , *1608*, 11-22.

[39] Zhang X, Tamot B, Hiser C, Reid GE, Benning C, Ferguson-Miller S. Cardiolipin-Deficiency in *Rhodobacter sphaeroides* Alters the Lipid Profile of Membranes and of Crystallized Cytochrome Oxidase, but Structure and Function are Maintained. *Biochemistry*. 2011;50(19):3879-3890. doi:10.1021/bi101702c.

[40] Svensson-Ek, M., et al., *The X-ray crystal structures of wild-type and EQ(I-286) mutant cytochrome c oxidases from* Rhodobacter sphaeroides. J Mol Biol (2002), 321(2): p. 329-39.

[41] Zhang, X., et al., *Combined genetic and metabolic manipulation of lipids in* Rhodobacter sphaeroides *reveals non-phospholipid substitutions in fully active cytochrome c oxidase.* Biochemistry (2011), 50(19): p. 3891-902.

[42] Laible PD, Scott HN, Henry L, Hanson DK. Towards higher-throughput membrane protein production for structural genomics initiatives, J Struct Funct Genomics. (2004), 5(1-2):167-72.

[43] Bangham, A.D. & Horne, R.W., Negative staining of phospholipids and their structural modification by surface-active agents as observed in the electron microscope. J. Mol. Biol. (1964), (8):660-668

[44] Bangham, A.D., Standish, M.M., and Watkins, J.C. Diffusion of univalent ions across lamellae of swollen phospholipids. J. Mol. Biol. (1965), (13):238-252

[45] Weissman.G, Sessa, G., Standish, M., Bangham, A. D. A direct effect of steroids on permeability of lipid membranes (liposomes). J. Clin. Invest. (1965), 44 (6), 1109-&.

[46] Allen, T.M. & Cullis, P.R. Liposomal drug delivery systems: From concept to clinical applications Advanced Drug Delivery Reviews (2013), 65 (1):36-48

[47] Pattni, B.S., Chupin, V.V., and Torchilin, V.P. New developments in liposomal drug delivery. *Chem. Rev. (2015), 115 (19):10938–10966*

[48] Zylberberg, C. & Matosevic, S. Pharmaceutical liposomal drug delivery: a review of new delivery systems and a look at the regulatory landscape, Drug Delivery (2016), DOI: 10.1080/10717544.2016.1177136

[49] Keller, B. C. Liposomes in nutrition. Trends in Food Science & Technology (2001), 12 (1): 25-31.

[50] Khanniri, E., Bagheripoor-Fallah, N., Sohrabvandi, S., Mortazavian, A.M., Khosravi-Darani, K., & Mohammad, R. Application of Liposomes in Some Dairy Products, Critical Reviews in Food Science and Nutrition (2016), 56 (3), 484-493, DOI: 10.1080/10408398.2013.779571

[51] Müller, R. H., Petersen, R. D., Hommoss, A., Pardeike, J. Nanostructured lipid carriers (NLC) in cosmetic dermal products. Advanced Drug Delivery Reviews 2007, 59 (6), 522-530.

[52] Hougeir, F.G. & Kircik, L. A review of delivery systems in cosmetics Dermatologic Therapy (2012), Vol. 25: 234–237

[53] Karamdad K., Law, R.V., Seddon, J.M., Brooks, N.J., Ces, O. Preparation and mechanical characterisation of giant unilamellar vesicles by a microfluidic method. Lab Chip. (2015),15 (2):557-62. DOI: 10.1039/c4lc01277a.

[54] Gael Clergeaud Veiga, Liposomes as versatile tools: nanoreactors, membrane models and drug delivery carriers, Doctoral Thesis, Rovira i Virgili University, 2014.

[55] Israelachvili, J. N.; Mitchell, D. J.; Ninham, B. W. Theory of self-assembly of hydrocarbon amphiphiles into

micelles and bilayers. *Journal of the Chemical Society, Faraday Transactions 2: Molecular and Chemical Physics (*1976), *72* (0), 1525-1568.

[56] Mouritsen, P. O. G. Life — As a Matter of Fat; Springer-Verlag: Berlin/Heidelberg, 2005.

[57] Mouritsen, O.G., Lipids, curvature, and nano-medicine. Eur. J. Lipid Sci. Technol. (2011), 113: 1174–1187

[58] Gennis, R.B., Biomembranes: molecular structure and function, Springer-Verlag, New York, 1989.

[59] Marsh, D. Lateral pressure in membranes. Biochimica et Biophysica Acta (1996), 12 (86): 183–223.

[60] Demel, R. Monomolecular layers in the study of biomembranes. Chapter 3, Physicochemical methods in the study of biomembranes. Hilderson, H. J., Ralston, G.B. (Eds.), Subcellular Biochemistry Volume 23 1994, Springer US

[61] Van den Brink-van der Laan, E. , Chupin, V. , Killian, J.A. , and De Kruijff, B. Stability of KcsA Tetramer Depends on Membrane Lateral Pressure *Biochemistry* (2004), *43* (14): 4240–4250

[62] Van den Brink-van der Laan, E., Killian, J.A. , and De Kruijff, B. Nonbilayer lipids affect peripheral and integral membrane proteins via changes in the lateral pressure profile. Biochimica et Biophysica Acta (BBA) - Biomembranes (2004), 1666 (1-2): 275-288

[63] McLaughlin, S. 1989. The electrostatic properties of membranes. Annu. Rev. Biophys. Biophys. Chem. 18:113–136.

[64] Voelker, D. and Smejtek, P. Adsorption of Ruthenium Red to Phospholipid Membranes. Biophysical Journal (1996), 70:818-830.

[65] Murray, Diana et al. Electrostatic Properties of Membranes Containing Acidic Lipids and Adsorbed Basic Peptides: Theory and Experiment. Biophysical Journal (1999), 77 (6):3176-3188

[66] Eeman, M., Deleu, M. From biological membranes to biomimetic model membranes. Biotechnol. Agron. Soc. Environ. (2010) 14(4): 719-736

[67] MacDonald, R.C., & Simon, S.A. Lipid monolayer states and their relationships to bilayers. PNAS. (1987), 84(12): 4089–4093.

[68] Maget-Dana, R. The monolayer technique: a potent tool for studying the interfacial properties of antimicrobial and membrane-lytic peptides and their interactions with lipid membranes**.** Biochimica et Biophysica Acta (BBA) - Biomembranes (1999), 1462 (1-2):109-140

[69] Butt, H-J., Graf, K., Kappl, M., Physics and Chemistry of Interfaces (2003), Wiley/VCH, Berlin

[70] White, S.H. Membrane proteins of known structure (2015). http://blanco.biomol.uci.edu/mpstruc/. Accessed 12 Oct 2015

[71] Dörr JM, Scheidelaar S, Koorengevel MC, et al. The styrene–maleic acid copolymer: a versatile tool in membrane research. *European Biophysics Journal*. 2016;45:3-21. doi:10.1007/s00249-015-1093-y.

[72] Le Maire, M., Champeil, P., Møller, J.V. Interaction of membrane proteins and lipids with solubilizing detergents. Biochim Biophys Acta (2000), 1508:86–111

[73] Lichtenberg D, Ahyayauch H, Goñi FM The mechanism of detergent solubilization of lipid bilayers. Biophys J (2013), 105:289–299

[74] Arachea, B.T., Sun, Z., Potente, N., Malik, R., Isailovic, D., Viola, R.E. Detergent selection for enhanced extraction of membrane proteins. Protein Expression Purif (2012), 86:12–20

[75] Privé, G.G. Detergents for the stabilization and crystallization of membrane proteins. Methods (2007) , 41:388–397

[76] Bordag, N., Keller, S. α-Helical transmembrane peptides: a “divide and conquer” approach to membrane proteins. Chem Phys Lipids (2010) 163:1–26

[77] Zhou, H-X., Cross, T.A. Influences of membrane mimetic environments on membrane protein structures. Ann Rev Biophys (2013), 42:361–392

[78] Quick, M., Shi, L., Zehnpfennig, B., Weinstein, H., Javitch, J.A. Experimental conditions can obscure the second high-affinity site in LeuT. Nat Struct Mol Biol (2012), 19:207–211

[79] Zhou, H-X., Cross, T.A. Modeling the membrane environment has implications for membrane protein structure and function: influenza A M2 protein. Protein Sci (2013), 22:381–394

[80] Zoonens, M., Comer, J., Masscheleyn, S., Pebay-Peyroula, E., Chipot, C., Miroux, B., Dehez, F. Dangerous liaisons between detergents and membrane proteins. The case of mitochondrial uncoupling protein 2. J Am Chem Soc (2013), 135:15174–15182

[81] Frotscher, E., Danielczak, B., Vargas, C., Meister, A., Durand, G., Keller, S. A fluorinated detergent for membrane-protein applications. Angew Chem Int Ed (2015), 54:5069–5073

[82] Chae, P.S. et al Maltose–neopentyl glycol (MNG) amphiphiles for solubilization, stabilization and crystallization of membrane proteins. Nat Methods (2010) , 7:1003–1008

[83] Bayburt ,T.H., Grinkova, Y.V., Sligar, S.G. Self-assembly of discoidal phospholipid bilayer nanoparticles with membrane scaffold proteins. Nano Lett (2002) , 2:853–856

[84] Bayburt, T.H., Sligar, S.G. Membrane protein assembly into nanodiscs. FEBS Lett (2010) 584:1721–1727

[85] Schuler, M.A., Denisov, I.G., Sligar, S.G. Nanodiscs as a new tool to examine lipid–protein interactions . Methods Mol Biol (2012) , 974:415–433

[86] Hagn, F., Etzkorn, M., Raschle, T., Wagner, G. Optimized phospholipid bilayer nanodiscs facilitate high-resolution structure determination of membrane proteins. J Am Chem Soc (2013), 135:1919–1925

[87] Wang, X., Mu, Z., Li, Y., Bi, Y., Wang, Y. Smaller nanodiscs are suitable for studying protein lipid interactions by solution NMR. Protein J (2015), 34(3):205–211

[88] Grinkova, Y.V., Denisov, I.G., Sligar, S.G. Engineering extended membrane scaffold proteins for self-assembly of soluble nanoscale lipid bilayers. Protein Eng Des Sel (2010), 23:843–848

[89] Chromy, B.A. et al (2007) Different apolipoproteins impact nanolipoprotein particle formation. J Am Chem Soc 129(46):14348 14354

[90] Park, S.H., Berkamp, S., Cook, G.A., Chan, M.K., Viadiu, H., Opella, S.J. Nanodiscs versus macrodiscs for NMR of membrane proteins. Biochemistry (2011), 50:8983–8985

[91] Bayburt, T.H. et al (2010) Monomeric rhodopsin is sufficient for normal rhodopsin kinase (GRK1) phosphorylation and arrestin-1 binding. J Biol Chem (2010), 286:1420–1428

[92] Civjan, N.R., Bayburt, T.H., Schuler, M.A., Sligar, S.G. Direct solubilization of heterologously expressed membrane proteins by incorporation into nanoscale lipid bilayers. Biotechniques (2003), 35:556–563

[93] Boldog, T., Grimme, S., Li, M., Sligar, S.G., Hazelbauer, G.L. Nanodiscs separate chemoreceptor oligomeric states and reveal their signaling properties. Proc Natl Acad Sci USA (2006), 103:11509–11514

[94] Shi, L. et al. SNARE proteins: one to fuse and three to keep the nascent fusion pore open. Science (2012), 335:1355–1359

[95] Roos, C. et al. Characterization of co-translationally formed nanodisc complexes with small multidrug transporters, proteorhodopsin and with the *E. coli* MraY translocase. Biochim Biophys Acta (2012) ,

1818:3098–3106

[96] He, W. et al. Cell-free expression of functional receptor tyrosine kinases. Sci Rep (2015), 5:12896

[97] Zeev-Ben-Mordehai, T., Vasishtan, D., Siebert, C.A., Whittle, C., Grünewald, K. Extracellular vesicles: a platform for the structure determination of membrane proteins by cryo-EM. Structure (2014) , 22(11):1687–1692

[98] Mizrachi, D. et al Making water-soluble integral membrane proteins in vivo using an amphipathic protein fusion strategy. Nat Commun (2015) , 6:6826

[99] Shirzad-Wasei, N., van Oostrum, J., Bovee-Geurts, P.H.M., Kusters, L.J.A., Bosman, G.J.C.G.M., DeGrip, W.J. Rapid transfer of overexpressed integral membrane protein from the host membrane into soluble lipid nanodiscs without previous purification. Biol Chem (2015) , 396:903–915

[100] Knowles, T.J., Finka, R., Smith, C., Lin, Y-P., Dafforn, T., Overduin, M. Membrane proteins solubilized intact in lipid containing nanoparticles bounded by styrene maleic acid copolymer. J Am Chem Soc (2009) , 131:7484–7485

[101] Tighe, B.J., Tonge, S.R. Lipid-containing compositions and uses thereof. UK patent number WO/1999/009955 (2000)

[102] Tonge, S.R. Compositions comprising a lipid and copolymer of styrene maleic acid. UK Patent Number WO/2006/129127 (2006)

[103] Jamshad, M. et al. Structural analysis of a nanoparticle containing a lipid bilayer used for detergent-free extraction of membrane proteins. Nano Research (2015), 8:774–789

[104] Orwick, M.C. et al. Detergent-free formation and physicochemical characterization of nanosized lipid–polymer complexes: lipodisq. Angew Chem Int Ed Engl (2012), 51:4653–4657

[105] Dörr, J.M. et al. Detergent-free isolation, characterization, and functional reconstitution of a tetrameric K+ channel: the power of native nanodiscs. Proc Natl Acad Sci USA (2014), 111:18607–18612

[106] Long, A.R., O'Brien, C.C., Malhotra, K., Schwall, C.T., Albert, A.D., Watts, A., Alder, N.N. A detergent-free strategy for the reconstitution of active enzyme complexes from native biological membranes into nanoscale discs. BMC Biotechnol (2013) , 13:41

[107] Maeda, H., Takeshita, J., Kanamaru, R. A lipophilic derivative of neocarzinostatin. A polymer conjugation of an antitumor protein antibiotic. Int J Pept Protein Res (1979) , 14:81–87

[108] Maeda, H. SMANCS and polymer-conjugated macromolecular drugs: advantages in cancer chemotherapy. Adv Drug Del Rev (2001), 46:169–185

[109] Tonge, S.R., Tighe, B.J. Responsive hydrophobically associating polymers: a review of structure and properties. Adv Drug Del Rev (2001), 53:109–122

[110] Alfrey, T., Lavin, E. The copolymerization of styrene and maleic anhydride. J Am Chem Soc (1945), 67:2044–2045

[111] Hill, D.J.T., O'Donnell, J.H., O'Sullivan, P.W. Analysis of the mechanism of copolymerization of styrene and maleic anhydride. Macromolecules (1985), 18:9–17

[112] Deb, P.C., Meyerhoff, G. Study on kinetics of copolymerization of styrene and maleic anhydride in dioxane. Eur Polym J (1984), 20:713–719

[113] Klumperman, B. Mechanistic considerations on styrene–maleic anhydride copolymerization reactions. Polym Chem (2010), 1:558–562

[114] Montaudo, M.S. Determination of the compositional distribution and compositional drift in styrene/maleic anhydride copolymers. Macromolecules (2001), 34:2792–2797

[115] Yao, Z., Li, B-G., Wang, W-J., Pan, Z-R. Continuous thermal bulk copolymerization of styrene and maleic anhydride. J Appl Polym Sci (1999), 73:615–622

[116] Fried, J.R. Polymer science and technology, 2nd edn. Prentice Hall, Upper Saddle River (2003)

[117] Scheidelaar, S., Koorengevel, M.C., Dominguez Pardo, J., Meeldijk, J.D., Breukink, E., Killian, J.A. Molecular model for the solubilization of membranes into nanodisks by styrene–maleic acid copolymers. Biophys J(2015), 108:279–290

[118] Banerjee, S., Pal, T.K., Guha, S.K. Probing molecular interactions of poly(styrene-co-maleic acid) with lipid matrix models to interpret the therapeutic potential of the co-polymer. BBABiomembranes (2012), 1818:537–550

[119] Henry, S.M., El-Sayed, M.E.H., Pirie, C.M., Hoffman, A.S., Stayton, P.S. pH-responsive poly(styrene-alt-maleic anhydride) alkylamide copolymers for intracellular drug delivery. Biomacromolecules (2006), 7:2407–2414

[120] Sugai, S., Ebert, G. Conformations of hydrophobic polyelectrolytes. Adv Colloid Interface Sci (1985), 24:247–282

[121] Sugai, S., Nitta, K., Ohno, N. Studies on conformational transition of the maleic acid copolymer with styrene in aqueous salt solution by derivative spectroscopy. Polymer(1982), 23:238–242

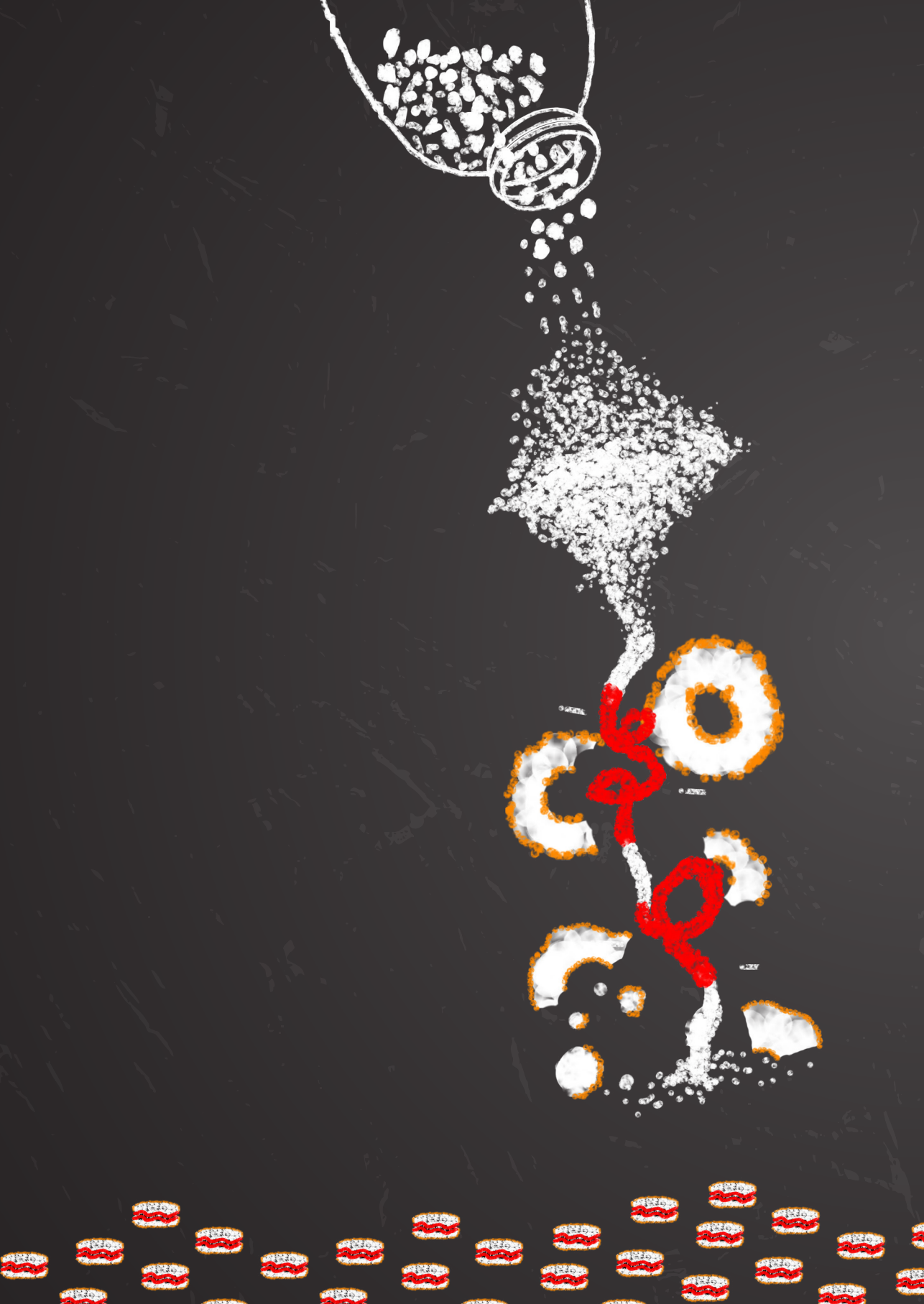

CHAPTER 2

MOLECULAR MODEL FOR THE SOLUBILIZATION OF MEMBRANES INTO NANODISKS BY STYRENE MALEIC ACID COPOLYMERS

STEFAN SCHEIDELAAR, MARTIJN C. KOORENGEVEL, JUAN DOMINGUEZ PARDO, JOHANNES D. MEELDIJK, EEFJAN BREUKINK, AND J. ANTOINETTE KILLIAN

S. SCHEIDELAAR, M.C. KOORENGEVEL, J.J. PARDO DOMINGUEZ, J.D. MEELDIJK, E. BREUKINK, AND J.A. KILLIAN, (2015), MOLECULAR MODEL FOR THE SOLUBILIZATION OF MEMBRANES INTO NANODISKS BY STYRENE MALEIC ACID COPOLYMERS. *BIOPHYS. J.* 108, 279-290.

KEYWORDS: STYRENE MALEIC ACID (SMA) COPOLYMER, MOLECULAR MECHANISM, LIPID BILAYERS, MODEL MEMBRANES

ABSTRACT

A recent discovery in membrane research is the ability of styrene-maleic acid (SMA) copolymers to solubilize membranes in the form of nanodisks allowing extraction and purification of membrane proteins from their native environment in a single detergent-free step. This has important implications for membrane research because it allows isolation as well as characterization of proteins and lipids in a near-native environment. Here, we aimed to unravel the molecular mode of action of SMA copolymers by performing systematic studies using model membranes of varying compositions and employing complementary biophysical approaches. We found that the SMA copolymer is a highly efficient membrane-solubilizing agent and that lipid bilayer properties such as fluidity, thickness, lateral pressure profile, and charge density all play distinct roles in the kinetics of solubilization. More specifically, relatively thin membranes, decreased lateral chain pressure, low charge density at the membrane surface, and increased salt concentration promote the speed and yield of vesicle solubilization. Experiments using a native membrane lipid extract showed that the SMA copolymer does not discriminate between different lipids and thus retains the native lipid composition in the solubilized particles. A model is proposed for the mode of action of SMA copolymers in which membrane solubilization is mainly driven by the hydrophobic effect and is further favored by physical properties of the polymer such as its relatively small cross-sectional area and rigid pendant groups. These results may be helpful for development of novel applications for this new type of solubilizing agent, and for optimization of the SMA technology for solubilization of the wide variety of cell membranes found in nature.

INTRODUCTION

A recent finding in membrane research is the ability of styrene maleic acid (SMA) copolymers to solubilize membranes into lipid nanodisks without the assistance of detergents (1–6). This has two implications: 1) it allows direct solubilization and purification of membrane proteins while maintaining their lipid environment (5,6), thereby avoiding cumbersome, detergent-based procedures (7) with concomitant risk of protein aggregation and/or denaturation; and 2) the embedding into nanodisks ensures a stable lipid environment for membrane proteins, yet with a small particle size that allows characterization by a wide range of biophysical approaches (1–6).

Other advantages of the use of nanodisks are that the embedded proteins are accessible to both sides of the membrane, facilitating functional studies (8), and that a defined oligomerization state of the proteins is maintained, which may be important for understanding mechanistic processes (9). A disadvantage of nanodisks, however, is that they do not allow the study of vectorial function such as solute transport or signal transduction, which requires a membrane that separates two distinct aqueous compartments.

Most of the studies on nanodisks described in literature so far involve nanodisks that

are stabilized by amphipathic membrane scaffolding proteins (MSPs), as developed by Bayburt and Sligar (10) and Denisov et al. (11). In these systems, many new applications of nanodisks for studies of membrane proteins have been developed (9,12–14). However, reconstitution of membrane proteins in MSP-bounded nanodisks typically requires several steps, including prior purification of the protein in detergent (10,11). The SMA technology thus combines the advantages of a straightforward protocol for detergent-free purification of membrane proteins with embedding of the proteins into nanodisks as a stable and native host in which they maintain their activity.

Despite this huge potential of SMA for membrane research, very little is known about the molecular mechanism of SMA-induced nanodisk formation. In this study, we investigate the physico-chemical properties of membranes that regulate the kinetics and efficiency of nanodisc formation by using model membrane systems. The main advantage of these model systems is that they allow systematic modulation of a wide range of physical and chemical properties of the membrane simply by variation of lipid composition. By using complementary biophysical techniques, we will show that the SMA copolymer is a very efficient membrane solubilizing agent and that lipid bilayer physico-chemical properties, such as lipid packing and electrostatic interactions, play an important role in determining the efficiency of the solubilization process. We present a model for the mode of action of SMA copolymers and compare this to the action of similar amphipathic polymers as well as MSPs. The fresh insights obtained in this study will be helpful to exploit the full potential of the SMA copolymer for research on membranes and membrane proteins.

MATERIALS AND METHODS

Materials

Lipids were purchased from Avanti Polar Lipids (Alabaster, AL). The following lipids were used: di-13:0 PC (1,2-ditridecanoyl-*sn*-glycero-3-phosphocholine); di-14:0 PC (1,2-dimyristoyl-*sn*-glycero-3-phosphocholine); di-14:0 PG (1,2-dimyristoyl-*sn*-glycero-3-phosphoglycerol); di-16:0 PC (1,2-dipalmitoyl-*sn*-glycero-3-phosphocholine); di-16:0 PG(1,2-dipalmitoyl-*sn*-glycero-3-phosphoglycerol); di-18:0 PC (1,2-distearoyl-*sn*-glycero-3-phosphocholine); di-18:0 PG (1,2-distearoyl-*sn*-glycero-3-phosphoglycerol); 16:0-18:1 PC (1-palmitoyl- 2-oleoyl-*sn*-glycero-3-phosphocholine); di-14:1 PC (1,2-dimyristoleoyl-snglycero- 3-phosphocholine); di-16:1 PC (1,2-dipalmitoleoyl-*sn*-glycero-3-phosphocholine); di-18:1 PC (1,2-dioleoyl-*sn*-glycero-3-phosphocholine); di-20:1 PC (1,2-dieicosenoyl-*sn*-glycero-3-phosphocholine); di-22:1 PC (1,2-dierucoyl-*sn*-glycero-3-phosphocholine); di-18:2 PC (1,2-dilinoleoyl-*sn*-glycero-3-phosphocholine); lyso-18:1 PC (1-oleoyl-2-hydroxy-*sn*-glycero-3-phosphocholine); di-18:1 PE (1,2-dioleoyl-*sn*-glycero-3-phosphoethanolamine); di-18:1 Rh-PE (1,2-dioleoyl-*sn*-glycero-3-phosphoethanolamine-n-lissamine rhodamine B sulfonyl-

Rhodamine PE); and TLE (total polar lipid extract) of *Escherichia coli* membranes (catalog No. 100600P). SMAn (Styrene maleic anhydride) copolymer was obtained as a kind gift from Cray Valley (Exton, PA). Membrane scaffold protein MSP1D1 was kindly provided by the NMR Department, Bijvoet Center for Biomolecular Research, Utrecht University, where MSP1D1 was expressed and purified as described by Bayburt and Sligar (15). Amphipol A8-35 was purchased from Affymetrix (Santa Clara, CA), and TRIS (tris-hydroxymethyl-aminomethane), NaCl, chloroform, and methanol were purchased from Sigma Aldrich (St. Louis, MO).

SMA copolymer preparation

The SMA2000 copolymer used throughout this study was prepared in exactly the same way as described in Swainsbury et al. (6). Briefly, a 5% (w/v) SMAn suspension in 1 M KOH was refluxed for at least 4 h after which the SMA was recovered by acid precipitation in 1.1 M HCl. The precipitated SMA was washed at least four times with 10 mM HCl. Finally, the SMA was lyophilized and stored at room temperature until required. 5% (w/v) SMA solutions used for experiments were prepared by dissolving lyophilized SMA in 50 mM Tris-HCl, after which the solution was adjusted to pH 8.0.

Large unilamellar vesicle preparation

Phospholipid stock solutions were prepared by dissolving dry lipid powder in 2:1 (v/v) chloroform/methanol at a concentration of 10 mM. Multilamellar vesicles (MLVs) at a concentration of 10 mM phospholipid were prepared by hydration of vacuum-dried lipid films using 50 mM Tris-HCl pH 8.0 buffer with 150 mM NaCl or without NaCl. After hydration, at least 10 freeze-thaw cycles were performed using liquid nitrogen and a water bath set at a temperature at least 10°C above the gel-to-liquid crystalline phase transition temperature (Tm) of the respective phospholipids. Subsequently, MLV dispersions were extruded through either a 200-nm or 400-nm Whatman polycarbonate filter using the Avanti mini-extruder (Sigma Aldrich) at least 15 times >Tm to prepare large unilamellar vesicles (LUVs) of 200-nm or 400-nm diameter. Phospholipid concentrations were determined by the phosphate assay according to Rouser et al. (16).

Nanodisk preparation for transmission electron microscopy and dynamic light-scattering experiments

Nanodisks of saturated and unsaturated phospholipids used for transmission electron microscopy (TEM) and dynamic light-scattering (DLS) experiments were prepared by the addition of SMA copolymer (5% w/v) in a 3:1 (w/w) SMA/phospholipid (~1:3.7 molar ratio) to lipid vesicles of either 200 nm or 400 nm in diameter at a phospholipid concentration of 10 mM in 50 mM Tris pH 8.0 and 150 mM NaCl at Tm for saturated PC lipids and at 25 °C for unsaturated lipids. The only exception was di-22:1 PC, which

required a 9:1 (w/w) SMA/phospholipid and a temperature of 60 °C for complete solubilization. All nanodisk samples were equilibrated overnight.

Turbidity experiments

The kinetics of solubilization of vesicles (400-nm diameter) by SMA copolymers was monitored by turbidity measurements at 350 nm using a Lambda 18 spectrophotometer (PerkinElmer,Waltham, MA) equipped with a Peltier element. In all experiments a quartz cuvette was used holding a total volume of 700 µL. The phospholipid vesicle dispersions (0.5mMphospholipid in 50 mM Tris-HCl pH 8.0 with either 150 mM or without NaCl) were temperature- equilibrated for at least 15 min before addition of 15 µL of a 5% (w/v) SMA 2000 solution yielding a final SMA copolymer concentration of 1.05 mg/mL (~0.1% w/v). This corresponds to a SMA/phospholipid of 3:1 (w/w) (1:3.7 molar ratio), and unless otherwise noted this ratio was used throughout this study. SMA addition was directly followed by quickly mixing the contents of the cuvette using a 200-µL pipette after which the starting point was set to zero (t = 0). Stirring the solutions yielded similar time traces but was avoided due to higher noise levels. Similar conditions were used in experiments with membrane scaffold protein MSP1D1. More specifically, MSP1D1 in 100 mM Tris pH 7.4 and 200 mM NaCl buffer was added to LUV dispersions (0.5 mM phospholipid, total volume of 700 µL) in either a 1:1 (w/w) or 3:1 (w/w) phospholipid/MSP1D1. Time traces of optical absorbance at 350 nm for all experiments were reproducible. The curves displayed are representative, and from a single experiment.

Analysis of lipid composition by thin layer chromatography (TLC) and gas chromatography (GC)

MLVs of *Escherichia coli* total polar lipid extract (Avanti Polar Lipids) were prepared as described above at a lipid concentration of 0.5 mM in 50 mM Tris-HCl pH 8 and 150 mM NaCl buffer. Vesicles were treated with an amount of SMA that is insufficient for complete solubilization (1.4:1 (w/w) SMA/lipid) for 15 min at 25 °C while shaking gently. Nanodisks (supernatant) and unsolubilized lipid material (pellet) were separated by ultracentrifugation at 115,000 g for 1 h at 4 °C. Lipids were purified from the supernatant, the pellet, and intact vesicles by the Bligh and Dyer extraction method (17). Purified lipid samples were applied to an HPTLC Silica gel 60 plate (Macherey Nagel, Düren, Germany) using a Linomat 5 sample applicator (CAMAG, Muttenz, Switzerland) that was developed with chloroform/methanol/ammonia/water (68:28:3:1 by volume) in a ADC2 developing chamber (CAMAG). The plate was preincubated in a 1.2% (w/v) boric acid solution in water/ethanol 1:1 (v/v), which was dried for 2 h at 160 °C. Lipids were visualized by dipping the plate into a methanol solution of 10% copper(II) sulfate (w/v) in 8% sulfuric acid (98%), and 8% phosphoric acid (85%)

and then drying the plate by heating at 130 °C for 15 min. Relative intensities were determined by densitometry using QUANTITY ONE software (BioRad, Hercules, CA). Molar percentages were determined from a concentration calibration of the TLE of *E. coli* membranes. The fatty acid composition of the samples was analyzed as follows: After extraction, a part of the lipid material was esterified by methyl esterification of the lipids in 2.5% volume sulfuric acid (98%) for 2 h at 70 °C. The reaction was stopped by the extra addition of water/methanol (1:1 v/v) and the methylated fatty acids were captured in the organic phase by the addition of hexane (2:1 v/v aqueous phase to hexane). The hexane phase was washed with water twice after which 0.2 mL of isopropanol was added. Samples were then dried under a nitrogen flow and the purified methylated fatty acids, redissolved in hexane, were analyzed by gas chromatography on a Trace GC Ultra (InterScience, Troy, NY) using a Stabilwax polar column (Thermo Fisher Scientific, Waltham, MA) of 30 min with a 0.31-mm internal diameter and a 0.25-mm film thickness. Fatty acid assignment was facilitated by using two standards: GLC 63b (Nu-Check Prep, Elysian, MN), and BAME (Bacterial Acid Methyl Ester) Mix (Sigma-Aldrich).

Size exclusion chromatography

LUVs of 200 nm in diameter of di-14:0 PC containing 0.5% mol Rh-PE (di- 18:1 phosphatidylethanolamine rhodamine sulfonyl, 10 mM phospholipid) in 50 mM Tris-HCl pH 8.0 treated with different concentrations of SMA copolymer were applied after 15 min of incubation with SMA at 30 °C to a Sephacryl S300 10/300 column (Pharmacia, Uppsala, Sweden) that was pre-equilibrated with Tris-HCl 50 mM pH 8.0 buffer at room temperature. Sample loading (200 µL) and elution were controlled manually using a model No. P-6000 pump (Pharmacia). The flow rate was set to 0.5 mL/min and at least 30 fractions of 200 µL were collected. Elution profiles were determined by measuring the Rh-PE absorption at 572 nm for each collected fraction using a Lambda 18 spectrophotometer (PerkinElmer).

TEM

Di-14:0 PC vesicles (untreated and treated with SMA) were visualized using cryo-TEM. A 3-µL aliquot (10 mM phospholipid) was pipetted onto a glow-discharged holey carbon copper grid in the environmental chamber of a Vitrobot (FEI, Hillsboro, OR) at 26 °C with a relative humidity kept >98%. The copper grids were blotted once for 2 s and quickly plunged into liquid ethane. A No. 20 Philips Tecnai electron microscope (FEI) was used, operating at an acceleration voltage of 200 kV. Di-14:0 PC intermediate vesicle structures were obtained by the addition of SMA copolymers in the SMA/lipid 1:4 (limiting concentration, i.e., insufficient amount of SMA to induce complete solubilization) to vesicles of di-14:0 PC at 30 °C. Nanodisks of di-14:0 PC and of other

lipid composition were visualized with negative-staining TEM. Aliquots (5 µL) of nanodisk dispersions (10 mM phospholipid) were adsorbed to glow-discharged carbon-coated copper grids for 120 s. Subsequently, the grids were washed twice with water for 15 s and negatively stained with 2% (w/v) uranyl acetate for 45 s. Excess solution on the grids was removed with filter paper. The grids were air-dried and examined using a model No. 10 Philips Tecnai electron microscope (FEI) operating at an acceleration voltage of 100 kV.

DLS

DLS experiments were performed on a Zetasizer Nano ZS (Malvern Instruments, Worcestershire, United Kingdom) at 25 °C. Nanodisks of different lipid composition (10 mM phospholipid) and vesicle dispersions ($5x10^{-4}$ mM phospholipid) in 50 mM Tris-HCl, 150–250 mM NaCl pH 8.0 buffer were measured for at least 15 times each measurement, being an average of 20 subruns of 15 s. Size-intensity distributions were generated using ZETASIZER softwares Ver. 6.20 and Ver. 7.03 and analyzed using the multiple narrow distribution. Hydrodynamic diameters (DH) were calculated from the intensity distributions with the assumption that nanodiscs are spherically shaped.

Lipid monolayers

Surface pressure isotherms versus time were recorded for lipid monolayers of di-14:0 PC, di-14:0 PG, and mixtures of both (4:1 mol PC/PG) while adding 20 µL 5% (w/v) SMA (1 mg/20 mL, which is an excess amount). Lipid monolayers were spread at the air-water interface by spreading a phospholipid solution (0.5 mM phospholipid in 9:1 v/v chloroform/methanol) until the required initial surface pressure was reached. Equilibration of the initial surface pressure and solvent evaporation was allowed for 15 min before each experiment. All measurements were performed in a 6 x 5.5 cm compartment of a homemade Teflon trough filled with 20 mL buffer of 50 mM Tris-HCl pH 8.0 with 150 mM or without NaCl at 25 ± 1 °C and constant area. The surface pressure in time was recorded using a commercially available monolayer system (Micro-TroughXS; Kibron, Helsinki, Finland). The reproducibility of the surface pressure increase in each experiment was within the maximum error of ±1 mN/m.

RESULTS

The SMA copolymer is a highly efficient membrane-solubilizing agent

LUVs scatter light efficiently, but nanodisks are too small to do so. Therefore the kinetics of vesicle solubilization upon addition of SMA copolymers can be followed simply by monitoring the decrease in optical density.

Initially, the effect was investigated of SMA addition to vesicles of saturated di-14:0 PC lipids, which undergo a gel to liquid-crystalline phase transition at 23 °C (17).

Fig. 1 A shows that the kinetics are temperature-dependent, with slow solubilization below the phase transition temperature (Tm), slightly faster solubilization when Tm is approached, and very fast solubilization within seconds at and above Tm. In all experiments, the SMA/lipid was kept constant at 3:1 (w/w). This represents an excess of SMA, based on the observation that the kinetics of solubilization for di-14:0 PC vesicles did not change when the ratio was lowered to 1:1 (w/w). At lower SMA/lipid, slower kinetics was observed at all temperatures (data not shown).

Similar solubilization trends were observed for vesicles of saturated lipids with different acyl-chain length (see Fig. S1 in the Supporting Material for full traces). Fig. 1 B shows the relative optical density value of the LUV dispersions after 10 min of SMA incubation as function of temperature. For all lipids, rapid solubilization occurs at and above Tm. In case of the shortest lipid, di-13:0 PC (red line), it was found that also at <Tm the LUV dispersion clarifies rapidly, even within seconds. For the longer lipids, at <Tm, the rate of solubilization is relatively slow but becomes faster when the temperature approaches Tm. Upon overnight incubation all lipid dispersions clarified except for those for which the temperature was set to 15 °C <Tm or more. In those cases, the rate of solubilization was so slow that no complete solubilization could be observed overnight (data not shown).

The SMA copolymer solubilizes lipid vesicles much more efficiently than the membrane scaffolding protein MSP1D1

For comparison, the ability of the membrane scaffold protein MSP1D1 to solubilize lipid vesicles was also tested. MSP1D1 is a widely used recombinant form of apolipoprotein A-I designed by Bayburt and Sligar (10,15), Denisov et al. (11), and Nath et al. (18) to reconstitute membrane proteins into nanodisks that are bounded by MSP1D1. The relative optical density was recorded as function of incubation time of MSP1D1 (1:1 w/w protein/lipid) in di-13:0 PC, di-14:0 PC, and di-16:0 PC lipid dispersions at different temperatures (see Fig. S2 for full traces). Fig. 1 C shows that after 10 min of incubation, a significant effect occurs only for di-13:0 PC and di-14:0 PC at Tm. In the case of di-16:0 PC even at Tm, no significant solubilization is observed. Similar results were obtained for all lipids when the experiments at Tm were performed at an increased protein/ lipid of 3:1 (w/w) (data not shown), demonstrating that the inability of MSP1D1 to solubilize vesicles was most likely not due to an insufficient amount of protein being present. These results are in agreement with results from previous studies on MSPs and model membranes under similar conditions as described, e.g., apoA-1 (19) and apoLp-III (20).

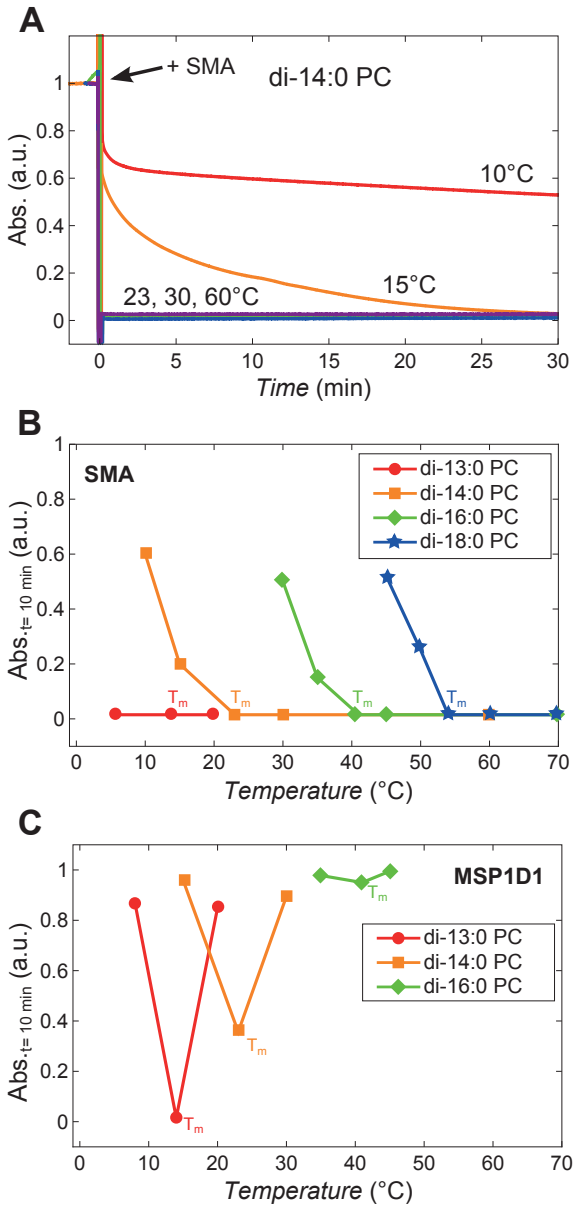

Figure 1

Kinetics of solubilization of lipid vesicles (400 nm) induced by the SMA copolymer and membrane scaffold protein MSP1D1. (A) Normalized time trace of absorbance at 350 nm showing the kinetics of solubilization of di-14:0 PC vesicles induced by the SMA copolymer at different temperatures. (B) Normalized absorbance values at 350 nm of saturated lipid vesicle dispersions after 10 min of incubation with SMA copolymer (3:1 w/w SMA/lipid) at different temperatures (*solid lines* are added to guide the eye). Tm values of the different lipids are indicated. (C) Normalized absorbance values at 350 nm of saturated lipid vesicle dispersions after 10 min of incubation with the membrane scaffold protein MSP1D1 (1:1 w/w MSP1D1/lipid) at different temperatures (*solid lines* are added to guide the eye).

The SMA copolymer induces a complete conversion of vesicles into nanodisks

The solubilization process of lipid vesicles by the SMA copolymer was further characterized using di-14:0 PC as model lipid. Fig. 2 A shows size-exclusion chromatograms of 200-nm lipid vesicles treated with different concentrations of SMA. In the absence of SMA, the vesicles elute at ~1.5 mL (red line). When the vesicles are mixed with a subsolubilizing amount of SMA, corresponding to a 1:4 (w/w) SMA/lipid (green line), the elution profile shows a decreased signal at 1.5 mL while a broad peak appears at higher retention volumes indicating the elution of smaller particles in addition to intact vesicles. When mixed with an excess amount of SMA, corresponding to a 3:1 (w/w) SMA/lipid (blue line), a single peak at ~3.0 mL is observed suggesting conversion of vesicles into even smaller particles.

The eluted samples were characterized by electron microscopy. As illustrated in Fig. 2 B, left, intact vesicles were found to have an average diameter of 175 nm. Treatment of vesicles with a subsolubilizing amount of SMA resulted in the appearance of open vesicular intermediates and membrane fragments (Fig. 2 B, middle). Vesicles treated with an excess amount of SMA reveal disk-like particles of ~10 –12 nm in diameter (Fig. 2 B, right), consistent with previous observations by Jamshad et al. (21), who also used the SMA 2000 copolymer, and Orwick et al. (3), who used the more hydrophobic SMA 3000 copolymer.

DLS experiments confirmed the transition of lipid vesicles into nanodisks (Fig. 2 C). Lipid vesicles were found to have a hydrodynamic diameter of ~190 nm and nanodiscs were found to have a fairly homogeneous apparent diameter of ~10–12 nm, both in good agreement with the electron microscopy experiments. Characterization of the intermediate structures by DLS led to irreproducible size-intensity distributions due to the formation of differently sized and shaped intermediate vesicular particles, and are, for that reason, omitted.

The size of nanodisks does not significantly change upon variation of acyl-chain length

We next investigated whether fatty acid chain length of the lipids affects the size of the nanodisks. Vesicles of saturated PC lipids with varying length of acyl chains were treated with an excess amount of SMA at Tm in order to form nanodisks (see Materials and Methods). TEM and DLS analysis showed that the particle shapes as well as the average diameter of the nanodisks (12 ± 2 nm) are very similar, regardless of the acyl-chain length. Similar particle shapes and nanodisk diameters were also observed for vesicles of unsaturated lipids with different chain lengths (see Fig. S3). However, the presence of unsaturated chains in the lipids resulted in very different kinetics of vesicle solubilization, as will be discussed next.

Lipid packing strongly influences the efficiency of solubilization

Based on the fast solubilization of saturated lipids in the liquid-crystalline phase, one would also expect that addition of SMA to unsaturated lipids would lead to fast solubilization,

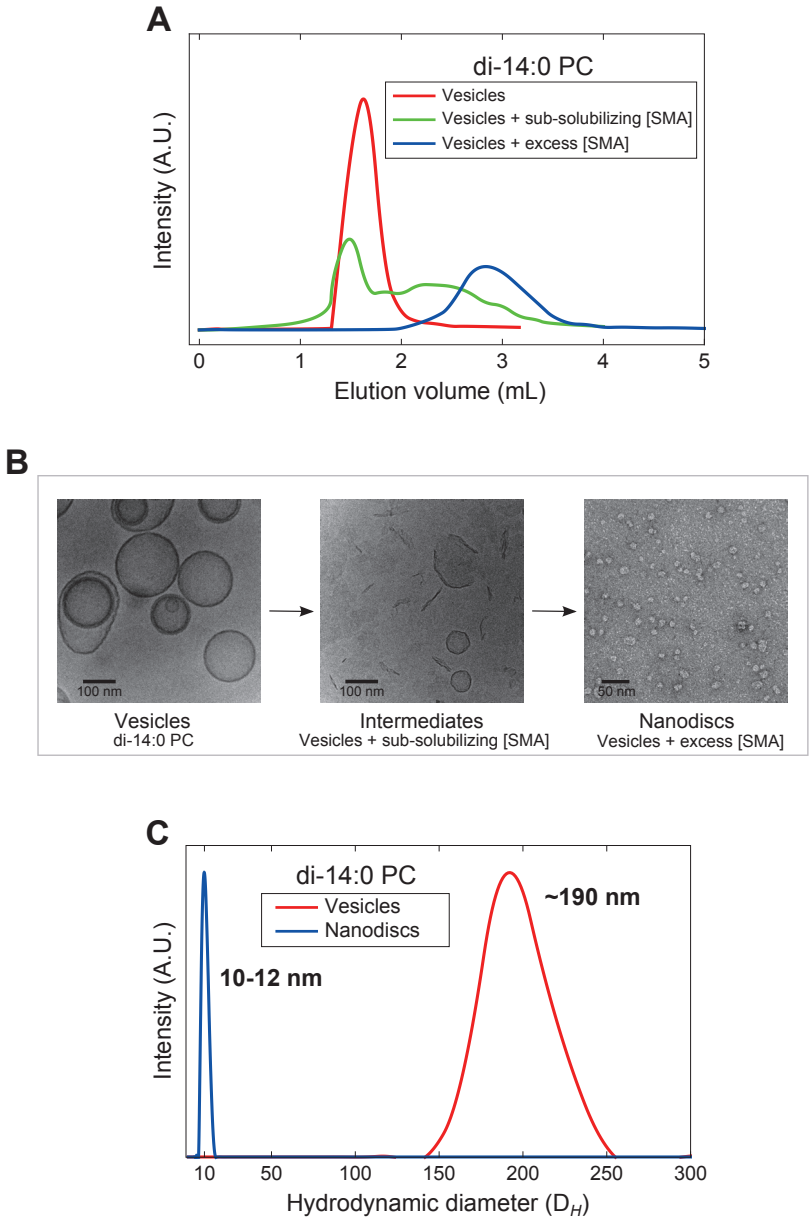

Figure 2

Structural characterization of di-14:0 PC lipid vesicle (200 nm) solubilization by the SMA copolymer. (A) Size-exclusion chromatograms of di-14:0 PC lipid vesicles (*red*), di-14:0 PC lipid vesicles incubated with a subsolubilizing amount of SMA corresponding to a 1:4 (w/w) SMA/phospholipid (*green*), and di-14:0 PC lipid vesicles incubated with excess SMA, which corresponds to a 3:1 (w/w) SMA/phospholipid (*blue*). (B) Cryo- (*left, middle*) and negative staining (*right*) transmission electron microscopy images of particles obtained from the fractions corresponding to the three chromatograms from Fig. 2 A showing vesicles (*left*), intermediate vesicular structures and open bilayer fragments (*middle*), and nanodisks *(right*). (C) Size distributions from DLS experiments on vesicles (*red*) and nanodisks obtained by incubating vesicles with excess SMA (*blue*).

because these lipids are in the fluid phase around room temperature. Surprisingly, this was not the case. Fig. 3 A shows the changes in relative optical density in time for di-18:1 PC vesicles. At 10◦C and 20◦C, solubilization is relatively slow and the curves display more complex kinetics than saturated PC lipids, possibly due to differences in the kinetics of formation and size of intermediate vesicular structures. At increased temperatures, solubilization becomes faster, with complete solubilization occurring within 10 min at 30◦C and above. A similar trend was observed for unsaturated lipids with other acyl-chain lengths (see Fig. S4 for full traces). Fig. 3 B shows the relative optical density after 10 min of incubation with SMA. At 30◦C and above, complete solubilization is obtained for all unsaturated lipids, except for the longest lipid di-22:1 PC. From this figure, two trends are clearly visible: 1) the rate of solubilization decreases with increasing acyl-chain length and 2) solubilization becomes faster at higher temperature.

Fig. 3 B also shows that bilayers of 16:0-18:1 PC are solubilized much faster than di-18:1 PC vesicles, while the effect of an extra double bond per acyl chain (di-18:2 PC vesicles) does not show significantly slower kinetics.

To further investigate the effect of lipid packing on solubilization, PE lipids were incorporated into PC lipid bilayers. This results in an increase of the lateral pressure in the acyl-chain region and an increase of the order of the lipid acyl chains due to the negative intrinsic curvature of PE lipids (22–25). Fig. 3 C shows that the presence of di-18:1 PE in di-18:1 PC vesicles results in incomplete solubilization, with a quick initial drop in optical density but no further change. By contrast, incorporation of lyso-PC lipids, which tend to decrease the lateral chain pressure due to their positive intrinsic curvature (22–24), results in immediate solubilization. Together, these data show that lipid packing has a strong influence on the kinetics of solubilization by SMA.

Electrostatic interactions affect membrane insertion and solubilization

At physiological pH, SMA copolymers carry multiple negative charges due to the partial deprotonation of maleic acid groups (26,27). In biological membranes, which often contain anionic lipids, this might lead to repulsive electrostatic interactions during membrane solubilization. Such electrostatic interactions would be particularly relevant when the polymer interacts with the membrane surface and inserts into the membrane. This step can be conveniently monitored by monolayer experiments.

Fig. 4 A shows that the addition of SMA copolymers to lipid monolayers of di-14:0 PC in the presence of salt results in an increase in surface pressure of 17 mN/m at an initial surface pressure of 25 mN/m. This increase is strong, because reported increases in surface pressure from other surface active molecules such as proteins are usually between 5 and 15 mN/m at similar initial surface pressure (28,29). Fig. 4 A also shows that the addition of 20 mol% anionic di-14:0 PG lipids has very little effect on the insertion of SMA copolymers into the lipid monolayer. However, a

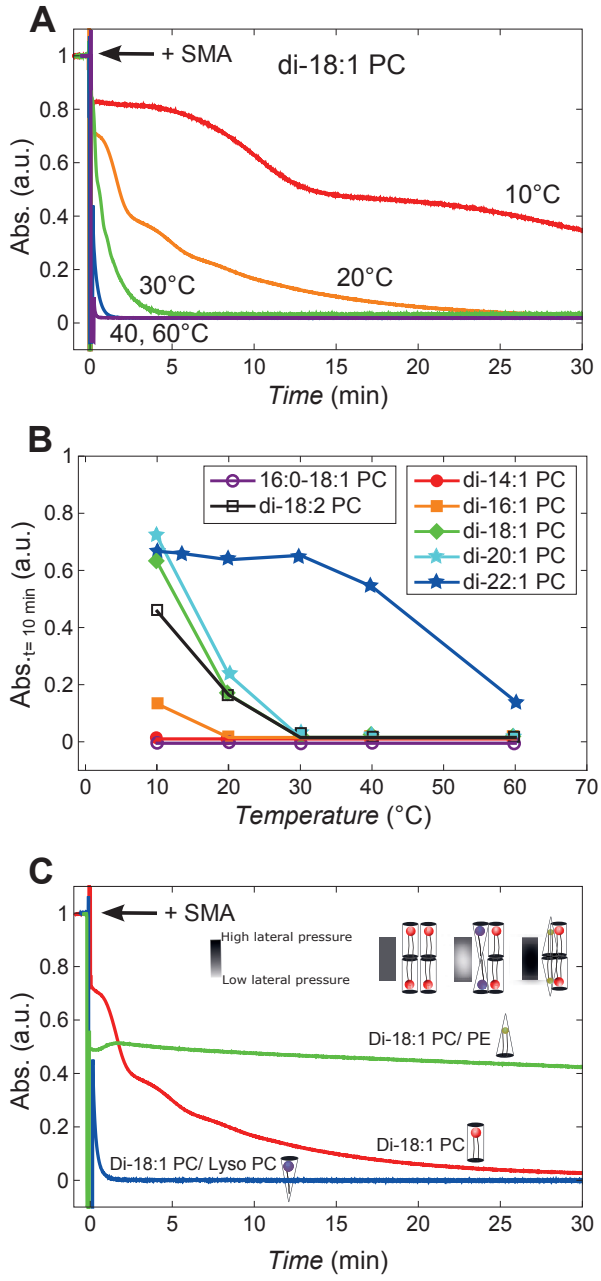

Figure 3

(A) Kinetics of solubilization of unsaturated lipid vesicles (400 nm) induced by the SMA copolymer and the effect of lateral chain pressure. In all cases, a 3:1 (w/w) SMA/lipid solubilization kinetics of di-18:1 PC vesicles is induced by the SMA copolymer at different temperatures. (B) Normalized absorbance values at 350 nm of unsaturated lipid vesicle dispersions after 10 min of incubation with SMA copolymer at different temperatures (*solid lines* are added to guide the eye). (C) Normalized absorbance time trace of di-18:1 PC vesicles (*red*), di-18:1 PC/di-18:1 PE (1:1 molar ratio, *green*), and di-18:1-PC/lyso-18:1-PC (4:1 molar ratio, *blue*) after the addition of SMA copolymer, all at 20 °C. (*Inset*) Schematic representation of the expected changes in the lateral chain pressure.

significantly lower increase in surface pressure is observed when monolayers of pure anionic lipids are used and when salt is absent, implying that electrostatic repulsions are no longer screened. This shows that repulsive electrostatic interactions between SMA copolymers and anionic lipids can inhibit membrane insertion to a certain extent. Fig. 4 B displays the increase in surface pressure at different initial surface pressures for di-14:0 PC and di-14:0 PG lipid monolayers in the presence of NaCl. From the linear relationship between the surface pressure increase and the initial surface pressure, the maximal insertion pressure can be extrapolated to be ~48 mN/m for both PC and PG lipid monolayers. This demonstrates that SMA readily inserts into lipid monolayers far above the surface pressure of ≈30 mN/m estimated for biological membranes (30). The observation that this happens even when the monolayer is completely negatively charged further highlights the strong insertion capability of the polymer.

We next investigated to what extent electrostatic interactions influence the kinetics of solubilization by analyzing the effects of incorporation of anionic lipids on solubilization kinetics of vesicles in the presence and absence of salt (see Fig. S5 for full traces). Fig. 4 C shows the optical density values after 10 min of incubation of SMA with di-14:0 PC/PG, di-16:0 PC/PG, and di-18:0 PC/PG vesicles in the presence of salt (*solid lines*). The trends are similar to those observed with pure PC lipids (Fig. 1 B), but with solubilization rates that are slightly slower at >Tm. This is particularly true for the case where salt is absent (dashed lines). Above Tm, solubilization is fast for di-14:0 PC/PG but it becomes significantly slower for the longer chain lipids di-16:0 PC/PG and di-18:0 PC/PG in the absence of salt. Rather surprisingly, in this case solubilization is getting more difficult with increasing temperature. Possibly, this effect is related to changes in the intrinsic membrane curvature, as will be discussed later. In any case, these results indicate that increased repulsive electrostatic interactions slow down the overall rate and efficiency of solubilization.

The SMA copolymer does not preferentially solubilize specific lipid species

Finally, we tested the effect of SMA copolymers on vesicles of a native extract of *E. coli* membranes. This system was chosen because *E. coli* is often used for the expression of membrane proteins, and therefore efficient solubilization is required for extraction of these proteins from the membrane by using SMA. The acyl-chain composition of *E. coli* lipids is governed by c16:0 and c18:1 fatty acids (Fig. 5 D). Based on the results of solubilization of 16:0–18:1 PC vesicles (Fig. 3 B), there is no reason to expect that the acyl-chain composition would significantly slow down solubilization in this case. However, the overall lipid composition of *E. coli* membranes may make it difficult to solubilize: the TLE of *E. coli* membrane consists for a large part of the nonbilayer lipid PE (~65 mol %) and furthermore contains the anionic lipids PG (~25 mol %) and cardiolipin (~10 mol %). As shown in Fig. 5 A, solubilization of

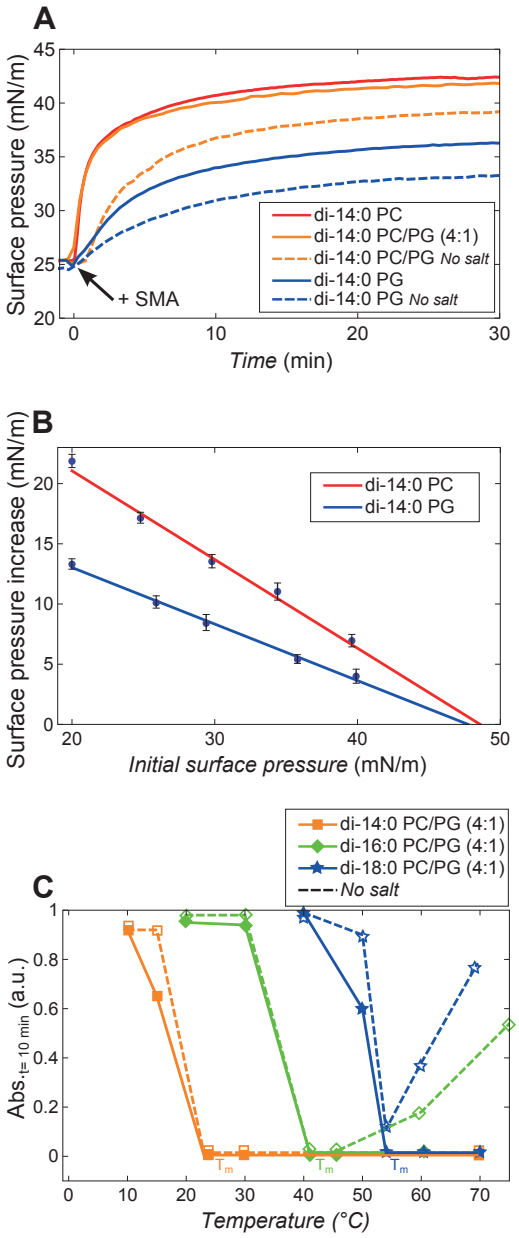

Figure 4

Effect of electrostatic interactions on membrane insertion and solubilization by SMA copolymers. (A) Surface pressure increase in time upon the addition of excess SMA to monolayers of di-14:0 PC (*red*), di-14:0 PC/PG (4:1) (*orange*), and di-14:0 PG (*blue*) in 50 mM Tris HCl pH 8.0 with 150 mM NaCl (*solid*) or without NaCl (*dashed*). (B) Surface pressure increase as function of initial surface pressure for di-14:0 PC and di-14:0 PG lipid monolayers in 50 mM Tris-HCl pH 8.0 with 150 mM NaCl as subphase. (*Solid lines*) Linear fit with the maximum insertion pressure extrapolated to be ~48 mN/m. Error bars are standard errors based on at least two independent measurements. (C) Normalized absorbance values at 350 nm of lipid vesicle dispersions after 10 min of incubation with the SMA copolymer at different temperatures. The diameter of the vesicles was 400 nm and a 3:1 (w/w) SMA/lipid was used. (*Solid lines*) Data recorded in Tris-HCl pH 8.0 buffer with 150 mM NaCl; (*dashed lines*) without NaCl.

vesicles of *E. coli* lipids is indeed inefficient at the standard 3:1 (w/w) SMA/lipid. On the other hand, solubilization could be significantly improved by increasing the SMA/lipid to 9:1 (w/w) and raising the salt concentration to 450 mM. Apparently, by increasing the concentrations of SMA and/or salt, polymer binding to the membrane is promoted and thereby solubilization. Also in this case, TEM and DLS analysis of the solubilized *E. coli* vesicles showed that nanodisks are formed with an average diameter of 8–10 nm (Fig. 5 B), similar to that found for pure PC lipids (see Fig. S3).

The observation that the efficiency of solubilization is modulated by lipid packing properties and electrostatic interactions raises the question whether SMA may preferentially solubilize specific lipids. To test this, a subsolubilizing amount of SMA (1.4:1 w/w SMA/lipid) was added to vesicles of the native extract to induce only partial solubilization (see Fig. S6). The samples were then centrifuged to separate pellet (nonsolubilized vesicles) and supernatant (nanodisks) and their lipid compositions were determined from TLC analysis. As shown in Fig. 5 C, the lipid composition in the supernatant is not significantly different from that of the pellet or that of the intact vesicles. Similarly, GC analysis revealed that the fatty acid composition of the lipids is similar in all cases (Fig. 5 D). Hence, SMA copolymers do not seem to selectively solubilize phospholipid species in this system.

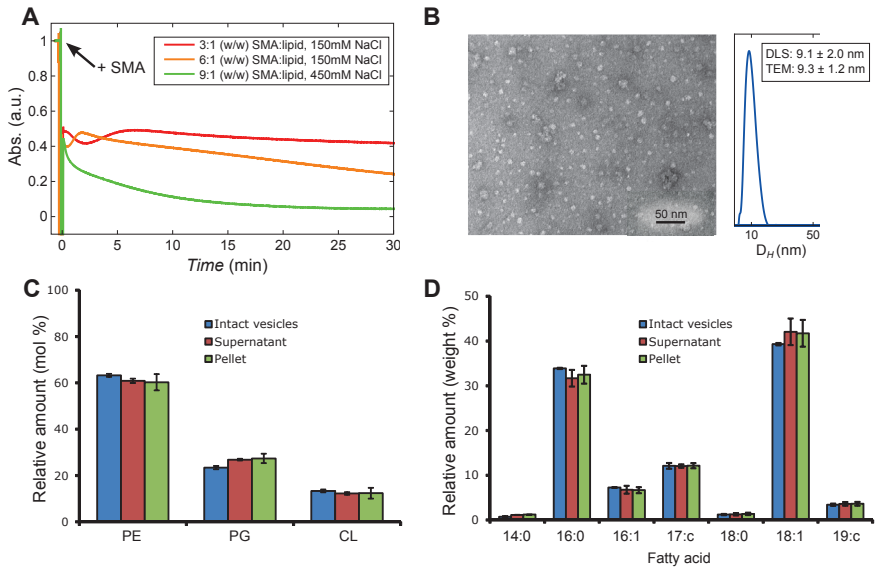

Figure 5

Characterization of the solubilization of vesicles (400 nm) of an *E. coli* native lipid extract by the SMA copolymer. (A) Time traces of absorbance at 350 nm of *E. coli* vesicle solubilization at different SMA copolymer and salt concentrations, all at 20 °C. (B) Negative staining TEM image and DLS size distribution of *E.coli* nanodiscs as prepared by the addition of SMA in a 9:1 (w/w) SMA/lipid in the presence of 450 mM NaCl. (*Inset*) Average diameters and standard deviations that were found. Analysis by TEM was based on 20 individual nanodisk particles and analysis by DLS was based on multiple measurements on a single independent sample as described in Materials and Methods. (C) Lipid composition (mol %) and (D) fatty acid composition (weight %) of intact vesicles of *E. coli* lipids, and of pellet and supernatant obtained after partial solubilization by SMA. Error bars represent the standard deviation of three independent experiments.

DISCUSSION

Insight into the mode of action of SMA copolymers is important to optimally exploit its use in the purification and characterization of membrane proteins but also for development of novel applications in membrane research. Here, it was found that the SMA copolymer is a very efficient membrane solubilizing agent but that the kinetics of solubilization are modulated by physico-chemical properties of the lipids in very distinct ways.

How does the SMA copolymer exert its action and how can we understand the effects of lipid composition? Below, we present a model for the molecular mechanism of membrane solubilization by SMA and discuss how it is related to our experimental findings. We then discuss the physico-chemical properties of SMA that are responsible for its high solubilizing efficiency and we will compare this with the mode of action of other amphiphilic polymers that are used in membrane research.

Model for the mode of action of the SMA copolymer

The effect of lipid composition on vesicle solubilization by SMA copolymers can be understood based on the model presented in Fig. 6.

Step 1: membrane binding

In a first step, SMA copolymers bind to the membrane. In our model, the extent of binding depends on the SMA concentration. It is modulated by electrostatic interactions between SMA copolymers and the copolymers and anionic lipids at the membrane surface. Despite these repulsive electrostatic interactions, SMA has a strong interaction with membranes. This is most clearly illustrated by the lipid monolayer experiments, which showed a fast and exceptionally strong insertion of SMA in films of zwitterionic as well as anionic lipids. In both cases, the polymers are able to insert even at surface pressures far above those estimated for biological membranes, suggesting that SMA copolymers will insert into any biological membrane.

What is the driving force for the interaction of SMA with membranes? We propose that binding is mainly driven by the hydrophobic effect via the polymer styrene moieties and the lipid acyl chains (21,31) and that this driving force is sufficiently strong to overcome any repulsive electrostatic interactions. Nevertheless, electrostatic repulsion does modulate the extent of binding, as illustrated by the effects of increasing the salt concentration or decreasing the amount of anionic lipids in the membrane. Both changes would lead to increased binding, and hence to an increased efficiency of solubilization in the next step of the process.

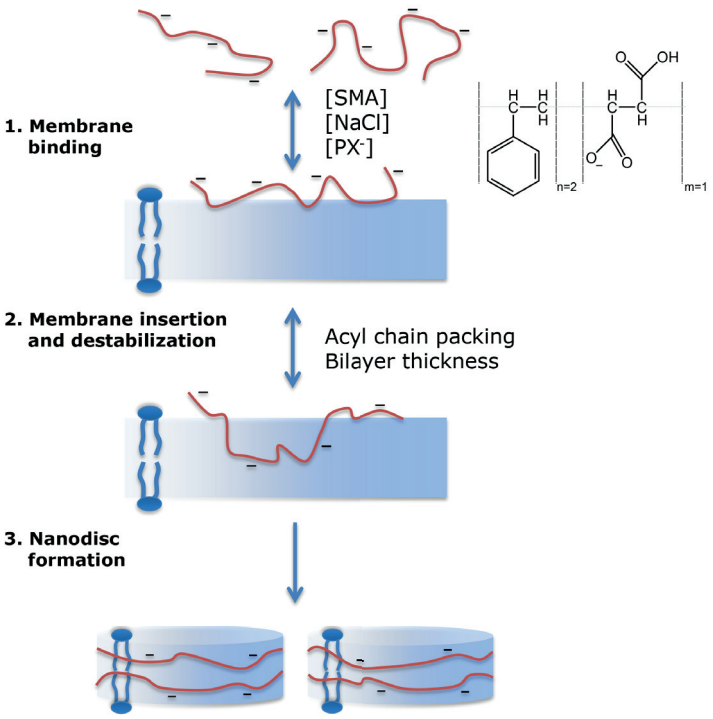

Figure 6
Schematic illustration of membrane solubilization by the SMA copolymer. (*Inset*) Schematic representation of the SMA copolymer used in this study. Step 1: anionic SMA copolymers bind to the lipid membrane, a process that is driven mainly by hydrophobic interactions and modulated by electrostatic interactions. Binding increases when the salt concentration increases and the number of anionic lipids (PX^-) decreases. Step 2: insertion of the SMA copolymer in the membrane hydrophobic core, a process mainly determined by acyl-chain packing. A high lateral pressure in the acyl-chain region will decrease the efficiency of insertion. Step 3: insertion into the hydrophobic core leads to membrane destabilization and to the formation of vesicular intermediates. Further solubilization will lead to the formation of nanodisks, which are stabilized by a SMA copolymer belt around the nanodisk. The kinetics and efficiency of membrane destabilization and nanodisk formation is determined by acyl-chain packing properties and bilayer thickness.

Step 2: membrane insertion and destabilization

In this step, SMA copolymers insert more deeply into the hydrophobic core of the membrane. We envision that SMA will need packing defects in the membrane for efficient insertion. This is supported by the observation that in all systems of saturated lipids, maximal solubilization of SMA occurs at Tm of the lipids, where gel-phase domains coexist with domains of lipids in the liquid-crystalline phase, leading to large packing defects (32). However, also in the absence of large packing defects, lipid packing is important for solubilization, as evident from the observation that at >Tm, solubilization takes place much faster than at <Tm, when the lipids are in the gel phase and are thus more tightly packed. Interestingly, unsaturated lipids were found to be more difficult to solubilize than saturated lipids in the fluid phase. At first glance this is surprising, because unsaturated chains are more disordered and thus are more loosely

packed. On the other hand, due to their double bonds, these membranes have an increased lateral pressure in the acyl-chain region (24,33,34), and this might lead to a less efficient insertion of the polymers. The observations that incorporation of PE, with its negative intrinsic curvature, inhibits solubilization, while incorporation of lyso-PC, with its positive intrinsic curvature, has the opposite effect, are consistent with the notion that the acyl-chain pressure plays an important role in solubilization.

In most cases, solubilization was improved by increasing temperature. This can be expected because increasing temperature will lead to a general increase in reaction kinetics and hence to faster solubilization. However, there is one exception: solubilization does not increase as a function of temperature upon SMA addition to anionic saturated lipids that have long acyl chains in the liquid-crystalline phase in the absence of salt (Fig. 4 C). Most likely this is a direct consequence of the low membrane binding of SMA, due to strong repulsive electrostatic interactions in this particular case. We propose that this low binding allows an opposing temperature-dependent effect to become dominant, namely the increase of lipid chain dynamics. This would lead to an increased negative curvature of the membrane at higher temperatures and hence, based on the result discussed above, to slower and inefficient solubilization. Such an increase in negative curvature will be stronger for longer lipids and would explain the trend of less efficient solubilization for increasing bilayer thickness.

In general, we suggest that the bilayer thickness plays an important role especially at the stage where the vesicles disintegrate and fall apart into intermediate vesicular structures and membrane fragments. This is simply because it will be more difficult to break up thicker membranes due to an increase of the forces that hold the membrane together, such as van der Waals interactions and the hydrophobic effect. This view is in line with the observations that short-chained saturated lipids are easily solubilized, even in the gel phase, and that unsaturated lipids at lower temperature are less efficiently solubilized when the effective length of the acyl chains increases (Fig. 4 B).

Together, these results show that the rate and yield of solubilization by SMA copolymers depends greatly on the lipid composition of the model membranes. Despite this, we found that the lipid composition of nanodisks largely reflects that of the initial membrane. This has also been observed recently for nanodisks that contain a membrane protein purified from the purple bacterium *Rhodobacter sphaeroides* (6). These findings thus imply that it is the physical properties of lipid membranes, rather than those of individual lipid constituents, that determine the solubilization kinetics and efficiency.

Step 3: nanodisk formation

In the last step, membrane fragments are further solubilized and the formation of nanodisks is facilitated. Recently, Jamshad et al. (21) and Orwick et al. (3) structurally characterized the nanodisks of di-14:0 PC bounded by SMA. In these studies it was

shown that nanodisks are indeed shaped like a disk and that the SMA copolymer places its phenyl groups between the lipid acyl chains, thereby stabilizing the nanodisks. The reported disk-like shape and average diameter of the nanodisks is very similar to what we observed here. In addition, we found that the average nanodisk diameter of 10 –12 nm is completely independent of lipid chain length and unsaturation. However, the parameters that control this nanodisk diameter are still unclear (see discussion below).

The SMA copolymer forms nanodisks efficiently because of its chemical structure

The hydrophobic effect drives the interaction between SMA copolymers and membranes. But what sets this polymer apart from other amphiphilic polymers? We argue that the properties of the phenyl and carboxylic acid pendant groups are responsible for this in several ways (Fig. 6).

1) These residues are small, thereby giving SMA a small cross-sectional area. This makes it relatively easy for the polymer to insert into membranes even when no packing defects are present.
2) Insertion of the short residues, and in particularly the rigid phenyl groups, in between the acyl chains (22) leads to a minimal loss in conformational entropy of the residues when the polymer is wrapped around a nanodisk compared to when the polymer is in solution.
3) Because there is minimal steric hindrance, the short sidegroups allow the polymer to adopt a curvature that is required to encircle a nanodisk.

An additional helpful property of the SMA copolymer might be its ability to interact with membranes via the polar moments of the side-groups. It was recently suggested that polyacids interact with the membrane based on the favorable interaction between the dipole moment of their carboxylic acid groups and the dipole potential of membranes (35). The same would hold not only for the carboxylic acid groups of SMA but for the phenyl side-groups as well. Due to the orientation of the lipid fatty acid carbonyls and the preferential orientation of water molecules that hydrate the lipid headgroups, a positive potential arises in the center of the bilayer (36). Because the phenyl side-groups have a large quadrupolar moment with a negative potential on both sides of the aromatic ring (37), this would favor their insertion into the interior of the bilayer.

Support for the special role of these side-groups in SMA comes from comparison with the chemistry and mode of action of other amphiphilic polymers. The A8-35 amphipol, for example, is a polymer that is often used as replacement for detergents to stabilize membrane proteins (38,39). Its pendant groups are mainly carboxylic acid and large alkyl groups (see Fig. S7 A). These alkyl chains give the polymer a large cross-sectional area, which would interfere with membrane solubilization and

nanodisk formation due to steric hindrance, while their flexibility would cause a large loss in conformational entropy when it hypothetically would be wrapped around a nanodisk. Instead, it is much more favorable for the polymer to wrap around membrane proteins directly. Another interesting example is PEAA (poly(ethyl)acrylic acid; see Fig. S7 B). This polymer consists of relatively small pendant carboxylic acid and ethyl groups. Thomas et al. (40) and Chung et al. (41) reported that PEAA is able to solubilize saturated di-14:0 PC and di-16:0 PC vesicles. This situation leads to the formation of structures similar in shape and size to SMA-bounded nanodisks. However, the solubilization kinetics is much slower, and range of lipid composition able to be solubilized much more limited than for SMA. This is in line with the notion that the presence of small pendant groups such as phenyl groups rather than the alkyl group is helpful for efficient solubilization of membrane into nanodisks.

Finally, we address MSPs, which are amphiphilic biopolymers that, like SMA, are able to assemble nanodisks. They form α-helices with a relatively large cross-sectional area, which would require the presence of large surface defects for membrane insertion. Indeed, as described here and previously, MSPs can only efficiently solubilize PC vesicles at T_m (19,20) when there are large surface defects, and then only in the case of short-chained lipids, when lipid-lipid interactions are less strong and solubilization occurs more easily.

The SMA copolymer versus membrane scaffold proteins

These fresh insights into the mode of action of SMA allow us to compare some aspects of the assembly of nanodisks by MSPs and SMA. Due to the efficient solubilizing properties of SMA, it can solubilize a wide variety of lipids with different acyl-chain lengths and headgroups. Thus SMA, in contrast to MSPs, is able to directly solubilize a wide variety of biological membranes into nanodisks without the help of detergents (5,6,8). Importantly, we showed that SMA does not solubilize lipids in a preferential way. This implies that the native lipid environment is retained for membrane proteins isolated in nanodisks by using SMA (5,6). In apparent contrast, for MSPs it is possible to choose which lipids are used for reconstitution. However, it should be realized that for SMA-bounded nanodisks it is also possible to capture membrane proteins in a specific lipid composition; this can be accomplished by first reconstituting the protein in vesicles of the desired lipids by conventional methods, and then solubilizing these reconstituted vesicles with SMA.

An advantage of the use of MSP-bounded nanodisks is that the diameter can be conveniently controlled between 7 and 20 nm by choosing an MSP of a certain length (42). The nanodisk diameter is an important parameter because, in principle, it determines the size of a membrane protein (complex) that can be captured in a nanodisk. For the SMA copolymer, it is not (yet) clear what controls the nanodisc diameter and

how this can be modulated (43). Here, we found that the SMA 2000 copolymer always yielded nanodiscs with a diameter of ~10 nm, regardless of the actual lipid used. Interestingly, it has been reported that both SMA 2000 and the more hydrophobic SMA 3000 yield larger nanodisks when a membrane protein is embedded. Incorporation of a photosynthetic reaction center (6), the mitochondrial respiratory complex IV (5), and bacteriorhodopsin (4) all led to nanodisks of a diameter between 12 and 17 nm. The capturing of the staphylococcal penicillin-binding protein complex PBP2/PBP2a even led to nanodisks up to 24 nm in diameter (44). Apparently, the protein content, and most likely specifically its shape and diameter, are key parameters in determining the size of nanodisks.

CONCLUSIONS

We found that that SMA is a very efficient membrane solubilizing agent, displaying kinetics that are strongly influenced by lipid packing properties and electrostatic interactions. Its small phenyl and carboxylic acids pendant groups both account for the high solubilizing efficiency of the polymer as well as for its ability to stabilize nanodisks. The results will be helpful for optimization of procedures involving the use of SMA for isolation of membrane proteins from different membranes, the extraction of more complex lipid compositions that might include sphingolipids and sterols, and for development of new applications of this polymer in membrane research. From a broader perspective, they will contribute to the understanding of the mode of action of polymers as membrane-active agents to modify membrane properties with possible implications for drug delivery systems, among other uses.

SUPPORTING MATERIAL

Seven figures are available at http://www.biophysj.org/biophysj/supplemental/S0006-3495(14)04667-0.

ACKNOWLEDGMENTS

We thank Charles Mateer from Cray Valley (USA) for providing the SMAn copolymer; Mark Daniels and Sylke Lievestro from the NMR spectroscopy group, Utrecht University, for the expression and purification of MSP1D1 membrane scaffold protein; Bonny Kuipers for his assistance during dynamic light scattering experiments; and Ruud Cox for his assistance during gas chromatography experiments. We thank Francisco Calderón Celis for his contributions as master student in our group. Financial support via S.S. and J.A.K. of the research program of the Foundation for Fundamental Research on Matter and the support from a grant from the Netherlands Organization for Scientific Research (NWO-ECHO grant No. 711-013-005 to J.D.P.) is gratefully acknowledged.

REFERENCES

1. Knowles, T. J., R. Finka, ., M. Overduin. 2009. Membrane proteins solubilized intact in lipid containing nanoparticles bounded by styrene maleic acid copolymer. J. Am. Chem. Soc. 131:7484–7485.
2. Jamshad, M., Y.-P. Lin, ., T. R. Dafforn. 2011. Surfactant-free purification of membrane proteins with intact native membrane environment. Biochem. Soc. Trans. 39:813–818.
3. Orwick, M. C., P. J. Judge, ., A. Watts. 2012. Detergent-free formation and physicochemical characterization of nanosized lipid-polymer complexes: Lipodisq. Angew. Chem. Int. Ed. Engl. 51:4653–4657.
4. Orwick-Rydmark, M., J. E. Lovett, ., A. Watts. 2012. Detergent-free incorporation of a seven-transmembrane receptor protein into nanosized bilayer Lipodisq particles for functional and biophysical studies. Nano Lett. 12:4687–4692.
5. Long, A. R., C. C. O'Brien, ., N. N. Alder. 2013. A detergent-free strategy for the reconstitution of active enzyme complexes from native biological membranes into nanoscale discs. BMC Biotechnol. 13:41.
6. Swainsbury, D. J. K., S. Scheidelaar, ., M. R. Jones. 2014. Bacterial reaction centers purified with styrene maleic acid copolymer retain native membrane functional properties and display enhanced stability. Angew. Chem. Int. Ed. http://dx.doi.org/10.1002/anie.201406412.
7. Seddon, A. M., P. Curnow, and P. J. Booth. 2004. Membrane proteins, lipids and detergents: not just a soap opera. Biochim. Biophys. Acta. 1666:105–117.
8. Gulati, S., M. Jamshad, ., A. J. Rothnie. 2014. Detergent-free purification of ABC (ATP-binding-cassette) transporters. Biochem. J. 461:269–278.
9. Shi, L., Q.-T. Shen, ., F. Pincet. 2012. SNARE proteins: one to fuse and three to keep the nascent fusion pore open. Science. 335:1355– 1359.
10. Bayburt, T. H., and S. G. Sligar. 2003. Self-assembly of single integral membrane proteins into soluble nanoscale phospholipid bilayers. Protein Sci. 12:2476–2481.
11. Denisov, I. G., Y. V. Grinkova, ., S. G. Sligar. 2004. Directed selfassembly of monodisperse phospholipid bilayer nanodiscs with controlled size. J. Am. Chem. Soc. 126:3477–3487.
12. Frauenfeld, J., J. Gumbart,., R. Beckmann. 2011. Cryo-EM structure of the ribosome-SecYE complex in the membrane environment. Nat. Struct. Mol. Biol. 18:614–621.
13. Hagn, F., M. Etzkorn, ., G. Wagner. 2013. Optimized phospholipid bilayer nanodiscs facilitate high-resolution structure determination of membrane proteins. J. Am. Chem. Soc. 135:1919–1925.
14. Mazhab-Jafari, M. T., C. B. Marshall, ., M. Ikura. 2013. Membranedependent modulation of the mTOR activator Rheb: NMR observations of a GTPase tethered to a lipid-bilayer nanodisc. J. Am. Chem. Soc. 135:3367–3370.
15. Bayburt, T. H., and S. G. Sligar. 2010. Membrane protein assembly into nanodiscs. FEBS Lett. 584:1721–1727.
16. Rouser, G., S. Fleischer, and A. Yamamoto. 1970. Two-dimensional then layer chromatographic

separation of polar lipids and determination of phospholipids by phosphorus analysis of spots. Lipids. 5:494–496.

17. Silvius, D. J. R. 1982. Thermotropic phase transitions of pure lipids in model membranes and their modifications by membrane proteins. In Lipid-Protein Interactions. John Wiley, New York.
18. Nath, A., W. M. Atkins, and S. G. Sligar. 2007. Applications of phospholipid bilayer nanodiscs in the study of membranes and membrane proteins. Biochemistry. 46:2059–2069.
19. Pownall, H. J., and J. B. Massey. 1982. Mechanism of association of human plasma apolipoproteins with dimyristoylphosphatidylcholine: effect of lipid clusters on reaction rates. Biophys. J. 37:177–179.
20. Wan, C.-P. L., M. H. Chiu, ., P. M. Weers. 2011. Apolipoproteininduced conversion of phosphatidylcholine bilayer vesicles into nanodisks. Biochim. Biophys. Acta. 1808:606–613.
21. Jamshad, M., V. Grimard, ., T. R. Dafforn. 2014. Structural analysis of a nanoparticle containing a lipid bilayer used for detergent-free extraction of membrane proteins. Nanotechnology. http://dx.doi.org/10.1007/s12274-014-0560-6.
22. Gruner, S. M. 1985. Intrinsic curvature hypothesis for biomembrane lipid composition: a role for nonbilayer lipids. Proc. Natl. Acad. Sci. USA. 82:3665–3669.
23. Marsh, D. 2007. Lateral pressure profile, spontaneous curvature frustration, and the incorporation and conformation of proteins in membranes. Biophys. J. 93:3884–3899.
24. Frolov, V. A., A. V. Shnyrova, and J. Zimmerberg. 2011. Lipid polymorphisms and membrane shape. Cold Spring Harb. Perspect. Biol. 3:a004747.
25. Separovic, F., and K. Gawrisch. 1996. Effect of unsaturation on the chain order of phosphatidylcholines in a dioleoylphosphatidylethanolamine matrix. Biophys. J. 71:274–282.
26. Ferry, J., D. Udy, ., D. Fordyce. 1951. Titration and viscosity studies of two copolymers of maleic acid. J. Colloid Sci. 6:429–442.
27. Garrett, E. R., and R. L. Guile. 1951. Potentiometric titrations of a polydicarboxylic acid: maleic acid-styrene copolymer. J. Am. Chem. Soc. 73:4533–4535.
28. Demel, R. A. 1994. Monomolecular layers in the study of biomembranes. In Physicochemical Methods in the Study of Biomembranes. Vol. 23, Subcellular Biochemistry. H. Hilderson and G. Ralston, editors. Springer, New York, pp. 83–120.
29. Calvez, P., S. Bussie`res, ., C. Salesse. 2009. Parameters modulating the maximum insertion pressure of proteins and peptides in lipid monolayers. Biochimie. 91:718–733.
30. Marsh, D. 1996. Lateral pressure in membranes. Biochim. Biophys. Acta. 1286:183–223.
31. Tonge, S. R., and B. J. Tighe. 2001. Responsive hydrophobically associating polymers: a review of structure and properties. Adv. Drug Deliv. Rev. 53:109–122.
32. Noordam, P. C., A. Killian,., J. De Gier. 1982. Comparative study on the properties of saturated phosphatidylethanolamine and phosphatidylcholine bilayers: barrier characteristics and susceptibility to phospholipase A2 degradation. Chem. Phys. Lipids. 31:191–204. 33. Cantor, R. S. 1999. Lipid composition and the lateral pressure profile in bilayers. Biophys. J. 76:2625–2639.
34. Mouritsen, O. G. 2011. Lipids, curvature, and nano-medicine. Eur. J. Lipid Sci. Technol.

113:1174–1187. |

35. Berkovich, A. K., E. P. Lukashev, and N. S. Melik-Nubarov. 2012. Dipole potential as a driving force for the membrane insertion of polyacrylic acid in slightly acidic milieu. Biochim. Biophys. Acta. 1818:375–383.
36. Clarke, R. J. 2001. The dipole potential of phospholipid membranes and methods for its detection. Adv. Colloid Interface Sci. 89 90:263–281.
37. Battaglia, M., A. Buckingham, and J. Williams. 1981. The electric quadrupole moments of benzene and hexafluorbenzene. Chem. Phys. Lett. 78:421–423.
38. Tribet, C., R. Audebert, and J.-L. Popot. 1996. Amphipols: polymers that keep membrane proteins soluble in aqueous solutions. Proc. Natl. Acad. Sci. USA. 93:15047–15050.
39. Popot, J.-L., T. Althoff, ., M. Zoonens. 2011. Amphipols from A to Z*. Annu. Rev. Biophys. 40:379–408.
40. Thomas, J. L., B. P. Devlin, and D. A. Tirrell. 1996. Kinetics of membrane micellization by the hydrophobic polyelectrolyte poly(2 ethylacrylic acid). Biochim. Biophys. Acta. 1278:73–78.
41. Chung, J. C., D. J. Gross, ., L. R. Opsahl-Ong. 1996. pH-Sensitive, cation-selective channels formed by a simple synthetic polyelectrolyte in artificial bilayer membranes. Macromolecules. 29:4636–4641.
42. Ritchie, T., Y. Grinkova, ., S. Sligar. 2009. Chapter 11—Reconstitution of membrane proteins in phospholipid bilayer nanodiscs. In Vol. 464, Liposomes, Part F, of Methods in Enzymology. N. Duzgunes, editor. Academic Press, New York, pp. 211–231.
43. Zhang, R., I. D. Sahu, ., G. A. Lorigan. 2014. Characterizing the structure of Lipodisq nanoparticles for membrane protein spectroscopic studies. Biochim. Biophys. Acta. www.sciencedirect.com/science/article/pii/S0005273614001801.
44. Paulin, S., M. Jamshad, ., P. W. Taylor. 2014. Surfactant-free purification of membrane protein complexes from bacteria: application to the staphylococcal penicillin-binding protein complex PBP2/PBP2a. Nanotechnology. 25:285101.

Supporting Material

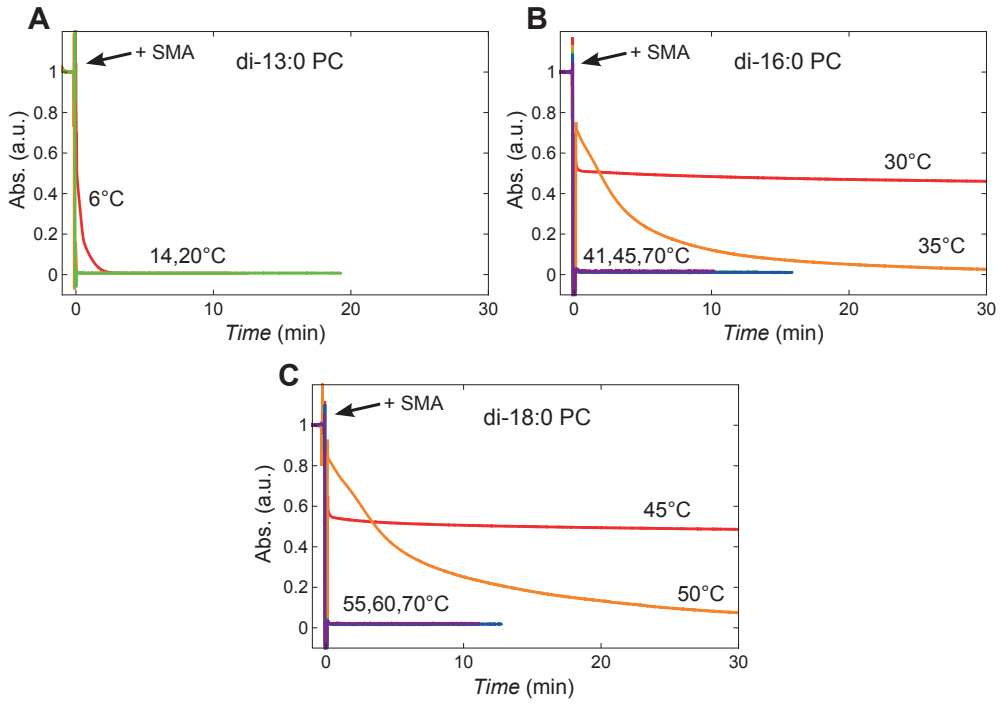

Figure S1
Kinetics of solubilization of saturated PC lipid vesicles (400 nm) induced by the SMA copolymer at a 3:1 (w/w) SMA to lipid ratio. Normalized time traces of the absorbance at 350 nm showing the kinetics of solubilization of (A) di-13:0 PC (Tm= 14 °C), (B) di-16:0 PC (Tm= 41 °C), and (C) di-18:0 PC vesicles (Tm= 55 °C). Tm values are taken from (1).

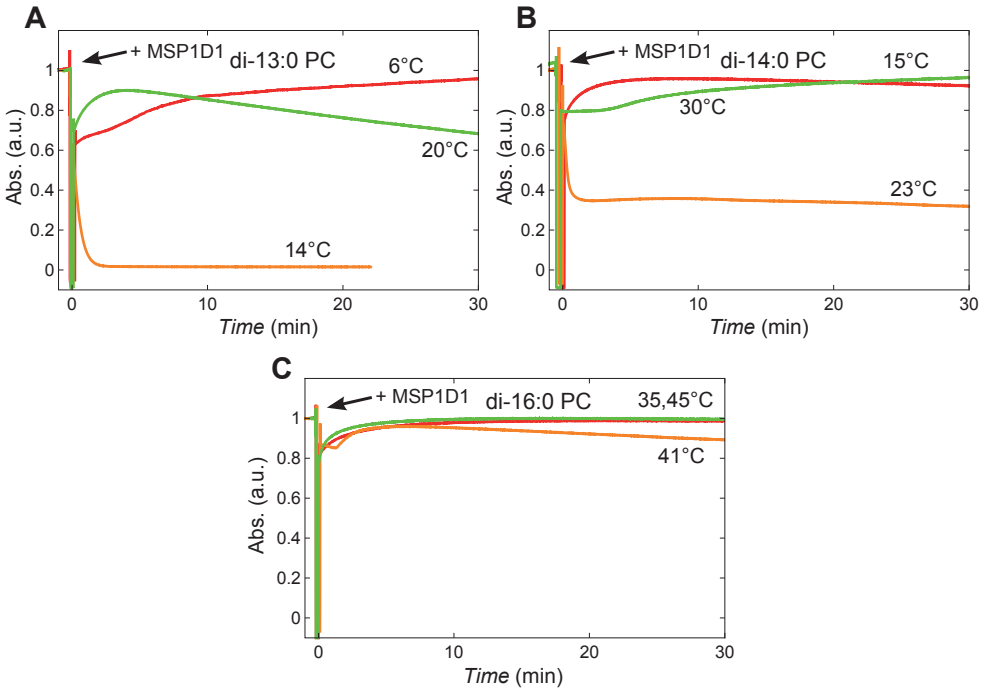

Figure S2

Kinetics of solubilization of saturated PC lipid vesicles (400 nm) induced by the membrane scaffold protein MSP1D1 at a 1:1 (w/w) protein to phospholipid ratio. Normalized time traces of the absorbance at 350 nm showing the kinetics of solubilization of (A) di-13:0 PC (Tm= 14 °C), (B) di-14:0 PC (Tm= 23 °C), and (C) di-16:0 PC vesicles (Tm= 41 °C).

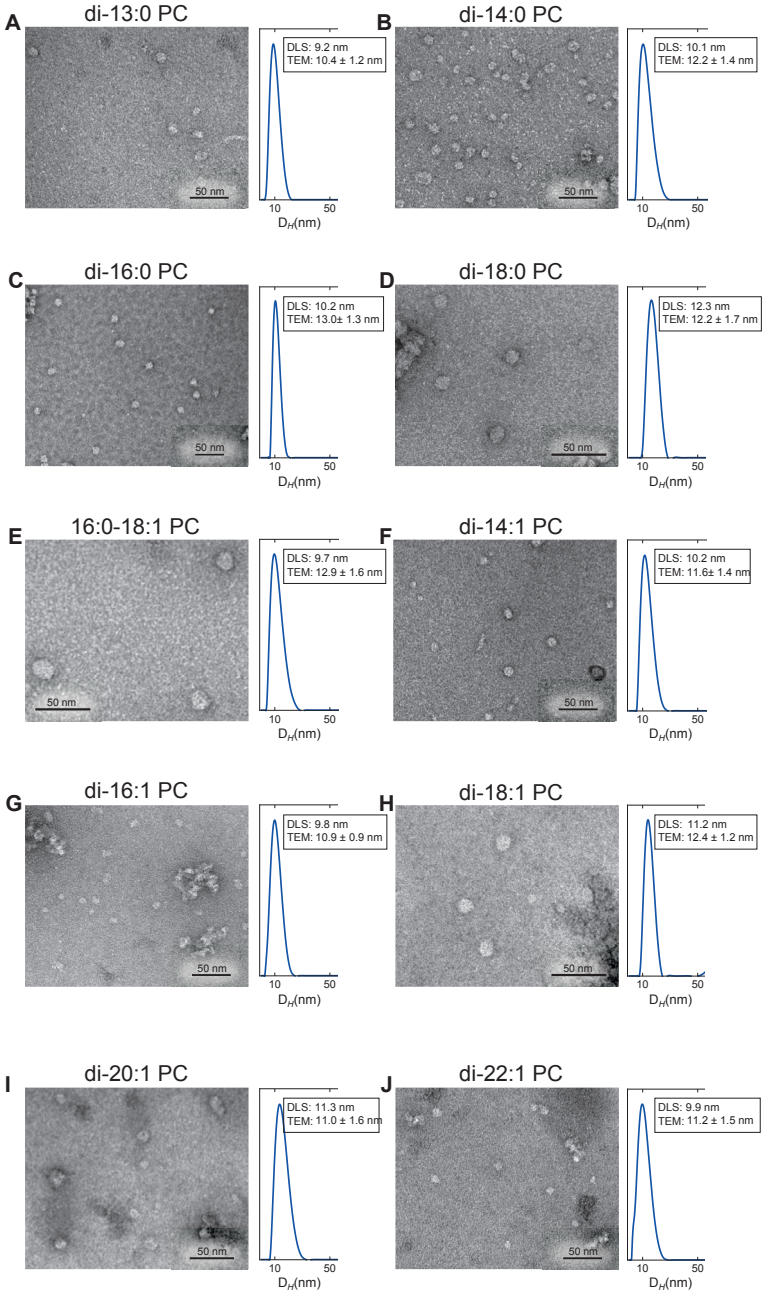

Figure S3
Negative staining transmission electron microscopy (TEM) images and dynamic light scattering (DLS) data on nanodiscs of saturated and unsaturated PC lipids. The average diameter and standard deviation found by TEM is based on the analysis of 20 individual nanodiscs. Scale bars are indicated. Aggregation of nanodiscs and uranyl acetate stain were sometimes found in the samples (for example in panel D and G) and were likely to be induced by drying effects. Aggregates were not considered for analysis. The average diameter and standard deviation found with DLS is based on multiple measurements on single independent samples as described in the method section.

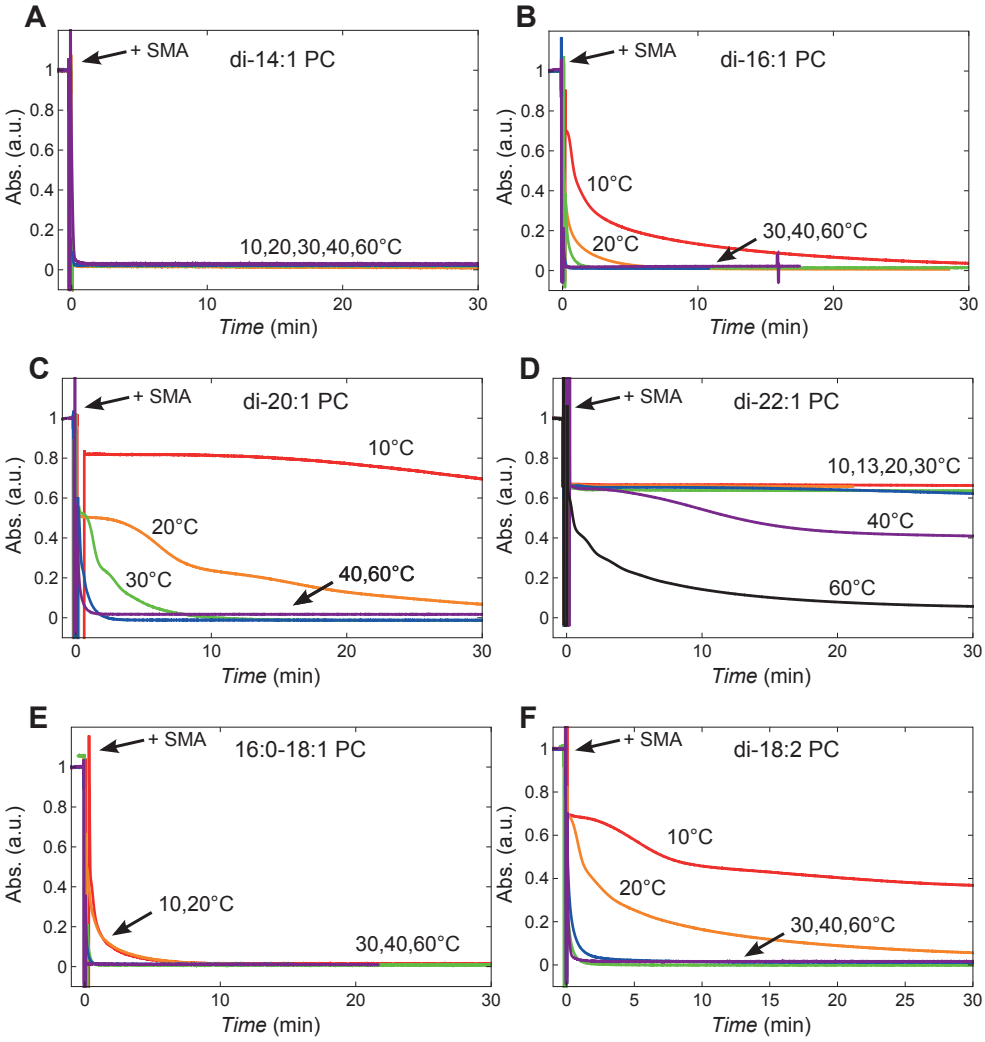

Figure S4

Kinetics of solubilization of unsaturated lipid vesicles (400 nm) induced by the SMA copolymer at a 3:1 (w/w) SMA to lipid ratio. Normalized time traces of the absorbance at 350 nm showing the kinetics of solubilization of (A) di-14:1 PC, (B) di-16:1 PC (Tm= -36 °C), (C) di-20:1 PC vesicles (Tm= -4 °C), (D) di-22:1 PC (Tm= 13 °C), (E) 16:0-18:1 PC (Tm= 2 °C), and (F) di-18:2 PC (Tm= -57 °C).

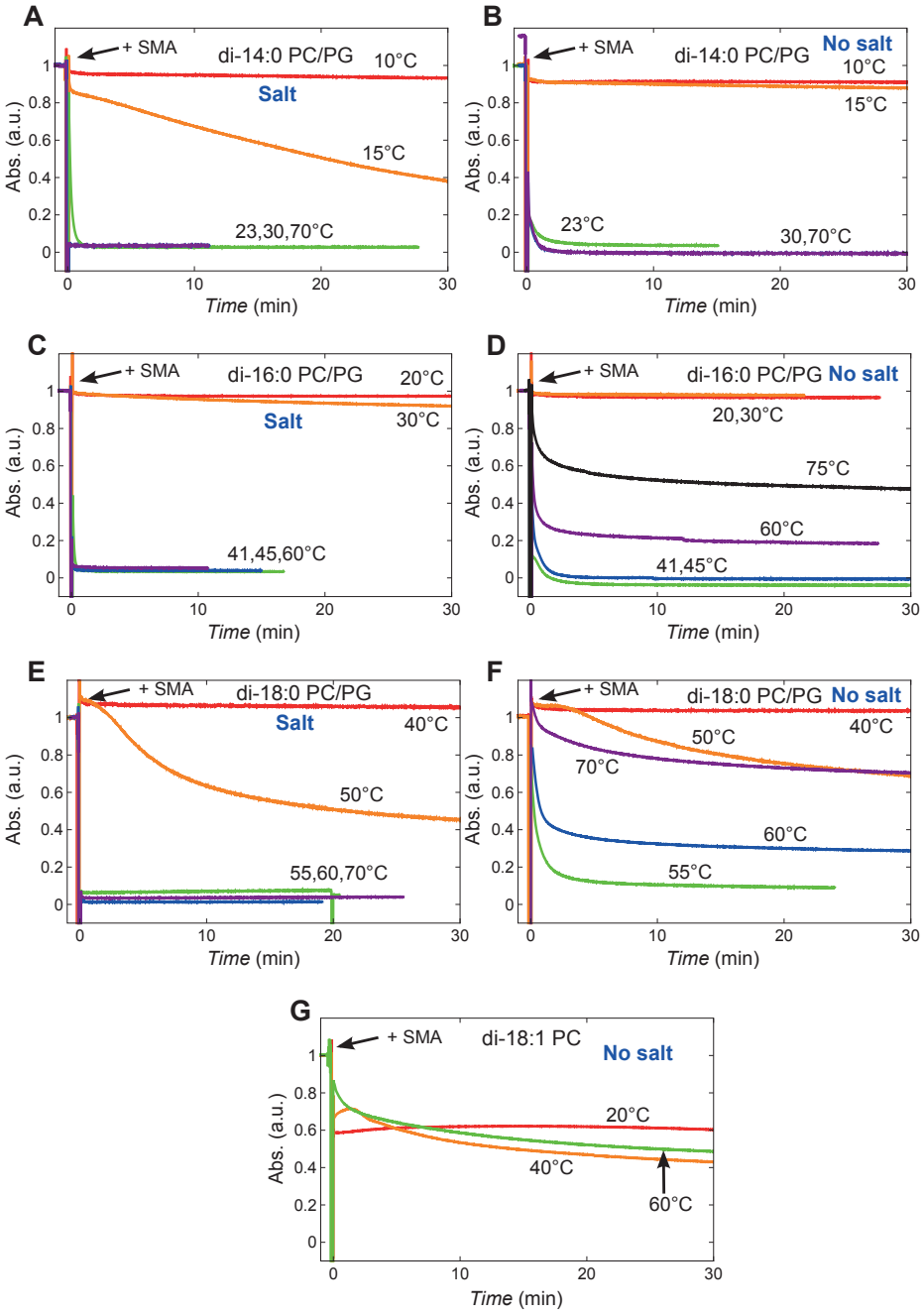

Figure S5

Kinetics of solubilization of saturated PC/PG (4:1) mol lipid vesicles (400 nm) and di-18:1 PC lipid vesicles in the absence of salt induced by the SMA copolymer at a 3:1 (w/w) SMA to lipid ratio. Normalized time traces of the absorbance at 350 nm showing the kinetics of solubilization of (A), (B) di-14:0 PC/PG (Tm= 23°C), (C), (D) di-16:0 PC/PG (Tm= 41°C), (E), (F) di-18:0 PC/PG (Tm= 55°C), and (G) di-18:1 PC (Tm= -20°C) in the presence and absence of salt, respectively.

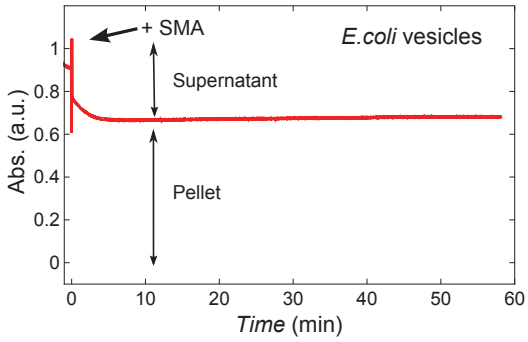

Figure S6
Partial solubilization of vesicles (400 nm) upon the addition of the SMA copolymer at a 1.4:1 (w/w) SMA to lipid ratio at 20°C. Normalized time trace of the absorbance at 350 nm. Supernatant and pellet were obtained after centrifugation as described in the method section.

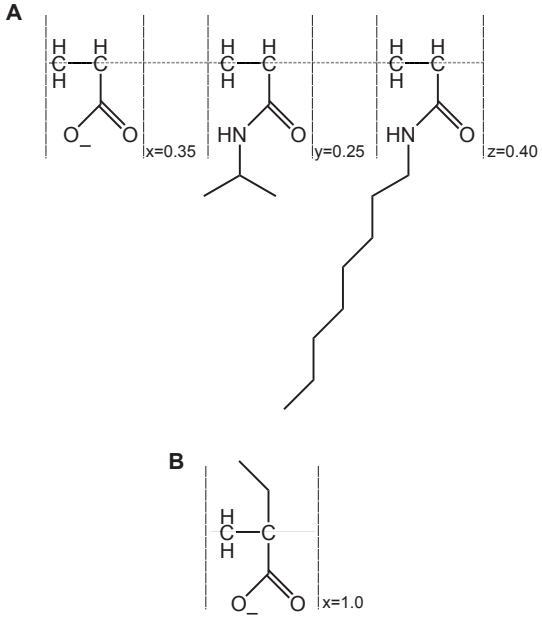

Figure S7
Chemical structures of (A) Amphipol A8-35 and (B) PEAA.

Supporting References

[1] Silvius, D. J. R., 1982. Thermotropic phase transitions of pure lipids in model membranes and their modifications by membrane proteins, volume Lipid-Protein Interactions. John Wiley & Sons, Inc. New York.

CHAPTER 3

EFFECT OF POLYMER COMPOSITION AND PH ON THE SOLUBILIZATION OF LIPID MEMBRANES BY STYRENE-MALEIC ACID COPOLYMERS

S. SCHEIDELAAR, M.C. KOORENGEVEL, C.A. VAN WALREE, J.J. DOMINGUEZ[1], J.M. DÖRR, AND J.A. KILLIAN

S. SCHEIDELAAR, M.C. KOORENGEVEL, C.A. VAN WALREE, J.J. DOMINGUEZ, J.M. DÖRR, AND J.A. KILLIAN, EFFECT OF POLYMER COMPOSITION AND PH ON THE SOLUBILIZATION OF LIPID MEMBRANES BY STYRENE-MALEIC ACID COPOLYMERS. BIOPHYS. J. MANUSCRIPT *SUBMITTED AFTER REVISION.*

KEYWORDS: STYRENE-MALEIC ACID (SMA) COPOLYMER, SMA COMPOSITION, PH, POLYMER CONFORMATION, MEMBRANE SOLUBILIZATION, SMALPS

Abstract

The styrene-maleic acid (SMA) copolymer is rapidly gaining attention as tool in membrane research due to its ability to directly solubilize lipid membranes into nanodisc particles without the requirement of conventional detergents. Although many variants of SMA are commercially available, so far only SMA variants with a 2:1 and 3:1 styrene-to-maleic acid ratio have been used in lipid membrane studies. It is not known how SMA composition affects the solubilization behavior of SMA. Here, we systematically investigated the effect of varying the styrene-to-maleic acid ratio on the properties of SMA in solution and on its interaction with membranes. Also the effect of pH was studied, because the proton concentration in the solution will affect the charge density and thereby may modulate the properties of the polymers. Using model membranes of 1,2-dimyristoyl-*sn*-glycero-3-phosphocholine (di-14:0 PC) lipids at pH > pH_{agg}, we found that membrane solubilization is promoted by a low charge density and by a relatively high fraction of maleic acid units in the polymer. Furthermore, it was found that a collapsed conformation of the polymer is required to ensure efficient insertion into the lipid membrane and that efficient solubilization may be improved by a more homogenous distribution of the maleic acid monomer units along the polymer chain. Altogether, the results show large differences in behavior between the SMA variants tested in the various steps of solubilization. The main conclusion is that the variant with a 2:1 styrene-to-maleic acid ratio is the most efficient membrane solubilizer in a wide pH range.

INTRODUCTION

The styrene-maleic acid (SMA) copolymer has recently gained much attention as solubilizing agent in the field of membrane protein and lipid bilayer research (for reviews see (1–3)). It has been shown that this polymer is able to directly solubilize lipid membranes into nanodisc particles without the help of detergents. In this way, membrane proteins can be solubilized in their native lipid environment (4–7) which was found to help stabilize the protein (5, 6, 8). This has opened options to purify membrane proteins that are unstable in detergent micelles and to study native protein-lipid interactions by biochemical methods. A further advantage of these so-called native nanodiscs is that they are small, with sizes in the range of 10 – 25 nm (4–6, 9–15). This makes them suitable to be characterized by a variety of biophysical approaches including UV/Vis- and fluorescence spectroscopy (5, 6, 8), as well as light scattering techniques (6, 14).

The SMA copolymer consists of hydrophobic styrene and hydrophilic maleic acid monomer units (Fig. 1), and variants with different monomer ratios and molecular weights are commercially available. Table 1 introduces some of these SMA variants and summarizes their physico-chemical properties. In all currently available studies using SMA for membrane solubilization and membrane protein isolation, the polymer variants used had a styrene-to-maleic acid ratio of 2:1 (SMA 2:1) or 3:1 (SMA 3:1). The pH in solubilization experiments is typically in the range of 7.5 to 8.0, independent of the SMA variant used. The choices for using a specific SMA variant and/or pH so far have not been discussed in the literature and the effects of varying polymer composition or pH have not been investigated. Yet these parameters are likely to be important for the solubilization properties of SMA, because they determine essential factors such as hydrophobicity, ionization state, and charge density (16).

In this study, we systematically investigate the effects of polymer composition and pH on the solubilization efficiency of SMA using model membranes. 1,2-Dimyristoyl-*sn*-glycero-3-phosphocholine (di-14:0 PC) is selected as lipid because it has been used in different SMA studies where the mode of action of SMA (3, 15) and the structural properties of styrene maleic acid lipid particles (SMALPs) (14) have been characterized in molecular detail. In the here presented systematic comparison we focus on different steps in the solubilization process of lipid membranes by SMA according to our previously proposed model (15). In brief, polymers that are initially dissolved in aqueous solution insert into the lipid membrane. The insertion of polymers then leads to membrane destabilization and subsequently to the formation of nanodiscs. Along these lines, we will start by addressing some properties of SMA in solution, such as water solubility and molecular conformation of the polymers. Next, we will discuss the insertion of SMA into di-14:0 PC lipids as monitored by lipid monolayer experiments. Third and last, we will focus on the destabilization of membranes by SMA which was investigated by means of a vesicle solubilization assay.

This study provides new insights into the relation between the monomer composition of SMA copolymers and their membrane-solubilizing properties, which will help to select the best SMA copolymer for the solubilization and isolation of membrane proteins from intact cells or for membrane solubilization under specific conditions such as low pH.

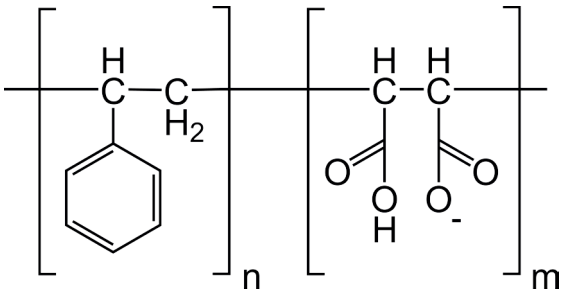

Figure 1
Chemical structure of the SMA polymer at 50% ionization. In this study, polymers with four different average styrene-to-maleic acid ratios of (n:m) = 1.4:1, 2:1, 3:1, and 4:1 have been used.

Table 1
SMA variants used in this study.

Brand name	Styrene-to-maleic acid ratio[a]	Mol % styrene	Mol % maleic acid	M_w (kDa)[b]
Xiran SZ 40005	1.4:1	57	43	5
Xiran SZ 30010	2:1	67	33	10
Xiran SZ 25010	3:1	75	25	10
Xiran SZ 20010	4:1	80	20	11

[a] Based on the acid value of the polymers as provided by the manufacturer
[b] Values were provided by the manufacturer and are given as weight-average molecular weight which is defined as

$$M_w \equiv \frac{\sum M_i^2 n_i}{\sum M_i n_i}$$

MATERIALS AND METHODS

Materials

Lipids were purchased from Avanti Polar Lipids (Alabaster, AL). The following two lipids were used: 1,2-dimyristoyl-*sn*-glycero-3-phosphocholine (di-14:0 PC); 1,2-dimyristoyl-*sn*-glycero-3 phosphoglycerol (di-14:0 PG). The different styrene maleic anhydride (SMAnh) copolymer variants were a kind gift from Polyscope Polymers B.V. (Geleen, The Netherlands). All other chemicals were purchased from Sigma Aldrich (St. Louis, MO).

Styrene-maleic acid (SMA) copolymer preparation

The SMA variants used throughout this study (see Table 1) were prepared in the same way as described in Scheidelaar et al. (15). Briefly, 5% (w/v) SMAnh suspensions in 1 M KOH were refluxed for approximately 4 h after which the SMA was recovered by acid precipitation in 1.1 M HCl. The precipitated SMA was washed at least four times with 10 mM HCl. Finally, the SMA was dried and stored at room temperature until use. 5% (w/v) SMA solutions were prepared by dissolving SMA powder in Milli-Q water while stirring and heating at 60 °C. 1 M KOH solution was slowly added until the SMA powder was completely dissolved and the solution reached pH 8.0. Finally, the obtained SMA solutions were filtered through a 0.22 μm Whatman filter to remove any residual particles that could possibly interfere with turbidity measurements.

Preparation of large unilamellar vesicles

Lipid stock solutions were prepared by dissolving dry lipid powder in chloroform/methanol 9:1 (v/v). Multilamellar vesicles (MLVs) at a concentration of 5 mM phospholipid were prepared by hydration of vacuum-dried lipid films in a 40 mM Britton-Robinson buffer (40 mM of acetic acid, boric acid, and phosphoric acid) containing 150 mM NaCl (will be referred to as standard BR-buffer) at the desired pH between 4.0 and 9.0. After hydration, at least 10 freeze-thaw cycles were performed using a dry ice/ethanol bath and a water bath set at a temperature at least 10 °C above the gel-to-liquid crystalline phase transition temperature (T_m) of di-14:0 PC (T_m= 23 °C). Subsequently, large unilamellar vesicles (LUVs) were prepared by extruding MLV dispersions at least 15 times at temperatures above T_m through a 400-nm Whatman polycarbonate filter using an Avanti mini-extruder (Avanti Polar Lipids). The average size of LUVs was checked by dynamic light scattering (DLS) and was found to be centered around 400 nm. Phospholipid concentrations of LUVs were determined by a phosphate assay according to Rouser et al. (17).

Determination of aqueous solubility of SMA copolymers

The solubility of the different SMA variants in water was determined in the following way. SMA solutions at a concentration of 0.1% (w/v) in a volume of 1.0 mL were prepared in a BR-buffer containing 150 mM, 300 mM, or 500 mM NaCl at the desired pH. The solutions were vortexed and allowed to equilibrate overnight at 20 °C. Subsequently, after vortexing and 10 min equilibration the optical density of the SMA solutions was measured at a wavelength of 350 nm using a Lambda 18 spectrophotometer (PerkinElmer,Waltham, MA) in a 10-mm quartz cuvette holding a total volume of 900 μL. The SMA copolymer is considered to be water soluble in the pH range where an optical density of zero was observed, i.e. the value of pH_{agg} is determined as the pH value of the first examined SMA solution for which a non-zero optical density value was

observed upon decreasing pH.

Acid-base titrations on SMA copolymers

Titrations on SMA copolymers were performed as follows. Milli-Q water was degassed by purging N_2(g) through it for 30 min to remove traces of carbon dioxide. Approximately 40 mg of dried SMA was dissolved in 0.5 mL methanol and added dropwise while stirring to 50 mL degassed Milli-Q water containing 150 mM KCl to assure a constant ionic strength during titration. A constant stream of N_2 saturated with water was gently blown above the surface of the SMA solution to prevent dissolution of carbon dioxide from the air. The temperature was kept at 25 °C using a temperature-controlled water bath. The SMA solution was titrated with a 0.1 M KOH solution using a T80/50 automatic titration system (Schott, Mainz, Germany). A Sevenmulti pH meter (Mettler-Toledo, OH, USA) was used to measure the pH after each addition of base. The pH meter was calibrated using calibration pH buffers at pH 4.0, 7.0, and 12.0 (Sigma Aldrich). The measured pH values were corrected for possible errors caused by non-linear electrode responses in the extreme pH regions using the Avdeef–Bucher four parameter equation (see Supporting M&M). The corrected pH versus added volume of base curves were converted into the ionization state versus pH graphs as described in the Supporting M&M.

Nile Red fluorescence experiments

SMA solutions at a concentration of 0.1% (w/v) and a volume of 1.0 mL were prepared in a standard BR-buffer at the desired pH. A 0.25-mM Nile Red stock solution was prepared in ethanol and added to SMA solutions to a concentration of 1 µM. The critical aggregation concentration (CAC) was determined by preparing SMA solutions in a standard BR-buffer at pH 8.0 at different polymer concentrations in the range from 10^{-5} mg/mL to 10 mg/mL all containing 1 µM of Nile Red. The solutions were vortexed and allowed to equilibrate overnight at 20 °C. Subsequently, Nile Red fluorescence was measured after vortexing and 10 min equilibration on a Varian Cary Eclipse fluorescence spectrophotometer (Agilent Technologies, CA, USA) using a 10-mm quartz cuvette, 5-nm excitation slit, 5-nm emission slit, 1-nm resolution, 0.5-s averaging time, 120-nm/min scan speed, and a Savitzky-Golay smoothing factor of 9. The temperature was controlled with a Peltier device at 20 °C. SMA solutions with Nile Red at different pH were excited at 490 nm because at that wavelength Nile Red molecules in a more hydrophobic environment are selectively excited (18) which is convenient for the detection of a possible collapse of the polymer chain. SMA solutions prepared at different polymer concentrations in order to detect a possible CAC were excited at 550 nm as mentioned in the literature (18). The emission was recorded in the 550 – 700 nm region. The CAC was determined from a weighted least-square fitting

using an adjusted Sigmoidal function given by:

$$\lambda_{\mathrm{em,\ max}} = B + \frac{(A-B)}{1+\left(\frac{[SMA]}{CAC}\right)^{n}}$$

in which A is the average $\lambda_{em,max}$ before the transition, B the average $\lambda_{em,max}$ after the transition, and n the cooperativity factor of the transition.

Lipid monolayer experiments

Surface pressure isotherms versus time were recorded for lipid monolayers of di-14:0 PC and di-14:0 PC/di-14:0 PG (1:1, molar) while adding 20 µL 5% (w/v) SMA, which represents a final concentration of 0.005% w/v. Addition of more SMA did not lead to a further increase in the surface pressure. Lipid monolayers were spread at the air–water interface by addition of a phospholipid solution (0.5 mM in 9:1 v/v chloroform/methanol) until the required initial surface pressure of 25 mN/m was reached. Solvent evaporation and equilibration of the initial surface pressure was allowed for at least 10 min before each experiment. All measurements were performed in a 6.0 x 5.5 cm compartment of a homemade Teflon trough filled with 20 mL standard BR-buffer at the desired pH at 20 ± 1 °C and at constant area while stirring of the subphase. The surface pressure in time was recorded using a commercially available monolayer system (Micro-TroughXS; Kibron, Helsinki, Finland). The increase in surface pressure as determined after 45 min in each experiment was reproducible within ± 1 mN/m.

Vesicle solubilization experiments

The kinetics of solubilization of lipid vesicles (400-nm diameter) by the different SMA variants was monitored by turbidity measurements at 350 nm using a Lambda 18 spectrophotometer (PerkinElmer,Waltham, MA) equipped with a Peltier element. In all experiments a 10-mm quartz cuvette was used holding a total volume of 700 µL. The phospholipid vesicle dispersions (0.5 mM phospholipid in standard BR-buffer at the desired pH) were temperature-equilibrated at 15 °C for at least 10 min before addition of 15 µL of a 5% (w/v) SMA solution yielding a final SMA concentration of 0.1% (w/v). This corresponds to a SMA/phospholipid ratio of 3:1 (w/w). SMA addition was followed by quickly mixing the contents of the cuvette using a 200-µL pipette after which the starting point was set to zero (t = 0). Similar time traces were obtained by stirring the solutions, but this yielded higher noise levels and was therefore avoided. Time traces of the optical density at 350 nm were reproducible for all experiments. The curves displayed in the result section are representative, and from a single experiment.

Analysis of the monomer sequence of SMA copolymers

The monomer sequences of the SMA copolymers were simulated according to the pen-ultimate unit model with the assumption that maleic anhydride monomers do not homo-polymerize (19, 20). In this model, the probability *P* to add a styrene (=1) or maleic anhydride (=2) monomer unit to a growing polymer chain for which the last two monomers are either 21 or 11 are given by

$$P_{211} = \frac{\frac{F_1}{F_1-1} + \sqrt{\left(\frac{F_1}{1-F_1}\right)^2 + 4\left(\frac{2F_1-1}{1-F_1}\right)\left(\frac{r_{11}}{r_{21}}-1\right)}}{2\left(\frac{r_{11}}{r_{21}}-1\right)} \quad \text{and} \quad P_{112} = \frac{-F_1 + (1-F_1)\sqrt{\left(\frac{F_1}{1-F_1}\right)^2 + 4\left(\frac{2F_1-1}{1-F_1}\right)\left(\frac{r_{11}}{r_{21}}-1\right)}}{2(2F_1-1)\left(\frac{r_{11}}{r_{21}}-1\right)}.$$

F_1 is the styrene fraction in the SMA copolymer of interest, and r_{11}/r_{21} is called the reactivity ratio. A value of $r_{11}/r_{21} = 0.43$ was used as has been described by Klumperman et al. (21). Models of 50000 polymers with 100 units each were generated and used for the analysis of styrene segments between two maleic acid units in the polymer. The results were not significantly influenced by the number of polymers and number of monomer units per polymer unless the number was reduced below 100 polymers or below 9 monomer units per polymer. The computer model was implemented and run using the free programming software JustBASIC v1.01 (Framingham, MA). The validity of our pen ultimate unit model was checked by constructing a styrene-centered triad fraction versus SMA composition graph. The graph was compared to the results as produced by Klumperman et al. (21) and found to be completely equal.

RESULTS

A lower styrene fraction in the polymer increases the pH range in which SMA is soluble.

The preparation of nanodiscs from lipid membranes is usually performed by the addition of SMA copolymers in aqueous solution to a membrane suspension. Therefore, knowledge about the aqueous solubility of SMA variants is important for determining their suitability for membrane solubilization under given experimental conditions. A particularly relevant parameter is the pH, because this determines the actual number of charges on the polymers. The pH range in which SMA is soluble is furthermore expected to vary with SMA composition, because a change in the styrene to maleic acid ratio alters both the overall hydrophobicity and the maximum number of charges of the polymer.

Fig. 2A shows the solubility of dfferent SMA variants as function of pH at 150 mM NaCl as monitored by turbidity measurements. In general, SMA copolymers are soluble at high pH, but become insoluble at low pH (starting at pHagg) as indicated by the increase in the apparent optical density due to light scattering from aggregated polymer. The solubility range was found to be dependent on the styrene to maleic acid ratio of the

polymer, an increase in the styrene content decreasing the range in which SMA is water soluble. The SMA 1.4:1, which is the most hydrophilic polymer used, is soluble above pH 4.0, whereas the SMA 4:1, the most hydrophobic polymer used, is only completely soluble in the range from pH 7.0 to 9.0. At first sight, it might be surprising that for this polymer at pH values below 5.0 a decrease in optical density is observed. This however does not correspond to dissolution, but rather signifies polymer precipitation.

Because negative charges on the polymer promote aqueous solubility, it is expected that an increase in ionic strength will decrease the polymer solubility due to Debye charge screening. This is indeed the case as illustrated in Fig. 2B for the SMA 2:1 variant. At higher ionic strength the polymer becomes less soluble shifting the solubility range to higher pH values. Nevertheless, at pH 7.0 or higher the SMA 2:1 variant is soluble even at 500 mM NaCl. Reduced polymer solubility with increasing ionic strength was also found for the other SMA variants (see Fig. S1 in the Supporting Material).

In the following two sections the physical properties of the SMA variants are studied in more detail, starting with the ionization state of the polymers.

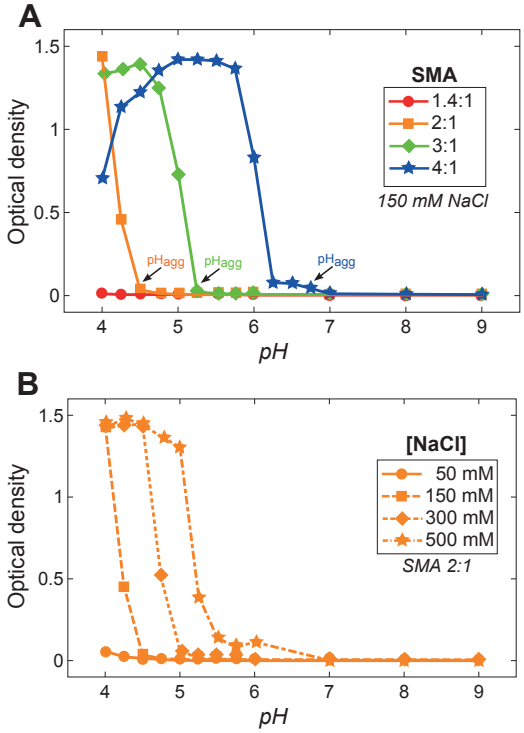

Figure 2

Solubility of SMA in aqueous solution. (A) pH dependence of optical density values of SMA solutions in standard BR buffer, which represent the solubility of the polymers. (B) pH dependent optical density of solutions of the SMA 2:1 variant in BR buffer at varying ionic strength. All measurements were performed at a polymer concentration of 0.1% w/v. The optical density was measured at λ=350 nm. Lines have been added to guide the eye.

The number of charges per unit length of polymer determines the pH range in which SMA is soluble.

The charges of the carboxylic groups of the maleic acid units, and with that the ionization state of SMA, is an important factor for the aqueous solubility of the polymer as well as for the interactions between SMA and lipid membranes (15). The ionization state at a given pH is determined by the acid strength (pKa) of the acid groups in SMA. Since the pKa values of acid groups are sensitive to the nearby presence of hydrophobic groups and negative charges, it is possible that the SMA variants have different pKa values and thus different ionization states at a given pH.

A convenient way to characterize the ionization state of a polymer is to evaluate the ionization state of a monomol unit. The monomol unit is defined as the smallest unit of the polymer that represents its overall composition. This means that per monomol unit each SMA variant will contain one maleic acid unit and a varying number of styrene units according to the styrene to maleic acid ratio of the polymer. In this definition, the maximal number of charges per monomol unit for each SMA variant is always two.

To determine the ionization states of the SMA variants as function of pH, acidbase titrations were performed and the obtained titration curves were converted into ionization states versus pH curves (see supporting M&M). For all SMA variants a titration curve could be produced, except for the most hydrophobic SMA variant, the SMA 4:1. The poor aqueous solubility of this polymer frustrated the recording of a reliable titration curve and is therefore not presented. Fig. 3A shows the protonation state (left axis) and corresponding ionization state (right axis) with the associated apparent pKa values which are found at an ionization state of -0.5 and -1.5. The SMA 1.4:1 variant shows a steep increase in ionization between pH 4.0 and pH 5.0 after which the ionization state increases more gradually to a maximum ionization at above pH 11. The pKa values of the two acid groups in each monomol are well separated with a pK_{a1} value around 4.4 and a pK_{a2} value around 9.0. This large difference is caused by the short distance between the acid groups in the maleic acid units of the SMA copolymer. After ionization of the first acid group, the presence of a negative charge will cause the other acid group to be more resistant towards releasing its proton. In addition, the singly protonated state may be stabilized by an internal hydrogen bridge in the maleic acid group (22).

The 2:1 and SMA 3:1 variants show a more gradual increase in ionization state with curves that are similar in shape. The increase in styrene content decreases the acid strength of SMA as illustrated by the increase in the pK_{a1} value, which is around 5.5 for the SMA 2:1 variant and around 5.9 for the SMA 3:1 variant. Despite their different monomer composition, the curves almost overlap, suggesting that the maleic acid units in both polymers experience a similar chemical environment. This similarity in chemical environment is possibly caused by a similarity in the molecular conformation of these polymer as will be discussed later.

The pH dependent solubility of SMA suggests a prominent role for the number of maleic acid units and their ionization state. The more hydrophobic SMA variants contain fewer maleic acids units per polymer and thus require a higher ionization state to remain water soluble which is essential for their ability to solubilize lipid membranes. This is illustrated in Fig. 3B by combining the solubility curves (Fig. 2A) with the ionization state curves (Fig. 3A). The obtained plot shows the optical density as a function of the average charge density along polymer chains. This linear charge density is given as the number of charges per monomer unit, where a monomer unit represents either maleic acid or styrene. For each of the three SMA variants tested, the aggregation point was found to be at approximately 0.045 charges per monomer unit. This means that the aqueous solubility of SMA is mainly governed by the linear charge density of the polymer which in turn is determined both by pH and the styrene content of the polymer.

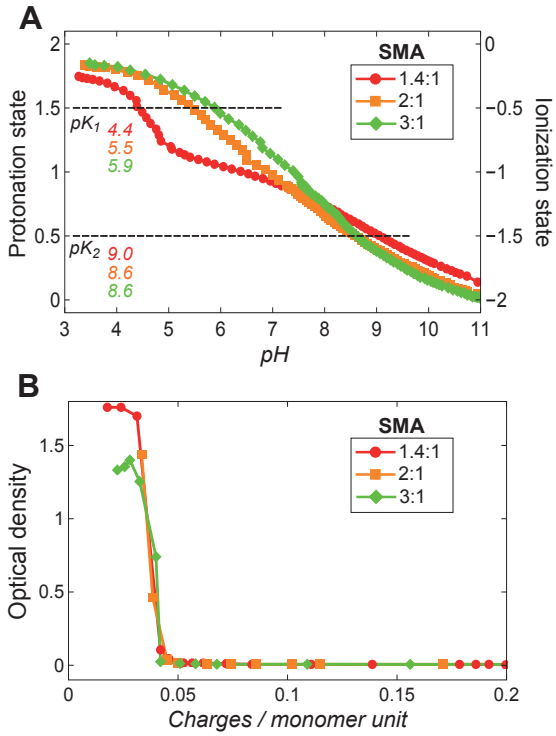

Figure 3

Influence of ionization state on aqueous solubility of SMA. (A) Protonation state (left axis) and corresponding ionization state (right axis) of the monomol of three SMA variants. The monomol is defined as the smallest unit of the polymer that represents its overall monomer composition. Titrations were performed in triplicate and gave very similar results. From the three repeated experiments the maximum error in pKa values is estimated to be ± 0.2. For clarity, only a single representative ionization curve is shown for each SMA variant. (B) Aqueous solubility of the SMA variants as function of the linear charge density, which is given as the number of charges per monomer unit where a monomer unit represents either maleic acid or styrene. This graph was prepared by combining the results that are shown in Fig. 2A and Fig. 3A. Solid lines have been added to guide the eye.

A decrease in pH or an increase in the styrene fraction in the polymer induces a conformational change in SMA.

Since water is a poor solvent for the hydrophobic styrene units in SMA, the polymer may adapt its conformation to minimize energetically unfavorable styrenewater contacts. Indeed, in previous studies it was found that at low pH the 1:1 SMA variant collapses into a globular conformation that contains hydrophobic domains while the polymer is still water soluble (23). Such hydrophobic domains may occur within one polymer chain, but they also may be formed as a consequence of intermolecular interactions, when the polymers are present in aggregates containing multiple polymer chains termed polymeric micelles (24, 25), as will be discussed later. Since the conformational state of the polymers is likely to be important for their interaction with lipid membranes, it was investigated how polymer conformation may be affected by the styrene to maleic acid ratio and pH.

The conformational behavior of the SMA copolymers was studied using the lipophilic fluorophore Nile Red (NR). This fluorophore is solvatochromic which means that its absorption and emission spectra are sensitive to the polarity of the environment in which it resides. In water, NR emits around 660 nm with low intensity, but when it resides in a hydrophobic solvent like t-butanol, NR shows a emission around 620 nm with relatively high intensity (18). Thus, when SMA collapses into a conformation that contains hydrophobic domains, NR should be able to partition into those domains and show a blueshift in emission accompanied by an increase in intensity.

Fluorescence spectra of SMA solutions that contain NR at pH 8.0 are shown in Fig. 4A. The excitation wavelength chosen was at 490 nm, because at this wavelength NR molecules that are present in a hydrophobic environment are selectively excited which makes it convenient to detect a collapsed polymer conformation (18). For the SMA 1.4:1 variant, the emission intensity under these conditions is very low with the emission maximum positioned around 655 nm, indicating that the NR molecules reside in an aqueous environment. However, when the styrene to maleic acid ratio of SMA increases to 2:1 and above, the maximum emission wavelength shifts to lower values and the emission intensity increases dramatically. This means that at least a fraction of the NR molecules experience a more hydrophobic environment, which may then indicate the collapsing of the polymer chain containing hydrophobic domains into which the NR molecules have partitioned. The increase in blueshift and intensity of the emission maximum with increasing styrene fraction of SMA is likely to be caused by an increase in the size and/or number of the hydrophobic domains in the polymer.

To determine how the conformational behavior of SMA is related to pH, the maximum emission wavelength is plotted versus the pH range in which the SMA variants were found to be water soluble (Fig. 4B). Above a pH of 6.0, the SMA 1.4:1 variant shows maximum emission wavelengths values around 655 nm. However, from

pH 6.0 to pH 4.0 the emission maximum decreases to a value of around 615 nm, consistent with a transition of NR to a more hydrophobic environment. Remarkably, the polymer is still well-dissolved at this low pH, although it has become progressively protonated. A likely explanation for these results is a transition from an extended coil conformation of the polymer at high pH to a collapsed conformation at low pH.

The more hydrophobic SMA variants show a completely different trend than the SMA 1.4:1 variant. Despite the relatively high charge density at pH 9.0, the emission maxima are low with values between 615 and 625 nm suggesting the presence of hydrophobic domains. An increase in styrene content of the polymer leads to a lower emission maximum because of the increase in size and/or number of the hydrophobic domains. The small decrease in emission maximum at lower pH values can simply be explained by the decrease in linear charge density of the polymer that decreases the polarity of the polymer. At low pH, close to the point where these polymers start to become insoluble in water, the emission maxima converge to the same value of approximately 615 nm for all SMA variants.

The presence of hydrophobic domains leads to the formation of polymeric micelles

Polymeric micelles are particles that consist of multiple polymer chains. Their formation is the result of intermolecular interactions driven by the balance in the hydrophobic effect and electrostatic repulsions (25). The existence of polymeric micelles can be detected by monitoring the maximum emission wavelength of NR as function of polymer concentration (18, 26). At very low concentrations of SMA, the polymers exist as single molecules. Under these conditions NR molecules in the hydrophobic domains have a relatively hydrophilic environment leading to emission around 650 nm. At higher concentration, the hydrophobic domains of multiple polymers may cluster together in order to decrease the hydrophobic surface area that is in contact with water, thereby decreasing the polarity of the environment of NR shifting the maximum emission to values around 625 nm. The concentration at which a break-point in the maximum emission wavelength is observed that is characteristic for the formation of polymeric micelles is in the case of polymers often referred to as the critical aggregation concentration (CAC) (25), which is analogous to the critical micelle concentration (CMC) in the case of detergents.

Fig. 4C displays the maximum emission wavelength as function of polymer concentration at pH 8.0. The SMA 1.4:1 variant shows maximum emission wavelength values between 650 nm and 660 nm over a large concentration range without showing a clear transition. This indicates that no polymeric micelles are formed, suggesting that this SMA variant exists as single molecules. Only at 10 mg/mL (1% w/v) the maximum emission wavelength drops below 650 nm to approximately 642 nm. This may indicate the start of a CAC or it may indicate the point where the polymers start to physically

influence each other due to crowding effects.

The other three SMA variants do show a clear transition in emission maximum as a function of concentration and all three were found to have a similar CAC value around 5.9 μg/mL. This is in accordance with the formation of polymeric micelles for these variants which already takes place at very low polymer concentration. Despite the difference in styrene content and linear charge densities of these polymer variants, the similar CAC values suggest that their polymeric micelles may be similar in molecular structure.

It is important to note here that the solubility experiments were performed at 1 mg/mL (0.1% w/v), a concentration where these SMA variants exist in the form of polymeric micelles rather than as single polymer chains. The same holds for typical lipid monolayer insertion and membrane solubilization experiments, which also were performed above the CAC of SMA and may have consequences for the interactions between SMA and lipids.

Insertion of SMA into a lipid monolayer is determined by electrostatic interactions and polymer conformation.

One of the steps in the proposed model for the solubilization of lipid membranes by SMA is the insertion of the polymer into the membrane (15). The effect of SMA composition and pH on insertion can be conveniently monitored by lipid monolayer experiments.

Fig. 5A shows the time traces of the insertion of the different SMA variants in a di-14:0 PC lipid monolayer at pH 8.0 and at an initial surface pressure of 25 mN/m. The SMA 1.4:1 variant is able to insert into the lipid monolayer, but increases the surface pressure only by ≈ 5 mN/m. The other SMA variants also insert but induce a remarkably large increase in surface pressure of about ≈ 17 mN/m. Despite their different styrene content and linear charge density, the 2:1, 3:1, and SMA 4:1 variants all show similar insertion behavior at pH 8.0.

The effect of pH on insertion of the polymers is summarized in Fig. 5B where the increase in surface pressure is shown as function of pH (see Fig. S2 for full traces). The SMA 1.4:1 variant shows a strong pH dependent insertion behavior. At high pH the increase in surface pressure is relatively low with a value of ≈ 5 mN/m. However, a drop in pH causes the insertion to increase drastically as demonstrated by the large surface pressure increase of ≈ 20 mN/m at pH 5.0 and 4.0. The surface pressure increase at lower pH can be ascribed to the presence of hydrophobic domains present in the collapsed state of the polymer at low pH. These domains can insert into the lipid monolayer. In addition, the decrease in charge density at lower pH reduces electrostatic repulsions between single polymer chains at the membrane surface and in solution allowing more polymers to insert. The latter is consistent with the notion that electrostatic interactions

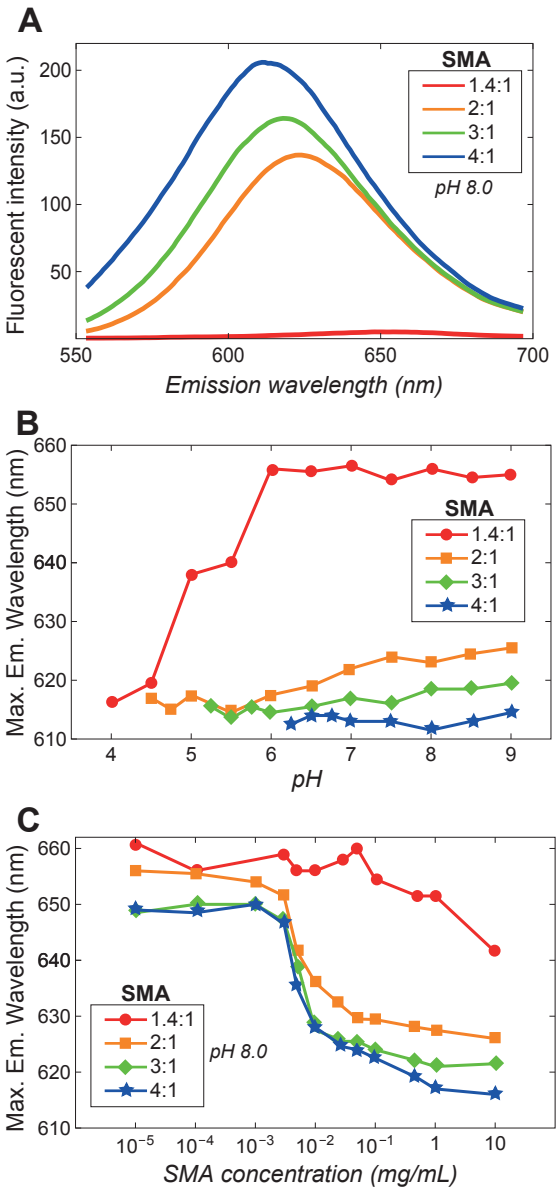

Figure 4

Fluorescence of Nile Red (NR) in SMA solutions to probe polymer conformation. (A) Emission spectra of NR in 0.1% w/v SMA solutions at pH 8.0 excited at 490 nm. (B) Maximum emission wavelength as function of pH in 0.1% w/v SMA solutions (λ_{ex} = 490 nm). (C) Maximum emission wavelength as function of SMA concentration (λ_{ex} = 550 nm). The CAC values for the 2:1, 3:1, and SMA 4:1 variants found to be 5.8, 5.9, and 5.9 µg/ml, respectively. For SMA 1.4:1 a CAC could not be determined in this concentration range. In (B), only the pH range is shown where the SMA variants were found to be water soluble according to Fig. 2A. The maximum emission wavelengths were estimated to have a maximum error of about ± 1 nm (n=3), except for the SMA 1.4:1 variant in (C) where the error is larger (± 3 nm) due to very low emission intensities. Solid lines are added to guide the eye.

are an important factor for the insertion of SMA copolymer into a lipid monolayer, as observed before for a SMA 2:1 variant (15).

The more hydrophobic SMA variants show a large increase in surface pressure already at pH 9.0 (≈ 15 mN/m), which increases by an additional 2 or 3 mN/m when the pH is lowered to 6.0. Remarkable is the similar insertion behavior of the 2:1, 3:1, and SMA 4:1 variants in a wide pH range. Differences in insertion between these variants were initially expected because an increase in their styrene content will increase the hydrophobicity and will decrease the linear charge density of the polymer. By contrast, the similar pH dependent insertion of these three polymers might suggest that despite their different monomer compositions, the overall charge density on the outside of their polymeric micelles is rather similar.

This is supported by results obtained by repeating the monolayer experiments using a lipid mixture containing 50 mol% of the negatively charged di-14:0 PG lipid (Fig. 5C). In this case, the absolute values for the increase in surface pressure are lower due to increased electrostatic repulsion between SMA and PG lipids. However, the trends of surface pressure increase versus pH for the different SMA variants are again very similar.

In summary, efficient insertion of the SMA copolymer into the lipid monolayer only seems to happen under the conditions where the polymer has a collapsed state that contains hydrophobic domains. A decrease in pH allows then more polymer to insert due to the reduction of electrostatic repulsion between SMA copolymers. In the next section, the solubilization efficiency of di-14:0 PC vesicles is investigated to test whether the trends observed for polymer insertion also hold for the complete solubilization process.

The SMA 2:1 variant is the most efficient solubilizer of di-14:0 PC vesicles.

The solubilization of di-14:0 PC vesicles by SMA was monitored by turbidimetry at 15 ˚C, at which temperature the lipids are in the gel phase. Under these conditions solubilization by the SMA copolymer is significantly slowed down as compared to the situation when lipids are at the gel-to-liquid-crystalline phase temperature (T_m) or in the liquid-crystalline phase (15). The slower solubilization in the gel-phase allows a convenient comparison of the effects of monomer composition and pH on the efficiency of solubilization.

Fig. 6A shows the solubilization in time of the different SMA variants at pH 8.0. The SMA 1.4:1does not solubilize the vesicles efficiently. After a quick initial drop, the optical density stabilizes and no further solubilization is observed. When the temperature is increased to the T_m at 23 ˚C (27) (marked by the asterisk), the optical density reduces quickly, showing fast and complete solubilization. This fast solubilization is attributed to the large surface defects that exist in the membrane at T_m, which makes it easy for the polymers to enter into the hydrophobic core and induce nanodisc formation (15).

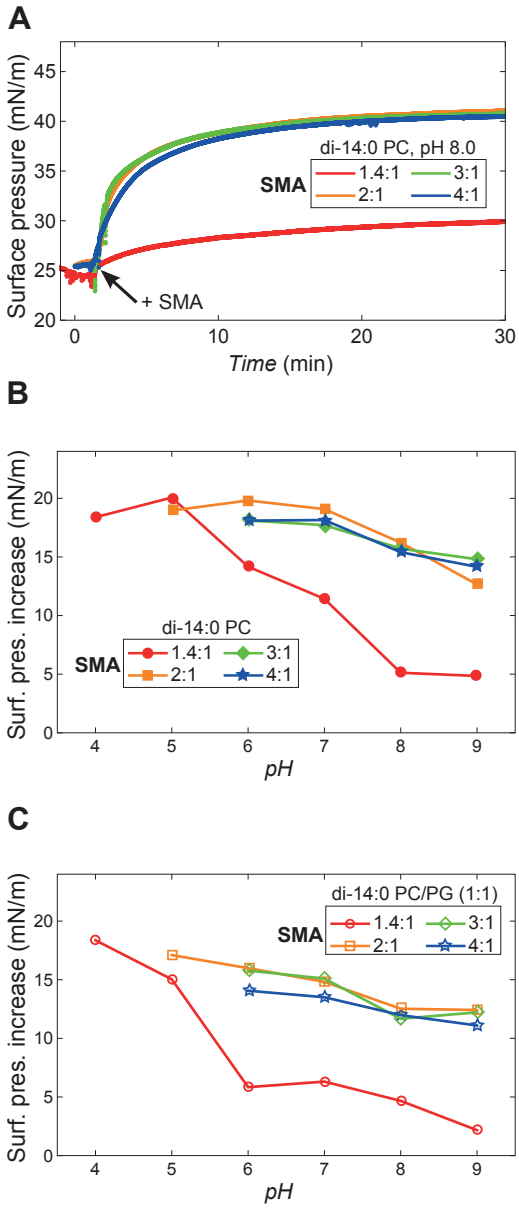

Figure 5

Effect of SMA composition and pH on the insertion into a lipid monolayer. (A) Insertion of the SMA variants into a di-14:0 PC lipid monolayer at pH 8.0. (B) pH dependent insertion of the SMA variants into a di-14:0 PC monolayer. (C) pH dependent insertion of the SMA variants into a di-14:0 PC/PG (1:1) monolayer. In (B) and (C), only the data points are shown where no polymer precipitation was observed during the time course of the experiment. The maximum increase in surface pressure was determined from the time point at which the signal was found to be stable, mostly around 45 min. In all experiments the initial surface pressure was 25 mN/m, a standard BR-buffer was used, and the SMA concentration was 0.005% (w/v). Subsequent addition of more SMA did not increase the observed surface pressure any further, demonstrating that the experiments were performed under conditions of excess SMA. The maximum error in surface pressure increase for each experiment is estimated to be ±1 mN/m as determined from repeated experiments (n=2 or n=3). Lines have been added to guide the eye.

Solubilization at T_m can therefore be used as a control to show that any slow solubilization is due to an inability of the polymer to efficiently insert and destabilize the membrane rather than an inability of the polymer to form nanodiscs.

Fig. 6A furthermore shows that the SMA 2:1 variant solubilizes the vesicles efficiently at pH 8.0 clarifying the vesicle suspension within 20 min. However, when the styrene to maleic acid ratio of the polymer increases, the rate of solubilization decreases again. Nevertheless, both the 3:1 and SMA 4:1 variant display fast solubilization at T_m. Because the 2:1, 3:1, and SMA 4:1 variant also show similar insertion behavior (Fig. 4B) the difference in solubilization between these polymers seems to be determined mainly by the solubilization step where the membrane is destabilized.

The influence of pH on membrane solubilization by the different SMA variants is shown in Fig. 6B (see Fig. S3 for full traces). The SMA 1.4:1 variant solubilizes poorly at high pH, but shows a steep increase in solubilization efficiency when the pH drops below 6.0. This may be ascribed to the increased insertion of the polymer in the membrane (Fig. 5B). This insertion is promoted by the presence of hydrophobic domains in the collapsed conformation of the polymer at low pH (Fig. 4B), and by the decrease in charge density (Fig. 3A) reducing electrostatic repulsions.

The three more hydrophobic SMA variants all show a similar trend: poor solubilization at high pH, an increase in efficiency upon decreasing pH, most likely as a consequence of reduced repulsive electrostatic interactions between polymers, and no solubilization at low pH due to insolubility of the polymers in water. However, there are two distinct differences among these SMA variants. First, the efficiency of SMA to solubilize membranes increases with an increase in the maleic acid content, most clearly visible in the pH range from 7.0 to 9.0. Second, the pH range in which the SMA variants show vesicle solubilization becomes wider with an increase in their maleic acid content, which can be ascribed to an increase in their water solubility.

The open symbols in Fig. 6B denote the pH values where SMA was found not to be water soluble anymore (i.e. below pHagg, see Fig 2A). While the SMA 4:1 variant does not solubilize anymore below its pHagg of 6.75 as expected, the SMA 2:1 (pHagg= 4.50) and SMA 3:1 (pHagg= 5.25) variants surprisingly could not induce solubilization at pH 5.25 and pH 5.75, respectively, where these variants are still water soluble. A possible explanation for this could be that at the membrane surface high local concentrations of polymer promote polymer– polymer interactions. Especially at the verge of water solubility, where the polymers are rather hydrophobic, these polymer–polymer interactions may compete with the ability of the polymer to solubilize or even may induce aggregation of the polymer coated vesicles.

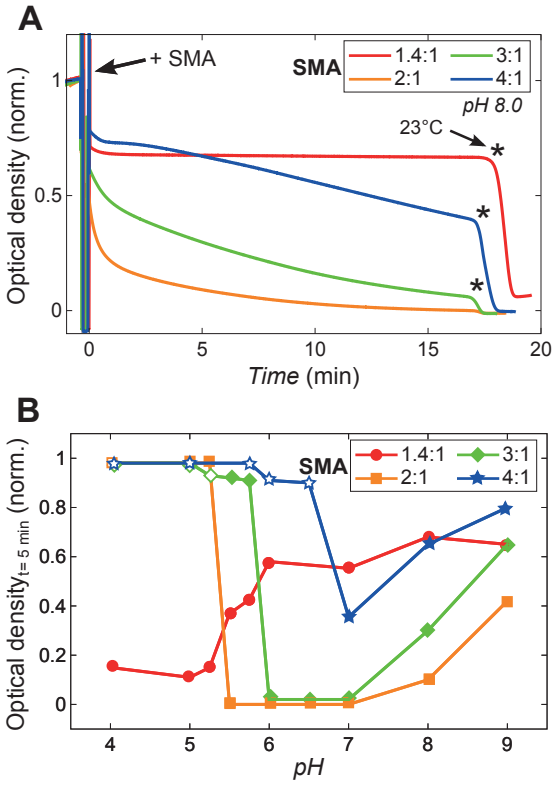

Figure 6
Efficiency of different SMA variants in solubilizing lipid vesicles. (A) Time course solubilization of di-14:0 PC vesicles in standard BR-buffer at 15 °C (gel phase) by the SMA variants at pH 8.0. The asterisks denote the time where the temperature was set to 23 °C which is the Tm of di-14:0 PC. (B) Normalized optical density values of the di-14:0 PC vesicle suspension 5 min after SMA addition. The open symbols in (B) indicate that the polymer is not water soluble in the absence of lipids according to Fig. 2A. Experiments where the optical density increased above the value before SMA addition have been set to a value of 1 to enhance the clarity of the figure. The relative optical density values could be reproduced with a maximum error estimated to be ± 0.05 A units (n=3). All measurements were performed at a polymer concentration of 0.1% (w/v). Solid lines have been added to guide the eye.

The styrene to maleic acid ratio poorly represents the monomer sequence along the polymer chain.

To gain further insight into the nature of the differences in solubilization behavior between the 2:1, 3:1, and SMA 4:1 variants, the monomer sequence of SMA was analyzed. The SMA variants used in this study have styrene-to-maleic acid ratios in the range from 1.4:1 to 4:1. This ratio reflects the average fraction of the monomer units in the polymer, but does not specify anything about the monomer sequence. Yet, this might be an important factor for the mode of action of SMA; for example, a hypothetical polymer chain that has only two separate blocks, one consisting of polystyrene and one consisting of poly-maleic acid, is expected to have very different solubilization properties

than a polymer with perfectly alternating monomer units.

The monomer sequence of a SMA copolymer is determined by the polymerization kinetics of the styrene and maleic anhydride monomers. The polymerization process can be described by the so called pen ultimate-unit model (19, 20). In brief, this model implies that the chances of whether a styrene or maleic anhydride monomer is added to a growing polymer chain is determined by (i) the styrene to maleic acid ratio of the polymer and (ii) the composition of the last two monomers on the growing chain. Another property of the polymerization of SMA copolymers is that maleic anhydride never adds to a maleic anhydride on the growing chain (19, 20). This means that neighboring maleic acid units in the SMA copolymer are virtually non-existent.

The monomer sequence of the SMA variants used here was modeled by simulating SMA copolymer formation according to the pen ultimate-unit model with the assumption that maleic anhydride monomers do not homo-polymerize. From the simulated polymers that all had a length of 100 monomer units (see M&M for more details) the number of adjacent styrene monomer units in each styrene segment between consecutive maleic acid units were counted. If the monomer sequence would be perfectly represented by the styrene to maleic acid ratio then, for instance, the SMA 2:1 variant would have two adjacent styrene monomer units between every two maleic acid units along the polymer chain: MA-*S*-*S*-MA-*S*-*S*-MA-*S*-*S*-MA-etc.

Fig. 7 shows the relative abundance of styrene monomer units that are present in styrene segments of different length. The SMA 1.4:1 variant consists mainly of styrene segments of one and two styrene units (example of a possible monomer sequence in that case: MA-*S*-*S*-MA-*S*-MA-*S*-MA-*S*-*S*-MA-etc.). However, the SMA 2:1 variant has only about 35% of all styrene monomer units in a segment of two. The 2:1 styrene-to-maleic acid ratio of this polymer thus poorly represents the monomer sequence since most of the incorporated styrene units are present in longer or shorter styrene segments. This becomes progressively worse when the styrene fraction in SMA increases. The distribution of styrene segments increases and the distribution becomes much broader. Some polymers of the SMA 4:1 may even contain styrene segments that are twelve styrene monomer units long. Thus, analysis of the polymer sequence shows that an increase in the styrene fraction of SMA not only leads to a lower number of maleic acid units per polymer chain, but also leads to a more heterogeneous distribution of these maleic acid monomer units. The possible influence of the monomer sequence on membrane solubilization will be addressed in the discussion.

DISCUSSION

Previous studies on SMA and lipid membranes all described the use of either the 2:1 or the SMA 3:1 variant at a pH in the range of about 7.5 to 8.0. However, it is not clear whether these were the optimal choices, because the effects of varying the

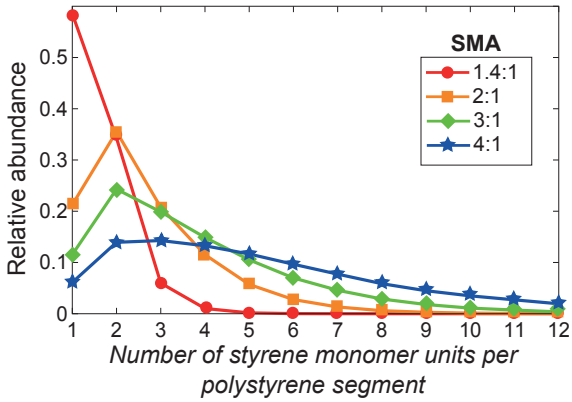

Figure 7
Analysis of the monomer sequence of the SMA variants. The distribution of styrene monomer units is shown as a function of the length of the polystyrene segment they are found in. Each polystyrene segment connects two consecutive maleic acid units. Polymer models were generated according to the pen-ultimate unit model with the assumption that neighboring maleic acid units are non-existent (see M&M and references therein for details of this model). Solid lines have been added to guide the eye.

styrene to maleic acid ratio or pH had not been investigated. In this study, we aimed at understanding how SMA composition and pH affect the molecular conformation and solubilization properties of SMA. We discuss the results of the different SMA variants tested according to Fig. 8, which is a schematic overview that summarizes the outcomes of the experiments. Finally, we suggest how the SMA copolymer might be improved in its composition in order to increase its solubilizing efficacy.

The SMA 1.4:1 variant

The SMA 1.4:1 variant clearly has properties very different from the other SMA variants. It is the most hydrophilic variant used and unlike the other variants it is water soluble over the whole pH range from 4.0 to 9.0, as demonstrated by the solubility experiments. Nile Red fluorescence experiments revealed that at a pH of about 5.5 this polymer variant undergoes a conformational change from a random coil at high pH to a collapsed conformation in which the polymer contains hydrophobic domains at low pH. A likely explanation for this pH dependence is that the decrease in ionization state and thus charge density of the polymer upon going from pH 6.0 to 4.0, as determined by acid–base titration, shifts the balance between electrostatic repulsions favoring the random coil conformation at high pH and the hydrophobic effect favoring the collapsed conformation at low pH. When the polymer has a random coil conformation it does not insert and solubilize membranes efficiently due to its high charge state (blue region in Fig. 8). However, when it adopts a collapsed conformation the polymer can solubilize membranes efficiently (green region in Fig. 8). Under these conditions at low pH, the hydrophobic domains insert into the membrane while the lower charge density decreases

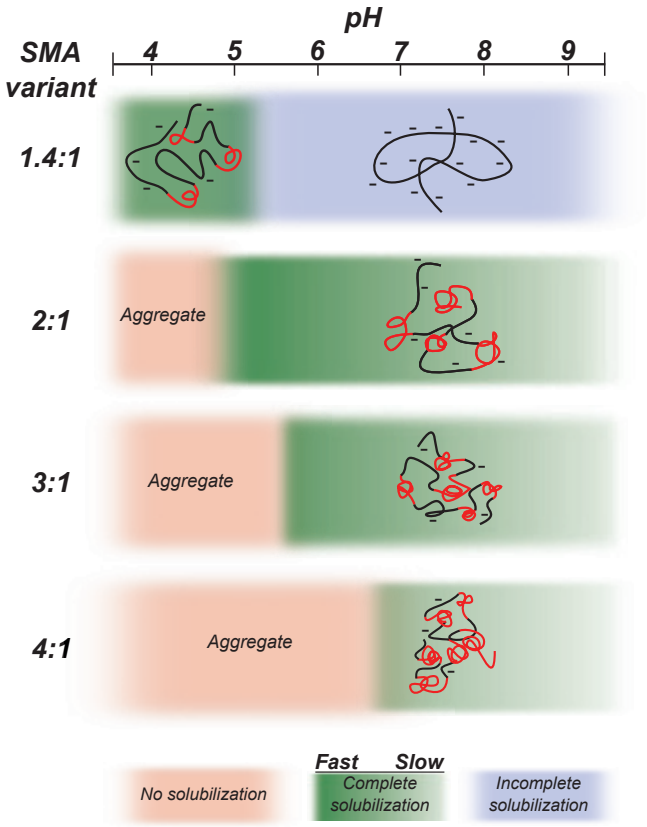

Figure 8
Schematic diagram that summarizes the effect of SMA composition and pH on the molecular conformation and solubilization efficiency of the SMA copolymer. The polymer conformation is shown as a cartoon in which the hydrophobic domains enriched in styrene units are shown in red, while the maleic acid-rich part of the polymer is shown in black. The efficiency of solubilization is depicted according to a color coding (see above). Dark green means complete and fast solubilization, blue means that solubilization is induced but remains incomplete, whereas red means that the polymer is not able to solubilize at all.

repulsive electrostatic interactions between polymers allowing more polymer to insert into the membrane. Although this polymer may not be very suitable for solubilization of (biological) membranes or membrane proteins at neutral and high pH, it would in fact be the polymer of choice for special circumstances that require a low pH.

The 2:1, 3:1, and SMA 4:1 variants

The more hydrophobic SMA variants all have similar properties that are different from the 1.4:1 variant in two ways. First, they are not soluble over the whole pH range. Instead, they aggregate at low pH (red region). An increase in the styrene to maleic ratio narrows the pH range in which the polymers are water soluble since the linear charge density decreases as well. Second, the polymers do not adopt a random coil conformation

at high pH, but they have a collapsed conformation at every pH value tested. This observed polymer conformation is in line with a previous study that showed that SMA copolymers with a 3:1 styrene to maleic acid ratio contain hydrophobic domains in their polymer conformation as investigated by pyrene fluorescence (24). An increase in the styrene fraction of the polymer also leads to an increase in the number and/or sizes of the hydrophobic domains. This was demonstrated by Nile Red fluorescence experiments; the more hydrophobic SMA variants showed only a small change in maximum emission wavelength over the whole pH range, and the polymers with higher styrene fractions had lower maximum emission values, indicating an increased overall hydrophobicity of the polymers. However, we should note that we cannot rule out that the collapsed conformation of SMA copolymers in general can actually be described by a single hydrophobic styrene rich core that is stabilized by a hydrophilic maleic acid rich outside, rather than by the presence of multiple hydrophobic domains. It is also possible that the polymers possess a combination of both, the exact structure depending on many variables, such as polymer composition, ionization state, and type of solvent (25, 28).

The more hydrophobic SMA variants all show efficient insertion into the membrane as observed by lipid monolayer experiments. These similarities of the polymers indicate that the presence of hydrophobic domains enriched in styrene is necessary for efficient membrane insertion. However, the absolute fraction of styrene in the polymer does not seem to be very important for insertion. This is in contrast to the solubilization of membranes where the styrene fraction in the polymer does play a significant role. Solubilization of di-14:0 PC vesicles in the gel phase showed that an increase in the styrene fraction in general decreases the efficiency of the polymer to solubilize a lipid membrane. Because monolayer experiments showed similar insertion behaviors for these polymers, and because fast and complete solubilization was observed at the T_m of di-14:0 PC lipids (23 °C), it may be concluded that the differences in solubilization efficiency between the polymers are mainly due to differences in efficiency to destabilize the membrane.

The main difference between the SMA variants is not only the absolute number of styrene and maleic acid units in the polymer, but also the distribution of these monomers along the polymer chain. We propose that these two properties are important for destabilization of the membrane and that in particular a relatively high fraction of maleic acid in the polymer promotes efficient destabilization. The absolute amount of maleic acid in the polymer is important because it is energetically unfavorable for its carboxylic acid groups to come into contact with the hydrophobic core of the membrane upon polymer insertion. This will speed up the thermodynamically favorable formation of nanodiscs (1, 29). The distribution of the monomer units is important because a more homogenous distribution along the polymer chain can promote uncoiling of the styrene rich hydrophobic domains (30) into the specific conformation that is required

to stabilize a nanodisc. It has been shown that when bound to the nanodisc, the SMA copolymer adopts a specific uncoiled conformation forming a rim around the lipids in which, with the styrene groups intercalating between the acyl chains and the maleic acid groups pointing towards the aqueous solution (14).

Altogether, our results show that the SMA 2:1 copolymer has the most beneficial properties for efficient membrane solubilization. Its hydrophobic domains ensure efficient membrane insertion, while its relatively high maleic acid content ensures a relatively homogeneous distribution of styrene and maleic acid along the polymer, leading to efficient destabilization of the membrane. Moreover, the high maleic acid fraction guarantees water solubility at pH values above 5.0, providing the broadest pH range for solubilization of all polymers tested.

Concluding remarks

In this study, the effects of polymer composition and pH on membrane solubilization have been systematically investigated. This will help to select the best SMA copolymer variant for solubilization of membranes and membrane proteins under specific conditions. For example, the SMA 1.4:1 would be the best option for membrane solubilization at low pH, which may be required for stabilization of specific membrane proteins. As another example, it has been shown that increasing the salt concentration may promote membrane solubilization by reducing repulsive interactions between SMA copolymers and membranes with anionic lipids (15). However, here we show that increasing the salt concentration has a risk of inducing polymer aggregation depending on the pH of the solution. Especially when using polymers with a relatively high styrene-to-maleic acid ratio this may become a problem, because for such polymers aggregation in the presence of salt may occur close to physiological pH.

All the presented results can be explained by the differences in the styrene-to-maleic acid ratios of the polymers. However, at this point we cannot exclude that the deviating behavior of the SMA 1.4:1 variant is in part due to a lower weight-average molecular weight (Table 1). The SMA variants used in this study typically have a broad distribution in molecular weight (see (1) for more detail) and it is not understood yet how this affects membrane solubilization. Thus, it is possible that an optimum for membrane solubilization exists for SMA molecules of a defined molecular weight/polymer chain length. The effect of polymer length on membrane solubilization is presently being investigated in our laboratory. Depending on the outcome, it may be worthwhile to consider options for the synthesis of SMA copolymers that have both a defined monomer composition and molecular weight. These polymers then would allow systematic investigation of the optimal composition and length for membrane solubilization, which may widen the range of membrane proteins from various origin that can be isolated and characterized using the SMA solubilization approach.

SUPPLEMENTARY MATERIAL

An online supplement to this article can be found by visiting BJ Online at http://www.biophysj.org.

ACKNOWLEDGMENTS

We thank Pieter Hanssen & Onno Looijmans from Polyscope Polymers B.V. (Geleen, The Netherlands) for providing the SMAnh copolymers and for useful discussions on the fabrication of SMA copolymers, and we thank Eefjan Breukink for critically reading the manuscript and providing helpful comments. We are grateful for the contributions of Maria Teresa Piane & Ilias Theodorakopoulos as master student in our group. Financial support of the research program of the Foundation for Fundamental Research on Matter, the Netherlands Organization for Scientific research (NWO-ECHO grant No. 711.013.005 to J.D.P.) and the seventh framework program of the European Union (Initial Training Network 'ManiFold', Grant 317371 to J.M.D.) are gratefully acknowledged.

References

[1] Dörr, J. M., S. Scheidelaar, M. C. Koorengevel, J. J. Dominguez, M. Schäfer, C. A. van Walree, and J. A. Killian, 2016. The styrene– maleic acid copolymer: a versatile tool in membrane research. European Biophysics Journal 45:3– 21. http://dx.doi.org/10.1007/s00249-015-1093-y.

[2] Lee, S. C., S. Khalid, N. L. Pollock, T. J. Knowles, K. Edler, A. J. Rothnie, O. R.T.Thomas, and T. R. Dafforn, 2016. Encapsulated membrane proteins: A simplified system for molecular simulation. Biochimica et Biophysica Acta (BBA)-Biomembranes http://www.sciencedirect.com/science/article/pii/S0005273616300797.

[3] Wheatley, M., J. Charlton, M. Jamshad, S. J. Routledge, S. Bailey, P. J. La-Borde, M. T. Azam, R. T. Logan, R. M. Bill, T. R. Dafforn, and D. R. Poyner, 2016. GPCR– styrene maleic acid lipid particles (GPCR– SMALPs): their nature and potential. Biochemical Society Transactions 44:619–623. http://www.biochemsoctrans.org/content/44/2/619.

[4] Long, A. R., C. C. O'Brien, K. Malhotra, C. T. Schwall, A. D. Albert, A. Watts, and N. N. Alder, 2013. A detergent-free strategy for the reconstitution of active enzyme complexes from native biological membranes into nanoscale discs. BMC Biotechnol 13:41. http://dx.doi.org/10.1186/1472-6750-13-41.

[5] Dörr, J. M., M. C. Koorengevel, M. Schäfer, A. V. Prokofyev, S. Scheidelaar, E. A. W. van der Cruijsen, and Dafforn, 2014. Detergent-free isolation, characterization, and functional reconstitution of a tetrameric K+ channel: The power of native nanodiscs. PNAS 111:18607–18612.

[6] Swainsbury, D. J. K., S. Scheidelaar, R. van Grondelle, J. A. Killian, and M. R. Jones, 2014. Bacterial Reaction Centers Purified with Styrene Maleic Acid Copolymer Retain Native Membrane Functional Properties and Display Enhanced Stability. Angewandte Chemie International Edition n/a– n/a. http://dx.doi.org/10.1002/anie.201406412.

[7] Prabudiansyah, I., I. Kusters, A. Caforio, and A. J. Driessen, 2015. Characterization of the annular lipid shell of the Sec translocon. Biochimica et Biophysica Acta (BBA) - Biomembranes 1848:2050 – 2056. http://www.sciencedirect.com/science/article/pii/S0005273615002047.

[8] Jamshad, M., J. Charlton, Y.-P. Lin, S. J. Routledge, Z. Bawa, T. J. Knowles, M. Overduin, N. Dekker, T. R. Dafforn, R. M. Bill, D. R. Poyner, and M. Wheatley, 2015. G-protein coupled receptor solubilization and purification for biophysical analysis and functional studies, in the total absence of detergent. Bioscience Reports 35. http://www.bioscirep.org/content/35/2/e00188.

[9] Knowles, T. J., R. Finka, C. Smith, Y.-P. Lin, T. Dafforn, and M. Overduin, 2009. Membrane Proteins Solubilized Intact in Lipid Containing Nanoparticles Bounded by Styrene Maleic Acid Copolymer. Journal of the American Chemical Society 131:7484– 7485. http://pubs.acs.org/doi/abs/10.1021/ja810046q, pMID: 19449872.

[10] Jamshad, M., Y.-P. Lin, T. J. Knowles, R. A. Parslow, C. Harris, M. Wheatley, D. R. Poyner, R. M. Bill, O. R. Thomas, M. Overduin, and T. R. Dafforn, 2011. Surfactant-free purification of membrane proteins with intact membrane environment. Biochemical Society Transactions 39:813–818. http://www.biochemsoctrans.org/bst/039/0813/bst0390813.htm.

[11] Orwick, M. C., P. J. Judge, J. Procek, L. Lindholm, A. Graziadei, A. Engel, G. Grabner, and A. Watts, 2012. Detergent-Free Formation and Physicochemical Characterization of Nanosized Lipid-Polymer Complexes: Lipodisq. Angewandte Chemie International Edition 51:4653– 4657. http://dx.doi.org/10.1002/anie.201201355.

[12] Orwick-Rydmark, M., J. E. Lovett, A. Graziadei, L. Lindholm, M. R. Hicks, and A. Watts, 2012. Detergent Free Incorporation of a Seven-Transmembrane Receptor Protein into Nanosized Bilayer Lipodisq Particles for Functional and Biophysical Studies. Nano Letters 12:4687– 4692. http://pubs.acs.org/doi/abs/10.1021/nl3020395.

[13] Paulin, S., M. Jamshad, T. R. Dafforn, J. Garcia-Lara, S. J. Foster, N. F. Galley, D. I. Roper, H. Rosado, and P. W. Taylor, 2014. Surfactant-free purification of membrane protein complexes from bacteria: application to the staphylococcal penicillin-binding protein complex PBP2/PBP2a. Nanotechnology 25:285101. http://dx.doi.org/10.1088/0957-4484/25/28/285101.

[14] Jamshad, M., V. Grimard, I. Idini, T. J. Knowles, M. R. Dowle, N. Schofield, P. sridhar, Y.-P. Lin, R. Finka, M. Wheatley, O. R. Thomas, r. E. Palmer, M. Overduin, C. Govaerts, J.-M. Ruysschaert, K. Edler, and T. R. Dafforn, 2014. Structural analysis of a nanoparticle containing a lipid bilayer used for detergent-free extraction of membrane proteins. Nanotechnology DOI: 10.1007/s12274-015-0560-6.

[15] Scheidelaar, S., M. Koorengevel, J. Pardo, J. Meeldijk, E. Breukink, and J. Killian, 2015. Molecular Model for the Solubilization of Membranes into Nanodisks by Styrene Maleic Acid Copolymers. Biophysical Journal 108:279 – 290. http://www.sciencedirect.com/science/article/pii/S0006349514046773.

[16] Goddard, A. D., P. M. Dijkman, R. J. Adamson, R. I. dos Reis, and A. Watts, 2015. Chapter Nineteen - Reconstitution of Membrane Proteins: A GPCR as an Example. In A. K. Shukla, editor, Membrane Proteins– Production and Functional Characterization, Academic Press, volume 556 of Methods in Enzymology, 405 – 424. http://www.sciencedirect.com/science/article/pii/S0076687915000178.

[17] Rouser, G., S. Fleischer, and A. Yamamoto, 1970. Two dimensional thin layer chromatographic separation of polar lipids and determination of phospholipids by phosphorus analysis of spots. Lipids 5:494– 496. http://dx.doi.org/10.1007/BF02531316.

[18] Stuart, M. C. A., J. C. van de Pas, and J. B. F. N. Engberts, 2005. The use of Nile Red to monitor the aggregation behavior in ternary surfactant-water-organic solvent systems. Journal of Physical Organic Chemistry 18:929– 934. http://dx.doi.org/10.1002/poc.919.

[19] Klumperman, B., and K. F. O'Driscoll, 1993. Interpreting the copolymerization of styrene with maleic anhydride and with methyl methacrylate in terms of the bootstrap model. Polymer 34:1032 – 1037. http://www.sciencedirect.com/science/article/pii/003238619390226Z.

[20] Klumperman, B., 2010. Mechanistic considerations on styrene-maleic anhydride copolymerization reactions. Polym. Chem. 1:558– 562. http://dx.doi.org/10.1039/B9PY00341J.

[21] Klumperman, B., 1994. Free radical copolymerization of styrene and maleic anhydride. Kinetic studies at low and intermediate conversion. Ph.D. thesis, DSM Research & Technical University Eindhoven, The Netherlands.

[22] Haines, T., 1083. Anionic lipid headgroups as a proton-conducting pathway along the surface of membranes: a hypothesis. PNAS 80:160164.

[23] Tonge, S., and B. Tighe, 2001. Responsive hydrophobically associating polymers: a review of structure and properties. Advanced Drug Delivery Reviews 53:109 – 122. http://www.sciencedirect.com/science/article/pii/S0169409X0100223X, polymeric Materials for Advanced Drug Delivery.

[24] Claracq, J., S. F. C. R. Santos, J. Duhamel, C. Dumousseaux, and J.-M. Corpart, 2002. Rigid Interior of Styrene-Maleic Anhydride Copolymer Aggregates Probed by Fluorescence Spectroscopy. Langmuir 18:3829– 3835. http://dx.doi.org/10.1021/la0117146.

[25] Olea, A. F., 2012. Hydrophobic Polyelectrolytes, John Wiley & Sons, Inc., 211– 233. http://dx.doi.org/10.1002/9781118165850.ch7. [26] Tang, R., W. Ji, and C. Wang, 2011. pH-Responsive Micelles Based on Amphiphilic Block Copolymers Bearing Ortho Ester Pendants as Potential Drug Carriers. Macromolecular Chemistry and Physics 212:1185– 1192. http://dx.doi.org/10.1002/macp.201100007.

[27] Silvius, D. J. R., 1982. Thermotropic phase transitions of pure lipids in model membranes and their modifications by membrane proteins, volume Lipid-Protein Interactions. John Wiley & Sons, Inc. New York.

[28] Dobrynin, A. V., , and M. Rubinstein, 1999. Hydrophobic Polyelectrolytes. Macromolecules 32:915– 922. http://dx.doi.org/10.1021/ma981412j.

[29] Vargas, C., R. C. Arenas, E. Frotscher, and S. Keller, 2015. Nanoparticle self-assembly in mixtures of phospholipids with styrene/maleic acid copolymers or uorinated surfactants. Nanoscale 7:20685–20696. http://dx.doi.org/10.1039/C5NR06353A.

[30] Murnen, H. K., A. R. Khokhlov, P. G. Khalatur, R. A. Segalman, and R. N. Zuckermann, 2012. Impact of Hydrophobic Sequence Patterning on the Coil-to-Globule Transition of Protein-like Polymers. Macromolecules 45:5229– 5236. http://dx.doi.org/10.1021/ma300707t.

Supporting Material

Supporting Materials & Methods

Acid–base titrations on SMA copolymers

The measured pH values were corrected for possible errors caused by non-linear electrode responses in the extreme pH regions using the Avdeef–Bucher four-parameter equation (**Eq. S1**) (1). In here, pH is the measured pH, α and k are constants, p_cH is the corrected pH, j_H and j_{OH} the parameters that account for the non-linear electrode responses in the extreme pH regions, K_w the water dissociation constant, and $[H^+]$ the corrected proton concentration. The parameters α, k, j_H, and j_{OH} were determined from weighted least squares fitting of alkalimetric titrations of known concentrations of HCl (blank titration) (1). Once the values of these parameters are known, Eq. S1 can be solved for every data point in the titration curve.

(**Eq. S1**) $pH = \alpha + k\ p_cH + j_H\ [H^+] + j_{OH}\ \frac{K_w}{[H^+]}$

Curves of the corrected pH versus the volume of added base were converted into curves of protonation state/ionization state versus pH according to **Eq. S2** in which n_H is the protonation state, $[OH^-] = 10^{(p_cH - pK_w)}$ the hydroxide concentration, $[K^+] = \frac{[KOH]}{V_{initial}+V_{added}}$ the potassium concentration, $[H^+] = 10^{-p_cH}$ the proton concentration and $[SMA]$ the monomol concentration of the SMA variant used in the titration.

(**Eq. S2**) $n_H = 2 + \frac{[OH^-]-[K^+]-[H^+]}{[\mathrm{SMA}]}$

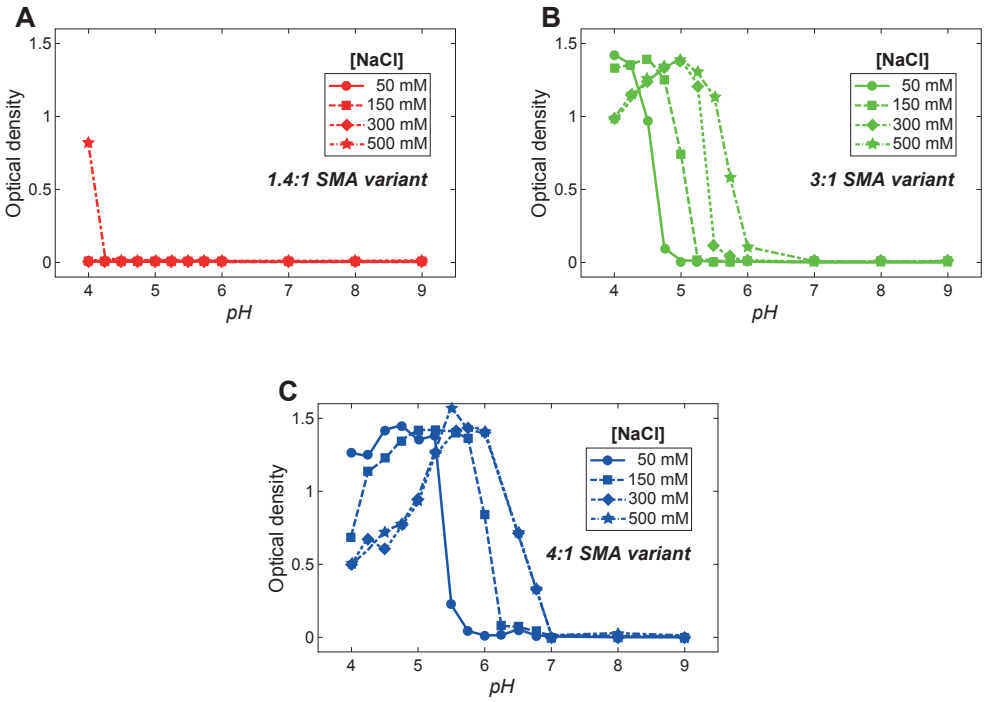

Figure S1
pH dependent solubility of different SMA variants in a 40 mM Britton-Robinson buffer at varying ionic strengths. All measurements have been performed at a polymer concentration of 0.1% (w/v). The optical density was measured at λ=350 nm. Lines have been added to guide the eye.

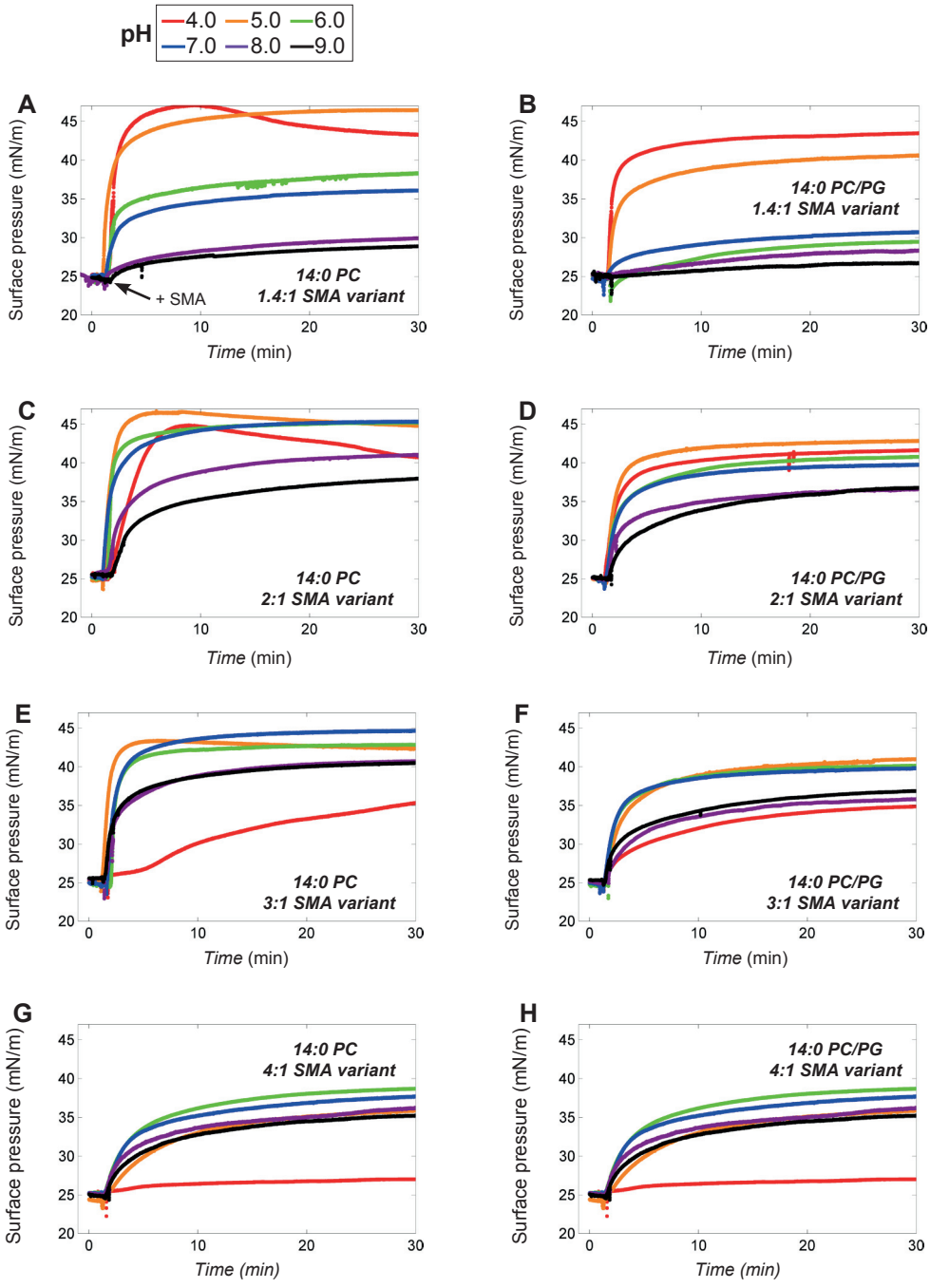

Figure S2

Insertion of the SMA variants in a di-14:0 PC and di-14:0 PC/PG (1:1 mol) lipid monolayer at different pH values. In all experiments the initial surface pressure was 25 mN/m, NaCl concentration is 150 mM and SMA concentration is 0.005% (w/v). Subsequent addition of more SMA did not increase the observed surface pressure any further, demonstrating that the experiments were performed under conditions of excess SMA.

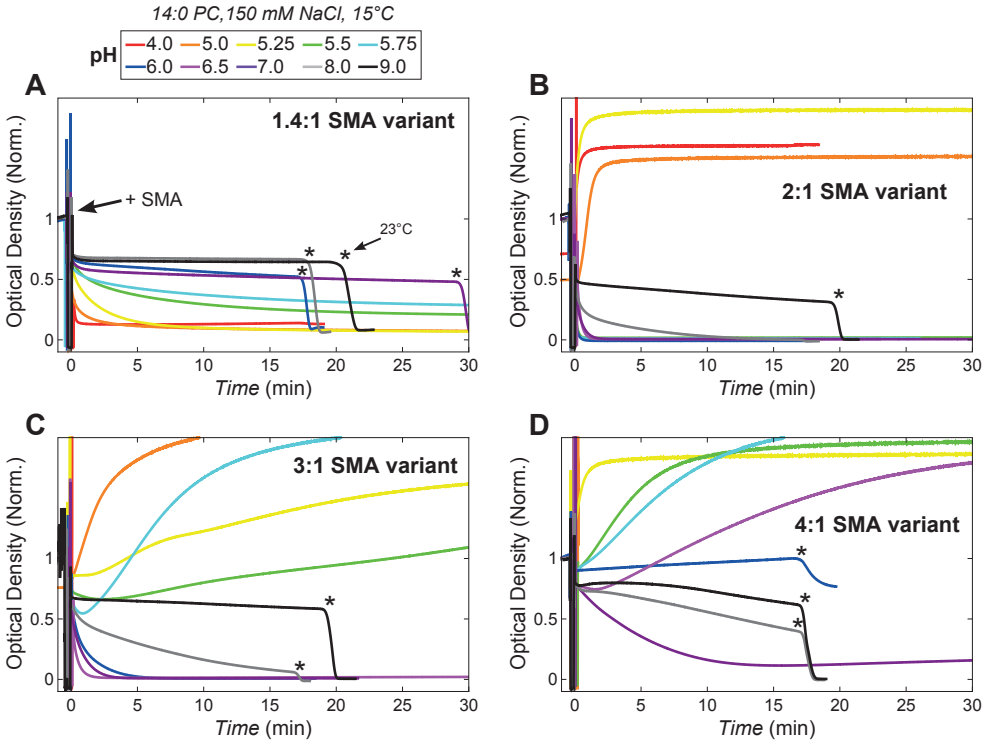

Figure S3
Time course solubilization of di-14:0 PC vesicles at 15 °C (gel phase) by each SMA variant at different pH values. The asterisks denote the time where the temperature was set to 23 °C, which is the Tm of 14:0 PC (2). For the 2:1, 3:1, and SMA 4:1 variants at lower pH, the relative optical density rises above 1. This means that the optical density increases after SMA addition, which is likely to be caused by polymer aggregation or clustering of vesicles due to the polymer. All measurements have been performed at a polymer concentration of 0.1% (w/v).

Supporting References

[1] Avdeef, A., 1983. Weighting scheme for regression analysis using pH data from acid-base titrations. Analytica Chimica Acta 148:237–244. http://www.sciencedirect.com/science/article/pii/S0003267000851685.

[2] Silvius, D. J. R., 1982. Thermotropic phase transitions of pure lipids in model membranes and their modifications by membrane proteins, volume Lipid-Protein Interactions. John Wiley & Sons, Inc. New York.

CHAPTER 4

BACTERIAL REACTION CENTERS PURIFIED WITH STYRENE MALEIC ACID COPOLYMER RETAIN NATIVE MEMBRANE FUNCTIONAL PROPERTIES AND DISPLAY ENHANCED STABILITY

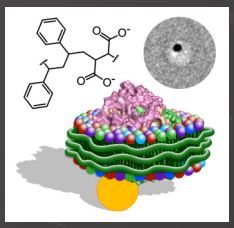

DAVID J. K. SWAINSBURY,[+] STEFAN SCHEIDELAAR,[+] RIENK VAN GRONDELLE, J. ANTOINETTE KILLIAN, AND MICHAEL R. JONES

[+] THESE AUTHORS CONTRIBUTED EQUALLY TO THIS WORK.

D.J.K. SWAINSBURY & **S. SCHEIDELAAR**, R. VAN GRONDELLE, J.A. KILLIAN, AND M.R. JONES, (2014), BACTERIAL REACTION CENTERS PURIFIED WITH STYRENE MALEIC ACID COPOLYMER RETAIN NATIVE MEMBRANE FUNCTIONAL PROPERTIES AND DISPLAY ENHANCED STABILITY. *ANGEW. CHEM. INT. ED.* 53, 11803–11807.

KEYWORDS: DETERGENTS, MEMBRANE PROTEINS, NANODISC REACTION CENTERS, STYRENE MALEIC ACID

Abstract

Integral membrane proteins often present daunting challenges for biophysical characterization, a fundamental issue being how to select a surfactant that will optimally preserve the individual structure and functional properties of a given membrane protein. Bacterial reaction centers offer a rare opportunity to compare the properties of an integral membrane protein in different artificial lipid/surfactant environments with those in the native bilayer. Here, we demonstrate that reaction centers purified using a styrene maleic acid copolymer remain associated with a complement of native lipids and do not display the modified functional properties that typically result from detergent solubilization. Direct comparisons show that reaction centers are more stable in this copolymer/lipid environment than in a detergent micelle or even in the native membrane, suggesting a promising new route to exploitation of such photovoltaic integral membrane proteins in device applications.

Biophysical characterization of integral membrane proteins and their use in biotechnology usually requires their removal from the native lipid bilayer environment using detergents. Identification of the best detergent for purification of a given protein typically involves a process of trial and error, and the final choice may not fulfill all requirements for optimal stability or native functionality[1]. An important concern is the extent to which transfer of a protein to a detergent environment strips away structurally and functionally important annular lipids. A recently developed alternative is the use of an amphipathic styrene maleic acid (SMA) copolymer (Figure 1A) that is able to remove the protein from a membrane with its associated lipids intact in the form of a protein/lipid nanodisc bounded by the polymer[2-5]. This approach has been used to successfully solubilize membrane proteins from artificial liposomes[2,6] and native membranes[7,8], and is one of a number of alternatives being developed for housing membrane proteins outside the native membrane[9].

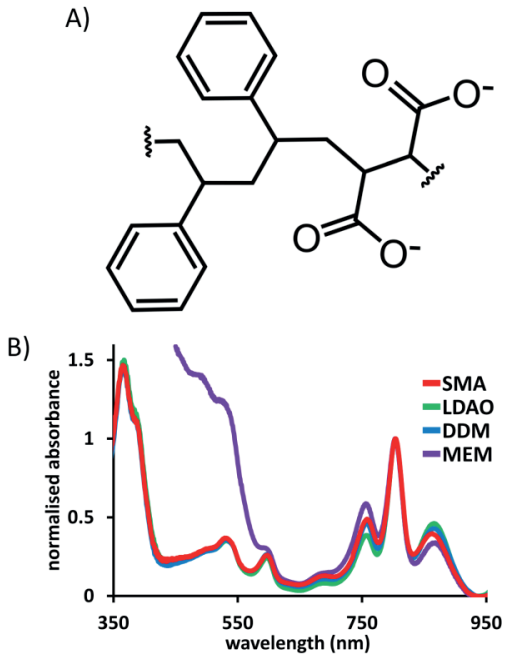

Figure 1
(A) Chemical structure of the average repeating unit of the SMA copolymer. (B) Absorbance spectra of *Rba. sphaeroides* RCs in different environments after normalisation and correction for scattering (for details see Experimental Procedures in the Supporting Information).

In the present report, a SMA copolymer (Figure 1A) was used to purify the photoreaction center (RC) from the purple bacterium *Rhodobacter (Rba.) sphaeroides*. This classic alphahelical integral membrane pigment-protein complex, which has a strong, distinctive bacteriochlorin absorbance spectrum that provides information on both structural and functional integrity, has been structurally characterized[10] and subjected to an extensive biophysical characterization.[11] It conducts an extremely efficient charge separation that lends itself to applications in photovoltaics, molecular electronics, biosensing, and photocatalysis.[12] However, such applications require the preparation of large amounts of protein that is structurally stable and optimally active. This presents challenges because the functional properties of the RC are known to be modulated when it is removed from the native membrane, [13–15] and its stability is known to be dependent on the detergent/lipid environment.[16]

To determine the usefulness of the SMA copolymer as a new vehicle for housing integral membrane proteins such as RCs, the properties of SMA-purified RCs were systematically compared with those of purified RCs in the commonly used detergents *N,N*-dimethyldodecylamine *N*-oxide (LDAO) and *n*-dodecyl β-D-maltoside (DDM), as well as with those of RCs in intact native photosynthetic membranes. The latter

was possible through the use of a strain of *Rba. sphaeroides* that lacks the genes that encode the native light-harvesting complexes, leaving the RC accessible as the sole bacteriochlorin-containing complex in the membrane.[13] RCs modified with a His_{10} tag were solubilized by the addition of SMA, LDAO or DDM, and purified using nickel affinity and size-exclusion chromatography (see Supporting Information).

The strong absorbance spectrum of the RC provides a simple way to monitor its properties. In the near-infrared it comprises three main bands arising from the bacteriochlorin cofactors (Figure 1B), the relative intensities and wavelength maxima of which are known to be modulated somewhat by the lipid/detergent environment of the protein[13,14]. The SMA-solubilized RCs had an absorbance spectrum that was similar to that of RCs in native membranes or solubilized in either LDAO or DDM, showing that it is structurally intact in the SMA/lipid nanodiscs (Figure 1B). Small differences in intensity of the bands at 865 and 760 nm in the four preparations are a consequence of the sensitivity of cofactors at, or close to, the surface of the protein to its detergent/lipid environment.

The purity of LDAO- or DDM-solubilized RCs can be conveniently quantified from the ratio between protein absorbance at 280 nm and bacteriochlorophyll absorbance at 802 nm[17]. Pure RCs gave a ratio of approximately 1.3, as determined by SDS-PAGE.[17] For SMA-solubilized RCs purified to the same degree, this ratio was around 1.5 (see Figure S1 in Supporting Information for discussion).

Analysis by dynamic light scattering (DLS) showed that the average diameter of purified SMA/lipid/RC nanodiscs was 12.2 ± 7.1 nm, significantly larger than RCs in micelles formed from DDM (7.8 ± 4.8 nm) or LDAO (5.1 ± 2.7 nm). Images of SMA/lipid/RC nanodiscs obtained by negative staining transmission electron microscopy (TEM; Figure 2A) showed particles with a diameter of approximately 12–15 nm, in good agreement with the DLS data. Pre-treatment of the discs with 5 nm Ni-nitrilotriacetic acid functionalized gold nanoparticles allowed detection of the RC His_{10} tag. The off-center position of this gold nanoparticle in most labeled nanodiscs (Figure 2A) is consistent with the expected off-center location of the His_{10} tag on the periplasmic surface of the RC. This point is illustrated in the schematic model of a gold-labeled SMA/lipid/RC nanodisc in Figure 2B. It may also indicate that individual RCs do not necessarily reside at the center of their SMA/lipid nanodisc.

Thin layer chromatography (TLC) of extracts of RC native membranes (Figure 3A) identified phosphatidylethanolamine (PE), phosphatidylcholine (PC), cardiolipin (CL), phosphatidylglycerol (PG) and sulphoquinovosyl diacylglycerol (SQDG) as the principal lipids, in agreement with previous studies on wild-type strains of *Rba. sphaeroides*[18]. In the SMA/lipid/RC nanodiscs, the same five lipids were found in similar proportions (Figure 3B), supporting the usefulness of nanodiscs as mimics of the membrane environment for biophysical analysis of a membrane protein in the pure

state. Analysis of the phosphate content of SMA-purified RCs produced an estimate of around 150 lipids per RC, corresponding to a nanodisc with an average of three layers of lipids around the RC, assuming that a typical lipid occupies an area of approximately 0.7 nm^2 [19] (Figure 2B). No lipids could be detected by TLC in samples of RCs solubilized in either DDM or LDAO at up to a five-fold higher protein concentration, showing that they had been stripped away to below detectable levels (Figure 3A).

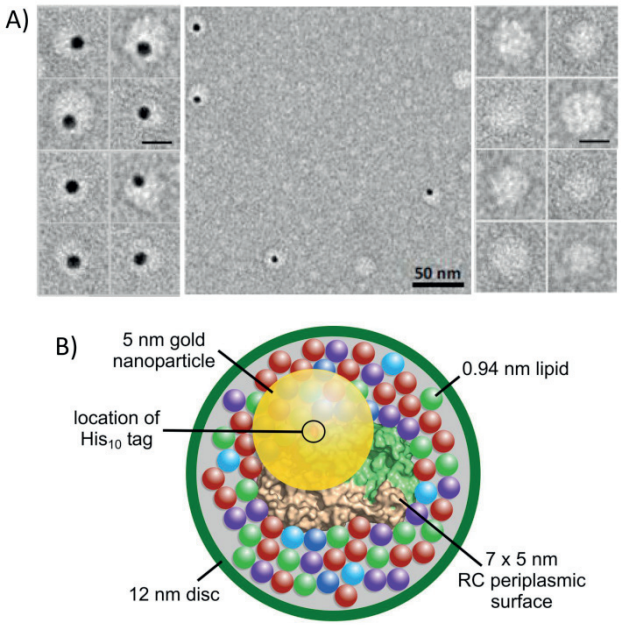

Figure 2.
Negative stain TEM and model of SMA-purified RC nanodiscs. (A) The galleries show enlarged views (scale bar 10 nm) of individual nanodiscs with (left) and without (right) 5 nm gold nanoparticles attached to the His_{10} tag of the RC. (B) Model of a nanodisc viewed orthogonal to the roughly elliptical periplasmic surface of the RC. Distances are diameters of the protein (lime/beige), each of five species of lipid (75 in total—colors and proportions as Figure 3B), a gold nanoparticle (yellow) and an overall nanodisc (green). The gold nanoparticle is centered on the point of connection of the His_{10} tag to the periplasmic surface of the RC (red, circled).

Modulation of the functional properties of RCs by the lipid/detergent/copolymer environment was investigated through two readily-measurable parameters. First, the mid-point oxidation potential was determined for the bacteriochlorophyll pair (P865) that form the primary donor of electrons during charge separation (see Section 2 of the Supporting Information). This was achieved by monitoring the intensity of their ground-state absorbance band at 865 nm during cycling of the applied potential in an electrochemical cell;[20] this band bleaches when P865 is oxidized (inset to Figure 4A).

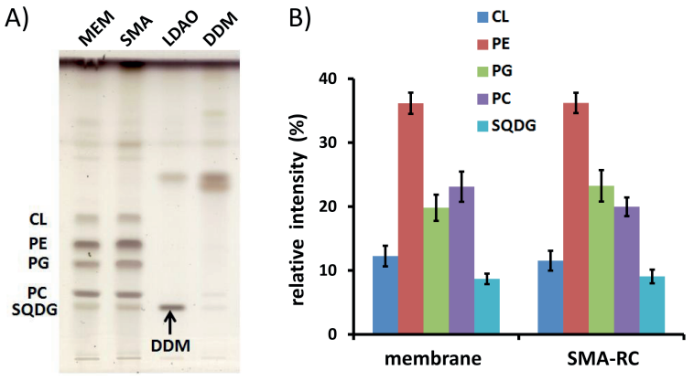

Figure 3.
Lipid content of intact membranes and purified RCs. (A) Lipid profiles determined by TLC. Lipids were identified by running pure samples of each as a standard (not shown). Bands above the labelled lipids are attributed to RC pigments. DDM was visualized but LDAO did not stain. Additional bands in the DDM and LDAO profiles are unidentified. (B) Relative populations of lipids in intact membranes and SMA/lipid nanodiscs from six independent lipid extractions, quantified by densitometry.

The mid-point potential obtained for RCs in SMA/lipid nanodiscs, 443 mV, was similar to the 449 mV obtained for RCs in native membranes and significantly lower than the 465 and 485 mV obtained for RCs in DDM and LDAO, respectively (Figure 4A).

Second, a short flash of light was used to form the charge-separated state $P865^{+}Quinone^{-}$, and the rate of recombination of this radical pair was monitored through recovery of bleaching of the same ground-state absorbance band of P865 (Figure 4B). Photo-excitation triggers membrane-spanning charge separation on a picosecond timescale, the electron arriving first on the tightly bound Q_A ubiquinone acceptor and then moving on to, if present, the dissociable Q_B ubiquinone acceptor (see the Supporting Information, Section 2, and Figure S2). In LDAO-solubilized RCs, the $P865^{+}Q_B^{-}$ radical pair recombines with a lifetime of around 1 s whereas, if the Q_B quinone is not present, the $P865^{+}Q_A^{-}$ radical pair recombines with a lifetime of around 100 ms[11a,21]. Furthermore, the recombination of $P865^{+}Q_B^{-}$ is slower in RCs in a lipid bilayer than in RCs in detergent by a factor of 1.5 to 3.5, depending on the lipid system used[15]. The kinetics of $P865^{+}Quinone^{-}$ recombination are therefore dependent on the occupancy of the Q_B site and on the detergent/lipid environment of the RC.

In the present study, charge recombination was monitored in the presence of a 7.5-fold molar excess of UQ_0 to largely reconstitute ubiquinone binding at the Q_B site. The overall rate of charge recombination in RCs in SMA/lipid nanodiscs was similar to that of RCs in native membranes, and in both cases was clearly slower than in RCs in LDAO or DDM (Figure 4B). Parameters from biexponential fits to the data in Figure 4B are shown in Table S1 in the Supporting Information; based on the lifetime of the dominant slower component, τ_2, recombination in membranes of SMA/lipid nanodiscs

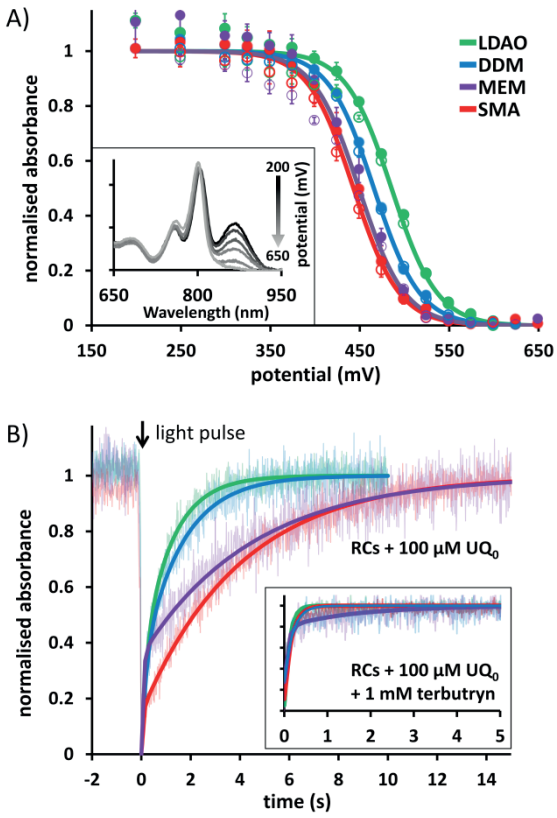

Figure 4

Effect of lipid/detergent/copolymer environment on RC functional properties. (A) Average variation of P865 absorbance over three oxidative (filled circles) and reductive (closed circles) titrations of applied potential, with the standard error for each data point. Solid lines show fits with the Nernst equation (n = 1); mid-point potentials are reported in the text and were associated with a standard error of ± 3 mV or less. Inset: Absorbance spectra for SMA-solubilized RCs at progressively increasing applied potentials (black to light-grey), showing oxidative bleaching of the band at 865 nm. (B) Averaged traces (faded lines) showing photobleaching and recovery of the same absorbance band at 865 nm, normalized to the maximal extent of the initial bleach for comparison. Inset: recovery portion of transients recorded in the presence of 1 mM terbutryn.

(4.5 and 4.0 s, respectively) was between 2.5 and 4 times slower than in RCs in detergent (1.2 s for LDAO, 1.6 s for DDM). The slower $P865^{+}Q_B^{-}$ charge recombination in RCs in intact membranes is a well-known phenomenon that is attributable to small environmental modulations of redox potential and/or reorganization energy. The fact that this modulation is preserved in RCs in SMA/lipid nanodiscs underlines the way in which they preserve a membrane-like environment for the purified protein.

One application of purple bacterial RCs is their use as the active element in a photoelectrochemical biosensor for herbicides such as terbutryn that block photosynthetic electron transfer in plants by binding to the equivalent Q_B site in Photosystem II[22]. To

be useful in this way, it is necessary for the intramembrane Q_B site in the bacterial RC to be accessible to herbicide molecules. In the present study, the addition of terbutryn led to almost complete loss of the slow-phase of recombination from Q_B^-, yielding a single component with a time constant of less than 200 ms, attributable to the recombination of $P865^+Q_A^-$ (inset to Figure 4B and Table S1 in the Supporting Information). This result shows that accessibility of the Q_B site to inhibitors is not occluded by housing RCs in SMA/lipid nanodiscs.

Successful exploitation of *Rba. sphaeroides* RCs in applications requires the protein to be stable under illumination. The integrity of the protein can be monitored through the bacteriochlorin absorbance bands at 803 and 760 nm, which show distinctive decreases in amplitude as the protein unfolds (see inset to Figure 5A; note that the band at 865 nm photobleaches immediately on strong illumination). As in previous work[23], degradation of the protein in response to light stress was assayed by simply monitoring the decrease in absorbance at 803 nm during incubation of RCs at room temperature in the light. The rate of photodegradation of RCs in SMA/lipid nanodiscs was similar to that for RCs in DDM, which has a reputation for being a "stabilizing" detergent, but was markedly slower than for either RCs in native membranes or LDAO micelles (Figure 5A). Although LDAO is used extensively for work on RCs, having the advantage that it is relatively inexpensive, it is not particularly stabilizing, and so the difference in the rate of photodegradation of RCs in DDM and LDAO was not a surprise.

More of a surprise was the relative instability of RCs embedded in native membranes when exposed to light stress. This instability was also observed for control samples incubated at room temperature in the dark for a period of weeks (Figure 5B). Over the first three days, the stability of RCs in native membranes was similar to that of RCs in nanodiscs or in DDM, but then steadily declined over the next two weeks. A possible explanation for the instability of the RCs in membranes is that protein damage is induced by the membrane environment via autocatalytic oxidation of the lipids. Although such lipid oxidation would also take place in the nanodiscs, it would be slowed down because the lipid material is divided over many membrane nanoparticles, which isolate the approximately 150 lipids occupying each nanodisc, reducing any autocatalytic propagation. Also other redox proteins present in native membranes that may play a role in the generation of the reactive oxidation species that initiate damage will not be present in the RC nanodiscs.

This finding highlights an additional aspect of the protection offered by the nanodisc environment to the encased protein. Intact photosynthetic membranes have been considered as a more stable alternative to detergent-purified proteins for the generation of photocurrents.[24] Our results indicate that the use of nanodiscs may provide the best of both worlds by offering a protective membrane-like environment that is less prone to membrane damage. Under long-term storage at room temperature (20–25

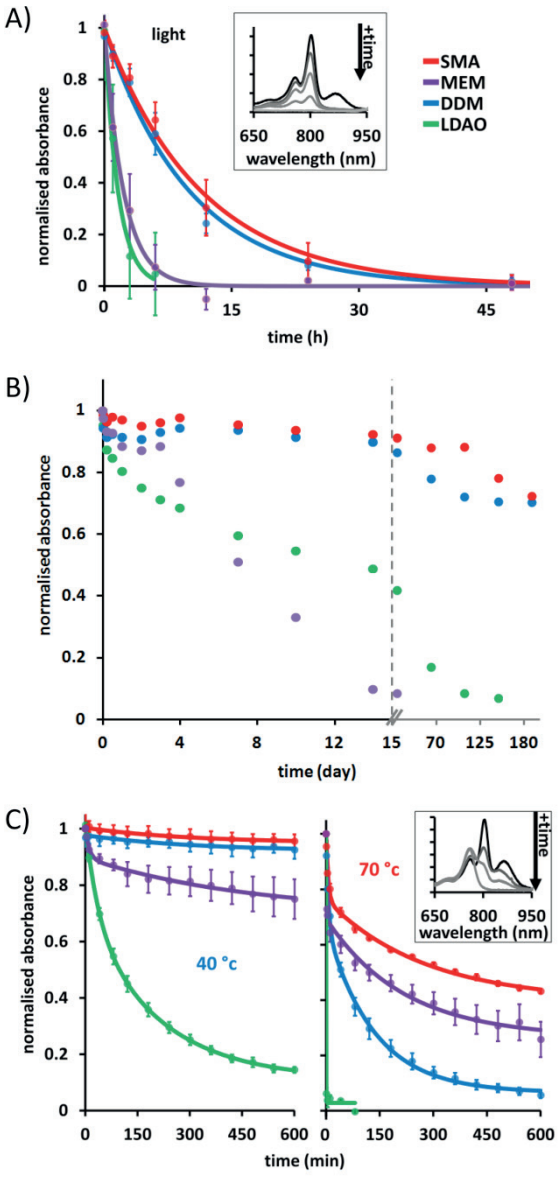

Figure 5

Stability of RCs under stress monitored through absorbance decreases at 803 nm. (A) Photostability of RCs at room temperature in the light. Circles show averages from three time courses with standard errors. Solid lines show fits to a single exponential decay as a guide to the eye. Inset: absorbance spectra of SMA-solubilized RCs before (black) and after (grey) strong illumination for 6, 12, 24 and 48 hours. (B) Data for duplicate RC preparations at room temperature in the dark. Colour coding as for panel A. (C) Thermal stability during a time course at 40 °C (left) or 70 °C (right). Circles show average data from three time courses with standard errors. Solid lines show fits to a double exponential decay. Inset: absorbance spectra of SMA-solubilized RCs before (black) and after (grey) heating at 80 °C for 2.5, 10 and 300 min.

°C) in the dark, membrane-embedded RCs showed complete degradation after 21 days and LDAO RCs after 100 days (Figure 5B). However, RCs in nanodiscs or DDM had

retained ≈ 70 % of their native absorbance after six months.

Another key issue is stability under thermal stress, which can also be assessed using the RC absorbance spectrum. During heating, the bands at 865 and 803 nm drop in intensity as the protein unfolds, while a band attributable to released bacteriochlorophyll will appear at around 760 nm (see inset to Figure 5C and previous accounts[23]). Assays showed that the stability of RCs in SMA/lipid nanodiscs is comparable to that of RCs in intact membranes or in DDM micelles at temperatures between 40 and 70 °C (Figure 5C), but that RCs in LDAO micelles are markedly less stable. The RCs in nanodiscs lost their native absorbance more slowly than RCs in DDM or intact membranes at all temperatures, the effect getting stronger as the temperature was increased. Again this highlights the strong protective environment that the SMA/lipid nanodiscs offer to the RC.

To summarize, the data outlined above show that it is possible to use a SMA copolymer to solubilize a His-tagged photovoltaic integral protein from a native membrane while maintaining its immediate native lipid environment, and purify it using standard affinity and size-exclusion chromatography in the complete absence of detergent. The SMA/lipid nanodiscs offer a membrane-like environment to RCs that preserves native functional properties. Notably, the RC protein is generally more stable when encased in the nanodiscs than in detergent solution or even in the native membrane. This is of particular interest, given that a major barrier to the exploitation of membrane proteins for technological applications is their limited stability under conditions of stress. The characteristics of currents generated by RC/SMA/lipid nanodiscs interfaced in a variety of ways with electrode materials are currently being explored, with focus on their stability and longevity.

Finally, it is important to emphasize the key roles that lipids play in membrane protein function and stability. A significant advantage of the SMA approach to membrane protein purification is that it enables the micromembrane environment to be maintained and analyzed without interference from detergent. Furthermore, given the preservation of native function evidenced above, it is possible that purification of membrane proteins using SMA could become the standard tool for biophysical studies of membrane proteins, and that the copolymer will greatly facilitate the wider use of these lipid/protein nanodiscs in biohybrid devices.

ACKNOWLEDGMENTS

Support is acknowledged from the Biotechnology and Biological Sciences Research Council of the UK (D.J.K.S., M.R.J.), the Foundation for Fundamental Researchon Matter (FOM, program no. 126), which is part of the Netherlands Organization for Scientific Research (NWO) (S.S., J.A.K., R.v.G.) and an ERC Advanced Investigator grant (R.v.G., 267333, PHOTPROT). We thank: Dr. Ross Anderson and Dan Watkins,

University of Bristol, for use of equipment for spectro-electrochemistry and helpful discussions; Hans Meeldijk, Bijvoet Center for Biomolecular Research, for assistance with negative stain electron microscopy; Martijn Koorengevel, Bijvoet Center for Biomolecular Research, for help with TLC and discussions.

SUPPORTING MATERIAL

Supporting information for this article is available on the WWW under http://dx.doi.org/10.1002/anie.201406412.

References

[1] a) M. le Maire, P. Champeil, J. V. MØller, *Biochim. Biophys. Acta* **2000**, *1508*, 86-111; b) A. M. Seddon, P. Curnow, P. J. Booth, *Biochim. Biophys. Acta-Biomemb.* **2004**, *1666*, 105-117; c) G. G. Prive, *Methods* **2007**, *41*, 388-397.

[2] T. J. Knowles, R. Finka, C. Smith, Y.-P. Lin, T. Dafforn, M. Overduin, *J. Am. Chem. Soc.* **2009**, *131*, 7484–7485.

[3] M. Jamshad, Y.-P. Lin, T. J. Knowles, R. A. Parslow, C. Harris, M. Wheatley, D. R. Poyner, R. M. Bill, O. R. T. Thomas, M. Overduin, T. R. Dafforn, *Biochem. Soc. Trans.* **2011**, *39*, 813-818.

[4] S. Rajesh, T. Knowles, M. Overduin, *New Biotechnology* **2011**, *28*, 250-254.

[5] M. Orwick-Rydmark, J. E. Lovett, A. Graziadei, L. Lindholm, M. R. Hicks, A. Watts, *Nano Lett.* **2012**, *12*, 4687-4692.

[6] M. C. Orwick, P. J. Judge, J. Procek, L. Lindholm, A. Graziadei, A. Engel, G. Gröbner, A. Watts, *Angew. Chem. Int. Ed.* **2012**, *51*, 4653-4657

[7] A. R. Long, C. C. O'Brien, K. Malhotra, C. T. Schwall, A. D. Albert, A. Watts, N. N. Alder, *BMC Biotechnology* **2013**, *13*, 41.

[8] S. Gulati, M. Jamshad, T. J. Knowles, K. A. Morrison, R. Downing, N. Cant, R. Collins, J. B. Koenderink, R. C. Ford, M. Overduin, I. D. Kerr, T. R. Dafforn, A. J. Rothnie, Biochem. J. 2014, 461, 269 – 278.

[9] a) J. L. Popot, Annu. Rev. Biochem. 2010, 79, 737 – 775;b) S. May, M. Andreasson-Ochsner, Z. Fu, Y. X. Low, D. Tan, H. P. de Hoog, S. Ritz, M. Nallani, E. K. Sinner, Angew. Chem. Int. Ed. 2013, 52, 749 – 753; Angew. Chem. 2013, 125, 777 – 781.

[10] J. P. Allen, G. Feher, T. O. Yeates, H. Komiya, D. C. Rees, *Proc. Natl. Acad. Sci. USA* **1987**, *84*, 5730-5734.

[11] a) G. Feher, J. P. Allen, M. Y. Okamura, D. C. Rees, *Nature* **1989**, *33*, 111-116; b) A. J. Hoff, J. Deisenhofer, *Physics Reports* **1997**, *287*, 2-247; c) M. R. Jones, *Biochem. Soc. Trans.* **2009**, *37*, 400-407; d) P. Heathcote, M. R. Jones, in *Comprehensive Biophysics*, Vol. 8 (Eds.: E. H. Egelman, S. Ferguson), Academic Press, Oxford, UK, **2012**, pp. 115-144.

[12] a) S. C. Tan, L. I.Crouch, S. Mahajan, M. R. Jones, M. E. Welland, *ACS NANO* **2012,** *6*, 9103-9109; b) O. Yehezkeli, R. Tel-Vered, D. Michaeli, I. Willner, R. Nechushtai, *Photosynth. Res.* **2014**, *120*, 71–85.

[13] M. R. Jones, R. W. Visschers, R. van Grondelle, C.N. Hunter, *Biochemistry* **1992**, *31*, 4458-4465

[14] S. S. Deshmukh, H. Akhavein, J. C. Williams, J. P. Allen, L. Kalman, *Biochemistry* **2011**, *50*, 5249-5262.

[15] a) P. Maroti, *J. Photochem. Photobiol. B: Biol.* **1991** *8*, 263-277; b) A. Agostiano, L. Catucci, M. Giustini, A. Mallardi, G. Palazzo, *Proc. Ind. Acad. Sci.-Chem. Sci.* **1998**, *110*, 251-264.

[16] a) P. K. Fyfe, N. W. Isaacs, R. J. Cogdell, M. R. Jones, *Biochim. Biophys. Acta* **2004**, *1608*, 11-22; b) T. Odahara, *Biochim. Biophys. Acta* **2004**, *1660*, 80-92; c) M. Kobayashi, Y. Fujioka, T. Mori, M. Terashima, H. Suzuki, Y. Shimada, T. Saito, Z. Y. Wang, T. Nozawa, Biosci. Biotech. Biochem. **2005**, *69*, 1130-1136; d) F. Böhles, P. Heathcote, M. Jones, S. Santabarbara, in: *Photosynthesis. Energy from the Sun*, (Eds.: J. F. Allen, E. Gantt, J. Golbeck, B. Osmond), Springer, Netherlands,

2008, pp. 29-34; e) G. Palazzo, F. Lopez, A. Mallardi, *Biochim. Biophys. Acta* **2010,** *1804*, 137-146.

[17] M. Y. Okamura, L. A. Steiner, G. Feher, *Biochemistry* **1974**, *13*, 1394-1403.

[18] a) C. N. Kenyon in *The Photosynthetic Bacteria*. (Eds.: R. K. Clayton, W. R. Sistrom) Plenum Press, New York, USA, **1978**, pp. 281-313; b) J. C. Onishi, R. A. Niederman, *J. Bacteriol.* **1982**, *149*, 831–839; c) T. J. Donohue, B. D. Cain, S. Kaplan, *J. Bacteriol.* **1982**, *152*, 595–606

[19] a) D. Marsh, L. I. Horvath, *Biochim. Biophys. Acta* **1998**, *1376*, 267–296; b) A.G. Lee, *Biochim. Biophys. Acta* **2003**, *1612*, 1–40.

[20] D. A. Moss, M. Leonhard, M. Bauscher, W. Mantele, *FEBS Letts* **1991**, *283*, 33-36

[21] D. Kleinfeld, M. Y. Okamura, G. Feher, *Biochemistry* **1984**, *23*, 5780-5786.

[22] a) R. R. Stein, A. L. Castellvi, J. P. Bogacz, C. A. Wraight, *J. Cell. Biochem.* **1984**, *24*, 243-259; b) D. J. K. Swainsbury, V. M. Friebe, R. N. Frese, M. R. Jones, *Biosens. Bioelectron.* **2014,** *58*, 172-178.

[23] a) A. V. Hughes, P. Rees, P. Heathcote, M. R. Jones, *Biophys. J.* **2006**, *90*, 4155-4166; c) K. Holden-Dye, L. I. Crouch, C. M. Williams, R.A. Bone, J. Cheng, F. Böhles, P. Heathcote, M. R. Jones, *Arch. Biochem. Biophys.* **2011**, *505*, 160–170.

[24] J. Magis, M.-J. den Hollander, W. G. Onderwaater, J. D. Olsen, C. N. Hunter, T. J. Aartsma, R. N. Frese, *Biochim. Biophys. Acta* **2010**, *1798*, 637–645.

Supporting Information

Table of Contents

1. Experimental Procedures

1.1. Preparation of styrene maleic acid.

Styrene maleic anhydride (SMA 2000, MW 7500, polydispersity index 2.5, ratio of 2:1 styrene to maleic anhydride) was a kind gift of Cray Valley, USA. SMA 2000 was refluxed for 6 hours at 5 % (w/v) in 1 M KOH, and the resulting hydrolyzed polymer was precipitated by addition of 6 M HCl to a final concentration of 1.1 M HCl. The precipitate was centrifuged at 16,000 x g for 30 minutes, the supernatant was removed and the polymer was washed by resuspension in an equal volume of 100 mM HCl. This cycle of centrifugation and resuspension was repeated five times to remove any traces of salt, and the styrene maleic acid (SMA) copolymer was then freeze dried. Completion of the reaction was confirmed by FTIR spectroscopy by the disappearance of the maleic anhydride carboxyl signal at 1780 cm^{-1} and the appearance of the maleic acid carbonyl signal at 1570 cm^{-1}. A solution of 6 % (w/v) SMA in 50 mM Tris (pH 8.0) was used for RC purification.

1.2. Purification of RCs in nanodiscs.

Cells of *Rba. sphaeroides* lacking light harvesting proteins and expressing RCs with a His_{10} tag[S1] were grown under dark/semiaerobic conditions[S2]. Cells harvested from 9 L of culture medium by centrifugation (5,000 x g for 20 mins) were suspended in 60 mL of 20 mM Tris (pH 8.0) containing a few crystals of DNAse I and two complete EDTA-free protease inhibitor tablets (Roche). Cells were lysed in a Constant Systems cell disruptor at 20,000 psi, cell debris being removed by centrifugation at 26,890 x g for 15 min at 4 °C. Aliquots of 6 % (w/v) SMA in 50 mM Tris (pH 8.0) and of 5 M NaCl were added to the membranes in the supernatant to give final concentrations of 1.5 % and 100 mM, respectively, in a total volume of 250 mL. This solution was incubated at room temperature in the dark for 1 h with gentle stirring, and membrane debris was then removed by ultracentrifugation at 100,000 x g at 4 °C for 30 minutes. The efficiency of RC solubilization by 6 % SMA was comparable to that achieved using a standard detergent-based protocol (0.5 % LDAO - see below). A 20 mL HisPrep FF 16/60 chromatography column (GE Healthcare) was equilibrated with 20 mM Tris/200 mM NaCl/10 mM imidazole at pH 8 (equilibration buffer) and the SMA-solubilized RCs were loaded by cycling the supernatant through the column overnight at a flow rate of approximately 3 mL min^{-1}. After loading, the column was washed with 20 column volumes of equilibration buffer, and the protein eluted by the addition of 20 mM Tris /200 mM NaCl/500 mM imidazole at pH 8. Fractions containing RCs were pooled and the SMA-solubilized RCs were further purified by passage through a Superdex 200 16/600 gel filtration column (GE Healthcare) pre-equilibrated with 20 mM Tris (pH 8). RC fractions with an absorbance ratio at 280 nm and 803 nm of ~1.5 (see below)

were pooled, concentrated and stored at -20 °C until required.

1.3. Purification of LDAO and DDM RCs. LDAO RCs were prepared in essentially the same way as SMA solubilized RCs except that extraction of the RCs from membranes was achieved with final concentrations of 0.5 % LDAO and 200 mM NaCl, and 0.1 % LDAO was included in all buffers used for purification. DDM RCs were prepared by the same method, except that the final gel filtration step was performed in 20 mM Tris (pH 8) containing 0.04% DDM to exchange LDAO for DDM. For all subsequent measurements the buffers used to dilute LDAO or DDM RCs were supplemented with 0.1% LDAO or 0.04% DDM, respectively.

1.4. Purity of RC preparations. Purity of RCs was assessed by UV/vis absorbance spectroscopy as described by Okamura and co-workers[15]. Column fractions containing LDAO or DDM purified RCs with a ratio of protein absorbance at 280 nm to bacteriochlorophyll absorbance at 802 nm of ~1.3 were retained for use (Figure S1, green and blue). Purity of these RC preparations was confirmed by SDS-PAGE, the only bands detected being the three constituent polypeptides of the RC (data not shown). The same spectroscopic assay was used during purification of SMA-solubilized RCs, and it was found that at the same degree of purity as assessed by SDS-PAGE these RCs had a A_{280}/A_{802} ratio of ~1.5, and a lower value could not be obtained (Figure S1, red). The source of the additional absorbance around 280 nm was not determined but could be attributable to the SMA copolymer, ubiquinone or carotenoid.

The RC has a single spheroidenone carotenoid with a broad absorbance band between 400 and 550 nm. Compared to detergent-solubilized RCs, some fractions of pure RCs in SMA/lipid nanodiscs showed additional carotenoid absorbance in this region (Figure S1, red compared with blue/green); this is consistent with the presence of free carotenoid in photosynthetic membranes from antenna-deficient strains[12]. Such carotenoid is washed away during detergent purification, but in some fractions a small amount appeared to have been retained in the protein/lipid nanodisc during SMA purification. The lower 865 nm band in the absorbance spectrum of SMA-solubilized RCs in Figure S1 is attributable to partial oxidation of the P865 bacteriochlorophylls under ambient conditions during purification. The fact that this was more pronounced for SMA-solubilized RCs than detergent-solubilized RCs is consistent with the lower $P865/P865^{+}$ redox potential in the former (see main text). This partial bleaching was not present in the spectra reported in Figure 1B in the main text due the presence of sodium ascorbate which reduces any $P865^{+}$.

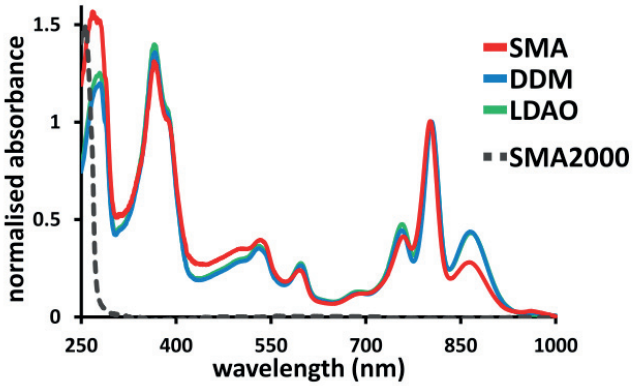

Figure S1. Absorbance spectra of pure RCs.
Spectra are for column fractions from gel filtration chromatography, recorded without addition of sodium ascorbate.

1.5. Preparation of native membranes for spectroscopy/potentiometry. A 1.5 L volume of cells of the antenna-deficient strain of *Rba. sphaeroides* expressing His_{10}-tagged RCs was grown as described above and harvested by centrifugation. Pelleted cells were suspended in 20 mM Tris (pH 8) containing a few crystals of DNAse I and lysed by passing twice through a French pressure cell at 20,000 psi. Cell debris was removed by centrifugation at 26,890 x g for 15 min at 4 °C, the lysate overlaid on a cushion of 60 % w/v sucrose, and centrifuged at 100,000 x g for 2 h. The tight membrane band on top of the sucrose layer was collected, the sucrose removed by dialysis against 20 mM Tris (pH 8), and the membrane suspension stored at -20 °C until required.

1.6. RC ground state absorbance spectra. RC concentrations were calculated using an extinction coefficient at 802 nm of 2.88×10^5 M^{-1} cm^{-1}[S3]. RCs were diluted to 0.5 µM in 20 mM Tris (pH 8) (containing detergent if appropriate). Sodium ascorbate (2 mM) was also present to prevent oxidative bleaching of the RC absorbance band at 865 nm. Absorbance spectra were recorded between 300 and 1000 nm after dark adaptation of each sample for 30 mins. The spectrum of membrane-embedded RCs was distorted by background light scatter, and this was corrected for by subtraction of a scatter curve comprising a modified Rayleigh function where Absorbance = $\lambda^{-2.6}$. This curve was calculated assuming that the absorbance at 950 nm is zero. The points at 950 and 650 nm were used to calculate the scatter curve and an offset of 0.07 was applied at 650 nm to match the values for the other conditions. The scattering power was reduced from -4 to -2.6 to give a better match in the 600-700 nm range, which is not expected to be altered by the RC environment. For comparison, spectra were then normalised to the strongest absorbance band in the near-infrared at ~802 nm.

1.7. Dynamic light scattering. RCs were diluted to 2 μM in 20 mM Tris (pH 8)/200 mM NaCl. DLS measurements were carried out in a 200 μL micro cuvette (Hellma) in a Zetasizer Nano ZS (Malvern Instruments). Correlation curves were produced from three sets of twelve spectra and processed using the Zetasizer software package. Particle diameters reported in the text were associated with a percentage mass of ≥ 99.9 %.

1.8. Transmission electron microscopy. A 5 μL aliquot of SMA solubilized RCs (8 mg mL^{-1}) was adsorbed onto a glow discharged copper grid for 2 minutes. Excess sample was removed with filter paper, and 10 μL of a 0.5 μM solution of 5 nm Ni-NTA functionalized gold nanoparticles were adsorbed onto the SMA solubilized RC copper grid for 20 minutes. Excess liquid was removed with filter paper and the copper grid was washed twice with water for 15 s. The copper grid was then stained with 2 % ammonium molybdate for 45 s and excess liquid was removed with filter paper. The copper grid was air-dried and examined using a Tecnai 12 Philips electron microscope operating at an acceleration voltage of 120 kV.

1.9. Thin layer chromatography and lipid analysis. Six independent lipid extractions were performed from the same batch of purified RCs or membranes. Lipids were extracted from native membranes, SMA solubilized RCs, RCs in DDM micelles and RCs in LDAO micelles by the Bligh and Dyer method[S4]. Extracted lipids were deposited onto a silica TLC plate (MACHEREY NAGEL GmbH & co) using a Linomat 5 sample applicator (Camag). The TLC plate was developed using a solution of chloroform:methanol:acetic acid:water (85:15:10:3.5) in an ADC2 Automatic Development Chamber (Camag). Lipids were visualized by dipping the plate into a methanol solution of 10 % copper(II) sulfate in 8 % sulfuric acid (98 %), and 8 % phosphoric acid (85 %) and then drying the plate by heating at 130˚C for 12 min. Copper(II) charring was used because it yields excellent signal-to-noise ratio in intensity, much better than for instance sulfuric acid charring[S5]. Only LDAO could not be visualized by copper(II) charring. Relative intensities were determined by densitometry using Quantity One (BioRad). The image shown in Figure 3A is slightly contrast enhanced (Adobe Photoshop CS6).

Lipid phosphate concentration was measured by the Rouser method[S6] using samples of known RC concentration. Amounts of lipid per nanodisc assumed that every His-tag purified nanodisc contains a single RC. It should be noted that the SQDG lipid content does not contribute because it does not contain a phosphate. On the other hand, cardiolipin (CL) adds two phosphates per molecule. The amounts of these two lipids in the SMA nanodiscs were similar, and so these effects approximately cancel out.

1.10. Redox potentiometry. Determination of the mid-point redox potential of the RC primary electron donor P865 was based on the method by Moss *et al.*[18]. RCs were diluted to 20 μM in 50 mM KH_2PO_4 (pH 7.5)/1 M KCl/10 mM UQ_0/10 mM potassium ferricyanide/2 mM TMPD (*N*,*N*,*N*',*N*'-tetramethyl-p-phenylenediamine)/20% v/v glycerol, with detergent if appropriate. An aliquot was placed in a sealed 200 μL transparent cell with a 0.3 mm path length fitted with a platinum gauze working electrode, platinum counter electrode and Ag/AgCl reference electrode. A series of potentials between 0 and 450 mV versus the reference electrode were applied and at each potential absorbance spectra were collected continuously between 650 and 1000 nm until there was no change in lineshape, the final spectrum at each potential being used for the subsequent analysis. In each titration the mid-point potential was determined by fitting the absorbance at 865 nm as a function of applied potential to a one electron Nernst function in Origin 8 (OriginLab). The standard error reported by this fitting process was typically no greater than ± 3 mV. The instrument was calibrated by carrying out a titration in the absence of RC protein, monitoring the absorbance band at 410 nm arising from ferricyanide and using the known mid-point potential of 430 mV for the ferricyanide/ferrocyanide couple.

1.11. Measurement of $P^+Q_B^-$ recombination kinetics. Measurements of P865 photo-oxidation and re-reduction through recombination were performed using a Cary60 spectrophotometer connected to an external CUV 1 cm cuvette holder (Ocean Optics) via a pair of optical fibres. Light pulses of 50 ms duration were applied to the sample at 90° to the pulsed measuring beam using an HL-2000-FHSA shutter controlled white light source (Ocean Optics) delivering approximately 25 W m^{-2} light intensity at the cuvette surface via an optical fiber; rapid shutter opening and closing was triggered by a TGP110 pulse generator (tti instruments). Solutions of 13.2 μM RCs were prepared in 20 mM Tris (pH 8) containing 100 μM UQ_0 and detergent if appropriate. RC samples were loaded in to a 3 x 3 mm fluorescence cuvette (Hellma) and the absorbance at 865 nm was measured before and for 20 s after delivery of the excitation pulse. Eight transients were recorded for each sample and averaged before analysis. Charge recombination kinetics were fitted with a single or double exponential function in Origin 8 (OriginLab). Parameters from the kinetic fits are shown in Table S1, below.

1.12. Thermal stability of RCs. Assays of thermal stability were performed in a Cary60 spectrophotometer equipped with a temperature-controlled multi-cell holder. Semi-micro cuvettes were filled with 1.6 ml of 20 mM Tris (pH 8) (and detergent if appropriate) that had been pre-heated to the desired temperature. Melts were initiated by rapidly mixing in adding 150 μL of RC solution in the same buffer to give a final

RC concentration of 0.5 μM, and sealing the cuvette with a stopper, excluding any air bubbles. Absorbance spectra between 600 and 1000 nm were recorded at intervals after mixing from 1 min to 10 h.

1.13. Photostability of RCs. RCs prepared with LDAO, DDM, SMA or in native membranes were diluted to 0.5 μM in 20 mM Tris (pH 8) (with detergent if appropriate) and used to completely fill a pair of stoppered cuvettes. Initial absorbance spectra were recorded and one set of cuvettes was placed in front of a 100 W white light source shielded by a water filter, which delivered a light intensity of approximately 90 mW cm^{-2} at each cuvette surface. The water filter prevented heating of the cuvettes above ambient. The second set of cuvettes was placed in the dark as a control. Absorbance spectra were recorded between 600 and 1000 nm at intervals.

2. Reaction Center Charge Recombination

As shown in Figure S2, the initial steps in the mechanism of the *Rba. sphaeroides* RC involve photochemical charge separation (blue arrow) to create the radical pair $P865^{+}Q_A^{-}$ on a picosecond time scale. If the Q_B binding site is not occupied by an oxidized ubiquinone (panel on left) $P865^{+}Q_A^{-}$ recombines with a lifetime of around 100 ms. If the Q_B site is occupied (panel on right) the electron is transferred from Q_A^{-} to Q_B on a microsecond time scale, creating the radical pair $P865^{+}Q_B^{-}$. In the absence of additional external electron donors or acceptors, or further photoexcitation, $P865^{+}Q_B^{-}$ recombines with a lifetime that varies between 1 and 5 s, depending on the detergent/lipid environment of the RC. This process can be monitored through the absorbance band attributable to the ground state of the P865 bacteriochlorophyll pair; this band is bleached when P865 is oxidized and recovers as the electron returns from Q_A^{-} or Q_B^{-}.

In the present study, charge recombination was compared in RCs in native membranes, SMA/lipid nanodiscs and LDAO or DDM micelles. Data from the kinetic fits in Figure 4B in the main text are shown in Table S1, below. The fast phase (τ_1, A_1) represents recombination of $P865^{+}Q_A^{-}$ in RCs where Q_B is either absent or the site is blocked by the inhibitor terbutryn. The slow phase (τ_2, A_2) represents recombination of $P865^{+}Q_B^{-}$.

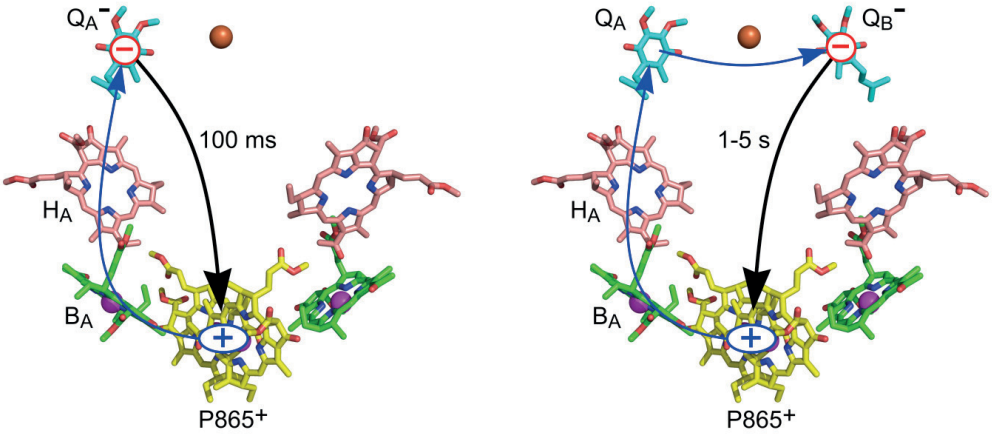

Figure S2. Charge recombination.
Recombination of $P865^{+}Q_A^{-}$ or $P865^{+}Q_B^{-}$ (black arrows) follows light-induced charge separation (blue arrows). The panels show the P865 bacteriochlorophyll pair (yellow carbons), two accessory bacteriochlorophylls (green carbons), two bacteriopheophytins (pink carbons) and either one or two ubiquinones (cyan carbons). Other atoms are oxygen (red), nitrogen (blue), magnesium (magenta spheres) and iron (brown sphere). Charge separation takes place along only one of the two cofactor branches, via a bacteriochlorophyll (B_A) and bacteriopheophytin (H_A). Hydrocarbon side chains of the RC cofactors and the carotenoid have been omitted for clarity.

Table S1.
Effect of RC environment on the lifetimes (τ) and amplitudes (A) of components of photoinduced charge recombination.

RC	τ_1 [a]	A_1 [a]	τ_2	A_2
	s	%	s	%
LDAO	0.20 ± 0.03	33 ± 3	1.19 ± 0.04	67 ± 3
DDM	0.18 ± 0.03	31 ± 3	1.58 ± 0.06	69 ± 2
nanodisc	0.06 ± 0.02	15 ± 3	4.03 ± 0.06	85.1 ± 0.4
membranes	0.07 ± 0.01	35 ± 4	4.52 ± 0.15	65 ± 1
LDAO + terb[b]	0.117 ± 0.003	100 ± 2		
DDM + terb[b]	0.195 ± 0.016	100 ± 5		
nanodisc + terb[b]	0.168 ± 0.005	100 ± 2		
membranes + terb[b]	0.085 ± 0.017	72 ± 8	1.64 ± 0.23	28 ± 3

[a] The significance of the precise lifetime and amplitude of the fast phase (τ_1, A_1) should be treated with caution as the ~50 ms excitation pulse is long relative to this component and noise levels in the averaged kinetic traces are high, especially for RCs in intact membranes.
[b] 1mM terbutryn added to inhibit electron transfer to Q_B

Supporting References

[S1] D. J. K. Swainsbury, V. M. Friebe, R. N. Frese, M. R. Jones, *Biosens. Bioelectron.* **2014**, *58*, 172-178.

[S2] M. R. Jones, M. Heer-Dawson, T. A. Mattioli, C. N. Hunter, B. Robert, *FEBS Letters* **1994**, *339*, 18-24.

[S3] S. C. Straley, W. W. Parson, D. C. Mauzerall, R. K. Clayton, *Biochim. Biophys. Acta* **1973**, *305*, 597-609.

[S4] E. G. Bligh, W. J. Dyer, *Can. J. Biochem. Physiol.* **1959**, *37*, 911-917.

[S5] A. A. Entezami, B. J. Venables, K. E. Daugherty, *J. Chromatogr.* **1987**, *387*, 323-331.

[S6] G. Rouser, S. Fleischer, A. Yamamoto, *Lipid* **1970**, *5*, 494-496.

[S7] K. Gibasiewicz, M. Pajzderska, J. A. Potter, P. K. Fyfe, A. Dobek, K. Brettel, M. R. Jones, *J. Phys. Chem. B* **2011**, *115*, 13037-13050.

CHAPTER 5

STYRENE–MALEIC ACID (SMA) COPOLYMER PURIFICATION OF DIVERSE INTEGRAL MEMBRANE PIGMENT-PROTEINS FROM SMA-RESISTANT MEMBRANES

DAVID J. K. SWAINSBURY, STEFAN SCHEIDELAAR, NICHOLAS FOSTER, RIENK VAN GRONDELLE, J. ANTOINETTE KILLIAN AND MICHAEL R. JONES

D.J.K. SWAINSBURY, **S. SCHEIDELAAR**, N. FOSTER, R. VAN GRONDELLE, J.A. KILLIAN, AND M.R. JONES, STYRENE-MALEIC ACID COPOLYMER PURIFICATION OF DIVERSE INTEGRAL MEMBRANE PIGMENT-PROTEINS FROM SMA-RESISTANT MEMBRANES. *MANUSCRIPT IN PREPARATION.*

KEYWORDS: STYRENE–MALEIC ACID, NANODISC, MEMBRANE PROTEIN, DETERGENT, REACTION CENTRE, LIGHT HARVESTING

INTRODUCTION

Styrene—maleic acid (SMA) is a copolymer of styrene and maleic acid moieties that shows great promise as an alternative to detergents for the solubilisation, purification and characterisation of integral membrane proteins [1—3]. Unlike detergents, which tend to strip away most or all of the lipids in the immediate environment of a membrane protein, SMA extracts proteins from the membrane in the form of a lipid/protein nanodisc [4]. These typically range in size from 10 to 15 nm, and estimates of the number of lipids they contain have ranged from 11 to 150 (see [2] for a review). A number of recent studies have shown that SMA can be used to produce highly pure preparations of integral membrane proteins from a variety of bacterial and eukaryotic sources [5—13]. Modification with a His-tag greatly assists this process by providing a means to separate nanodiscs containing the target protein from the heterogeneous population produced from a solubilised membrane.

In a recent review that included detailed protocols for preparation and application of SMA [3], Lee and co-workers commented that there may be size limits on proteins that can be solubilised, a constraint being the maximum diameter (~15 nm) of the SMA/lipid discs that can be formed. This may not be a fixed limit however, as particle sizes of 18 nm and 24 nm were reported for nanodiscs containing various proteins from *Staphylococcus aureus* [7], and a wide range of particle sizes were also reported for solubilised mitochondrial membranes [14]. Craig and co-workers have recently reported empty discs of up to 32 nm using a RAFT polymerised SMA with a different polymer structure to the commercially available SMAs employed here and in other studies [15]. Lee and co-workers also reported, on the basis of experience of purification of more than thirty membrane proteins, that proteins with more than 36 to 40 transmembrane α-helices may not be extractable using SMA [3, 16].

In previous work [5] we have shown that SMA can be used to extract and purify the relatively small "naked" reaction centre (RC) from membranes from a strain of the purple photosynthetic bacterium *Rhodobacter* (*Rba.) sphaeroides* lacking both types of light harvesting complex (see below). This photosynthetic pigment-protein complex comprises eleven membrane-spanning α-helices and has a mass of ~104 kDa [17—20]. Use of a strain of *Rba. sphaeroides* with the RC as the sole pigment-protein complex in the cell enabled comparison of the spectroscopic properties of SMA-purified RCs with those of RCs in intact bacterial membranes and purified in detergent [5]. Complete solubilisation of cytoplasmic membranes from this antenna-deficient strain was achieved at room temperature using SMA2000 (Cray Valley, USA), a SMA copolymer with a 2:1 ratio of styrene-to-maleic acid moieties and a mean molecular weight of 7.5 kDa [5]. The purified RCs showed a normal pigment absorbance spectrum, a good indication of native structure, and showed functional properties more consistent with RCs in native membranes than those in detergent. These findings demonstrated the ability of SMA to

preserve aspects of membrane protein function that are altered or lost in detergent [5]. Here, we explore the extent to which SMA is able to extract larger protein complexes from photosynthetic membranes that display a high degree of order and dense protein packing. In wild-type strains of *Rba. sphaeroides,* the RC is part of a larger RC-LH1-X complex along with the LH1 light harvesting pigment-protein (Figure 1A,B). LH1 forms an incomplete hollow cylinder with the RC (Figure 1C,D) at the centre [21, 22], and complete closure of the ring is prevented by the PufX protein (yellow in Figure 1A,B) [23—26]. In photosynthetic membranes these RC-LH1-X complexes associate with each other and with a peripheral LH2 pigment-protein, LH1 and LH2 forming an "antenna" that feeds the RC with excited state energy to power electron transfer [27, 28]. Monomers of RC-LH1-X complexes pack together in the membrane with a two-fold symmetry, such that two complexes with a C-shaped LH1 are arranged as a dimer [24] in which two RCs are surrounded and interconnected by a continuous S-shaped LH1 complex (Figure 1A,B) [21,25,29,30]. The strength of this dimer interaction is rather variable depending on growth conditions, such that even with mild detergents the predominant form of the complex that is isolated from membranes is the RC-LH1-X monomer when cells are grown under dark/semi-aerobic conditions [26,31,32]. Removal of the PufX protein by gene deletion results in a monomeric RC-LH1 complex [24] in which the RC is surrounded by a closed ring of LH1 pigment-protein (Figure 1E) [23]. A variety of techniques have shown that, in bacterial strains lacking the LH2 antenna, RC-LH1-X complexes form ordered, protein-rich arrays in the photosynthetic membrane [25, 29, 30, 34]; the packing model in Figure 1F is based on an electron microscopy image published by Jungas and co-workers [29]. Because the dimeric RC-LH1-X complex has a bend along its long axis the resulting ordered and densely-packed membranes have a tubular architecture [25, 30, 34—36]. Near circular monomeric RC-LH1 complexes also form extensive, protein-rich arrays that display hexagonal packing, forming membranes comprising large vesicles and sheets [25, 37].

Following from our recent work on purifying RCs [5], we attempted to use the same formulation of SMA to isolate larger RC-LH1-X and RC-LH1 complexes from photosynthetic membranes containing LH1, or both LH1 and LH2. As documented below, it was found that such membranes were markedly resistant to solubilisation by SMA. This raises questions over whether these RC-LH1-X complexes are too large to be accommodated in a SMA/lipid nanoparticle, whether the densely-packed composition of antenna-containing membranes disfavours permeation by this formulation of SMA, and how the latter may be overcome. To address these questions, we have explored methodologies to achieve more effective protein extraction from membranes from antenna-containing *Rba. sphaeroides* strains expressing His-tagged RC-LH1 complexes. We have also examined SMA-solubilisation of membranes from antenna-deficient strains in which the normally monomeric RC, which has eleven transmembrane α-helices, is

engineered to assemble in dimeric, trimeric or tetrameric forms to produce complexes with up to 44 transmembrane α-helices [38]. We also survey the effectiveness of the range of commercially-available SMA copolymers in solubilising RCs and RC-LH1 pigment-proteins from these membranes.

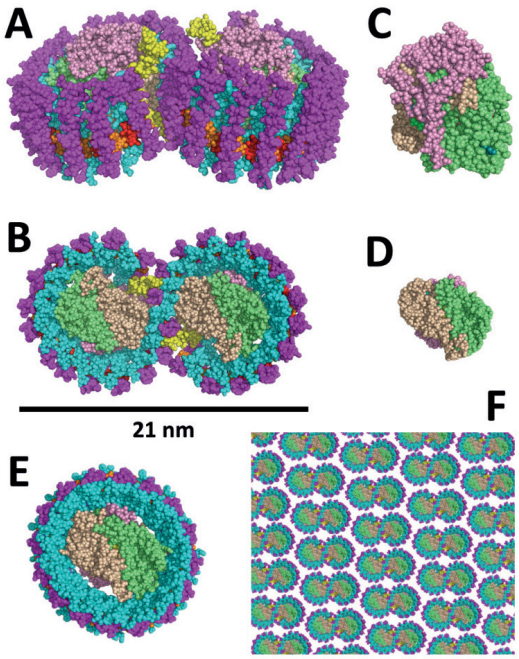

Figure 1.
Architectures of membrane proteins used to test SMA solubilisation. (A,B) Space-fill representations of the RC-LH1-X dimer from *Rba. sphaeroides* at 7.8 Å resolution (PDB entry 4V9G [21]) viewed (A) side-on and (B) perpendicular to the periplasmic side of the membrane. (C,D) Space-fill representations of the *Rba. sphaeroides* RC at 2.3 Å resolution (PDB entry 3ZUW [39]) viewed (C) side-on and (D) perpendicular to the periplasmic side of the membrane. (E) Space-fill representation of the Thermochromatium tepidum RC-LH1 complex at 3.0 Å resolution (PDB entry 3WMM [22]); this complex has the same architecture as the *Rba. sphaeroides* RC-LH1 complex with a complete ring of LH1 pigment-protein surrounding the RC. (F) Model of a semicrystalline array of closely-packed dimeric RC-LH1-X complexes based on a Fourier transform of an electron microscopy image of a photosynthetic membrane from an LH2-deficient strain of *Rba. sphaeroides* (Figure 3C from Jungas et al [29]). As the RC-LH1-X dimer is bent along its long axis (see panel A) membranes from such strains have a tubular architecture. In all panels, colour coding is: Magenta – LH1 β-polypeptide, cyan – LH1 α-polypeptide, yellow – PufX, red/orange – LH1 bacteriochlorophylls, pink – RC H-polypeptide, lime – RC M-polypeptide, beige – RC L-polypeptide. The models in B, D and E are shown on the same scale.

MATERIALS AND METHODS

Preparation of SMA copolymers

Styrene-maleic anhydride pellets were mixed at 5 % (w/v) with deionised water in a round bottom flask. Potassium hydroxide was added at a ratio of 0.3, 0.24, 0.2 or 0.14 g KOH per gram SMA for the 1.5:1, 2:1, 3:1 and 4.5:1 polymers, respectively. Solutions

were heated at 110 °C whilst refluxing with a condenser for 16 h. For 80 and 120 kDa polymers this period was extended up to a further 24 h if the solutions had not clarified. Clarified solutions were allowed to cool, the pH was adjusted to 8.0 with KOH, and they were stored at 4 °C for up to two weeks until required. The long-chain variants of the 3:1 SMA formulation had reduced solubility compared to the shorter chain SMAs. This increased the time required to convert them to the soluble form by up to 24 h and limited the maximum concentrations of stock solution achievable to approximately 3.5-4 % (w/v).

Biological materials

Cells of *Rba. sphaeroides* strain DD13 [40] were transformed with pRK415-based plasmids expressing native RCs [40], native RC-LH1 complexes with PufX [41], modified RC-LH1 complexes without PufX, and RCs modified with extra-membrane α-helical sequences that form dimeric, trimeric or tetrameric coiled-coil bundles [38]. Complementation was achieved by conjugative transfer from *Escherichia coli* strain S17-1 [35] and in all cases the RC component was modified with a sequence at the C-terminus of the PufM polypeptide comprising a deca-histidine tag [40]. Bacterial cells were stored as thick suspensions in 70 % lysogeny broth/30 % glycerol at -80 °C. Glycerol stocks were used to inoculate a 10 mL starter culture of M22+ minimal medium [35] in a 30 mL universal bottle that was grown for 24 h in the dark at 34 °C and 180 rpm in an orbital incubator. This was then used to inoculate 70 mL of M22+ in a 100 mL conical flask and this culture was grown on for 24 h under the same conditions. This intermediate culture was then used to inoculate 1.5 L of M22+ medium in a 2 L conical flask. This culture was grown for 48 h under the same conditions, and scaled up as necessary. Cells were harvested by centrifugation and cell pellets were stored at -20 °C until required. For all cells expressing photosynthetic complexes neomycin and tetracycline were added to the media at 100 μg mL, but cells of strain DD13 were grown in the presence of neomycin only. For growth under high aeration 1 L of M22+ media containing tetracycline and neomycin in a 2 L baffled conical flask was inoculated with an 80 mL intermediate culture, and flasks were incubated overnight in the dark at 34 °C and 250 rpm in an orbital incubator.

For the preparation of photosynthetic membranes, harvested bacterial cells were resuspended in 20 mM Tris (pH 8) containing a few crystals of bovine DNAse I (Sigma). Cells were lysed at 20,000 psi using a cell disruptor (Constant Systems) and debris was removed by centrifugation at 27,000 g at 4 °C for 15 min. The supernatant was overlaid onto a cushion of 60 % (w/w) sucrose in 20 mM Tris (pH 8) and centrifuged at 167,000 g for 2 h at 4 °C. The membrane band was harvested and used fresh or stored at -20 °C until required.

Solubilisation screen

Solutions of membranes containing RC, RC-LH1-X or RC-LH1 complexes at a concentration of 3 μM were prepared in 20 mM Tris (pH 8) containing 200 mM NaCl. SMA from a 5 % (w/v) stock solution was mixed in a 1:1 (v:v) ratio with 500 μL of membrane solution, an absorbance spectrum recorded between 400 and 1000 nm, and the resulting mix incubated in the dark at room temperature for 1 h. The mixture was then loaded into a 1 mL ultracentrifuge tube and insoluble material was pelleted at 100,000 g for 2 h at 4 °C. The supernatant was carefully removed and an absorbance spectrum recorded. For detergent extraction the SMA was replaced by 2.5 % (w/v) dodecyl maltoside (DDM).

As the expression level of artificially multimeric RCs was not uniform the concentrations of membranes containing dimeric, trimeric and tetrameric RCs were adjusted to match the absorbance at 650 nm of membranes containing unmodified monomeric RCs such that the concentration of each membrane suspension was similar before the addition of SMA. This produced concentrations of ~0.5 μM dimeric RC, ~1.5 μM trimeric RC and ~1 μM tetrameric RC.

All absorbance spectra were corrected for light scatter as described previously [5]. Scatter corrected spectra were used to estimate the percentage of complex remaining in the soluble fraction using absorbance values at 803 nm (for RCs and RC multimers) or 875 nm (for RC-LH1-X and RC-LH1 complexes).

Purification of RCs and RC-LH1 complexes

RC multimers and RC-LH1 complexes solubilised using SMA were purified by nickel affinity chromatography using SMA-free buffers as previously described for the native monomeric RC [5]. The SMA used was Xiran SZ30010 which has a 2:1 styrene:maleic acid formulation and an average molecular weight of 10 kDa. Concentration of samples after purification was performed in an Amicon stirred cell with a 100,000 MWCO PVDF membrane (Generon). Aggregation was often observed in this step and can be ascribed to the presence of large membrane fragments in the sample.

Dynamic light scattering

Purified SMA/lipid/protein nanodiscs were diluted to 2 μM protein concentration in 20 mM Tris (pH 8) containing 200 mM NaCl and passed through a 0.1 μm spin filter. DLS was measured at 25 °C in a 200 μL quartz cuvette inserted into a Zetasizer Nano ZS instrument (Malvern). Three data sets consisting of ten repeats of a ten-second measurement were averaged and analysed by volume to estimate average hydrodynamic diameter.

Fusion of lipids with high-expression membranes

A 2.5 % (w/v) dispersion of 1-palmitoyl-2-oleoyl-*sn*-glycero-3-phosphocholine (POPC) or *E. coli* total lipid extract was prepared in 20 mM Tris (pH 8) by vortexing followed by incubation at 42 °C for 15 min. Each dispersion was then sonicated on ice with a probe sonicator for a total of two minutes, alternating 10 sec on and 10 s off to prevent overheating. These lipids were mixed 5:1 with photosynthetic membranes containing RC-LH1-X complexes isolated from cells grown under high expression conditions. The membrane/lipid mix was vortexed and subjected to five rounds of freezing in liquid nitrogen and thawing for 15 min in an ultrasonic bath. Each sample was then sonicated with a probe sonicator for 2 min on ice, pulsing 10 sec on and 10 s off, followed by five more rounds of freeze-thaw and one further round of probe sonication.

For fusion of DD13 membranes with RC-LH1-X high expression membranes, the two types of membrane were prepared to the same OD at 650 nm, mixed in a 1:1 ratio and diluted 2.5 fold in 20 mM Tris (pH 8). Samples were then subjected to the same procedure of a total of ten freeze-thaw cycles and two probe sonication cycles described above.

A volume of 75 µL of each sample was used to perform a SMA solubilisation assay with 2.5 % (w/v) 10 kDa Xiran SZ30010.

For preparative-scale fusion of fusion of DD13 membranes with RC-LH1-X high expression membranes, 50 mL of each were mixed. The solution was divided equally between three 50 mL Falcon tubes, frozen in liquid nitrogen for 5 min and thawed in a bath sonicator for 45 min. This freeze/thaw cycle was repeated five times. After the final thaw each solution was sonicated with a probe sonicator on ice for a total of 52 mins per tube, pulsing with cycles of 2 min on and 5 min off to prevent overheating. Five more rounds of freeze-thaw were performed followed by one more round of probe sonication. RC-LH1-X complexes were purified from these fused membranes using SMA as described above.

Flash induced charge recombination kinetics

The kinetics of charge recombination were measured as described previously for RCs [5], except the protein concentration was reduced to 2 µM and LDAO in the buffer was replaced with 0.04% β-DDM.

Transmission electron microscopy

Copper grids for negative staining were prepared following the carbon flotation technique. Samples were diluted to ~0.05 mg/mL with 20mM Tris pH 8.0 buffer and small aliquots were adsorbed on carbon-coated mica. The mica was then transferred to a staining solution containing 2% (w/v) sodium silico tungstate, causing detaching of the carbon film. Subsequently, a copper grid was placed on top of the detached carbon which

was recovered and dried under air flow. Images were taken under low dose conditions at a nominal magnification of 23000x or 30000x with a T12 electron microscope (FEI, Hillsboro, OR) at an operating voltage of 120 kV using an ORIUS SC1000 camera (Gatan, Inc., Pleasanton, CA). We are very grateful to Dr. C. Moriscot from the Electron Microscopy Platform of the Integrated Structural Biology of Grenoble (ISBG, UMI3265) for performing the TEM imaging.

Thin layer chromatography and lipid analysis.
Four independent lipid extractions were performed from the same batch of solubilized RC-LH1 after fusion with DD13 membranes and from high expression membranes by the Bligh and Dyer method [33]. Extracted lipids were deposited onto a silica TLC plate (MACHEREY NAGEL GmbH & co) using a Linomat 5 sample applicator (Camag). The TLC plate was developed using a solution of chloroform:methanol:acetic acid:water (85:15:10:3.05) in an ADC2 Automatic Development Chamber (Camag). Lipids were visualized by dipping the plate into a methanol solution of 10 % copper(II) sulphate in 8 % sulfuric acid (98 %), and 8 % phosphoric acid (85 %) and then drying the plate by heating at 130˚C for 12 min. Relative intensities were determined by densitometry using Quantity One (BioRad).

RESULTS AND DISCUSSION

Efficiency of RC and RC-LH1 complex extraction by different formulations of SMA

To our knowledge, all previous reports on the use of SMA to extract proteins from a lipid bilayer have employed a formulation with a 3:1 or 2:1 ratio of styrene to maleic acid, but none of these have compared the relative abilities of a range of SMAs to isolate a single target protein. Our previous report on RC isolation and purification employed SMA2000, a 2:1 formulation with an average molecular weight of 7.5 kDa. However, as outlined in Table 1, 2:1 and 3:1 SMA copolymers are commercially available in a range of average molecular weights from 7.5-120 kDa, and low molecular weight 1.5:1 and 4.5:1 formulations are also available. As described in Materials and Methods, these copolymers were tested for their abilities to solubilise His-tagged RC complexes from membranes prepared from a strain of *Rba*. *sphaeroides* that lacks the LH1 and LH2 light harvesting proteins.

Solubilisation efficiency was estimated by absorbance spectroscopy of the starting membrane material and the extracted soluble fraction, utilising the strong and distinctive spectroscopic properties of the RC bacteriochlorin cofactors. The soluble fraction was separated from unsolubilised membrane material by ultracentrifugation at 100,000 g for 2 h at 4 °C. All 2:1 or 3:1 variants of SMA with a molecular weight of 30 kDa or below were effective to similar extents, extracting 70-90 % of RCs (Figure 2A). The two

Table 1.
Range of SMA preparations used in this work

Ratio of styrene: maleic acid	Molecular weight (weight—average)	n styrene per chain (weight—average)	n maleic acid per chain (weight—average)	Commercial name	Supplier
1.47	5000	29.2	19.9	Xiran SZ40005	Polyscope
2.00	7500	49.0	24.5	SMA2000	Cray Valley
2.16	10000	66.8	31.0	Xiran SZ30010	Polyscope
2.16	30000	200.5	93.0	Xiran SZ30030	Polyscope
3.19	10000	74.1	23.3	Xiran SZ26030	Polyscope
3.02	80000	585.7	193.8	Xiran SZ26080	Polyscope
3.02	120000	878.6	203.5	Xiran SZ26120	Polyscope
4.53	11000	87.4	19.3	Xiran SZ20010	Polyscope

versions of the 3:1 formulation with much higher average molecular weights (80 and 120 kDa) were also able to solubilise RCs but at a significantly lower efficiency than the 10 kDa version. SMAs with a 1.5:1 and 4.5:1 ratio of styrene to maleic acid were unable to solubilise RCs to a significant degree. The conclusion, therefore, was that low molecular weight 2:1 or 3:1 SMAs are the most effective for extraction of RCs, but longer chain variants with the same styrene to maleic acid ratio are able to achieve a somewhat less efficient extraction.

The same assay was carried out using intracytoplasmic membranes containing RC-LH1-X complexes that had been prepared from a *Rba. sphaeroides* strain lacking the LH2 light harvesting complex. As shown in Figure 2B, for this protein the solubilisation efficiency was less than four percent for all SMAs tested. One possible reason for this could be that the RC-LH1-X complex is too large to be accommodated in a SMA/lipid nanodisc, a monomer of the native RC-LH1-X complex being expected to have approximately three times the mass and twice the diameter of a RC at ~300 kDa and ~13 nm (Figure 1). As outlined above it has been reported that SMAs typically form discs of 10-15 nm diameter when incorporating proteins, and so a ~13 nm diameter

RC-LH1 complex may be too large to encapsulate. An additional factor could be that native RC-LH1 complexes form dimers when in the native membrane [21, 24, 25, 29, 30], which doubles their mass and increases their diameter along the long axis to ~21 nm [21] (Figure 1A,B).

To explore this latter point we also conducted a survey of SMA extraction efficiencies using membranes from an LH2-deficient strain containing RC-LH1 complexes lacking the PufX protein, which results in the assembly of exclusively monomeric RC-LH1 complexes in which the LH1 forms a complete ring around the central RC (Figure 1E). The efficiency of extraction of this type of complex was also uniformly low (Figure 2C). This showed that the possibility that native RC-LH1-X complexes assemble in a dimeric arrangement in the membrane was not the reason for inefficient solubilisation by SMA. It should be noted that an increase in SMA concentration or the length of incubation had no effect on the low extraction efficiencies obtained for either RC-LH1-X or RC-LH1 complexes, nor did carrying out the extraction using membranes that also contained the LH2 antenna complex (data not shown).

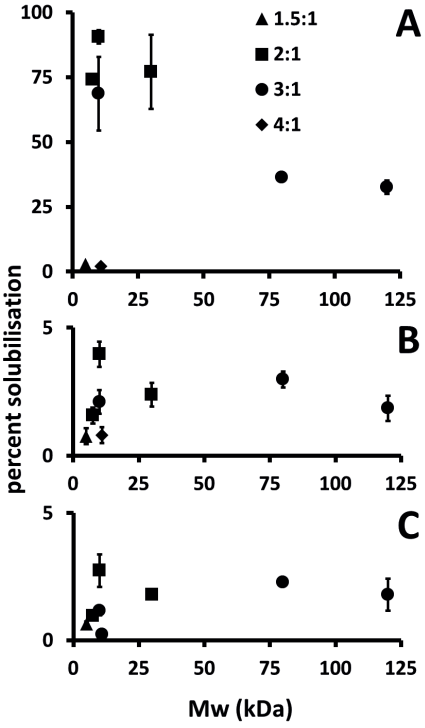

Figure 2.
Efficiency of membrane protein solubilisation us different SMAs. (A) RCs; (B) RC-LH1-X complexes; (C) RC-LH1 complexes. Different symbols are used for different ratios of styrene to maleic acid. Error bars show standard deviations (three replicates).

Attempts to overcome the recalcitrance of RC-LH1-X membranes to solubilisation by SMA.

In addition to the obvious issue of their size, another factor that may prevent SMA solubilisation of RC-LH1-X or RC-LH1 complexes is an unfavourable membrane composition and organisation. As oxygen is the primary regulator of photosynthesis gene expression in *Rhodobacter*, under semi-aerobic growth conditions the expression levels of the RC-LH1-X complex are high and protein crowding leads to the formation of highly-ordered RC-LH1-X arrays [25, 29, 30, 34] (Figure 1F). Although high resolution structural information is not available for such membranes, it is likely that the amount of lipid bilayer in such protein-rich membranes is limited, and there are extensive protein-protein interactions between adjacent RC-LH1-X complexes, producing a structure that has limited fluidity and limited opportunities for SMA to interact with contiguous regions of lipid bilayer.

It is known that RC-LH1-X complexes can be solubilised intact from highly-ordered LH2-deficient membranes by treatment with mild detergents such as dodecyl maltoside (DDM). To measure the maximal extent to which RC-LH1-X complexes could be extracted from the high-expression membranes prepared in the present work, these membranes were treated with 2.5 % (w/v) DDM. The mean extraction efficiency over multiple experiments was 72 %, some 30-fold greater than that achieved with the same membranes using the 10 kDa, 2:1 formulation of SMA (Figure 3A).

As the high degree of order shown by RC-LH1-X complexes is a consequence of their high concentration in the membrane [25, 29, 30, 34], a possible way to enable more efficient extraction of RC-LH1-X complexes by SMA is to dilute their concentration by increasing the lipid-to-protein ratio. . Experiments on membranes from a wild-type strain of *Rba. sphaeroides* fused with phosphatidyl choline (PC) liposomes have previously shown a loss of energy transfer from LH2 to LH1 when exogenous lipid is added, likely resulting from loss of protein-protein contacts and the surrounding of complexes with complete belts of lipid [42]. A number of methodologies were explored to achieve dilution of complexes in the membrane, using the 10 kDa 2:1 SMA formulation to test the effect on solubilisation efficiency. In the first, cells of *Rba. sphaeroides* were grown at high aeration (see Methods) to down-regulate RC-LH1-X levels in membranes (Figure 3B). When complexes were extracted from these reduced expression membranes the solubilisation efficiency increased to 28 %, some ~12-fold higher than was achieved with membranes prepared from high-expressing cells grown under standard semi-aerobic/dark conditions (Figure 3A). In the second, high expression membranes were fused with pure 1-palmitoyl-2-oleoyl-*sn*-glycero-3-phosphocholine (POPC) lipid by subjecting a mixture of the two to multiple freeze-thaw cycles. This increased the solubilisation efficiency by ~13-fold over the same membranes without POPC treatment (Figure 3A). Thus, it would appear that lowering the concentration of RC-LH1-X complexes in these

membranes made them somewhat more amenable to solubilisation by SMA.

One attractive aspect of the use of SMA is the possibility of purifying proteins along with their immediate native lipid environment. Clearly, addition of a synthetic lipid such as POPC has the potential to disturb this environment and directly impact on native protein-lipid interactions that may be crucial for function or stability. Accordingly, the ability of two non-synthetic preparations to increase the efficiency of RC-LH1-X complex extraction was also tested. The first of these was a commercial preparation of total lipids from *E. coli*, which is predominantly phosphatidylethanolamine (PE) with lower percentages of cardiolipin (CL) and phosphatidylglycerol (PG). Both *E. coli* and *Rba. sphaeroides* are gram-negative bacteria, and the latter also has PE as the main lipid with PG and CL, the main difference being that it also has PC [5, 43—45]. This preparation of *E. coli* total lipid, when fused with high RC-LH1-X expression membranes by freeze/thaw, enabled an extraction efficiency of approximately 15 % (Figure 3A).

The next approach was to fuse high RC-LH1-X expression membranes with membranes purified from a strain of the DD13 strain of *Rba. sphaeroides* in which all photosynthetic complexes are absent. This DD13 strain has a deletion of the *puf* operon which abolishes RC and LH1 expression and of the *puc1BAC* operon which abolishes LH2 expression. This double deletion strain was used to make the RC and RC-LH1-expressing strains used for the main part of the work described above (see Methods). This approach to dilution of RC-LH1-X high expression membranes enabled 13 % extraction of RC-LH1 complexes with SMA, similar to that achieved with *E. coli* total lipids. Although this efficiency was around half that achieved with pure POPC, the advantage was one of scale and cost, in that it was straightforward to produce a large quantity of DD13 membranes for fusion with high expression RC-LH1-X membranes, and therefore produce a large amount of SMA-solubilised RC-LH1-X complexes for further analysis. Obviously, another advantage is that these DD13 membranes comprised native *Rhodobacter* lipids.

We were also able to extract approximately 10 % of complexes by fusing high expression membranes with a crude lipid extract from the same DD13 membranes (data not shown). However, these extracted *Rba. sphaeroides* lipids caused some protein unfolding, probably due to the crude nature of this method of lipid purification (a 1:1 methanol:chloroform extract) complicating the spectroscopic assay of extraction efficiency. Nevertheless these findings suggest that lipids chemically extracted from a recalcitrant membrane system could be used to make that membrane more amenable to solubilisation by SMA.

Characteristics of SMA-solubilised RC-LH1-X complexes

RC-LH1-X complexes solubilised using SMA from high expression membranes,

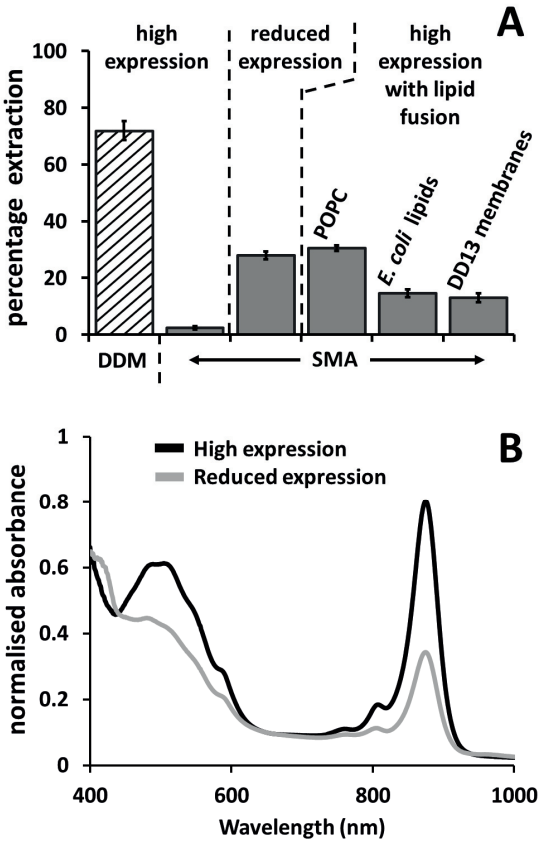

Figure 3.
Efficiency of extraction of RC-LH1-X complexes. (A) Efficiency of solubilisation of RC-LH1-X complexes with DDM or the 10 kDa 2:1 SMA. Error bars show standard deviations (three replicates). (B) Absorbance spectra of membranes with high RC-LH1-X expression (black) and lowered expression achieved by growing cells at high aeration (grey). Spectra are normalised to the same membrane scatter at 650 nm.

reduced expression membranes and from high-expression membranes fused with membranes from strain DD13, were purified by nickel affinity chromatography, making use of the His-tag on the RC component. For comparison, RC-LH1-X complexes were also purified from high-expression membranes after solubilisation by DDM, again by nickel affinity chromatography. Transmission electron microscopy (TEM) of DDM-purified protein showed particles of dimensions consistent with monomeric RC-LH1-X complexes (expected to be ~13 nm in diameter) aggregated into larger, structures (Figure 4A). It was not clear whether this aggregation took place in solution (which did not contain any visible aggregates) or was an artefact of the drying and staining procedures required for TEM.

TEM showed that the SMA-solubilised material eluted from the nickel affinity column consisted mainly of small fragments of membrane rather than individual,

discrete nanodiscs. Membrane fragments liberated in small amounts by SMA from untreated high-expression membranes were typically 50-100 nm in diameter, and some images showed internal, periodic structure consistent with the presence of densely-packed RC-LH1 complexes (Figure 4B). Fragments solubilised in higher amounts from reduced expression membranes had similar characteristics (Figure 4C). Strikingly, fragments isolated from high expression membranes that had been fused with DD13 membranes were markedly smaller, typically below 50 nm in diameter (Figure 4D). The conclusion therefore was that SMA-solubilisation of these highly ordered RC-LH1-X membranes resulted in the production of small membrane fragments rather than individual complexes, these being small enough to stay in solution during a standard clearing ultracentrifugation spin and passage through the matrix of a nickel affinity column.

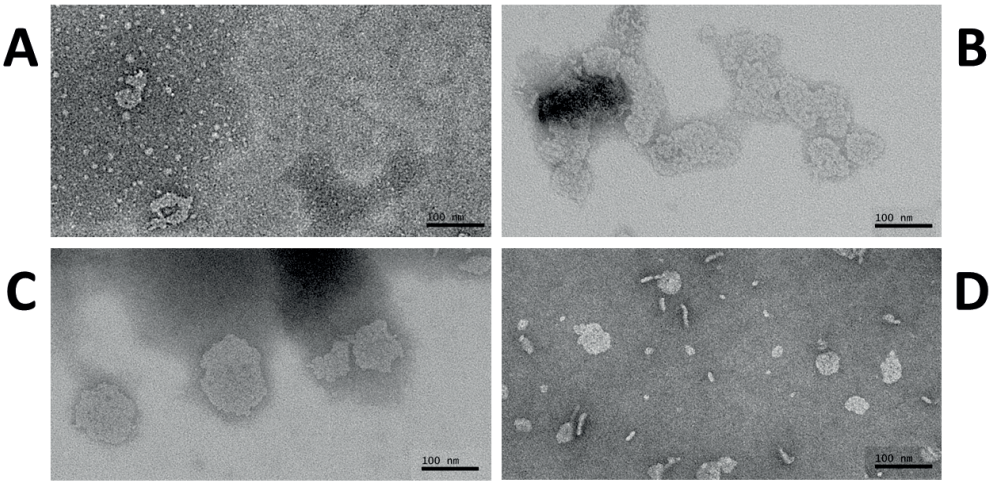

Figure 4.
TEM images of RC-LH1-X complexes (A) purified in DDM detergent, (B) solubilized with SMA from untreated high-expression membranes, (C) solubilized with SMA from reduced expression membranes, and (D) solubilized with SMA from high expression membranes that had been fused with DD13 membranes.

The impact on the structural integrity of the RC-LH1-X complex of the various treatments to make RC-LH1-X membranes more amenable to solubilisation by SMA was assessed by absorbance spectroscopy. As shown in Figure 5A, the spectral line shape was similar in all cases with a band between 820 and 950 nm attributable to the LH1 BChls, a broad band between 430 and 560 nm attributable to the LH1 carotenoids and small bands at 805 and 760 nm attributable to the RC bacteriochlorins. Absorbance spectra of RC-LH1-X complexes from SMA-treated high expression membranes (Figure 5A, orange) or SMA-treated reduced expression membranes (Figure 5A, blue) were virtually identical to that of RC-LH1-X complexes in intact high-expression membranes (Figure

5A, purple), with a main absorbance maximum at 875 nm. These three spectra differed from that of DDM-purified RC-LH1-X complexes (Figure 5A, green) in two respects. First, the LH1 BChl band was noticeably blue-shifted to 871 nm in the spectrum of DDM-purified complex, an effect of the change in environment from a lipid bilayer to a detergent micelle. Second, the contribution of the RC at 807 nm was a little higher in the spectrum of DDM-purified RC-LH1-X complexes. There are two possible reasons for this. The first is that, along with a blue-shift in absorbance maximum of the main LH1 BChl band to 871 nm there is a decrease in its intrinsic intensity such that, after normalisation, the RC absorbance is more prominent; in support of this the full width at half maximum of this band was 2-3 nm wider in the spectrum of DD13-purified complexes than those in SMALPs or intact membranes. The second reason is the presence of a small amount of free RCs in the DDM-purified material (bearing in mind that the His tag used to purify RC-LH1-X complexes is on the L-polypeptide of the RC component).

Turning to the absorbance spectrum of RC-LH1-X complexes from SMA-treated high expression membranes that had been fused with DD13 membranes, contributions from the RC at 801 nm and 760 nm were particularly high relative to the (normalised) absorbance intensity of LH1 at 873 nm. Such a pronounced effect strongly suggests the presence of a population of some LH1-free RCs. The most probable explanation for this is either that the freeze/thaw process used for membrane fusion caused some selective degradation of the LH1 component, or that it causes physical separation of LH1 and RCs (i.e. breakage of LH1 rings and release of RCs) such that the preparation of containing His-tagged RC-LH1-X complexes is "contaminated" with a minor population of His-tagged RCs. With regard to the first of these, it is the case that the LH1 pigment protein is less structurally-robust than the RC, for example being unfolded by strong detergents such as LDAO (lauryl diamine oxide) that are used routinely to purify RCs. Whatever the correct explanation, these data highlight a potential drawback of the membrane fusion approach to overcoming SMA recalcitrance if there is scope for the target protein complex to be damaged by steps in this treatment or, in the case of a multicomponent target, to dissociate into its component parts.

To assess the functional integrity of the solubilised RC-LH1 complexes, a flash of excitation light was used to trigger photochemical charge separation between the primary electron donor pair of BChl molecules near the periplasmic face of the RC-LH1 complex and the secondary acceptor ubiquinone, Q_B, near the cytoplasmic face of the complex, forming the radical pair $P^+Q_B^-$. Conversion of P to P^+ causes an absorbance decrease at 865 nm that recovers due return of the P BChls to their ground state through recombination of $P^+Q_B^-$. The lifetime for this recombination is very sensitive to the environment sensed by the dissociable Q_B ubiquinone, being around 3.5-fold longer in purified RC-LH1 complexes than in purified RCs [46, 47], and in the case of RCs,

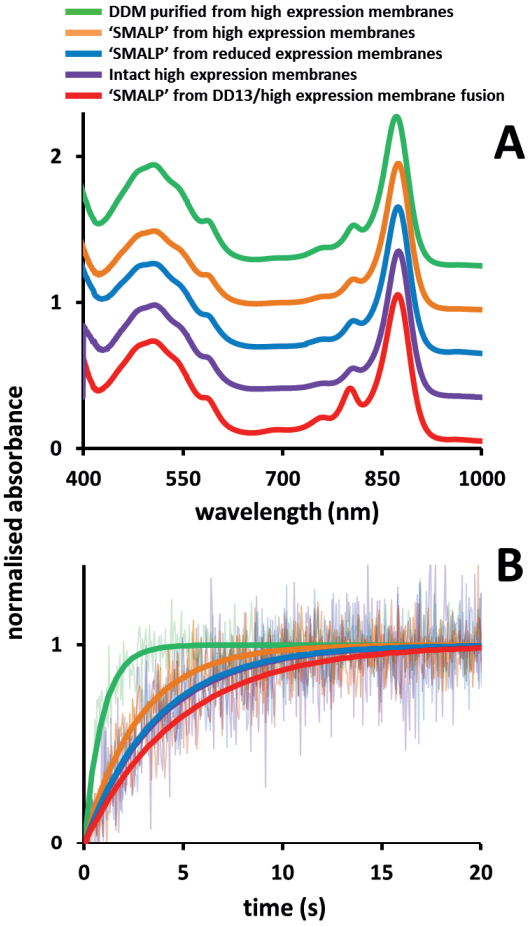

Figure 5.
Effect of lipid/detergent/copolymer environment on protein structural and functional integrity. (A) Absorbance spectra of RC-LH1-X complexes in membranes, SMA, and DDM micelles. (B) Kinetics of charge recombination in RC-LH1-X complexes (initial light-induced bleaching is not shown). All measurements were performed in the presence of 1 mM UQ_0 and are averaged from 16 datasets (shown in faded lines) with fits to a single exponential decay (overlaid in solid lines). Time constants were 0.9 ± 0.1s in detergent, 3.7 ± 0.2 s in native membranes, and 2.8 ± 0.1 , 3.64 ± 0.2 and 4.8 ± 0.2 s for SMALPs produced from untreated high expression, reduced expression and DD13 fused membranes, respectively.

being slower in bilayer membranes than in detergent micelles by a factor of between 1.5 and 3.5 depending on the type of bilayer [48, 49].

For each sample, averaged experimental data (Figure 5B) was fitted with a single exponential decay. The fitted time constant was markedly shorter in RC-LH1-X complexes purified from high-expression membranes using DDM (0.9 s – Figure 5B, green)) than for RC-LH1-X complexes in untreated high-expression membranes (3.7 s – Figure 5B, purple), or for RC-LH1-X complexes from these membranes after

treatment with SMA (2.8 s – Figure 5B, orange). RC-LH1-X complexes isolated from low expression membranes using SMA produced a time constant of 3.6 s (Figure 5B, blue), and given the noise in the experimental data this value is not significantly different from that for intact high expression membranes or SMA-solubilised material from these (i.e. Figure 5B, blue, purple and orange – note that the blue and purple fits are almost coincident). Recombination of $P^+Q_B^-$ was slowest for RC-LH1-X complexes isolated from fused membranes using SMA (4.8 s – red), a preparation which, as discussed above, probably consisted of a mixture of RC-LH1-X complexes and free RCs (likely in the form of SMALPS). Given the level of noise in the experimental data the difference in the fitted time constant between this sample and those prepared from high or low expression membranes was probably not significant. We have previously reported a time constants of 4.0 s for $P^+Q_B^-$ recombination in RCs in SMALPS [5], which would rule out a significant kinetic distortion by a sub-population of RC SMALPs.

Thin layer chromatography (TLC) of lipid extracts of high expression membranes (Table 2) identified phosphatidylethanolamine (PE), phosphatidylcholine (PC), cardiolipin (CL), phosphatidylglycerol (PG), and sulphoquinovosyl diacylglycerol (SQDG), which is in accordance with the lipid content of antenna-deficient membranes in *Rba. sphaeroides* [5]. The same five lipids were also detected in fragments isolated from high expression membranes that had been fused with DD13 membranes. The relative amounts of lipids in high expression membranes and in the isolated membrane fragments are similar, however, CL seems to be slightly enriched in the membrane fragments mostly on the expensive of PE.

Taken with the data from absorbance spectroscopy and $P^+Q_B^-$ recombination kinetics, it was possible to conclude that the treatments explored to make RC-LH1-X high expression membranes more amenable to solubilisation by SMA did not have an adverse effect on the structural or functional integrity of the complex.

Table 2.
Lipid composition of RC-LH1 expressing membranes and SMA solubilized RC-LH1 after fusion with DD13 membranes

Lipids	Membrane	SMA solubilized RC-LH1
CL	5.5 ±0.6	11.0 ±1.5
PE	34.4 ±1.4	30.4 ±1.9
PG	22.6 ±0.4	21.2 ±0.6
PC	28.2 ±0.3	25.8 ±2.0
SQDG	9.3 ±1.2	11.6 ±2.2

Extraction of synthetic RC oligomers with SMA

To explore further the issue of how size affects the efficacy with which SMA can isolate a membrane protein in the form of a nanodisc, a set of engineered RCs were used that assemble as synthetic, programmable dimeric, trimeric and tetrameric complexes (Figure 6A). This was achieved as described in previous work by tethering monomeric RCs together through genetically-encoded fusion of the N-terminus of one of the component polypeptides to an extra-membrane α-helix that forms a water-soluble coiled-coil bundle [38]. The sequence of this α-helix determines the oligomeric state of the bundle [50], and hence that of the tethered RCs [38]. Together with the native monomer, these artificial oligomers provide a set of RC complexes with calculated masses of 104, 216, 324 and 436 kDa respectively, housed in an antenna-deficient membrane system that has been proven to be amenable to solubilisation with SMA2000 [5]. X-ray crystal structures of the oligomers have not been determined but molecular models of each of them in a bilayer have been constructed and validated by AFM images of individual oligomers [38]. Views of these molecular models perpendicular to the plane of the membrane are shown in Figure 6A. In terms of gross dimensions in the plane of the membrane, monomeric and dimeric RCs can be represented by ellipsoids with approximate dimensions of 5 x 7 nm and 6 x 13 nm, respectively. Trimeric and tetrameric RCs can be represented by circles with diameters of 14 nm and 17 nm, respectively.

When isolated from antenna-deficient membranes using detergent, RCs modified in this way have been found to be a mixture of monomers and the programmed oligomer, with a yield of ~80 % of the total RC population in the dimer or trimer form, and ~50 % of the total RC population in the tetramer form (based on the separation of the monomeric and multimeric species by size-exclusion chromatography) [38]. It should be noted that the percentage of RCs in the oligomeric form in membranes may be substantially higher than this as the extent to which detergent extraction causes monomerisation has not been determined. As illustrated in Figures 6B-D, if a RC oligomer is regarded as a single molecule, these minimal estimates mean that "dimer membranes" contained 67 % RC dimers and 33 % RC monomers (Figure 6B), "trimer membranes" contained 57 % RC trimers and 43 % RC monomers (Figure 6C), and "tetramer membranes" contained 20 % RC tetramers and 80 % RC monomers (Figure 6D).

As shown in Figure 6E and 6F, lower molecular weight 2:1 and 3:1 SMA formulations that achieved >80 % extraction of RC monomers were also able to extract RCs from membranes containing a proportion of artificially oligomeric RCs, but the efficiency of extraction decreased as the oligomer became larger. Hence, organising a sub-population of RCs into larger structures in the membrane impacted on the ability of SMA to liberate the total RC population into solution. Such a gradual decline in extraction efficiency

could not be accounted for simply by an inability of the SMA to solubilise RCs when in the oligomeric form, as this should be expected to cause a much sharper drop-off of efficiency for membranes containing dimers and trimers (where the monomer RC population is only 33 % or 43 % of the total, respectively – Figure 6B,C), and a recovery to higher extraction efficiency for tetramers (where the monomer population is ~80 % of the total – Figure 6D). The conclusion therefore, was that although a decrease in the proportion of monomeric RC complexes may have contributed to the gradual reduction in extraction efficiency across the four types of membrane, it was likely that artificial tethering of RC complexes into larger and larger oligomers also contributed to this reduction, these formulations of SMA gradually becoming less effective at solubilising RCs as the size of the oligomer became larger.

Interestingly, a different trend was seen when the longer chain formulations of SMA were used (Figure 6G and 6H). Here there was a sharp drop-off in extraction efficiency on moving from monomers to dimers, and the extraction efficiency seemed to recover somewhat with trimers and then tetramers. Here there was a hint that this trend may be related to the relative size of the monomer population, which changes through 100 % to 33 % to 43 % to 80 % on moving from monomers through to tetramers, but a clear correlation could not be drawn. However, it was the case that a simple correlation with oligomer size was no longer seen. Intriguingly, focussing just on the data for monomeric and tetrameric RCs, although the longer chain SMAs were clearly less effective at solubilising monomers than the shorter chain SMAs, the efficiency of extraction from membranes containing RC tetramers was similar for the long and short chain forms. When solubilised with DDM all RC-oligomer variants were extracted to a ~70 % or greater efficiency, again showing that these effects are specific to SMA.

Characteristics of SMA-solubilised RC oligomers

Using a protocol previously reported for the purification of monomeric RCs in SMA [5], membranes expressing engineered dimeric, trimeric and tetrameric RCs were treated with 2:1 SMA (10 kDa from Polyscope) and the solubilised RCs were purified nickel affinity chromatography. Due to the high mass of the SMA/lipid/protein nanoparticles it was not possible to separate nanoparticles containing oligomers from those containing monomeric RCs in the way that is possible when RC monomers and oligomers are solubilised using LDAO.

DLS showed that nanoparticles prepared from membranes containing RC dimers were similar in size to those prepared from membrane containing exclusively RC monomers, with diameters of 11.9 ± 9.7 nm and 11.1 ± 7.5 nm, respectively. For the former this value was similar to that of 12.2 ± 7.1 nm reported by us previously for RC monomers prepared with a similar, but not identical, formulation of 2:1 SMA (SMA2000, 7.5 kDa from Cray Valley) [5]. Also based on DLS, SMA/lipid nanoparticles purified from

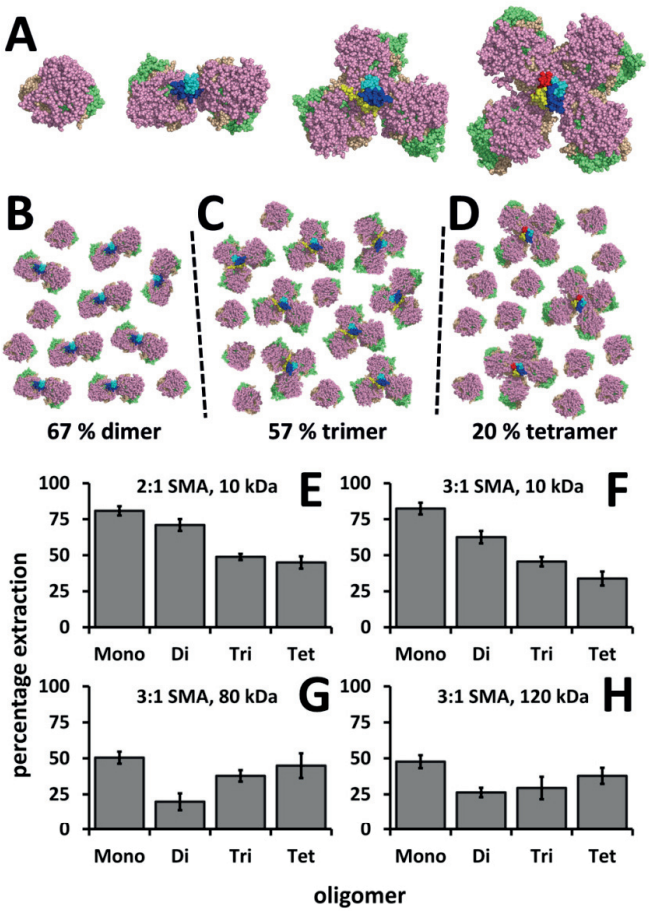

Figure 6.
Efficiency of solubilisation of native monomeric and artificially oligomeric RCs with four variants of SMA. (A) Molecular models of monomeric, dimeric, trimeric and tetrameric RCs. View is from the cytoplasmic side of the membrane, RCs are shown as in Figure 1 with the fused coiled-coil bundle in blue/cyan for dimers, blue/cyan/yellow for trimers or blue/cyan/yellow/red for tetramers; (B) extraction using 2:1 SMA, 10 kDa. (C) Extraction using 10 kDa 3:1 SMA. (D) Extraction using 80 kDa 3:1 SMA. (E) Extraction using 120 kDa 3:1 SMA. In all panels, Mono refers to extraction from antenna-deficient membranes containing native monomeric RCs whilst Di, Tri and Tet refer to extraction from antenna-deficient membranes that contain engineered dimeric, trimeric and tetrameric RCs, respectively. Error bars show standard deviations (three replicates).

membranes containing RC trimers and tetramers were consistently somewhat larger at 14.3 ± 8.3 nm and 12.9 ± 16.1 nm, respectively. As indicated above, modelling suggests that RC trimers and tetramers can be approximated in the plane of the membrane by circles of the order of 14 and 17 nm diameter, respectively, which would explain the need for a somewhat larger nanoparticle than is required to accommodate RC monomers or dimers. It should be remembered that DLS measures an average hydrodynamic

radius and so does not simply report on the diameter in the plane of the membrane. In addition, it is probable that each preparation of purified SMA/lipid/RC nanoparticles contained a substantial fraction of RC monomers in addition to RC oligomers, which could lead to an underestimate of the diameter of the sub-population of nanoparticles accommodating oligomers, particularly for tetramers as in this system the oligomeric form made up only 20 % of the RC complexes in the membrane when viewing the RC tetramer as a single molecule. Such heterogeneity would also explain why the error associated with the estimate of mean diameter from DLS was larger for the nanoparticles prepared from membranes containing RC tetramers.

TEM of these nanoparticle preparations showed a range of particle sizes (data not shown), in broad agreement with the findings from DLS. However it was not possible to confirm from this imaging whether some of these particles housed oligomeric RCs.

The mechanism of SMA solubilisation of membrane proteins

Systematic investigations of the mechanism by which SMA solubilises membranes have employed liposome systems comprised of pure lipids [51—54]. It has been found that the polymer inserts into the membrane after which the hydrophobic styrene groups intercalate with the lipid tails [11, 51, 55]. The resulting nanodiscs have a diameter of 9 nm and are monodisperse. Nanodiscs incorporating proteins tend to be larger, at 10–15 nm diameter with some reports of structures up to 24 nm. These data indicate that intrinsic curvature of SMA may be involved in the formation of nanodiscs when inserted into a lipid bilayer, but that the degree of this curvature is somewhat flexible to allow the incorporation of membrane proteins through the formation of larger discs that is seen in ideal lipid-only systems. In this report we were able to use a variety of SMAs to solubilise monomeric RC-LH1 complexes which have a diameter of around 13 nm and comprise 43 membrane-spanning α-helices, and also artificially tetrameric RCs that have an expected diameter of 17 nm and comprise 44 membrane-spanning α-helices. It was also possible to isolate RC-LH1-X complexes which are known to assemble in the membrane as dimers with a total of 80 membrane-spanning α-helices and dimensions of 21 x 12 nm in the plane of the membrane. However, it should be noted that even with mild detergents such as DDM it is difficult to isolate the dimeric form of the RC-LH1-X complexes from the type of high-expression membrane system employed here, and so it is likely that those RC-LH1-X complexes that were solubilised by SMA were monomers rather than dimers.

Examination of the literature shows that most studies have employed a SMA formulation with a 3:1 ratio of styrene to maleic acid, with a smaller number of studies using a 2:1 formulation. In the present work, both types were equally effective in solubilising monomeric RCs when average chain molecular weights were below 30 kDa. As far as we are aware there are no data published on the effectiveness of

more hydrophilic or more hydrophobic versions of SMA but, in our hands, neither a 1.5:1 nor a 4.5:1 formulation was able to solubilise monomeric RCs. A simple way to rationalise this would be to postulate that the 4.5:1 version is insufficiently hydrophilic to make the initial ionic interactions with the lipid headgroups, whilst the 1.5:1 version is insufficiently hydrophobic to insert into the membrane to the extent required to form the nanodisc. Therefore it is likely that the ratio of hydrophobic to charged groups required to form a SMA nanodisc occupies a small window.

As outlined above, initial failures to achieve substantial solubilisation of RC-LH1 complexes from photosynthetic membranes using any of the SMA variants were overcome by reducing the level of protein expression or by fusing high-expression membranes with pure lipids, lipid extracts or less SMA-recalcitrant membranes from the same organism. Although this remains to be proven, our hypothesis is that these treatments reduced the density of packing of RC-LH1 complexes in the membrane enabling permeation by SMA, which suggests that SMA needs regions of lipid bilayer in order to at least initiate nanodisc formation.

Having identified treatments that made RC-LH1-X membranes less resistant to solubilisation by SMA, it was interesting to note that the resulting nanodiscs purified by nickel affinity chromatography contained RC-LH1 complexes rather than just RCs (as assessed by the absorbance spectra of the purified nanodiscs). The isolation of intact RC-LH1 complexes by detergent purification requires the use of mild detergents such as DDM, treatment of membranes with more aggressive detergents such as lauryl diamine oxide (LDAO) resulting in preferential solubilisation of RCs and degradation of the surrounding LH1 pigment protein. The rationalisation of this is that LDAO disrupts molecular interactions between the LH1 and RC components of the RC-LH1-X complex whereas DDM preserves these interactions. The extraction of structurally and functionally intact RC-LH1 complexes using SMA suggests that the polymer is reasonably tolerant to weak interactions between membrane components. These findings suggest that SMA may be used to trap and identify through co-purification protein-protein interactions that would not withstand detergent purification or to solubilise multi-component complexes, such as supercomplexes, that do not retain their native interactions upon detergent treatment.

Conclusions

The data described in this report take a systematic look at the ability of different formulations of the SMA polymer to solubilise monomeric RC pigment-proteins from bacterial membranes. SMA copolymers with 2:1 and 3:1 ratios of styrene to maleic acid were equally effective in solubilising RCs, with no obvious differences between differently-sized polymers up to an average molecular weight of 30 kDa. In contrast, 1.5:1 and 4.5:1 formulations of SMA were unable to solubilise RCs, showing that a correct

balance of hydrophobic and hydrophilic groups is required for a SMA to effectively solubilise target complexes. Engineered RC oligomers with up to 44 transmembrane helices and a diameter of 12 nm in the plane of the membrane could be solubilised with low molecular weight 2:1 and 3:1 SMAs, and our data suggest the size limit for SMA solubilisation lies in excess of these values. Interestingly high molecular weight 3:1 SMAs (80 and 120 kDa) were less effective at solubilising monomeric RCs then their <30 kDa counterparts, but this trend was lost when RCs were tethered together into synthetic tetramers. This suggests that there may be some advantage to using longer chain variants of SMA for the purification of larger complexes. A resistance to SMA solubilisation was seen with membranes in which RC-LH1-X proteins are known to form highly ordered arrays, and altering the properties of the SMA did not enhance solubilisation. However, lowering protein expression levels or increasing the lipid-to-protein ratio through various lipid or membrane fusions enabled solubilisation of a greater proportion of RC-LH1-X proteins by SMA. This supports the notion that SMA interacts principally with lipids. However, these solubilised RC-LH1-X complexes still comprised small membrane patches rather than a homogeneous population of discrete nanodiscs containing a single protein. Overall we conclude that successful solubilisation of a membrane protein by the SMA copolymer requires the right balance of copolymer hydrophobicity/hydrophilicity and length, and that properties of the target membrane such as lipid:protein ratio and the degree of order shown by component proteins are also of crucial importance.

References

1 Jamshad, M., Lin, Y.-P., Knowles, T.J., Parslow, R.A., Harris, C., Wheatley, M., Poyner, D.R., Bill, R.M., Thomas, O.R.T., Overduin, M. and Dafforn, T.R. (2011) Surfactant-free purification of membrane proteins with intact native membrane environment. *Biochem. Soc. Trans.* **39**, 813-818.

2 Dörr, J. M., Scheidelaar, S., Koorengevel, M. C., Dominguez, J. J., Schäfer, M., van Walree, C. A. and Killian, J.A. (2016) The styrene–maleic acid copolymer: a versatile tool in membrane research. *Eur. Biophys. J.* **45**, 3-21.

3 Lee, S.C, Knowles, T.J., Postis, V.L.G., Jamshad, M., Parslow, R.A., Lin, Y.-P., Goldman, A., Sridhar, P., Overduin, M., Muench, S. P. and Dafforn T. R. (2016) A method for detergent-free isolation of membrane proteins in their local lipid environment. *Nature Protocols* **11**, 1149-1162.

4 Knowles, T. J., Finka, R., Smith, C., Lin, Y.-P., Dafforn, T. and Overduin, M. (2009) Membrane proteins solubilized intact in lipid containing nanoparticles bounded by styrene maleic acid copolymer. *J. Am. Chem. Soc.* **131**, 7484-7485.

5 Swainsbury, D.J.K., Scheidelaar, S., van Grondelle, R., Killian, J.A. and Jones, M.R. (2014) Bacterial reaction centers purified with styrene–maleic acid copolymer retain native membrane functional properties and display enhanced stability. *Angew. Chem. Int. Ed.* **53**, 11803–11807.

6 Dörr, J.M. *et al.* (2014) Detergent-free isolation, characterization, and functional reconstitution of a tetrameric K^+ channel: the power of native nanodiscs. *Proc. Natl. Acad. Sci. USA* **111**, 18607-18612.

7 Paulin, S. *et al* (2014) Surfactant-free purification of membrane protein complexes from bacteria: application to the staphylococcal penicillin-binding protein complex PBP2/PBP2a. *Nanotechnology* **25**, 285101.

8 Gulati, S., Jamshad, M., Knowles, T.J., Morrison, K.A., Downing, R., Cant, N., Collins, R., Koenderink, J.B., Ford, R.C., Overduin, M., Kerr, I.D., Dafforn, T.R. and Rothnie, A.J. (2014) *Biochemical J.* **461**, 269-278.

9 Postis, V. *et al* (2015) The use of SMALPs as a novel membrane protein scaffold for structure study by negative stain electron microscopy. *Biochim. Biophys. Acta Biomemb.* **1848**, 496-501.

10 Prabudiansyah, I., Kusters, I., Caforio, A. and Driessen, A.J.M. (2015) Characterization of the annular lipid shell of the Sec translocon. *BBA-Biomemb.* **1848**, 2050-2056.

11 Jamshad, M. *et al* (2015a) G-protein coupled receptor solubilization and purification for biophysical analysis and functional studies, in the total absence of detergent. *Biosci. Rep.* **35**, 1-10.

12 Logez, C., Damian, M., Legros, C., Dupré, C., Guéry, M., Mary, S., Wagner, R., M'Kadmi, C., Nosjean, O., Fould, B., Marie, J., Fehrentz, J.-A., Martinez, J., Ferry, G., Boutin, J. A. and Banères, J.-L. (2016) Detergent-free isolation of functional G protein-coupled receptors into nanometric lipid particles. *Biochemistry* **55**, 38-48.

13 Wheatley, M., Charlton, J., Jamshad, M., Routledge, S.J., Bailey, S., La-Borde, P.J., Azam, M. T., Logan, R.T., Bill, R.M., Dafforn, T.R. and Poyner, D.R. (2016) GPCR–styrene maleic acid lipid particles (GPCR–SMALPs): their nature and potential. *Biochem. Soc. Trans.* **44**, 619-623.

14 Long, A.R., O'Brien, C.C., Malhotra, K., Schwall, C.T., Albert, A.D., Watts, A. and Alder, N.N.

(2013) A detergent-free strategy for the reconstitution of active enzyme complexes from native biological membranes into nanoscale discs. *BMC Biotechnology* **13**, 41.

15 Craig, A.F., Clark, E.E., Sahu, I.D., Zhang, R., Frantz, N.D., Al-Abdul-Wahid, S., Dabney-Smith, C., Konkolewicz, D., Lorigan, G.A. (2016) Tuning the size of styrene-maleic acid copolymer-lipid nanoparticles (SMALPs) using RAFT polymerization for biophysical studies. *BBA Biomembranes.* In press.

16 Lee, S.C., Pollock, N.L. (2016) Membrane proteins: is the future disc shaped? Biochem. Soc. Trans. **44**, 1011–1018; doi:10.1042/BST20160015.

17 Feher, G., Allen, J.P., Okamura, M.Y. and Rees, D.C. (1989) Structure and function of bacterial photosynthetic reaction centres. *Nature* **33**, 111-116.

18 Hoff, A.J. and Deisenhofer, J. (1997) Photophysics of photosynthesis. Structure and spectroscopy of reaction centers of purple bacteria. *Physics Reports* **287**, 2-247

19 Jones, M.R. (2009) The petite purple photosynthetic powerpack. *Biochem. Soc. Trans.* **37**, 400-407.

20 Heathcote, P. and Jones, M.R. (2012) The structure-function relationships of photosynthetic reaction centers. in Comprehensive Biophysics, Vol. 8 (Eds.: Egelman E. H., Ferguson S.), Academic Press, Oxford, UK, pp. 115-144.

21 Qian, P. *et al.* (2013) Three-dimensional structure of the *Rhodobacter sphaeroides* RC-LH1-PufX complex: dimerization and quinone channels promoted by PufX. *Biochemistry* **52**, 7575-7585.

22 Niwa, S. *et al.* (2014) Structure of the LH1-RC complex from *Thermochromatium tepidum* at 3.0 angstrom. *Nature* **508**, 228-232.

23 Walz, T., Jamieson, S.J., Bowers, C.M., Bullough, P.A. and Hunter, C.N. (1998) Projection structures of three photosynthetic complexes from *Rhodobacter sphaeroides*: LH2 at 6 Angstrom, LH1 and RC–LH1 at 25 Angstrom. *J. Mol. Biol.* **282**, 833-845.

24 Francia, F., Wang, J., Venturoli, G., Melandri, B.A., Barz, W.P. and Oesterhelt, D. (1999) The reaction center-LH1 antenna complex of *Rhodobacter sphaeroides* contains one PufX molecule which is involved in dimerization of this complex. *Biochemistry* **38**, 6834-6845.

25 Siebert, C.A., Qian, P., Fotiadis, D., Engel, A., Hunter, C.N. and Bullough, P.A. (2004) Molecular architecture of photosynthetic membranes in *Rhodobacter sphaeroides*: the role of PufX. *EMBO J.* **23**, 690-700.

26 Holden-Dye, K., Crouch, L.I. and Jones, M.R. (2008) Structure, function and interactions of the PufX protein. *Biochim. Biophys. Acta Bioenerg.* **1777**, 613-630.

27 Hunter, C.N., Daldal, F., Thurnauer, M.C. and Beatty, J.T. (eds) (2009) The purple photosynthetic bacteria. Advances in Photosynthesis and Respiration, Vol 28. Springer, Dordrecht.

28 Niederman, R.A. (2016) Development and dynamics of the photosynthetic apparatus in purple phototrophic bacteria. *Biochim. Biophys. Acta* **1857**, 232-246

29 Jungas, C., Ranck, J.L., Rigaud, J.L., Joliot, P. and Verméglio, A. (1999) Supramolecular organization of the photosynthetic apparatus of *Rhodobacter sphaeroides*. *EMBO J.* **18**, 534-542.

30 Qian, P., Bullough, P.A. and Hunter, C.N. Three-dimensional reconstruction of a membrane-bending complex the RC-LH1-PufX core dimer of *Rhodobacter sphaeroides*. *J. Biol. Chem.* **283**, 14002-14011.

31 Ng, I.W., Adams, P.G., Mothersole, D.J., Vasilev, C., Martin, E.C., Lang, H.P., Tucker, J.D. and Hunter C.N. (2011) Carotenoids are essential for normal levels of dimerisation of the RC–LH1–PufX core complex of *Rhodobacter sphaeroides*: characterisation of R-26 as a crtB (phytoene synthase) mutant. *Biochim. Biophys. Acta Bioenerg.* **1807**, 1056-1063.

32 Ratcliffe, E.C., Tunnicliffe, R.B., Ng, I.W., Adams, P.G., Qian, P., Holden-Dye, K., Jones M.R., Williamson M.P. and Hunter C.N. (2011) Experimental evidence that the membrane-spanning helix of PufX adopts a bent conformation that facilitates dimerisation of the *Rhodobacter sphaeroides* RC–LH1 complex through N-terminal interactions. *Biochim. Biophys. Acta Bioenerg.* **1807**, 95–107.

33 Bligh, E.G., Dyer, M., (1959) A rapid method of total lipid extraction and purification. *Can, J. Biochem. Physiol.* **37**, 911-917.

34 Westerhuis, W.H., Sturgis, J.N., Ratcliffe, E.C., Hunter, C.N. and Niederman R.A. (2002) Isolation, size estimates, and spectral heterogeneity of an oligomeric series of light-harvesting 1 complexes from *Rhodobacter sphaeroides*. *Biochemistry* **41**, 8698-8707.

35 Hunter, C.N., Pennoyer, J.D., Sturgis, J.N., Farrelly, D. and Niederman, R.A. (1988) Oligomerization states and associations of light-harvesting pigment protein complexes of *Rhodobacter sphaeroides* as analyzed by lithium dodecyl-sulfate polyacrylamide-gel electrophoresis. *Biochemistry* **27**, 3459-3467.

36 Golecki, J.R., Ventura, S. and Oelze, J. (1991) The architecture of unusual membrane tubes in the B800–850 light-harvesting bacteriochlorophyll-deficient mutant 19 of *Rhodobacter sphaeroides*. *FEMS Micro. Letts.* **77**, 335-340.

37 Adams, P.G., Mothersole, D.J., Ng, I.W., Olsen, J.D. and Hunter, C.N. (2011) Monomeric RC–LH1 core complexes retard LH2 assembly and intracytoplasmic membrane formation in PufX-minus mutants of *Rhodobacter sphaeroides*. *Biochim. Biophys. Acta* **1807**, 1044-1055

38 Swainsbury, D.J.K, Harniman, R.L., Di Bartolo, N.D., Liu, J., Harper, W.F.M., Corrie, A.S., and Jones, M.R., (2016), Directed assembly of defined oligomeric photosynthetic reaction centres through adaptation with programmable extra-membrane coiled-coil interfaces, *BBA Bioenergetics, In Press.*

39 Gibasiewicz, K., Pajzderska, M., Potter, J.A., Fyfe, P.K., Dobek, A., Brettel, K., Jones, M.R. (2011) Mechanism of recombination of the $P^+H_A^-$ radical pair in mutant *Rhodobacter sphaeroides* reaction centers with modified free energy gaps between $P^+B_A^-$ and $P^+H_A^-$. *J Phys. Chem. B* **115**, 13037-13050.

40 Swainsbury, D.J.K., Friebe, V.M., Frese R.N. and Jones, M.R. (2014) Evaluation of a biohybrid photoelectrochemical cell employing the purple bacterial reaction centre as a biosensor for herbicides. *Biosens. Bioelectron.* **58**, 172-178.

41 Friebe, V.M., Delgado, J.D., Swainsbury, D.J.K., Gruber, J.M., Chanaewa, A., van Grondelle, R., von Hauff, E.L., Millo, D., Jones, M.R. and Frese, R.N. (2016) Plasmon enhanced photocurrent of photosynthetic pigment-proteins on nanoporous silver. *Adv. Func. Mat.* **26**, 285-292.

42 Pennoyer, J.D., Kramer, H.J., van Grondelle, R., Westerhuis, W.H., Amesz, J., Niederman, R.A. (1985) Excitation energy transfer in *Rhodopseudomonas sphaeroides* chromatophore membranes

fused with liposomes. *FEBS Letters*. **182**, 145-150.

43 Kenyon, C.N. Complex lipids and fatty acids of photosynthetic bacteria. in The Photosynthetic Bacteria. (Eds.: R. K. Clayton, W. R. Sistrom), Plenum Press, New York, 1978, pp. 281-313.

44 Onishi, J.C. and Niederman, R.A. (1982) *Rhodopseudomonas sphaeroides* membranes - alterations in phospholipid-composition in aerobically and phototrophically grown cells. *J. Bacteriol.* **149**, 831-839

45 Donohue, T.J., Cain, B.D. and Kaplan, S. (1982) Alterations in the phospholipid-composition of *Rhodopseudomonas sphaeroides* and other bacteria induced by TRIS. *J. Bacteriol.* **152**, 595-606.

46 Francia, F., Dezi, M., Rebecchi, A., Mallardi, A., Palazzo, G., Melandri, B. A. and Venturoli, G. (2004) Light-harvesting complex 1 stabilizes $P^+Q_B^-$ charge separation in reaction centers of *Rhodobacter sphaeroides*. *Biochemistry* **43**, 14199-14210.

47 Dezi, M., Francia, F., Mallardi, A., Colafemmina, G., Palazzo, G., Venturoli, G. (2007) Stabilization of charge separation and cardiolipin confinement in antenna – reaction center complexes purified from *Rhodobacter sphaeroides*. *Biochim. Biophys. Acta* **1767**, 1041-1056.

48 Maróti, P. (1991) Electron transfer and proton uptake of photosynthetic bacterial reaction centres reconstituted in phospholipid vesicles. *J. Photochem. Photobiol. B* **8**, 263-277

49 Agostiano A., Catucci L., Giustini M., Mallardi A. and Palazzo G. (1998) Charge recombination kinetics of photosynthetic reaction centres in phospholipid organized systems. *Proc. Indian Acad. Sci. Chem. Sci.* **110**, 251-264.

50 Fletcher J.M. *et al*. A basis set of *de novo* coiled-coil peptide oligomers for rational protein design and synthetic biology. *ACS SynBio.* **1**, 240-250

51 Scheidelaar, S., Koorengevel, M.C., Pardo, J.D., Meeldijk, J.D., Breukink, E. and Killian, J.A. (2015) Molecular model for the solubilization of membranes into nanodisks by styrene–maleic acid copolymers. *Biophys. J.* **108**, 279-290.

52 Tanaka, M., Hosotani, A., Tachibana, Y., Nakano, M., Iwasaki, K., Kawakami, T. and Mukai, T. (2015) Preparation and characterization of reconstituted lipid–synthetic polymer discoidal particles. *Langmuir* **31**, 12719–12726.

53 Vargas, C., Cuevas Arenas, R., Frotscher, E. and Keller, S. (2015) Nanoparticle self-assembly in mixtures of phospholipids with styrene/maleic acid copolymers or fluorinated surfactants. *Nanoscale* **7**, 20685-20696.

54 Zhang, R., Sahu, I.D., Liu, L., Osatuke, A., Comer, R.G., Dabney-Smith, C. and Lorigan, G.A. (2015) Characterizing the structure of lipodisq nanoparticles for membrane protein spectroscopic studies. *Biochim. Biophys. Acta Biomemb.* **1848**, 329-333.

55 Orwick-Rydmark, M., Lovett, J.E., Graziadei, A., Lindholm, L., Hicks, M.R. and Watts, A. (2012) Detergent-free formation and physicochemical characterization of nanosized lipid–polymer complexes: lipodisq. *Nano Lett.* **12**, 4687-4692.

CHAPTER 6

SUMMARIZING DISCUSSION & OUTLOOK

THIS CHAPTER IS PARTLY BASED ON THE PUBLICATION:

J.M. DÖRR, **S. SCHEIDELAAR**, M.C. KOORENGEVEL, J.J. DOMINGUEZ, M. SCHÄFER, C.A. VAN WALREE AND J.A. KILLIAN, (2016), THE STYRENE–MALEIC ACID COPOLYMER: A VERSATILE TOOL IN MEMBRANE RESEARCH. *EUR. BIOPHYS. J.* 45, 3-21.

6.1 The study of membranes and membrane proteins

Membranes are of great importance to life. They enclose the contents of cells, form a barrier to the external environment and are a dynamic and active part of cellular processes. Membrane proteins in the cell membrane can be considered as the gatekeepers of the cell regulating the transport of molecules over the membrane. For that reason, membrane protein have become important targets in the pharmaceutical industry; about 50-60 % of all approved drugs target a membrane protein [1,2]. In addition, one of the most vital processes for life on earth, that of photosynthesis, takes place in lipid membranes.

Insight in how membranes work will return much valuable information on how drugs can be efficiently transported into cells and how we can learn from photosynthesis in our search for sustainable energy sources. Unfortunately, the study of a lipid membrane or a specific membrane protein is challenging. The main difficulty is that membrane proteins are not water soluble, which gives problems with membrane protein isolation and stabilization. Membrane proteins require special synthetic systems to stabilize them in aqueous environment.

Various systems and approaches have been developed and include the use of detergent micelles, bicelles, amphipols, and membrane scaffold protein (MSP) nanodiscs. They all have their own advantages and limitations and comprehensive reviews of these systems can be found in the literature [3-5]. Ideally, the chemical environment of purified membrane proteins in a synthetic system is the same as the chemical environment in the native membrane. Clearly, that is impossible and as such the development of new synthetic systems will always continue.

Recently, a new approach for the stabilization of membrane proteins in aqueous solution based on the copolymer styrene–maleic acid (SMA) was introduced. SMA is able to solubilize lipids and membrane proteins in the form of nanodisc particles. This particular solubilization process is the central topic in this thesis.

6.2 The SMA copolymer in membrane research

The SMA copolymer is another approach for the stabilization of membrane proteins in aqueous solution. Why would SMA be better than any of the other approaches? The superior property of SMA is that it is the only approach that does not require detergents to solubilize a membrane. Consequently, the formation of nanodiscs with SMA is a single-step process in which the protein is captured along with a piece of the native lipid environment. The unique property of SMA to maintain the direct native lipid environment leads to a higher stability of the protein (Chapter 4), which may help to increase the number of membrane proteins that can be studied, and may allow the identification of novel protein-lipid interactions.

In 2001, Tonge and Tighe were the first to report that SMA copolymers are able to stabilize a small piece of lipid bilayer in the form of a nanodisc [6]. They found that the

nanodiscs can hold hydrophobic drugs and recognized that nanodiscs might be a new way to deliver drugs in cells. Later on, it was realized that nanodiscs of SMA might also be used as a platform for membrane proteins. In 2009, the solubilization of membrane proteins by SMA was demonstrated for the first time [7].

Although the potential of SMA in membrane research was made clear, many questions still needed to be answered. In this thesis, we focused mainly on two aspects: (I) the mode of action of SMA copolymers in the solubilization of lipid membranes (Chapter 2 & 3), and (II) the solubilization of photosynthetic proteins in native nanodiscs. In addition, we compared properties of these proteins in native nanodiscs with those obtained by conventional approaches in detergent micelles (Chapter 4 & 5).

Below, the main results are summarized and the potential of SMA copolymers in membrane research will be discussed.

6.3 The mode of action of SMA copolymers in model membrane systems

Model membranes offer an ideal way to study the mode of action of the SMA copolymer. They are easy and quick to prepare and the physical properties of the membrane can be systematically modulated by changing the lipid composition. In Chapter 2 & 3 large unilamellar vesicles (LUVs) of various lipid compositions were prepared and SMA was added to them to study the process of solubilization and nanodisc formation. Different biophysical techniques were applied to characterize membrane solubilization by SMA of which turbidity measurements played a major role. In turbidity experiments the amount of light scattering is monitored in time after the addition of SMA to LUVs. Since LUVs are large (200—400 nm) and nanodiscs are small (~10 nm) solubilization is conveniently monitored as a decrease in the amount of light scattering allowing the study of the solubilization process under various conditions. Such experiments however do not specify anything about the thermodynamics of the process or about the nature and lifetime of the intermediate structures that are formed during solubilization. More insight into the nature of the particles that are formed during solubilization was obtained by electron microscopy (EM). During solubilization by SMA, membranes are fragmented and many membrane fragments of different sizes are formed. Upon further solubilization these fragments decrease in size ultimately resulting in the formation of nanodiscs.

Membrane solubilization. The efficiency of membrane solubilization by the SMA 2:1 copolymer under various conditions was investigated by turbidity experiments. Based on the results of these experiments a three-step solubilization model was proposed as shown in Chapter 2.

Several parameters were found to have a positive effect on solubilization. For example, the presence of salt in solution, which decreases the electric potential at the

membrane surface that arises when negatively charged lipids such as PG are present and/or when anionic SMA copolymers adsorb. The decreased electric potential allows more SMA to insert thereby speeding up solubilization. It should be noted that monovalent ions are most suitable. Divalent ions like Ca^{2+} and Mg^{2+} can bind to a doubly charged maleic acid group thereby precipitating and inactivating the SMA copolymers.

Loosely packed lipids also have a positive effect on membrane solubilization. This is the case when lipids are in the liquid-crystalline phase and/or when the lateral pressure in the core of the membrane (also termed chain pressure) is relatively low. In those cases, SMA copolymers can easily insert into the membrane core and destabilize the membrane. When the lipids are tightly packed or when many non-bilayer lipids, such as PE, are present in the membrane solubilization is less efficient. These situations are likely to be encountered in biological membranes where the lipid and protein composition is much more complex and therefore slower solubilization is expected. In Chapter 3, SMA copolymers with different styrene-to-maleic acid ratio (1.4:1, 2:1. 3:1, and 4:1) were tested. The SMA 2:1 copolymer turned out to be the most efficient SMA variant mainly because this polymer has the optimal balance in the amount of styrene and maleic acid monomer units. A 2:1 styrene-to-maleic acid ratio leads to a collapsed state of the polymer in solution and a relatively homogenous distribution of the maleic acid units along the polymer chain. While the collapsed state with its hydrophobic domains ensures efficient membrane insertion, the homogenous distribution of the maleic acid units ensures efficient membrane destabilization. The SMA 3:1 variant showed similar efficient solubilization as the SMA 2:1 variant, but the SMA 1.4:1 and SMA 4:1 variants showed much less efficient solubilization. The SMA 1.4:1 variant is too hydrophilic lacking hydrophobic domains thereby inserting poorly into the membrane, while the SMA 4:1 is too hydrophobic having a minor amount and heterogeneous distribution of maleic acid units causing it to destabilize the membrane inefficiently.

Nevertheless, all tested SMA variants are able to form nanodisc as was shown by solubilization at the phase transition temperature, where large surface defects exist and the membrane is already partly destabilized. Apparently, it is thermodynamically favorable for the SMA to form nanodiscs regardless of its chemical composition. The resistance of the lipid membrane to these polymers determines then how efficient solubilization and nanodisc formation will be.

Properties of nanodiscs. Despite the individual contributions of lipids such as PG and PE to the kinetics of solubilization, SMA does not appear to preferentially solubilize certain lipid species, i.e., nanodiscs maintain the overall lipid composition of the vesicles as exemplified for a lipid mixture that reflects the composition of *E. coli* inner membranes (Chapter 2). This result implies that solubilization is mainly determined by the physical properties of the lipid membranes rather than by the properties of individual lipid species.

An interesting observation is that, regardless of the lipid composition, the size of nanodiscs from model membranes was found to be around 10 nm at a fixed SMA-to-lipid ratio of 3:1 (Chapter 2).

A possible explanation for this could be the intrinsic curvature (or sometimes called the persistence length) of the SMA copolymers when it is wrapped around a nanodisc. This property describes the stiffness of the polymer and allows a range of nanodisc sizes until a minimal size is reached (possibly ~10nm) where the polymer is bended optimally around the nanodisc. If the nanodisc gets any smaller, it will cost free energy to bend the polymer, hence it will become unfavorable to decrease the nanodisc in size. On the other hand, one might expect an increase in nanodisc size with decreasing SMA-to-lipid ratios. This is because it is favorable for the styrene units to insert and cover the hydrophobic rim of the nanodisc. When the SMA-to-lipid ratio decreases the nanodisc size will increase in order to match the number of styrene units in the system with the hydrophobic surface area of the nanodiscs.

Recently, the size of nanodiscs was related to the concentration of SMA used during solubilization [8,9]. Upon lowering the 3:1 SMA-to-lipid ratio the size of lipid nanodiscs was found to increase in size. Our proposed theory may thus explain why the nanodisc size increases with decreasing SMA concentration, and why a size of ~10 nm would be the smallest stable nanodisc possible.

Anyhow, our theory is an idea and further study is necessary in order to gain more insight in what drives the size of nanodiscs made by SMA copolymers.

6.4 The solubilization of reaction centers (RCs) by SMA copolymers

To study the application of membrane protein solubilization by SMA, the photosynthetic protein reaction center (RC) from the purple bacterium *Rhodobacter (Rba.) sphaeroides* was used. The main advantage of this membrane protein is that it comprises pigments which allow simple characterization of its properties, such as stability by its absorption spectra, but also that the protein structure and pigment organization have been well studied [11].

Solubilization of the RC from *Rba. sphaeroides* with the SMA 2:1 variant was efficient (~70—75% of the total RCs were solubilized) and resulted in the formation of nanodiscs (also named native nanodiscs, since they contain material of a native membrane) with a diameter between 12 to 15 nm (Chapter 4). Based on the dimensions of the protein and the determination of the amount of phospholipids in the nanodiscs it was estimated that around 150 lipids were co-isolated with the RC. Other proteins that were solubilized by SMA were also found to have native lipid co-purified with them, however, the number of lipids was found to vary a lot. For example, 40 lipids were found for the AcrB protein [12], whereas only 11 were co-extracted with the PagP protein [7]. Neither of the two low values would be in accordance with a full annular ring of lipids around the incorporated protein and thus some of

the hydrophobic surface of the protein would be in direct contact with the polymer.

There are several potential explanations for the large variation in lipid numbers. For instance, low amounts of lipids could originate from the formation of oligomeric complexes of the incorporated proteins. Furthermore, variations in experimental conditions, such as the SMA/lipid ratio used for initial solubilization could affect the composition and size of native nanodiscs. Systematic studies on this with biological membranes have not been reported yet, but the heterogeneity of SMA, the presence of structurally different membrane proteins and differences in membrane lipid composition will result in further deviations between samples. Thus, many different parameters will probably influence whether or not a full annular ring of lipids is co-extracted with the protein or whether there are alternating polymer and lipid contacts with the hydrophobic surface of the protein. For all systems in which the lipid content of native nanodiscs has been investigated, it was demonstrated that at least multiple native lipid molecules are co-isolated. [13—16]. This (near) native environment, whether organized in a genuine full bilayer or not, is likely the major reason for the higher stability of membrane proteins in native nanodiscs.

RCs in native nanodiscs showed higher stability under heating and light exposure as compared to RCs in detergent micelles and RCs in native membranes (Chapter 4). Intriguing is the higher stability in light of RCs in native nanodiscs as compared to RCs in native membranes. That is probably because native nanodiscs are less prone to damage by autocatalytic processes that have the characteristics of chain reactions than continuous bilayer systems. Light-induced oxidation processes may corrupt all molecules in a damaged liposome, whereas in nanodiscs the same process will affect much fewer lipids and generally only one protein. This principle may be important for potential future applications of native nanodiscs, for example in the construction of solar cells using a high concentration of RCs in native nanodiscs.

Comparison of two intrinsic properties of the RC, namely, the midpoint oxidation potential of the special pair, and the rate of recombination of the $P^{+}Q_{b}^{-}$ radical pair showed that RCs in native nanodiscs have properties that are very similar to RCs in the native membrane, but different from RCs in detergent micelles. Although it is likely that the increased stability and native-like properties of the RC in native nanodiscs is due to the native lipid environment, it is not certain that the *native* lipid environment is responsible for the increased stability or that the presence of lipids themselves is already sufficient. In any case, these results demonstrate that SMA offers a near-native environment for the RC that is superior to the environment of detergent micelles.

In Chapter 5, SMA formulations with variations in the styrene-to-maleic acid and molecular weight were studied for their solubilization activity. As in line with the solubilization of model membranes, the SMA 2:1 and SMA 3:1 variants are efficient and the SMA 1.4:1 and SMA 4:1 variants are not efficient in solubilization of the membranes and the subsequent extraction of the RC.

SMA resistant membranes. That solubilization of biological membranes and the formation of nanodisc particles may not be as straightforward as in case of the RC was made clear in attempts to solubilize RC-LH1 (core) complexes from *Rba. sphaeroides* (Chapter 5). In that case, the bacterium was modified to only express the core complex with or without the PufX protein. When the PufX protein is expressed the core complex dimerizes, while in the absence of PufX the core complex is present as monomer. In both cases, the solubilization efficiencies were similarly low with maximal extraction values around 5%.

A possible explanation for this resistance of the membrane to SMA solubilization is the high protein-to-lipid ratio and resulting high degree of order of the proteins in the membrane. Such an explanation is supported by the increased solubilization values of these proteins (up to ~25%) when lipids are fused in the membrane or when protein expressed was reduced. Both approaches lower the protein-to-lipid ratio in the membrane and as such partly reduce the ordered organization of the proteins. Although it was not determined how much the lipid to protein ratio changed, these results indicate that SMA benefits from the presence of lipid bilayer and loosely packed lipids. This would be in line with results from the solubilization of model membranes where loosely packed membranes are easier to solubilize than tightly packed membranes. Probably, if the protein-to-lipid ratio is reduced further it is possible to extract more core complexes.

Despite the success of solubilizing core complex with SMA copolymers upon diluting the protein content of the membrane, the solubilized material did not consist solely of monodisperse nanodisc particles. Electron microscopy (EM) revealed that solubilized material from highly-ordered core membranes predominantly consists of large membrane fragments (up to > 100 nm in size). Solubilized material of the diluted core membranes showed fragments that were much smaller (< 100 nm) with the possible presence of nanodisc particles in which a single core complex might be embedded. Although around 5% of cores could be extracted from highly-resistant membranes, the proteins were not solubilized into well-defined nanodiscs, but rather in large membrane fragments. Solubilization of protein-diluted membrane led to smaller particles, but not to a monodisperse nanodisc population. Possibly, when the protein-to-lipid ratio is lowered further, smaller particles may be formed and single protein complexes can be captured in nanodiscs.

Size limit of a protein in nanodiscs. That a single core complex could not be (efficiently) captured in a nanodisc might be due to the resistance of the membrane to SMA solubilization as discussed above. However, it is also possible that a single core complex is simply too big to fit in a nanodisc. The core complex in the monomeric form is approximately 13 nm in diameter, while the dimeric form is approximately 21 nm in diameter. It may be possible that a size limit for proteins in a nanodisc exists and that membranes full with such large proteins get solubilized partly or not at all.

To get more insight into this matter, oligomers (dimers, trimers and tetramers)

of the RC were expressed and solubilized with several SMA formulations (Chapter 5). The largest oligomer, the tetramer, is estimated to have a diameter of ~17 nm. Although the efficiency of extraction by the SMA 2:1 and SMA 3:1 formulations (both showed similar results) is different for the three oligomers, being less efficient for larger oligomers, all oligomers could be solubilized for at least ~30%. Inspection of the solubilized material by EM showed that particles are present that have sizes ranging from 10 to sometimes 100 nm, i.e. the oligomers are not solely in nanodisc particles. The less efficient solubilization of larger oligomers and the presence of large particles in the solubilized fraction of all at least indicate that the capturing of larger proteins (that consist of RCs) by SMA is less effective. Although we do not expect that the oligomers pack as tightly as cores do in the membrane, we cannot exclude that specific interactions between the oligomers (or interactions between oligomers and monomeric RCs) have a negative effect on the formation of nanodiscs.

SMA formulations with a higher molecular weight were also tried because they are longer and thus may be more efficient in embedding a large protein in a nanodisc. Unfortunately, these polymers show a more complex trend in the efficiency of oligomer solubilization. The solubilization efficiencies for dimers and trimers were lower and that of tetramers was similar to the low molecular weight SMA variants. This hints that the use of SMA formulations with higher molecular weights are not more beneficial per se.

The discussions about partial membrane solubilization and the existence of a possible size limit of proteins that fit in a native nanodisc are relevant for studies where SMA is used to solubilize membrane proteins from, for instance, plant thylakoid membranes. In these membranes, the protein-to-lipid ratio can be very high and the formation of super-complexes with sizes of ~35 nm has been observed [17]. For these membranes it may be expected that, depending on the nature of the protein, solubilization efficiencies will vary from protein to protein.

6.5 Outlook for the SMA copolymer in membrane research

Despite the fact that the SMA technique is still relatively young, the first report in the literature being 2009, it already has proven itself to be a very useful approach for the stabilization of membrane proteins in aqueous solution. In a number of recent studies it has been shown that SMA can extract membrane proteins directly from intact membranes of cells and organelles. The biological sources include bacteria, yeast, insect, and human cells (for review see [5]). The proteins incorporated into native nanodiscs range from those with a single membrane spanning α-helix to oligomeric complexes comprising up to 36 transmembrane helices. The variety of successfully solubilized membranes and incorporated proteins into nanodiscs bounded by SMA indicates a general applicability of SMA isolation for membrane proteins of any class.

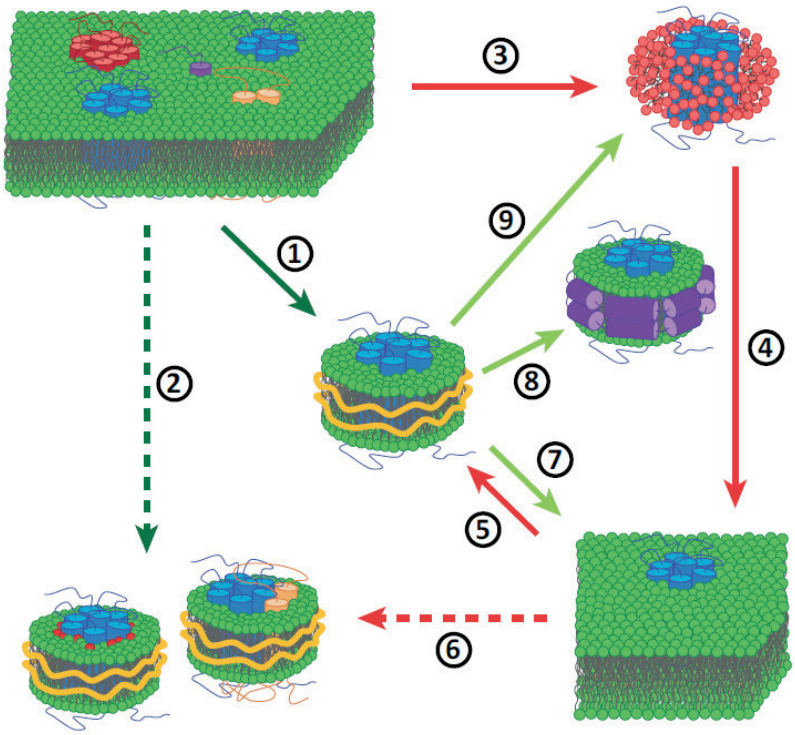

Figure 1.
Different applications of native nanodiscs. Dark green arrows indicate conservation of the native environment, light green arrows display possibilities for the transfer to controlled environments. Red arrows display approaches that generally use synthetic environments. The dashed arrows represent approaches in which complexes of membrane proteins with specific lipids (red) or other proteins (yellow) can be isolated from native (2) or synthetic (6) environments.

Applications of native nanodiscs and new possibilities offered by transfer to other environments. The various reports that have been published on the use of SMA have highlighted various applications in the study of membranes and membrane proteins. This shows that the system is rapidly gaining acceptance in the field. However, current use of the technique is still far from exploiting its full potential. Here, we will review some possibilities offered by current methods of SMA extraction and we will discuss some new applications of SMA that may become available in future membrane research.

Figure 1 illustrates established and potential future applications of membrane solubilization by SMA. The various applications are depicted as numbered arrows in the figure, which will be referred to in the text. In the following paragraphs, we will zoom in on the possibilities associated with each of the different arrows.

Arrow 1. As discussed extensively already, the isolation of membrane proteins in native nanodiscs offers exciting possibilities for their structural and functional characterization in a native environment. Native nanodiscs are readily amenable to single particle techniques right after purification and can thus be studied by many biophysical

techniques. EM in particular is a promising technique for structure determination of membrane proteins in native nanodiscs. Given a sufficient sensitivity of any technique employed, it would even be possible to study isolated membrane proteins at endogenous levels of expression. These properties make native nanodiscs a promising tool that will likely develop into a powerful platform for structural and functional characterization of membrane proteins.

Arrow 2 involves the co-purification of lipids and other proteins with membrane proteins in the same nanodisc. The results reported to date support the assumption that SMA-based extraction renders a snapshot view of a membrane protein in its natural context, allowing determination of preferential lipid–protein and protein–protein interactions [13,15,18]. Combined approaches involving different pull-down assays and separation techniques on native nanodiscs may thus provide a convenient tool to obtain detailed information on the interaction profile of membrane proteins.

Arrows 3–5. SMA can also be applied to model membranes (arrow 5) in which proteins are reconstituted in the conventional way by using detergent (arrows 3 and 4). This allows the preparation of nanodiscs containing an membrane protein embedded in a defined lipid environment. The big advantage would be that the lipid composition can be systematically varied in a similar way as has been established for MSP bounded nanodiscs [19].

Arrow 6. Nanodiscs derived from synthetic bilayers of specific lipid and/or protein composition can also be used as a tool to analyze preferential interactions of membrane proteins with lipids or other proteins. The underlying principle is similar to that already presented for native nanodiscs, but the advantage is that the interactions can be studied in a more controlled way. For instance, it is then possible to reconstitute proteins into bilayers at different lipid/protein ratios and then analyze the protein content of the purified nanodiscs. This would allow straightforward studies on protein–protein interactions and oligomerization processes and enable investigations on how they depend on, for instance, the lipid environment.

Arrow 7. A limitation of native nanodiscs is that they may be incompatible with certain downstream applications. Examples are techniques that require the presence of separate compartments such as transport assays and electrophysiology. In those cases, it would be convenient to reconstitute the protein from the native nanodisc directly into synthetic bilayers, as was recently reported for the channel protein KcsA [13]. Membrane proteins treated this way may thus be studied in a controlled and compartmentalized environment without ever being destabilized in detergent. A big challenge still remains in the quantitative reconstitution of the entire native protein material including surrounding lipids. This could have important implications because it might enable structure determination by X-ray crystallography of membrane proteins in a near-native lipid environment. Such reconstitution is not straightforward however, especially

because of the high affinity of SMA for lipids, which complicates their removal and may impair the formation of extended bilayers. It has been suggested that lowering the pH would solve this problem [20]. However, in our hands this approach was not successful (Koorengevel, Scheidelaar and Dörr, unpublished observations). Reconstitution via a decrease in pH is likely problematic because the increased hydrophobicity of a protonated polymer causes precipitation of the nanodiscs together with enclosed lipids and proteins. Nevertheless, it is an intriguing idea to exploit the pH dependence of SMA to destabilize nanodiscs. For instance, addition of excess lipid may be sufficient to facilitate reconstitution in bilayers using this approach.

Arrows 8 and 9. There might be several reasons why native nanodiscs may be incompatible with the assays or methods to be used. In such cases purification and stabilization of an membrane protein in native nanodiscs and further transfer into other membrane mimics may be a convenient approach. Depending on the applications, this environment may be compartment-forming systems, as discussed above, or it could be MSP nanodiscs or detergent micelles. In particular, transfer to MSP nanodiscs could be convenient because many applications already have been developed and tested for these particles. However, reconstitution directly from native nanodiscs into MSP nanodiscs has not been reported yet. Similarly, it could be advantageous to purify proteins in the form of native nanodiscs and replace the nanodiscs for detergent prior to functional or structural studies. This is the case for example when a protein is not stable enough in detergent for purification, but the analysis method is incompatible with nanodiscs bounded by SMA.

Preferential solubilization of membrane domains by SMA. Preferential solubilization of membrane domains by SMA may be another useful application for future membrane research. Although the polymer is promiscuous with respect to solubilization of phospholipid species [13—16, 21], it does solubilize certain types of membranes more easily than others. For example, membranes with very low lipid/protein ratios will be relatively difficult to solubilize. This was exploited in a recent study on plant thylakoid membranes to prepare a non-solubilized fraction that was enriched in certain membrane protein complexes [22]. As another example, membranes with lipids in a fluid phase are more efficiently solubilized than membranes with gel phase lipids [21]. This may be exploited to selectively solubilize the fluid phase lipids in membranes that exhibit phase separation. The same could hold for membranes containing liquid-ordered domains enriched in sphingolipids and cholesterol (often termed “lipid rafts”). In view of their tight packing, these domains are likely to be more resistant against solubilization by SMA than the more fluid phosphatidylcholine-rich domains, leading to a selective solubilization of the liquid disordered domain (Dominguez and Killian, manuscript in preparation). Thus, SMA could provide an alternative means of purifying liquid-

ordered domains without the need for conventional detergent. This would be a potential advantage over established detergent-based methods that can affect the phase behavior of the system [23].

SMALPs as membrane mimics to study membrane interactions with water–soluble proteins and peptides. An alternative application of nanodiscs bounded by SMA or MSP is their use as small soluble membrane mimics for any kind of study on membrane interaction of water-soluble peptides or proteins. Due to their limited size, nanodiscs may be particularly useful for studying initial stages in processes that involve membrane mediated peptide oligomerization. No such studies have been reported yet, but it is possible that nanodiscs are suitable to study early stages of pore formation in membranes by oligomeric species of amyloid forming proteins or by pore-forming antibiotic peptides. The same holds for amyloid aggregation at a membrane surface, where the small available surface area on nanodiscs may be exploited to trap smaller oligomeric intermediates.

SMA as acceptor system for cell–free protein production. SMALPs may possibly also find a use as acceptor bilayer system for cell-free MP production, as was shown for nanodiscs bounded by MSP [24]. So far, this has not been reported but advantages over the MSP-bounded discs would be that the preparation of SMALPs is cheaper and easier. Furthermore, the particles might be able to expand upon incorporation of a protein due to the flexibility of SMA that is less restricted to a specific arrangement than MSP.

Design of SMA derivatives for specific applications. Generally, the structure of SMA should provide plenty of opportunities for chemical modification to tune its properties in order to avoid undesired interactions. Also, the incorporation of fluorescent or radioactive labels or affinity tags is possible and thus an extensive toolbox of different SMAs and their derivatives may be generated for various applications. Recently, it was shown that SMA can be functionalized with thiol groups (R-SH) to which other functionalities can be chemically linked. This opens applications for attaching fluorophores to nanodiscs that can be used in single molecule spectroscopy and attaching biotin-derivatives for the binding of nanodiscs to solid surfaces [25].

Limitations. One should note, however, that the use of SMA also has potential limitations. As mentioned before (in the paragraph that describes reconstitution of nanodiscs, arrow 7 of figure 1) nanodiscs are incompatible with functional studies on vectorial transport of small molecules by transport proteins, since such assays usually require compartment-forming systems.

There are more limitations, for instance, the higher order of lipids in nanodiscs

from model membranes [26] could cause a higher rigidity of the lipid environment. Apart from a favorable increase in protein stability this could also hinder conformational transitions or helical movement and thus interfere with protein function in native nanodiscs. Furthermore, the presence of SMA could impair binding studies involving the use of (multiple) positively charged molecules, because the high negative charge density of SMA can interfere with binding of these molecules to their target proteins. Measurements at low pH or assays that require high amounts of Mg^{2+}or Ca^{2+} for example as cofactor may be a problem due to destabilization of the nanodiscs by protonation or chelated divalent cations, respectively. Finally, it is possible that insertion of the phenyl groups between the lipid chains induces changes in lipid packing in nanodiscs that may be unfavorable, or that the presence of phenyl groups is a disadvantage in processes involving cation–π or π–stacking interactions. Reconstitution from native nanodisc into bilayers or other membrane mimicking environments may overcome these problems.

6.6 Conclusions.

In this thesis, SMA copolymers have been successfully employed in the solubilization of a set of photosynthetic membrane proteins generally showing the superiority of the obtained native nanodisc environment over detergent micelles. The nanodiscs have been subject to complementary studies proving their suitability for a variety of biophysical and biochemical techniques that allowed insights into protein structure and function as well as native interactions of membrane proteins with both lipids and other proteins. Details of the mode of action of SMA-mediated membrane solubilization have been described, and are expected to be valuable for adaptations of the method to more difficult systems or conditions. Yet, many potential applications of the use of SMA copolymers and chemically modified or tailor-made variants thereof remain to be explored and discovered. Altogether, it can be concluded that SMA copolymers are highly promising versatile tools for the study of diverse membrane-related processes and that they are likely to make a large contribution to the field of membrane research in the future.

References

[1] Imming, P., Sinning, C., and Meyer, A. Drugs, their targets and the nature of drug targets. Nat. Rev. Drug. Disc. (2006), 5:821-834.

[2] Yildirim, M.A., Goh, K.I., Cusick, M.E., Barabasi, A.L., and Vidal, M. Drug - target network (2007) , Nat. Biotechnol., 25: 1119 – 1126 .

[3] Popot, J-L. Amphipols, Nanodiscs, and Fluorinated Surfactants: Three Nonconventional Approaches to Studying Membrane Proteins in Aqueous Solutions. Annual Rev. of Biochem. (2010), 79:737-775.

[4] Serebryany, E., Zhy, G.A., and Yan, E.C.Y. Artifical membrane-like environments for in vitro studies of purified G-protein coupled receptors. BBA Biomembranes (2012), (1818)2:225-233.

[5] Dörr JM, Scheidelaar S, Koorengevel MC, et al. The styrene–maleic acid copolymer: a versatile tool in membrane research. *European Biophysics Journal*. 2016;45:3-21. doi:10.1007/s00249-015-1093-y.

[6] Tonge, S.R., Tighe, B.J. Responsive hydrophobically associating polymers: a review of structure and properties. Adv Drug Del Rev (2001), 53:109–122.

[7] Knowles, T.J., Finka, R., Smith, C., Lin, Y-P., Dafforn, T., Overduin, M. Membrane proteins solubilized intact in lipid containing nanoparticles bounded by styrene maleic acid copolymer. J Am Chem Soc (2009) , 131:7484–7485.

[8] Vargas, C., Arenas, R.C., Frotscher, E., Keller, S. nanoparticle self-assembly in mixtures of phospholipids with styrene/maleic acid copolymers or fluorinated surfactants. Nanoscale (2015), (48)7:20686-20696.

[9] Cuevas Arenas, R., Klingler, J., Vargas, C., and Keller, S. Nanoscale (2016), DOI: 10.1039/C6NR02089E.

[10] Jamshad, M. et al. Structural analysis of a nanoparticle containing a lipid bilayer used for detergent-free extraction of membrane proteins. Nano Research (2015), 8:774–789.

[11] Jones, M.R., The petite purple photosynthetic powerpack, Biochemical Society Transactions (2009), 37 (2), 400-407, DOI: 10.1042/BST0370400.

[12] Postis, V. et al. The use of SMALPs as a novel membrane protein scaffold for structure study by negative stain electron microscopy. BBA-Biomembranes (2015), 1848:496–501.

[13] Dörr JM et al Detergent-free isolation, characterization, and functional reconstitution of a tetrameric K+ channel: the power of native nanodiscs. Proc Natl Acad Sci USA (2014), 111:18607–18612.

[14] Long, A.R., O'Brien, C.C., Malhotra, K., Schwall, C.T., Albert, A.D., Watts, A., Alder, N.N. A detergent-free strategy for the reconstitution of active enzyme complexes from native biological membranes into nanoscale discs. BMC Biotechnol (2013) , 13:41.

[15] Prabudiansyah, I., Kusters, I., Caforio, A., Driessen, A.J.M.Characterization of the annular lipid shell of the Sec translocon. BBABiomembranes (2015), 1848:2050–2056.

[16] Swainsbury, D.J.K., Scheidelaar, S., van Grondelle, R., Killian, J.A., Jones, M.R. Bacterial reaction centers purified with styrene–maleic acid copolymer retain native membrane functional properties and display enhanced stability. Angew Chem Int Ed Engl (2014), 53:11803–11807.

[17] Caffarri, S., Kouril, R., Kereiche, S., Boekema, E.J., and Croce, R. Functional architecture of higher plant photosystem II sumpercomplexes. EMBO (2009), 28:3052-3063.

[18] Paulin, S. et al. Surfactant-free purification of membrane protein complexes from bacteria: application to the staphylococcal penicillin-binding protein complex PBP2/PBP2a. Nanotechnology (2014), 25:285101.

[19] Schuler, M.A., Denisov, I.G., Sligar, S.G. Nanodiscs as a new tool to examine lipid–protein interactions . Methods Mol Biol (2012) , 974:415–433

[20] Jamshad, M. et al. Surfactant-free purification of membrane proteins with intact native membrane environment. Biochem Soc Trans (2011), 39:813–818

[21] Scheidelaar, S., Koorengevel, M.C., Dominguez Pardo, J., Meeldijk, J.D., Breukink, E., Killian, J.A. Molecular model for the solubilization of membranes into nanodisks by styrene–maleic acid copolymers. Biophys J(2015), 108:279–290

[22] Bell, A.J., Frankel, L.K., Bricker, T.M. High yield non-detergent isolation of photosystem I light-harvesting chlorophyll II membranes from spinach thylakoids. J Biol Chem (2015), 290:18429–18437

[23] Heerklotz, H. Triton promotes domain formation in lipid raft mixtures. Biophys J (2002), 83:2693–2701

[24] Roos, C. et al. Characterization of co-translationally formed nanodisc complexes with small multidrug transporters, proteorhodopsin and with the *E. coli* MraY translocase. Biochim Biophys Acta (20120, 1818:3098–3106

[25] Lindhoud, S., Carvalho, V., Pronk, J.W., and Aubin-Tam, M-E. SMA-SH: modified styrene—maleic acid copolymer for functionalization of lipid nanodiscs. Biomacromolecules (2016), 17(4): 1516-1522

[26] Orwick, M.C. et al. Detergent-free formation and physicochemical characterization of nanosized lipid–polymer complexes: lipodisq. Angew Chem Int Ed Engl (2012), 51:4653–4657

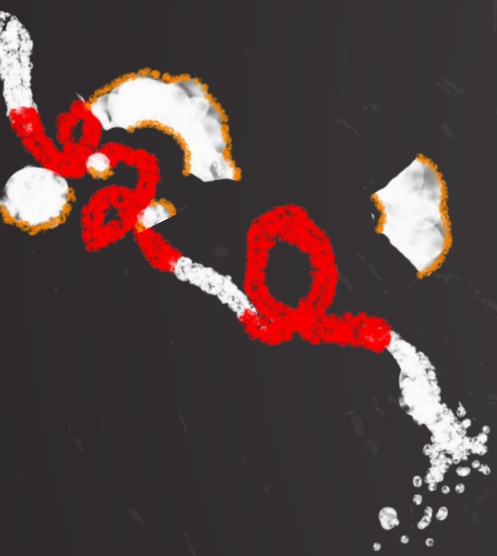

ADDENDUM

Nederlandse samenvatting

Deze samenvatting van mijn proefschrift is gericht aan iedereen. Aan iedereen die in een aantal minuten graag wil weten waar ik mij de afgelopen jaren mee bezig heb gehouden en wat het heeft opgeleverd. In het bijzonder is deze samenvatting voor diegene die niet thuis zijn in de wereld van de scheikunde, zoals mijn ouders en mijn vriendin. Ik heb dan ook geprobeerd het verhaal begrijpelijk en leesbaar te houden. Beschouw het als een wetenschappelijke reis op papier. Een reis die ons o.a. brengt langs de kleinste bouwstenen van het menselijk lichaam, bacteriën die leven op zonlicht en langs een bepaald soort plastic, welke je o.a. vindt in auto's.

Onze reis begint bij het menselijk lichaam. Deze is opgebouwd uit wel 100 miljard (!) cellen. Er bestaan veel verschillende celtypes die allemaal hun eigen functie hebben. Een kleine greep: zenuwcellen, spiercellen, longcellen, levercellen, huidcellen, rode bloedcellen, enz., enz. Cellen bouwen op tot weefsel en organen die ingenieus samenwerken om zo het menselijk lichaam te vormen. Ondanks dat er veel verschillende soorten cellen zijn, hebben ze een aantal dingen gemeen. Eén daarvan stond centraal in mijn onderzoek: het celmembraan. Dit is het omhulsel van de cel en zorgt daarmee dat de inhoud van de cel bij elkaar blijft. Dit klinkt misschien niet spannend, maar niks is minder waar. Een celmembraan is actief betrokken bij vele processen die in de cel plaatsvinden. Als barrière tussen binnen en buiten is het betrokken bij elk verkeer dat graag de cel in en uit wil.

Als we wat verder inzoomen op een celmembraan zien we dat deze bestaat uit hoofdzakelijk twee soorten chemische deeltjes (moleculen): lipiden en eiwitten. Lipiden zijn cilindervormige moleculen en bestaan uit een hydrofiele (waterminnend) kopgroep en een hydrofobe (vetminnend) staart. Als je lipiden in water stopt, waar ~70 % van het menselijk lichaam uit bestaat, zullen de hydrofiele kopgroepen contact maken met water en de hydrofobe staarten zullen elkaar opzoeken en juist weg van het water gaan. Op deze manier organiseert zich een dubbellaag waarvan de buitenkant bestaat uit kopgroepen en de binnenkant uit hydrofobe staarten. Dit is handig gedaan van de natuur, want op deze manier kunnen wateroplosbare stoffen niet zomaar de cel in en uit. Dat verkeer wordt gereguleerd door de andere component van een celmembraan: de membraaneiwitten. Deze zitten in het celmembraan en zijn dus eigenlijk de uitsmijters van de cel.

Nu wordt het interessant (Oké, ik bedoel: nog interessanter). Je zou misschien verwachten dat membraaneiwitten op z'n minst een belangrijke rol spelen bij het toelaten van medicijnen in de cel. En inderdaad, ongeveer 50 % van alle medicijnen op de markt grijpen aan op een membraaneiwit! Het is dus wel duidelijk dat het begrijpen van hoe

een membraaneiwit eruit ziet en functioneert van levensbelang kan zijn.

En niet alleen het membraaneiwit zelf. Ook de directe omgeving (lipiden en andere eiwitten) van een membraaneiwit kunnen bepalen hoe deze functioneert. Het is dus ook belangrijk om te weten welke soorten lipiden en eiwtten interactie met elkaar hebben. Maar dat is makkelijker gezegd dan gedaan. Hoe krijgen we inzicht in al die interacties die plaatsvinden in een celmembraan? Een apparaat waar je een cel instopt en analyseert wat er allemaal gaande is, klinkt als de oplossing. Alleen bestaat zoiets simpelweg niet.. Het is over het algemeen nodig om een membraaneiwit te kiezen en deze op te zuiveren, zodat die in detail bestudeerd kan worden. Maar daar dient zich de volgende moeilijkheid al aan. Hoe zuiveren we een membraaneiwit op, zodanig dat het nog functioneert zoals het in een celmembraan doet? Dat is een vraag die wetenschappers in het veld al tientallen jaren bezighoudt. Zodra een membraaneiwit uit een celmembraan gehaald wordt, bevindt het zich niet meer in zijn natuurlijke omgeving. Sterker nog, er zijn detergenten (ook wel zeepmoleculen genoemd) nodig om de membraaneiwitten op te zuiveren en oplosbaar in water te houden. Helaas zijn deze zeep moleculen vaak slecht voor het eiwit. Ondanks dat dit als slecht nieuws overkomt, heeft deze methode al heel veel informatie opgeleverd en ons gebracht waar we nu staan. Maar we moeten verder, het moet beter. En dat is waar dit proefschrift een klein beetje aan bijdraagt. En hulp komt uit overwachte hoek. Het is een soort plastic, een polymeer opgebouwd uit styreen en maleïnezuur dat veelvuldig in de chemische industrie gebruikt wordt van auto's tot aan schoonmaakmiddelen, dat ons verder helpt.

Een polymeer is te vergelijken met een gekookte spaghettisliert. Het bestaat uit heel veel aaneengeschakelde eenheden, in ons geval uit styreen en maleïnezuur eenheden. Niet verrassend heet dat dan een *styreen-maleïnezuur polymeer* (vanaf nu SMA). Styreen is hydrofoob, terwijl de maleinezuur hydrofiel is en afhankelijk van de pH van water neutraal of negatief geladen. De oplettende lezer weet nog dat lipiden ook deels hydrofoob en hydrofiel zijn. En dat is precies de reden waarom de ogenschijnlijke verschillende lipiden en SMA moleculen toch samen in één huwelijk te passen zijn.

Het blijkt namelijk dat de SMA op een hele zachte manier een membraaneiwit kan opzuiveren. SMA kan een membraan opdelen in kleine schijfjes (welke we nanodiscs noemen) waarin het membraaneiwit zit, samen met een klein stukje van de natuurlijke membraanomgeving. En dat is uniek. Er is geen enkele andere methode bekend die op deze manier werkt. Dat maakt de SMA methode een veelbelovende manier in het onderzoek naar celmembranen en membraaneiwitten. Echter, de SMA methode staat nog wel in de kinderschoenen. Pas sinds 2009 is de SMA methode bekend gemaakt in de wetenschappelijke wereld en er zijn nog veel onduidelijkheden over bijvoorbeeld het

werkingswechanisme van SMA. Hoe werkt de SMA op moleculair niveau en wat zijn mogelijke toespassingen en limitaties van de SMA methode?

Dit is het punt dat we (eindelijk..) overgaan op de resultaten van dit proefschrift. Hoofdstuk 1 is een introductie, een uitgebreide van o.a. wat hier boven beschreven staat. In hoofdstuk 2 onderzoeken we een commericeel verkrijgbare SMA variant met een streen/maleinezuur verhouding van 2:1 en een gewicht–gemiddelde molecuulgewicht van 7.5 kDa. We onderzoeken specifiek hoe SMA werkt op model membranen met verschillende lipide composities. Dit was experimenteel tot stand gebracht met behulp van lichtverstrooiing. Omdat de model membranen (~ 400 nm) wel licht verstrooit en de uiteindelijke nanodiscs (~ 10 nm) niet, kon mooi worden bijgehouden hoe snel en efficiënt SMA model membranen afbreekt (noemen we solubilizeren) tot nanodiscs. Daaruit bleek dat membranen die lipiden bevatten die negatief geladen zijn, een dubble binding in de hydrofobe staart hebben, of kegelvormig zijn veel moeilijker te solubilizeren zijn met SMA dan membranen die lipiden bevat die neutraal zijn, geen dubbele binding hebben, en cilindervormig zijn. Het komt er op neer dat repulsieve elektrostatische interacties en de druk (kracht/oppervlak) die heerst in de binenkant van een membraan bepaalt hoe snel en efficiënt SMA een membraan solubilizeert. Ook als je de concentratie van SMA verhoogt, kun je solubilizatie versnellen. Het proces van solubilizatie is ook vastgelegd op camera. In dit geval met een elektronenmiscroscoop (EM). Deze techniek heeft de resolutie om te kunnen kijken naar deeltjes zo klein als een aantal nanometer. Dat leverde mooie foto's op, kijk zelf maar eens in hoofdstuk 2.

Andere waardevolle bevindingen in hoofdstuk 2 zal ik kort benoemen. SMA blijkt veel efficiënter membranen te solubilizeren dan membrane scaffold proteins (MSPs), een ander veel gebruikt molecuul dat nanodiscs kan maken. Dat SMA nanodiscs maakt en daar ook nog eens efficiënt in is, heeft vooral te maken met zijn hydrofiele en hydrofobe karakter in één, maar ook dat zijn bouwstenen klein zijn. Ook blijkt het dat de lipidecompositie van het membraan precies behouden blijft in een nanodisc. Dat betekent dus dat het SMA geen voorkeur heeft voor de solubilizatie van een specifiek lipid, en dat is van cruciaal belang om de natuurlijk lipide compositie van een celmembraan te kunnen bestuderen.

In hoofdstuk 3 zijn de rollen omgedraaid. Daar wordt SMA met verschillende styreen/maleïnezuur verhoudingen in het polymeer getest (1.4:1, 2:1, 3:1, en 4:1) op hun solubilizatie eigenschappen op één soort membraan. Het doel was om te bekijken welk bestaand SMA polymeer het beste is in het solubilizeren, en of we zouden kunnen leren of we zelf een nieuw SMA polymeer kunnen fabriceren die mogelijk nog beter is. Verder zijn een aantal eigenschappen van SMA polymeren in water onderzocht zoals

wateroplosbaarheid, ionisatiegraad als functie van pH, en de moleculaire conformatie op verschillende pHs. Allen zijn van belang voor een optimale toepassing van SMA in het onderzoek naar celmembranen (soms moet je maar even aannemen dat zo'n bewering klopt).

De SMA met een 2:1 verhouding styreen tot maleïnezuur blijkt de beste in zijn vak. Deze verhouding is optimaal, omdat het genoeg hydrofoob styreen heeft om interactie te willen hebben met een membraan, en genoeg hydrofiel maleïnezuur om de styreen in bedwang te houden en het membraan op te breken in kleinere stukken. En als we de verdelingen van de styreen en maleïnezuur eenheden nog beter verdelen in de toekomst, zouden we een nog betere SMA kunnen ontwikkelen! Tenminste, dat is de verwachting.

Waar in hoofdstuk 2 & 3 vooral de eigenschappen van SMA en het solubilisatieproces van membranen werd bestudeerd, worden in hoofdstuk 4 & 5 de toepassing van SMA onderzocht: het solubilizeren van membraaneiwitten uit echte celmembranen. Het systeem om te bestuderen was de bacterie *Rhodobacter (Rba.) sphaeroides*. Deze bacterie leeft diep in bepaalde meren in de VS en gebruikt de zon als energiebron (fotosynthese), net als planten dat doen. Een bepaald soort eiwit in de fotosynthetische membranen, de reaction center (RC) is al in detail gekarakteriseerd en daardoor een ideaal model membraaneiwit om de SMA op toe te passen.

Hoofdstuk 4 beschrijft hoe de membranen van *Rba. sphaeroides* met SMA omgezet worden in nanodiscs die RCs bevatten. Voor membranen die alleen RCs bevat is dat een efficiënt proces. Ook het opzuiveren van de RCs in nanodiscs bleek goed te doen. En dan de karakterisatie van de RC-nanodisc. Wederom is de elektronenmicroscoop van grote waarde. Deze laat prachtige nanodisc deeltjes zien. De zwarte bolletjes in die plaatjes zijn hele kleine gouddeeltjes gebonden aan de RC. Het maakt de foto niet alleen fraaier, het is ook een direct bewijs dat de RC daadwerkelijk in de nanodisc zit.

Doordat we precies weten wat de dimensies van de nanodisc en de RC zijn, en hoeveel lipiden er gemiddeld per RC zijn, konden we schatten dat er ongeveer 150 lipiden in de nanodisc zitten om de RC heen. Dat zijn membraanstukjes van ongeveer drie lipide lagen dik. Fantastisch, niet waar?! Dat betekent namelijk dat we met SMA dus echt een stukje natuurlijke membraanomgeving van de RC meenemen in een nanodisc. Ter herinnering: via de standaard manier zou de RC in een bolletje met zeepmoleculen zitten zonder lipiden, laat staan de aanwezigheid van een stukje natuurlijk membraan.

Zoals gehoopt laat de RC in een nanodisc ook eigenschappen zien zoals hij die in zijn natuurlijke omgeving laat zien, en anders dan in zeepmoleculen. Nog mooier, een RC in een nanodisc is beter beschermd tegen verhitting en slechte lichtinvloeden dan in zeepmoleculen of zelfs in zijn natuurlijke omgeving in de membraan. Dit opent mogelijkheden RCs in nanodiscs te gebruiken voor applicaties als bio-zonnecellen waar de stabiliteit van de RC voorheen altijd een probleem was.

Hoofdstuk 4 is dus prachtige reclame voor de SMA methode. Maar.... eerlijk is eerlijk, dit is alleen getoond voor de RC van *Rba. sphaeroides*. Wie zegt dat SMA ook andere membranen zo goed kan solubilizeren en andere eiwtten zo goed in nanodiscs kan vangen?

In hoofdstuk 5 komen we daar een klein beetje op terug. Daar kijken we waar mogelijke limitaties van het SMA liggen om membraaneiwitten te vangen in nanodiscs vanuit een celmembraan. De focus lag op (1) het solubiliseren van membranen, en (2) een mogelijk maximale grootte van een membraaneiwit welke gevangen kan worden in nanodiscs. Hier speelt de RC van *Rba. sphaeroides* weer de hoofdrol. Maar deze keer op een iets andere manier dan in hoofdstuk 4. Nu worden membranen van RC-LH1 eiwitten en RC-oligomeren gebruikt. In het geval van de RC-LH1 heeft de RC nog een andere eiwitcomplex omzich heen: de light harvesting complex 1 (LH1). In het geval van RC-oligomeren zijn er meerdere RCs aan elkaar gekoppeld tot dimeren, trimeren en tetrameren. Daardoor worden ze vooral groter en pakken ze zich misschien wel anders in het membraan wat mogelijk problemen geeft voor het SMA ze te solubilizeren.

De RC-LH1 membranen blijken haast niet te solubilizeren. Waarom? Vooral omdat het membraan tjokvol van het eiwit zit waardoor ze ontzettend strak tegen elkaar zitten. Dit zorgt er voor dat de SMA bijna niet in staat is het membraan op te breken. SMA heeft namelijk lipiden nodig om dat te doen. De truc is dan ook om de eiwitexpressie te verlagen of extra lipiden in te fuseren. Om die manier komen de strak georganiseerde eiwitten los van elkaar en zijn er genoeg lipiden voor SMA om solubilizatie te induceren. Nog steeds is de efficiëntie niet zo hoog als met de RCs, maar er is tenminste solubilisatie te zien. Helaas zijn we er hier nog niet mee.. Elektronenmicroscopie liet zien dat de RC-LH1 deeltjes niet hoofdzakelijk in nanodiscs zitten, maar vooral in grotere membraanfragmenten (tot groter dan 100 nm soms!). Dus de membranen worden wel opgebroken, maar ergens in het proces van intact membraan naar nanodisc stopt het proces. De trend lijkt wel zo te zijn dat hoe meer lipiden/hoe minder eiwit, des te efficiënter de solubilizatie en des te kleiner de membraanfragmenten, dus des te groter de kans dat nanodiscs vormen.

Deze resultaten zijn vooral interessant voor membranen waar de eiwit tot lipide ratio erg hoog is. Een voorbeeld daarvan zijn de fotosynthestische membranen in planten. Die membranen noem ik ook liever eiwitmembranen dan lipidemembranen. Experimenten die wij hebben uitgevoerd op deze planten membranen laten inderdaad ook grote membraanfragmenten zien, maar gelukkig ook deeltjes die op nanodiscs lijken. Er ligt hier dan ook nog meer dan genoeg ruimte om de studie voort te zetten.

Wat betreft de grootte van eiwitcomplexen die in een nanodisc passen. Daar bestaat nog geen eenduidigheid over. Al de oligomeren van de RC zijn te solubiliseren, hetzij dat de efficiëntie wel minder wordt als het oligomeer groter wordt (dimeer-> trimeer-> tetrameer). Maar ook hier worden voornamelijk membraanfragmenten gevormd (wel

kleiner dan voor de RC-LH1, veelal tussen de 10 en 100 nm). Het kan goed zijn de de grootte van een eiwit in het membraan deels bepaalt hoe goed het membraan opgebroken wordt, naast de interacties tussen de eiwitten en lipiden in het membraan.

Een laatste opmerking wil ik maken over de lengte van de SMA polymeren die in hoofdstuk 5 worden gebruikt. Zou het zo kunnen zijn dat langere SMA polymeren grotere nanodisc maken, welke dan weer grotere eiwitten kan bevatten? Daar is geen enkel teken of bewijs voor, en het is dan ook nodig om hier nog verder studie aan te doen. En dat gebeurt. En wel in ons lab. Wel is het zo dat des te langer de SMA polymeren, des te minder efficiënt ze een membraan kunnen opbreken. Dat kan worden verklaard doordat langere polymeren meer interacties met zichzelf kunnen aangaan en daarmee het membraan meer links laten liggen. En dat leidt dan weer tot minder efficiëntere solubilizatie.

Misschien ben je al afgehaakt of overweeg je sterk dat nu te doen. Maar ik beloof, we zijn er bijna.

Alleen hoofdstuk 6 is nog over en deze bespreekt de mogelijkheden die SMA en nanodiscs hebben in de wetenschappelijke wereld. Maar ook limitaties, nadelen en concepten die we graag beter zouden willen begrijpen komen aan bod. Zo zijn nanodiscs niet handig als we de transport over een membraan willen bestuderen. De negatieve ladingen van de maleïnezuren kunnen ongewenste elektrostatische interacties geven en binden calcium en magneisum ionen. Dat laatste is ook ongewenst, omdat het de solubilizatie eigenschappen van SMA te niet doet en het vangt ionen weg die belangrijk zijn voor het stabiel en functioneel houden van sommige eiwitten.

Van alle onderdelen die we beter willen begrijpen aan het SMA en nanodisc systeem, is de terugreactie van nanodisc naar membraan wel één van de grootste. Het SMA wil graag nanodiscs maken van membranen en dat is juist de bedoeling. Maar soms willen we de nanodiscs ook weer terugzetten in andere membranen of juist een collectief aan nanodiscs laten fuseren tot een membraan. Het lastige is dat het SMA zo graag deel is van de nanodisc dat het niet meer los wil laten om de vorming van membranen mogelijk te maken. Trucjes met lage en hoge pH, en het gebruik van calcium en magnesium ionen hebben nog niet geleid tot het gewenste resultaat. Ik zou zeggen, denk eens mee en laat het mij weten..

Al met al beschouw ik dit proefschrift als een hele mooie bijdrage aan het gebruik van SMA en nanodiscs in membraanonderzoek. Het begrijpen van de eigenschappen van het SMA polymeer in water en membraansolubilizatie (hoofdstuk 2 & 3), het laten zien van hoe prachtig de SMA zijn werk kan doen in de solubilizatie van membranen en het vangen van een membraaneiwit in een nanodisc (hoofdstuk 4), welke problemen

SMA mogelijk tegen kan komen in de solubilizatie van membranen (hoofdstuk 5), en het laten zien welke potenties SMA en nanodiscs hebben in membraanonderzoek, maar ook het besef waar nog aan gewerkt moet worden (hoofdstuk 6) maken mij trots op wat ik en ons SMA-groepje in Utrecht hebben bereikt in die paar jaar.

List of publications

D.J.K. Swainsbury & **S. Scheidelaar**, R. van Grondelle, J.A. Killian, and M.R. Jones, (2014), Bacterial reaction centers purified with styrene maleic acid copolymer retain native membrane functional properties and display enhanced stability. *Angew. Chem. Int. Ed.* 53, 11803–11807.

J.M. Dörr, M.C. Koorengevel, M. Schäfer, A.V. Prokofyev, **S. Scheidelaar**, E.A.W. van der Cruijsen, T.R. Dafforn, M. Baldus, and J.A. Killian, (2014), Detergent-free isolation, characterization, and functional reconstitution of a tetrameric K^+ channel: the power of native nanodiscs. *Proc. Natl. Acad. Sci. USA* 111, 18607-18612.

S. Scheidelaar, M.C. Koorengevel, J.J. Pardo Dominguez, J.D. Meeldijk, E. Breukink, and J.A. Killian, (2015), Molecular model for the solubilization of membranes into nanodisks by styrene maleic acid copolymers. *Biophys. J.* 108, 279-290.

J.M. Dörr, **S. Scheidelaar**, M.C. Koorengevel, J.J. Dominguez, M. Schäfer, C.A. van Walree and J.A. Killian, (2016), The styrene–maleic acid copolymer: a versatile tool in membrane research. *Eur. Biophys. J.* 45, 3-21.

J.M. Gruber, **S. Scheidelaar**, H. Van Roon, J.P. Dekker, J.A. Killian, and R. Van Grondelle, Photophysics in single light–harvesting complexes II: from micelle to native nanodiscs, (2016), *Proc. SPIE* 9714, doi:10.1117/12.2211588.

S. Scheidelaar, M.C. Koorengevel, C.A. van Walree, J.J. Dominguez, J.M. Dörr, and J.A. Killian, Effect of polymer composition and pH on the solubilization of lipid membranes by styrene–maleic acid copolymers. *Biophys. J. Manuscript submitted after revision.*

J.J. Dominguez Pardo, J.M. Dörr, A. Iyer, R.C. Cox, **S. Scheidelaar**, M.C. Koorengevel, V. Subramaniam, and J.A. Killian, Solubilization of lipids and lipid phases by the styrene–maleic acid copolymer. *Manuscript submitted.*

D.J.K. Swainsbury, **S. Scheidelaar**, N. Foster, R. Van Grondelle, J.A. Killian, and M.R. Jones, Styrene–maleic acid copolymer purification of diverse integral membrane pigment–proteins from SMA–resistant membranes. *Manuscript in preparation.*

About the author

Stefan Scheidelaar was born July 12th 1988 in Nieuw-Lekkerland, Zuid-Holland. In 2006 he graduated from *Willem de Zwijger College* in Papendrecht (VWO). There, his interest for chemistry came alive and as such he went to Utrecht University to study chemistry. During his bachelor he was active for the student union "Proton" where he was a committee member of *de Chemograaph* (magazine for the department of chemistry) and *DIES* (committee that organizes the birthday of proton). During his bachelor research, he studied the energy transfer in lanthanide-doped crystals, which may find application in future generation solar cells, both experimentally and theoretically in the group of Condensed Matter and Interfaces (CMI).

His continuing growing interest in physics translated itself into the master "Chemistry & Physics: Nanomaterials" at Utrecht University. His master thesis was a continuation of his bachelor thesis in the group of CMI under the supervision of prof. Andries Meijerink and is named: *Theoretical modeling of luminescence from quantum cutting materials*. His master ended with a 5 month internship at the FOM AMOLF institute (Amsterdam) in the group of Prof. Huib Bakker, where he investigated the dynamics of water molecules around ions and ionic hydrophobic molecules using ultrafast infrared pump-probe spectroscopy.

After graduation in 2011, he started his PhD for Stichting FOM in the group Biochemistry of Membranes under the supervision of prof. Antoinette Killian at Utrecht University in Oktober 2011. From June 1st 2012 on, this group merged with the group of Membrane Enzymology into Membrane Biochemistry & Biophysics (MBB). During his PhD he did a lot on teaching. He supervised many bachelor- and master students on a SMA project, and assisted various courses that were part of bachelors in chemistry, pharmacy, biomedical sciences, and life sciences. He presented the SMA project at multiple conferences in the Netherlands, UK and USA. He won a total of 4 awards for presenting the SMA project to the scientific community, of which the most rememberable one was the Student Research Achievement Award (SRAA) awarded at the Biophysical Society meeting in Philadelphia, PA, USA in February 2013.

Dankwoord

Dit is als je het mij vraagt het moeilijkste gedeelte van een proefschrift. Ik wil niemand vergeten of tekort doen. Want een proefschrift vol met wetenschappelijk onderzoek maak je niet alleen. Nee, daar heb je namelijk een heel team om je heen voor nodig.

Ik begin met mijn promotor. Antoinette, ik ben heel blij dat wij het SMA avontuur aangegaan zijn. Dat wisten wij van te voren niet, want in de onderzoeksomschrijving kwam het woord SMA niet eens voor. Daarnaast waren wij allebei niet thuis in de fotosynthese, hetgeen wat er wel in stond. Maar kijk eens waar we na bijna 5 jaar staan met ons SMA cluppie. Dat is iets om trots op te zijn. Ik dank je voor je drive, de discussies, de hulp, het sturen van mijn eigenwijsheid, en het delen van de passie voor membranen.

Dan Martijn. Martijn, jij verdient eigenlijk een heel dankwoord voor jezelf. Ik kwam binnen als afgestudeerde van het Debye instituut en de woorden membraan en eiwit kon ik mij slechts nog vaag herinneren van vroegere colleges. Jij bent degene die mij wist om te vormen tot een membraanwetenschapper. Vanaf het begin hebben wij samen het SMA project in handen genomen en niet meer losgelaten. Dit proefschrift is dus voor een groot gedeelte ook van jou. In het niet-wetenschappelijke gedeelte was je er ook altijd. Van de eindeloze grappen en grollen tot aan serieuze onderwerpen. Echt gaaf vond ik ons avontuur in Philadelphia. Ik beschouw je inmiddels ook als een vriend en niet meer als een collega. Bedankt dat je mij bij staat als paranimf tijdens mijn verdediging.

I also want to show my gratitude to Dave Swainsbury & Mike Jones from the Bristol University in the UK. You guys are indispensable. Without you two this thesis was not as good as it is now. I'm in particular proud of chapter 4. My visit in Bristol in October 2014 was also something never to forget. For the first time visiting a lab abroad and experience the life there was absolutely fantastic. Thank you so much.

Dan de mensen binnen het FOM project. Het zijn er eigenlijk te veel om op te noemen, maar in het bijzonder gaat mijn dank uit naar Rienk, Jan, Henny, Michael, Laura en Marc. Rienk, jij hebt mij gelinkt aan Mike en Dave en je was altijd enthousiast over de SMA. Jan en Henny, jullie hebben je keihard ingezet om de SMA methode op plantenmembranen werkend te krijgen. Helaas was dit uitdagender dan misschien vooraf gehoopt was. Hopelijk worden SMA en thylakoids nog eens goede vrienden van elkaar. Michael, the SMA and LCHII did work out and a paper was the result. Laura, bedankt voor de hulp bij de elektronenmicroscopie in Groningen en de leuke gesprekken die we hadden. Marc, jij bedankt voor de Nile Red tip. Dat is nu één van mijn lievelingsmoleculen.

De vakgroep Membrane Biochemistry & Biophysics. Bijna 5 jaar mijn tweede thuis geweest. Velen hebben bijgedragen aan een hele leuke werksfeer en de gezellige uitjes en feestjes. Joost, jou wil in in het bijzonder noemen. Bijna mijn gehele promotietijd was jij mijn buurman op het kantoortje in W604 op die zesde verdieping. We zijn elkaar goed leren kennen en hebben een goede band opgebouwd in die tijd, niet in de laatste plaats omdat we allebei een dochter in ons leven kregen. Bedankt voor alle hulp (jij zat naast me en was dus vaak als eerste de klos als ik iets niet wist). Het was mij een grote eer paranimf te mogen zijn bij jouw verdediging, ik ben vereerd dat jij ook paranimf wilt zijn bij mijn verdediging. Iets wat ik niet zal vergeten is ons optreden tijdens een van de kerstdiners op de groep.

Eefjan, gelukkig kon jij mijn humor waarderen en ben ik blij dat je altijd je eerlijke en oprechte mening durfde te geven. Over alles. Onze samenwerking in het vak biofysische chemie voor 1e jaars life science studenten vond ik één van de leukste dingen die ik heb gedaan aan onderwijs. Hopelijk keert de Eefjan Breukink Coffee Corner (EBCC) nog eens terug, een man van jouw status kan zoiets echt niet ontbreken.

Ruud, ook bij jou kon ik mijn humor kwijt en ik vond het leuk om mijn sportervaringen met jou te delen en te bediscussiëren. Dankzij jou ben ik handbal gaan waarderen. Eén ding heb ik als geen ander van jou en Martijn geleerd: zonder de technici bestaat er geen vakgroep, bestaat er geen wetenschappelijk onderzoek.

Juan(ovic), having you as a roommate was awesome. We had good fun, great scientific discussions, and football was frequently the subject of our conversations. I will not remind you of the 5-1 score in Brazil, but I would like to remind you of the Baltimore trip. That is in my mind forever, and you know why..

Yao, thanks for the great conversations we had and all the help you always offered. Mike, met jou heb ik altijd kunnen lachen. Als ik zeg Japiejooooo, weet jij wel genoeg. En daarnaast, ik twijfel er niet aan je nog eens tegen te komen als Prof. Dr. Mike Renne, icoon in de wetenschap.

Michal, ik bewonder jouw kijk op de wetenschap en de successen die je daarmee bereikt. Bedankt voor je discussies over de wetenschap en over het leven daarnaast.

Jonas, your contributions to the SMA project are amazing and they have helped me a lot. I enjoyed your company, the conversations we had, and I am curious to find out what you will decide after the PhD life.

Kees, als polymeerchemicus en belangrijk onderdeel van het 1e jaars lab heb jij mij goed kunnen helpen. En daarnaast wil ik je ook gelijk geven: lunchtijd is lunchtijd.

Remko, hulp in het lab of een gezellig kletspraatje, het was allemaal geen probleem. Ik heb ook veel lol gehad in het voorbreiden van de video en quiz die we voor Joost zijn promotiefeestje hebben gemaakt.

Of course, I would like to thank the rest of the MBB group for their efforts and the great time at the lab: Toon, Maarten, Inge, Lisette, Sam, Sabine, Paulien, Saran, Amrah, Xue, Marre, Greg, Cecile, Caroline, Noortje, Tami.

Also a special thanks to the bachelor and master students that had to deal with me as their supervisor: Fran, Ines, and Maria. Of course, there is also Ilias. I will probably always remember you. But I'm not sure whether that is a good or bad thing..

De samenwerkingen met Hans en Jan vond ik heel erg leuk. Hans, wij hebben toch heel wat uur achter de elektronenmicrscoop gezeten en jouw plaatjes zijn een geweldige bijdrage aan mijn proefschrift. Jan, door mijn achtergond in de fysische kant van de chemie vond ik ons werk aan het nanodiscmodel erg leuk. Ik vind het eigenlijk heel jammer dat dit niet expliciet in mijn proefschrift is gekomen.

De samenwerking met Polyscope, in de personen van Pieter Hanssen en Onno Looijmans, waren zeer belangrijk voor mijn proefschrift. Ik bedank jullie voor de informatieuitwisseling en de goede discussise die we over SMA hadden. Onze bezoeken in Geleen vond ik heel erg leuk. Ook zeer bedankt voor de financiële bijdrage aan mijn promotie, daar ben ik heel blij mee. Op dit moment hoop ik dat er nog meer verschiet ligt tussen ons..

Bert, dankzij jou ben ik ook veel wijs geworden over het SMA als molecuul. Het onderonsje in het SMA onderzoek dat wij hadden met Martijn en Onno vond ik één van de leukste dingen van mijn promotietijd.

Ook wil ik de lees- en promotiecommissie graag bedanken. Maarten, Rienk, Andries, Willem, en Bert. Een samenstelling waar ik oprecht trots op ben.

Willem, jou wil ik speciaal ook nog noemen vanwege de fysische chemie colleges. Jouw stijl en manier van werken hebben mij altijd aangesproken, en mijn liefde voor de fysische chemie is voor een goed deel bepaald door jou.

Andries, als begeleider in mijn bachelor- en masterthesis ben jij heel belangrijk geweest voor de vorming van mij als wetenschapper. Niet voor niets heb ik zowel mijn bachelor- als masteronderzoek in jouw groep doorgebracht. Mijn liefde voor het geven van onderwijs heb jij altijd bij mij gestimuleerd. De klaverjaspotjes op de vakgroep zijn om nooit meer te vergeten.

Gerd, ook jou wil ik graag noemen in mijn dankwoord. Als leraar scheikunde (en mentor) in de bovenbouw op de middelbare school ben jij toch wel degene die mij heeft doen overtuigen dat scheikunde het ging worden. We zijn altijd contact blijven houden en ik hoop dat je op mijn promotie aanwezig kan zijn.

Voor de cover design van mijn thesis wil ik Stefanie van den Herik bedanken van BOXPress. Ik vind een mooie beeldende cover heel belangrijk en jij bent er in geslaagd dat voor elkaar te krijgen!

Mijn ouders bedank ik, uiteraard, voor de steun door alle jaren heen.

Tenslotte, Annika, mijn vriendin. Je hebt mij altijd door mijn promotietijd heen gesteund, ondanks dat ik je wel eens het bloed onder de nagels vandaan haalde. De mooiste gebeurtenis tijdens mijn promotieijd is toch wel de geboorte van ons prachtige dochtertje Lizzie op 20 maart 2015. Ik vind het super dat zij ook getuige mag zijn van tenminste een deel van mijn promotie. Ook al zal ze op het moment dat ze dit ooit nog eens mag lezen er niks meer van herinneren. Toch, Liz?

Lipids

Styrene-Maleic Acid copolymer

Nanodisc

SMALPs

Membrane Protein